



# **Genome-based Approaches for Understanding Nutritional Iron Homeostasis in *Chlamydomonas reinhardtii***

Vom Fachbereich Biologie der Technischen Universität Kaiserslautern  
zur Verleihung des akademischen Grades  
“Doktor der Naturwissenschaften“  
genehmigte Dissertation

vorgelegt von

**Anne G. Glaesener**

Datum der wissenschaftlichen Aussprache:

26. November 2019

## **Prüfungskommission**

1. Gutachter: Herr Prof. Dr. Michael Schroda  
2. Gutachter: Frau Prof. Dr. Sabeeha Merchant (UC Berkeley, USA)  
Vorsitzender: Herr Prof. Dr. Ekkehard Neuhaus

Berkeley, 2021

D 386







### **Zusammenfassung**

Angesichts des Klimawandels und einer stetig wachsenden Weltbevölkerung, gehören die Anpassung an die sich ändernden Umweltbedingungen und steigende Ernährungsbedürfnisse zu den größten Herausforderungen unserer Zeit, und werden daher auch für die Grundlagenforschung und die Biotechnologie immer wichtiger. Eisen ist ein essentieller Nährstoff für alle Lebensformen, steht jedoch in vielen Lebensräumen nur begrenzt zur Verfügung. Unter (Nutz-)Pflanzen ist Eisenmangel weit verbreitet und beeinträchtigt dadurch die Produktivität sowohl der Lebensmittelproduktion als auch der CO<sub>2</sub>-Fixierung. Eisen ist aufgrund seiner Funktion als Katalysator für Redoxreaktionen und Elektronentransport von wesentlicher Bedeutung. Aufgrund der Beschaffenheit dieser Reaktionen können überschüssige Mengen an Eisen zur Bildung schädlicher reaktiver Sauerstoffspezies führen, was eine genaue Feinabstimmung des zellulären Eisengehalts erfordert, um sowohl den wesentlichen Bedarf zu decken aber auch nachteilige Auswirkungen zu vermeiden.

Eine zentrale Frage dieser Doktorarbeit ist, wie der Pflanzenstoffwechsel unter eisenarmen Bedingungen verändert wird, und die Grünalge *Chlamydomonas reinhardtii*, ist der ideale Referenzorganismus dafür. Die metabolische Flexibilität von *C. reinhardtii*, insbesondere die Fähigkeit zum heterotrophen (auf Acetat) und autotrophen (auf CO<sub>2</sub>) Wachstum, bietet eine einzigartige Gelegenheit, die Auswirkungen der Eisenernährung auf die Photosynthese im Vergleich zur Zellatmung zu unterscheiden. Während des photoheterotrophen, eisenarmen Wachstums, bei dem die Zellen mit Licht, CO<sub>2</sub> und Acetat versorgt werden, aber kein extrazelluläres Eisen vorhanden ist, erhalten die Zellen die Atmungskette aufrecht, während der photosynthetische Beitrag zur Energetik der Zelle verringert wird. In diesem Zustand kann die Aufrechterhaltung des Photosyntheseapparates zur Last werden, da er große Mengen des limitierenden Nährstoffs Eisen bindet. In dieser Arbeit habe ich den Übergang von photoautotrophen (Licht und CO<sub>2</sub>) zu photoheterotrophen Kulturen in unterschiedlichen Eisenkonzentrationen untersucht, indem phototrophen Kulturen Acetat als reduzierte Kohlenstoffquelle zusetzte wurde und die sich entwickelnden Veränderungen des Stoffwechsels zeitabhängig in verschiedenen Bereichen dokumentiert wurden. Basierend auf der Transkriptomanalyse reagieren alle wichtigen zellulären Prozesse und Signalwege auf die Verfügbarkeit von

Acetat, aber eisenarme Zellen opfern die Photosynthesekapazität in den ersten 12 Stunden nach Verfügbarkeit der zusätzlichen Kohlenstoffquelle zugunsten der Atmungsaktivität und ermöglichen so mechanistische Einblicke in den Übergang zwischen verschiedenen Lebensweisen, abhängig von der Nährstoffzusammensetzung der Umwelt.

Der Einfluß von hohen Mengen extrazellulären Eisens auf *Chlamydomonas* mit allen einhergehenden Chancen und Gefahren war zu Beginn meiner Doktorarbeit wenig untersucht. Anhand physiologischer und photosynthetischer Parameter, Elementaranalyse, Transkriptomik und einer Mutante in einem potentiell wichtigen Speicherorganell, habe ich zum Verständnis beigetragen, mit welchen Mitteln *Chlamydomonas* die potentielle Gefahr zu hoher Eisenkonzentrationen mildern und überschüssiges Eisen in zukünftigen Mangelzeiten nutzen können.

Während der Laborarbeit fielen mir deutliche phänotypische Unterschiede zwischen verschiedenen Labor-Stämmen auf, insbesondere in Bezug auf die Effektivität der Aufnahme von geringen Eisenkonzentrationen. In einem dritten Teil habe ich die Variabilität der basalen Transkriptvorkommen, der photosynthetischen und respiratorischen Aktivität und der Fe-Homöostase der Stämme CC-124, CC4532, CC-1690, CC-1009 und CC-1691 charakterisiert.

Zusammen genommen zeigen die in dieser Arbeit vorgestellten Ergebnisse, wie *C. reinhardtii* erfolgreich als Modellorganismus für die Anpassung an hohe und niedrige Eisenverfügbarkeit in der Umwelt genutzt werden kann.

## Abstract

Facing climate change and a steadily growing human population, acclimation to changing environmental conditions and accommodating increased nutritional demands are among the premier challenges of our time, and therefore of increasing importance to basic plant research and biotechnology. Among the nutritional challenges experienced by plants is iron-deficiency. Iron is an essential nutrient for all life forms, but of limiting availability in many environments, affecting productivity of both food production and carbon capturing. Iron is essential because of its broad function as a catalyst of redox reactions and processes involving O<sub>2</sub> chemistry in the catalytic centers of enzymes. Because of the nature of these reactions, excess amounts of the nutrient can result in the production of deleterious reactive oxygen species, requiring a fine tuning of the cellular iron content, to both accommodate the essential demand and avoid detrimental effects simultaneously. Iron is the most abundant of the transition metals, found in cofactors like heme or inorganic Fe/S, that are utilized in enzymatic reactions or for electron transport in photosynthesis, respiration and many other essential reactions. A question of this project is how plant metabolism is modified in iron-deficient conditions, for which the green alga *Chlamydomonas reinhardtii* as a microbe is an excellent reference organism.

In the past decades, *Chlamydomonas reinhardtii* has been used as a model organism for studying fundamental processes in biology, including photosynthesis, biosynthesis of organelles, nutrient homeostasis, acclimation to changing environments, and specifically discovering mechanisms of acclimation to poor iron nutrition in the plant lineage.

The metabolic flexibility of *C. reinhardtii*, specifically the capacity for both heterotrophic (on acetate) and autotrophic (on CO<sub>2</sub>) growth, offers a unique opportunity to distinguish the impact of iron nutrition on photosynthetic versus respiratory metabolism. During steady-state photoheterotrophic Fe-limited growth, where the cells are provided with light, CO<sub>2</sub>, and acetate, but lack extracellular iron, cells maintain respiration while decreasing the photosynthetic contribution to the energetics of the cell. In this condition, the photosynthetic apparatus can be either an essential life raft or a burden, as sink for large amounts of the limiting nutrient Fe. In this thesis I analyzed the transition from photoautotrophic (light and CO<sub>2</sub>) to photoheterotrophic cultures in the context of Fe-

## Abstract

---

nutrition by adding acetate as reduced carbon source to phototrophic cultures and assessing the developing changes to the metabolism time-dependently, in various levels of readouts. Based on the transcriptome analysis, all major cellular processes and pathways respond to the availability of acetate, but Fe-limited cells specifically sacrifice photosynthetic capacity towards respiratory activity in the first 12h after the additional carbon source becomes available, allowing to gain mechanistic insights of transitioning between different ways of life, dependent on the nutritional makeup of the environment.

Secondly, exposure to high extracellular iron amounts, its opportunities and the mechanisms of avoiding deleterious effects as a result from it, had been under-investigated before the beginning of my PhD thesis. I used physiological and photosynthetic parameters, elemental analysis, transcriptomics and a mutant depleted of functional acidic vacuoles, proposed to be involved in the storage for transition metals, to further the understanding of the processes involved in *C. reinhardtii* mitigating high concentrations of extracellular iron.

Lastly, while performing the research for this thesis, I noticed distinct phenotypic differences between commonly used laboratory wild-type strains of *Chlamydomonas*, specifically with respect to the effectiveness of assimilating sparse Fe. In a third section, I compared the variability in basal transcriptome levels, photosynthetic and respiratory activity and Fe homeostasis of *Chlamydomonas* strains CC-124, CC4532, CC-1690, CC-1009 and CC-1691.

Altogether, the results presented in this thesis illustrate how *C. reinhardtii* can be successfully used as a model organism to study a large variety of aspects of cell and molecular biology, including dynamic acclimations to changing environments.



## Table of Content

<b>1</b>	<b>Introduction</b>	<b>1</b>
1.1	The green alga <i>Chlamydomonas reinhardtii</i>	1
1.1.1	<i>Chlamydomonas reinhardtii</i> laboratory strains	2
1.1.2	<i>Chlamydomonas</i> as a model organism.	3
1.1.3	Photosynthesis	5
1.2	Metal Homeostasis	10
1.2.1	The Ionome	12
1.2.2	Iron Homeostasis	14
1.3	Iron Homeostasis in <i>C. reinhardtii</i>	16
1.3.1	Iron-deficient and Fe-limited <i>C. reinhardtii</i>	19
1.3.2	Excess Iron	21
1.3.3	The Impact of Carbon Source on Iron Homeostasis	22
1.4	Aim of This Thesis	23
<b>2</b>	<b>Results</b>	<b>25</b>
2.1	Elemental Profile of <i>Chlamydomonas reinhardtii</i>	25
2.2	Steady State Photoheterotrophic Iron Homeostasis in the Green Alga <i>Chlamydomonas reinhardtii</i> .	26
2.2.1	Extracellular Fe Availability Affects Fe, Cu and Mn Levels.	26
2.2.2	Iron Accumulation Does Not Impact Micronutrient Content.	29
2.2.3	Excess Intracellular Iron Offers a Growth Advantage.	31
2.2.4	Over-accumulated Iron Did Not Impact Photosynthetic Activity.	32
2.2.5	Identification of Candidate Genes Facilitating Iron Accumulation.	34
2.2.6	Effect of Pre-culture Iron Status on Iron Accumulation.	37
2.2.7	Influence of C-source on Fe-status-dependent Elemental Profiles.	41
2.2.8	Iron Accumulation in Excess Fe Conditions is Affected in <i>vtc1</i> .	44
2.2.9	Comparative Transcriptome Analysis of the <i>vtc1</i> Mutant.	46
2.2.10	Common transcriptomic response to excess iron.	49
2.2.11	<i>vtc1</i> is More Sensitive to Oxidative Stress Fe-excess Conditions.	51
2.3	Dynamic acclimations to Changes in Extracellular Iron.	52
2.3.1	Over-accumulated Iron Can Be Remobilized When Necessary.	52
2.3.2	Iron Re-supply to Fe-starved <i>vtc1</i> Cultures.	53
2.4	Acclimation to Heterotrophic Carbon During Iron Starvation.	57
2.4.2	Untargeted Analysis of Transcript Abundance Changes upon Acetate Addition.	63
2.4.3	Cellular Processes and Pathways Affected by Iron and Acetate.	72
2.4.4	Photosynthetic Parameters Respond to the Addition of Acetate.	79
2.4.5	Acetate- and Fe-specific changes to the ionome.	82
2.4.6	Variations in the Experimental Procedure.	88
2.5	Examining the Range of Phenotypical Deviation in Wild-type Strains of <i>Chlamydomonas reinhardtii</i> .	90
2.5.1	Chlorophyll content is a Prominent and Easily Visible Difference Observed Between <i>C. reinhardtii</i> Wild-type Strains.	90
2.5.2	Variability in the Transcriptome of Different Wildtype Strains	92
2.5.3	Examples of Differentially Expressed Genes Between the Strains	95
2.5.4	Phenotypic Variability in Different Wild-type Strains.	99

## Contents

---

<b>3</b>	<b>Discussion</b>	<b>109</b>
3.1	Elemental Profile of <i>Chlamydomonas reinhardtii</i>	109
3.2	Steady State Photoheterotrophic Iron Homeostasis in the Green Alga <i>Chlamydomonas reinhardtii</i> .	111
3.3	Dynamic acclimations to Changes in Extracellular Iron.	113
3.4	Acclimation to Heterotrophic Carbon During Iron Starvation.	115
3.5	Examining the Range of Phenotypical Deviation in Wild-type Strains of <i>Chlamydomonas reinhardtii</i> .	117
<b>4</b>	<b>Materials and Methods</b>	<b>123</b>
4.1	Materials	123
4.1.1	<i>Chlamydomonas reinhardtii</i> Strains	123
4.1.2	Chemicals	123
4.1.3	Software, Computer Programs and Other Resources	124
4.2	Methods	125
4.2.1	<i>Chlamydomonas reinhardtii</i> Growth Conditions	125
4.2.2	Cell Density, Generation Time and Cell Volume	130
4.2.3	Photosynthetic Parameters	130
4.2.4	Elemental Analysis	133
4.2.5	Transcriptome Analysis	136
4.2.6	Calculations and Statistics	138
<b>5</b>	<b>References</b>	<b>140</b>
<b>6</b>	<b>Appendix</b>	<b>158</b>
6.1	Supplemental Figures	158
6.2	Supplemental Tables	188

## Abbreviations and Nomenclature

### Nomenclature

Nuclear encoded genes: e.g. *FOX1*

Nuclear encoded protein: e.g. FOX1

Mutated nuclear encoded genes: e.g. *vtc1*

### Abbreviations

$b_6f$	Cytochrome $b_6f$ complex
CEF	Cyclic electron flow
Chl	Chlorophyll
DCMU	3-(3,4-dichlorophenyl)-1,1-dimethylurea
EDTA	Ethylenediaminetetraacetic acid
e.g.	Exempli gratia, for example
ER	Endoplasmatic reticulum
$F_0$	Initial fluorescence
FDR	False discovery rate
$F_{max}$	Maximal fluorescence
FPKM	Fragments per kilobase per million mapped
$F_v$	Variable fluorescence
$g$	$g$ -force
ICP-MS/MS	Inductively coupled plasma tandem mass spectrometry analysis
ISTD	Internal standard
K	Kelvin
LEF	Linear electron flow
LHC	Light harvesting complex (LHCI, LHCII)
$m/z$	Mass-to-charge ratio
mt	Mating type
NDIR	Non-dispersive infrared
NPQ	Non-photochemical quenching
PPFD	Photosynthetic photon flux density
PCY	Plastocyanin

## Abbreviations and Nomenclature

---

ppt	Parts per trillion
PQ, PQH <sub>2</sub>	Plastoquinone, plastoquinol
PS	Photosystem (PSI, PSII)
QA	Quinone
ROS	Reactive oxygen species
rpm	Revolutions per minute
SD	Standard deviation
SDS	Sodium dodecyl sulfate
TAP	Tris-acetate-phosphate medium
TP	Tris-phosphate medium
TOC-TN	Total organic carbon and total nitrogen analysis
w/v	Weight per volume
v/v	Volume per volume

# 1 Introduction

## 1.1 The green alga *Chlamydomonas reinhardtii*

Algae represent a very large and diverse phylogenetic group of photosynthetic eukaryotes (Blaby-Haas and Merchant, 2019) and are major primary producers contributing tremendously to globally fixed carbon (Field et al., 1998). The *Chlamydomonas* genus within the *Chlorophyte* (green algae) lineage contains almost 600 identified species (<http://www.algaebase.org>, Guiry and Guiry, 2019), but *C. reinhardtii* is by far the most studied one. This single-celled biflagellate can be found in damp soil and fresh water and appears typically spherical to subspherical with an average diameter of 7-10  $\mu\text{m}$ . It contains a wall of hydroxyproline-rich glycoproteins that lacks cellulose, multiple mitochondria, an endoplasmic reticulum (ER), the Golgi apparatus, contractile vacuoles, and a single, cup-shaped chloroplast (Figure 1) (Harris, 2001; Salomé and Merchant, 2019).

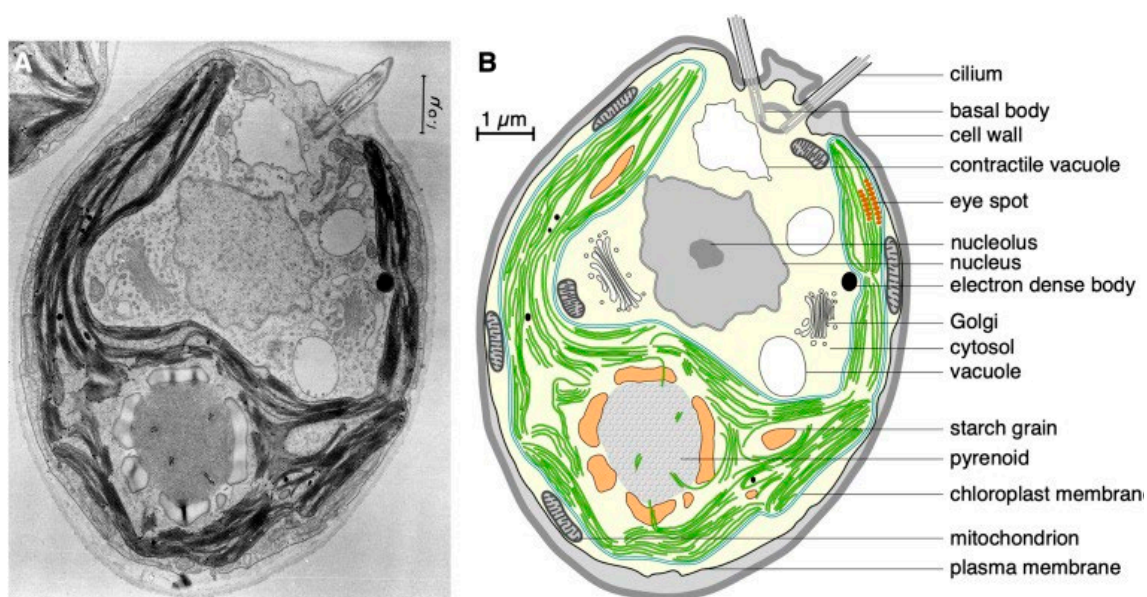


**Figure 1. Anatomy of *Chlamydomonas reinhardtii*.** **A:** Transmission electron micrograph (TEM) of a single cell and **B:** a cartoon based on the micrograph showing the single cup-shaped chloroplast, the pyrenoid, the central nucleus, mitochondria, the eyespot, vacuoles and anterior flagella anchored in a basal body. From Salomé and Merchant (2019), TEM image originally published by Ohad et al. (1967) and made available through the Cell Image Library (<http://www.cellimagelibrary.org>).

The chloroplast contains a structure called pyrenoid, where Ribulose-1,5-biphosphate carboxylase oxygenase (Rubisco) accumulates and surrounding starch sheets create a barrier to enrich  $\text{CO}_2$ . Also, within the chloroplast is a region composed of several layers

of pigment granules, the eyespot, that sense light and triggers phototaxis. *C. reinhardtii* vegetative cells are haploid, with 17 chromosomes and 17 741 gene models (Harris, 2001; Harris, 2009). *Chlamydomonas* cells can propagate either sexually by mating or asexually by mitotic division into clonal daughter cells. In optimal laboratory setting, cells divide asexually, but upon certain stressors, e.g. nitrogen starvation, cells differentiate into haploid gametes. The gametes can divide into two mating types,  $mt^+$  and  $mt^-$ , which fuse through the help of their flagella and form a non-flagellate diploid zygote. After meiosis, the zygote releases four flagellated vegetative daughter cells (Harris, 2001; Ferris et al., 2002).

### 1.1.1 *Chlamydomonas reinhardtii* laboratory strains

Even though many species exist, most research on *Chlamydomonas* uses a limited number of related standard laboratory strains of *C. reinhardtii*. The first laboratory strains were collected in Massachusetts (USA) by Gilbert M. Smith (Smith, 1946) and since then it has been widely used by the community as a model organism to study numerous aspects of cell and molecular biology, contributing to an increasing number of common laboratory strains. In October 2019, the *Chlamydomonas* Collection contained ~300 individual strains for purchase and recorded over 5000 unique CC- numbers (<http://www.chlamycollection.org>). Smith studied *Chlamydomonas* isolates with an interest in sexual recombination (Smith and Regnery, 1950), and in subsequent years, he began supplying strains to interested researchers at other institutions (Sager, 1955; Ebersold, 1956). Despite their recent common ancestry, there are many readily observable phenotypic differences between the common laboratory strains. For example, strains in the Ebersold-Levine lineage are unable to utilize nitrate as a nitrogen source, while those in the Sager lineage can (Harris, 2009). Strains differ in their ability to utilize micronutrients, in their responses to light, in the production of a cell wall and in triacylglycerol accumulation in response to stress (Pazour et al., 1995; Merchant et al., 2006; Siaux et al., 2011; Gallaher et al., 2015). Some of these phenotypes have been traced to specific mutations, such as the *nit1* and *nit2* mutations that prevent nitrate utilization (Fernández et al., 1989). CC-1690, the  $mt^+$  strain in the Sager lineage, remains green when grown in the dark, whereas CC-1691, the  $mt^-$  Sager strain, turns yellow due to a mutation at the *y1* locus (Sager, 1955). Many other phenotypes are due to the interplay of multiple genetic loci.

## 1. Introduction

Genome resequencing revealed genetic diversity of 39 common laboratory strains, many of which are widely and frequently used in the *Chlamydomonas* research community (Gallaher et al., 2015). Within this group of “wildtype” strains, the sequence divergence was not evenly distributed but consisted of two discrete blocks of haplotypes. About 25% of the genome was found to have either of the two haplotypes with 2% sequence variance between them. The sequence of the reference strain CC-503 was set as haplotype 1 (all blue, middle) and the alternate regions as haplotype 2 (yellow) (Figure 2).

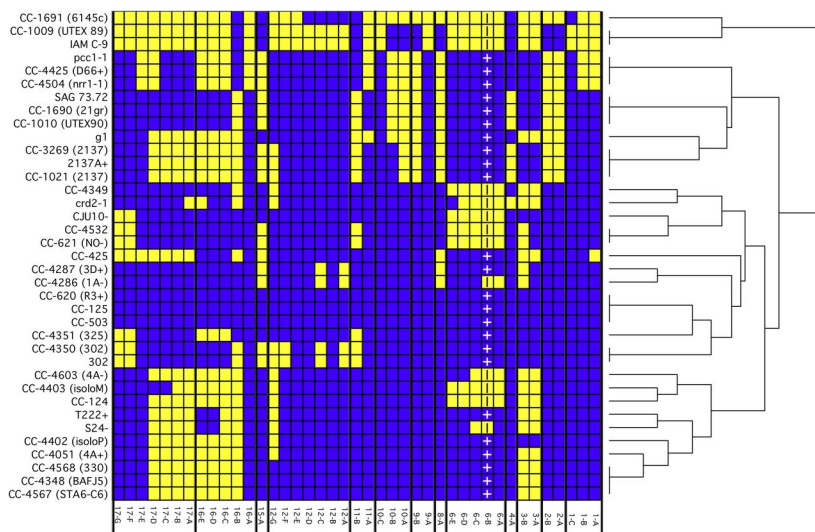


**Figure 2. Distribution of two haplotypes in laboratory strains.** Genomes of common laboratory strains contain large blocks of either of two haplotype blocks with comparatively low sequence divergence. From Gallaher et al. (2015).

The effect of haplotype 2 variants on gene models was generally small, with 0.2% of all variants amounting to nonsense changes (e.g. frame shift, premature stop codons). The majority resulted in synonymous codons or small insertions and deletions preserving the reading frames (>50%) and 40% caused nonsynonymous codon changes. Of those, 627 structural variants (change to amino acid from a different class), were predicted to have a high impact on one or more genes within the haplotype region (Gallaher et al., 2015).

### 1.1.2 *Chlamydomonas* as a model organism.

In the past decades, *C. reinhardtii* has been used as a model organism for studying fundamental processes in cell and molecular biology including photosynthesis (Levine, 1960; Grossman, 2000; Dent et al., 2001; Eberhard et al., 2008), sexual reproduction

## 1. Introduction

---

(Quarmby, 1994; Lee et al., 2008; Nishimura, 2010), flagella biology (Silflow and Lefebvre, 2001; Cole, 2003; Snell et al., 2004), biogenesis of organelles, micronutrient deficiency (Merchant et al., 2006), and algal biofuel production (Moellering and Benning, 2010; Radakovits et al., 2010). A number of traits make *Chlamydomonas* a particularly useful reference organism. The single-celled organism allows for uniform samples without distinct tissues. A simple life cycle with a rapid asexual (clonal) doubling time of as low as 8h in the vegetative state and growth in chemically defined growth medium, where e.g. metal deficiency can be established easier than in plants (soil). *Chlamydomonas* is very amenable to quick changes in growth conditions and is capable to grow photoautotrophic, photoheterotrophic and heterotrophic. This ability to grow under different light regimes is dependent on nutrient availability. In a culture medium lacking organic carbon and chemical energy sources, *C. reinhardtii* cells grow photoautotrophic in the light, but when an organic carbon source in the form of acetate is supplied, cells grow photoheterotrophic or heterotrophic in the dark (Harris, 2009). This flexibility of cultivation is very useful in the laboratory and enables different research approaches particularly suitable for studying photosynthetic mutants (Spreitzer and Mets, 1981; Rochaix, 1995) and conditions with a major impact on the photosynthetic capacity (Grossman et al., 2010). The ability to synchronize cultures with light/dark cycles allows studying the cell cycle. The nuclear genome exists in the haploid state during vegetative growth; thus, the effect of mutations can be observed directly (Harris, 2009). All three genomes (nuclear, mitochondrial, chloroplastic) have been sequenced and may be genetically manipulated (Maul et al., 2002; Popescu and Lee, 2007; Merchant et al., 2007; Gallaher et al., 2018). Classical genetic crosses are easy to perform (Jiang and Stern, 2009), a rigorous genetic system exists, making it amenable to metabolic manipulation through techniques such as gene knock-down or overexpression (Grossman et al., 2007; Merchant et al., 2007; Grossman et al., 2010; Wijffels and Barbosa, 2010) as well as molecular techniques, including transcriptomics, proteomics and systems level analyses. Over the years, a large collection of strains and mutants has been generated by the community that can be easily acquired through central stock collections in addition a large systematic mutant library has been generated (Li et al., 2016). It's unique evolutionary history, retaining features from the animal ancestor, that were later lost in land plants, for example flagella, which can be used as a model system for human ciliary disease (Silflow et al., 2001). And at the same time sharing many detailed photosynthetic features with higher plants.



### 1.1.3 Photosynthesis

Photosynthesis, the conversion of light energy into chemical energy and a single carbon (CO<sub>2</sub>) into complex carbohydrates, sustains virtually all life on Earth, providing the oxygen we breathe and the food we eat. It is believed that the Earth was formed 4.6 billion years ago, and life began around 3.4 billion years ago with non-oxygenic photosynthesis by bacteria and *Archea* (Lowe, 1980; Schopf, 1993; Han and Runnegar, 1992, Olson et al., 2006). During evolution, chlorophyll evolved as the light-absorbing pigment, the solar energy trapped by it was used to generate ATP, and reduced NAD(P)H became a stable end-product. Another consequence of oxygenic photosynthesis is the release of oxygen that started to accumulate in the atmosphere about 2.4 billion years ago by the action of cyanobacteria, triggering dramatic changes in the biosphere (Fischer, 2008; Czaja, 2010; Kasting, 2012; Planavsky et al., 2014, Fischer et al., 2016). Organisms were forced to cope with the presence of this strong oxidant, some presumably got extinct when they failed to adapt to this new environment, while many others evolved complex mechanism to cope with and utilize the oxygen. In their current evolutionary state modern plant and photosynthetic algal cells contain a specialized organelle to drive photosynthesis, the chloroplast. The evolution of plants cells began after a eukaryotic cell engulfed a photosynthesizing bacterium, referred to as the cyanobacterial ancestor, which remained and became a permanent part of the eukaryotic cell (Rockwell et al., 2014; Zimorski et al., 2014). After this endosymbiotic event, photosynthetic eukaryotes divided into three lineages: *Rhodophyta*, *Glaucophyta* and *Viridaplantae*. Around one billion years ago, the lineage of *Viridaplantae* further divided into the Chlorophyta, which include *Spermatophyta* (vascular plants) and *C. reinhardtii* (Reyes-Prieto et al., 2007; Leliaert et al., 2012). Surprisingly, even after 1 billion years of evolution, the photosynthetic machineries from vascular plants and cyanobacteria are still very similar (Meyer, 1994). The main modifications observed may be related to the development of a light harvesting complex (LHC) by modern plant cells (Grossman et al., 1995). Due to that, some polypeptides have been lost to make space for LHC-docking to the photosystems and others were gained to assist in this process. Additional pigments have been incorporated to extend the range of light wavelengths that can be harvested for photosynthetic conversion or to quench excess excitation energy (Moore et al., 1989).

## 1. Introduction

---

The process of oxygenic photosynthesis can be divided into two major parts, the light-dependent and light-independent reactions. The light reactions occur in thylakoid membranes of photosynthetic organisms. The basic principle involves the trapping of photons by chlorophyll to raise electrons to a higher energetic level. The electrons would naturally return to their basic state within  $10^{-9}$  s, releasing energy as heat and photons as fluorescence with a longer wavelength (Bowsher et al., 2008). Photosynthetic organisms move those high-energy electrons to an acceptor molecule (with a subsequently higher redox potential) before they return to their basic level. By that, the acceptor molecule is reduced, and chlorophyll is left in the oxidized state. To avoid an electron backflow from the acceptor back to chlorophyll, the acceptor molecule has to rapidly pass the electron to another acceptor. At the same time, oxidized chlorophyll is reduced with electrons gained from the oxidation of water in photosystem II (PSII) or by the oxidation of plastocyanin in photosystem I (PSI) to become available again to be excited by another photon. Cyanobacteria, algae and plants have these two photon-trapping, chlorophyll-containing photosystems operating in series. Their combined actions, together with the other photosynthetic complexes, the cytochrome  $b_6/f$  (Cyt  $b_6/f$ ) complex and the ATP synthase (ATPase), result in the reduction of the final acceptor NAD(P)H and phosphorylation of ADP to ATP (Donald et al., 1996). Both products, NAD(P)H and ATP fuel the light-independent reactions, which occur in the stroma part of chloroplasts. Alternatively, cyclic electron flow around PSI can produce ATP without the generation of NAD(P)H, which is used to adjust the ATP-to-NAD(P)H ratio to the requirements of the cell (Arnon, 1959). The light-independent reactions comprise of three parts, also called Calvin-Benson cycle, the carbon fixation, reduction reactions, and ribulose-1,5-bisphosphate (RuBP) regeneration (Calvin and Benson, 1948). As a result, carbon dioxide is reduced to produce the carbohydrate glyceraldehyde-3-phosphate, which can be further used to generate sugars and fatty acids.

There are two complexes in the thylakoid membranes, PSII and PSI, which can trap photons by chlorophyll to induce charge separate across the thylakoid membrane (Figure 3) (Johnson, 2016). Each complex is composed of a light-harvesting antenna, which absorbs radiant energy, and reaction centers, which contain a chlorophyll molecule that can convert the light energy captured from the antenna to chemical energy (Vasil'ev and Bruce, 2004; Koziol et al., 2007). The chlorophyll molecule in PSII reaction centers is

## 1. Introduction

most reactive to photons with a wavelength of 680 nm and 700 nm in PSII reaction centers. Therefore, PSII and PSI reaction centers are often referred to as P680 and P700, respectively. The linear electron flow from PSII to PSI occurs according to the Z-scheme, which refers to the redox potentials of carriers within the transport chain (Hill and Bendall, 1960). Accordingly, light-harvesting antenna of PSII capture photons and transfer the excitation energy to a chlorophyll molecule in the core of the PSII reaction center, P680 (Dekker and van Grondelle, 2000).

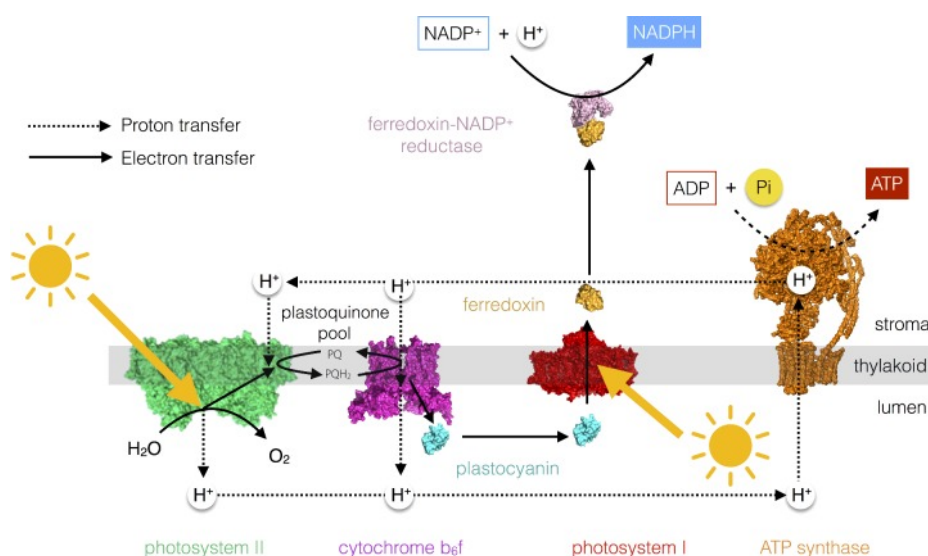


**Figure 3. Photosynthetic electron transfer chain.** The linear electron and proton transfer chain from water to NAD(P)H through PSII, PQ, PCY, PSI and Fd. For details see text. (Reviewed in Johnson, 2016).

After excitation, P680 becomes photo-oxidized and donated an electron to the first acceptor molecule pheophytin, and further transferred to plastoquinone (PQ) (Renger and Govindjee, 1985). The electron gap in the chlorophyll in PSII reaction center (P680<sup>+</sup>) leads to the oxidation of water molecules in the luminal oxygen-evolving complex (OEC). Molecular oxygen and protons are generated and P680 returns to the neutral state (Radmer and Kok, 1975). Plastoquinone takes a second electron from the next P680 excitation from the stromal space and is released as plastoquinol (PQH<sub>2</sub>) from the PSII binding site. PQH<sub>2</sub> diffuses to Cyt b<sub>6</sub>f and transfers the two electrons to plastocyanin (PCY), releasing two protons from the stroma to the lumen and in the process generating an electrochemical gradient across the thylakoid membrane. Consequently, PQ is recycled to PSII and PCY diffuses through the lumen to PSI (Kurisu et al., 2003; Nelson and Ben-Shem, 2004). In PSI, light absorbed by the antenna is transferred to the reaction center, P700. Upon

excitation, it releases an electron that eventually reduces ferredoxin (Fd). Electrons of two reduced ferredoxins are used by the Fd-NADP<sup>+</sup> reductase (FNR) to convert NAD(P)<sup>+</sup> into NAD(P)H. The electron gap in the chlorophyll in the PSI reaction center (P700<sup>+</sup>) is recycled by the electrons from PCY (Jordan et al., 2001). The accumulation of protons in the thylakoid lumen generates a proton gradient that drives the phosphorylation of ADP to ATP through the ATPase complex (Mitchell, 1961).

Alternative electron transfer routes are connected to the photosynthetic chain and act to modulate the ATP-to-NAD(P)H ratio and to avoid damage to the photosystems due to an over-reduced state. Those alternative pathways include cyclic electron flow around PSI, chlororespiration and the water-water cycle (Mehler, 1951; Peltier and Cournac, 2002; Rumeau et al., 2007). During cyclic electron flow (CEF), electrons can cycle between reduced Fd/NAD(P)H via PQ, Cyt *b<sub>6</sub>f*, PCY and PSI, to increase the pH gradient that in allows ATP synthesis (Shikanai, 2007, Jans et al., 2008). The biological meaning of CEF has been proposed to be related to the generation of an equilibrium between NAD(P)H and ATP in the thylakoid stroma and to the protection of the photosynthetic apparatus from photodamage (Munekage et al., 2004; Shikanai et al., 2007; Johnson et al., 2014). Chlororespiration is an alternative electron sink pathway in which electrons coming from NAD(P)H are redirected to the PQ pool (Peltier and Cournac, 2002), probably in a similar way as during CEF via NDH (Desplats et al., 2009). When the NAD(P)H-to-ATP ratio is high, oxygen is reduced by electrons coming from PSI or Fd to generate superoxide (O<sub>2</sub><sup>-</sup>), which is then enzymatically converted to H<sub>2</sub>O<sub>2</sub> by Fe-superoxide dismutase (SOD) (Asada, 2000; Kitayama et al., 2002), also called the water-water cycle.

Probing the biophysics of photosynthesis via chlorophyll fluorescence kinetic measurements is a powerful tool because the time course of changes in chlorophyll fluorescence quantum yield reveals many insights into subtle changes of the photosynthetic apparatus (Maxwell and Johnson, 2000; Baker, 2008; Stirbet et al., 2018). Many cellular stresses, including most types of metal-induced stress directly and indirectly affect photosynthetic performance. Chlorophyll *a* fluorescence is a highly sensitive, non-destructive, and reliable tool for measuring photosynthetic efficiency, particularly of PSII (Cao and Govindjee, 1990). When dark-adapted photosynthetic samples are exposed to saturating continuous light, a fast (up to 1 s) chlorophyll *a* fluorescence induction can be

## 1. Introduction

---

observed, also known as the Kautsky effect (Kautsky and Hirsch, 1931) or OJIP fluorescence transients. The chlorophyll fluorescence intensity rises from a minimum level (the O level), in less than 1 s, to a maximum level (the P-level) via two intermediate steps labeled J and I. This is followed by a decline to a lower semi-steady state level, the S level, which is reached in about one minute. The rate of PSII photochemical conversion is limited by the electron acceptor side (the side that is reduced by PSII). Further, the fluorescence yield was suggested to be controlled by plastoquinone in its oxidized state. In this theory, the fast fluorescence rise reflects the concentration of reduced quinone (QA), as affected by the kinetics of several different redox reactions in the photosynthetic electron transport chain. Thus, the OJIP transient has the potential to be used for the characterization of the photochemical quantum yield of PSII photochemistry, and the electron transport activity. In photosynthetic samples, which have been kept in darkness, the electron acceptor side of PSII is mostly in the oxidized state (i.e., the PSII reaction centers are open, and the fluorescence intensity is minimal,  $F_0$ , represented on the fluorescence transient, curve as O, for ‘Origin’, as mentioned earlier). The O to J rise, known as the photochemical phase, is very fast (approx. 2 ms), and depends strongly on the intensity of the exciting light, whereas J–I, and I–P parts of the fluorescence curve, known as thermal phases (temperature sensitive), are much slower (especially the I–P portion). In less than 1 s, chlorophyll *a* fluorescence reaches the peak P, when the exciting light intensity is high and saturating. At the  $F_{\max}$  level, all QA molecules are completely reduced (all active PSII reaction centers are closed), due to the reduction of the entire linear electron transport chain because of a “traffic jam” of electrons on the acceptor side of PSI (Papageorgiou et al., 2004; Stirbet and Govindjee, 2011).

Light and nutrients are important environmental factors that affect photosynthesis in algae and plants. Photosynthetic light harvesting is regulated by changes in both light quantity and quality. In response to high light intensities that exceed a photosynthetic organism's capacity for CO<sub>2</sub> fixation, nonphotochemical quenching (NPQ) mechanisms are induced that dissipate excess absorbed light energy harmlessly as heat (Erickson et al., 2015). The photosynthetic process is generally limited by its substrates, light and CO<sub>2</sub>, but also by nutrients such as N, P, S, and transition metals such as iron and copper. Electron transfer reactions commonly involve transition metal complexes. These nutrients are required as heteroatoms in macromolecular cellular constituents or serve as catalytic centers in redox

transformations (Pilon et al., 2009; Nouet et al., 2011; Yruela, 2013). Accordingly, the biogenesis and maintenance of the photosynthetic apparatus and the metabolic networks are regulated in response to fluctuations in resources (Grossman et al., 1993). In addition to iron, Cu is a required cofactor in photosynthesis. A mutant identified in a screen to dissect copper deficiency, *crd1* (Moseley et al., 2000), for example fails to accumulate PSI, LHCI and to a lesser extent LHCII under copper-deficient conditions. The gene product of *CRDI* was characterized as a 47 kDa protein with a di-iron binding site, giving another example of the intricate interplay of transition metals to perform complex biological functions (Moseley et al., 2000).

### 1.2 Metal Homeostasis

Metal homeostasis is the study of how cells regulate their internal environment to maintain an optimal level of essential metals, despite large extracellular fluctuations. It serves to ensure that the metal ions are accessible and the apoproteins only interact with the right metal for functional activity. Metal availability directly regulates genes involved in metal ion resistance. The metal assimilation pathways are induced at low nutrient concentrations and turned off at high concentrations. Metal ion permeases and transporters, metallochaperones that directly insert metal ions into their target enzymes and many other proteins associated with metal ions have been characterized for many organisms for decades. Transition metals, especially iron, copper, zinc, manganese, cobalt and nickel have unique chemical and physical properties that make them attractive molecules for use in biological systems. Nature has used these unique chemical properties of each metal ion, such as ligand preferences, coordination geometries and redox potential, generating a huge repertoire of catalytic abilities that are not readily provided by functional groups of amino acids (Andreini et al., 2008). This repertoire includes allowing harsh chemical reactions such as the reduction of dinitrogen to ammonium and the oxidation of water under gentle biological conditions. These catalytic activities are dependent on specific metal cofactors in unique active sites. With few exceptions, proteins have evolved to exploit the properties of a specific metal therefore it is critical that the right metal cofactor occupies its dedicated active site in the presence and often excess of competing metals.

The divalent ions Mn, Fe, Co, Ni, Cu, Zn bind functional groups in proteins according to thermodynamic preferences described by the Irving-Williams series (Irving et al., 1953), and based on that many metalloproteins bind  $\text{Cu}^{2+}$  with higher affinity than they bind  $\text{Zn}^{2+}$ ,

## 1. Introduction

---

followed by  $\text{Fe}^{2+}$  and then  $\text{Mn}^{2+}$  (Williams, 2001). Without mechanisms for selectivity in vivo, metal binding would be driven by the concentration of the metal ion and the Irving-Williams preferences toward the available binding sites (Dudev and Lim, 2008; Waldron et al., 2009). The best-understood mechanism for ensuring selectivity of metal-protein association include the function of metallochaperones (such as Cu chaperones) which effect transfer of the metal to its final target via specific protein-protein interaction and ligand exchange. Another is compartmentalized assembly (such as MncA) in which holoprotein formation is restricted to a compartment with the appropriate high concentration of the desired metal ion and low concentration of the undesired but thermodynamically preferred metal ions (Tottey et al., 2008; Waldron et al., 2009; Boal and Rosenzweig, 2009). Kinetic barriers generally preclude metal exchange or dissociation once the metalloprotein is in its final subcellular location.

Many of the same properties that allow the metals to provide essential biochemical activities and structural motifs to a multitude of proteins including enzymes and other cellular constituents also lead to a potential for cytotoxicity. Unchelated redox-active metal ions, such as iron and copper, can generate reactive oxygen species (ROS) via Fenton chemistry, leading to oxidative stress (Galaris et al., 2019). Even though zinc is less harmful by comparison, zinc toxicity symptoms have been observed, which could be due to mis-incorporation of zinc into proteins or generation of protein aggregates (Maret and Li, 2009). Metal storage proteins and small molecules inside the cell can buffer the concentration of free metal ions, but only to a certain degree, the influx and efflux of each metal must be tightly coordinated to ensure the right metal at the correct concentration is present in each compartment. Disruption of the homeostasis can lead to a variety of impacts and implications, including in human health and diseases, ranging from hemochromatosis and anemia to neurodegenerative disorders including Alzheimer's and Parkinson's disease. In eukaryotes, an additional mechanism to maintain metal homeostasis is the storage of metals in intracellular organelles. Plant and yeast vacuoles are well-established organelles to sequester and mobilize metals (Martinoia et al., 2007, 2012). More recently, other compartments, like acidocalcisomes and lysosome-related organelles, emerged as important players of metal homeostasis (Docampo et al., 2010; Blaby-Haas and Merchant 2014; Hong-Hermesdorf et al., 2014; Tsednee et al., 2019).

Although attempts are made to study the individual impact of each transition metal or element, perturbations in one inevitably are complicated by reflexive perturbations in other nutrients (Jacobsen et al., 2011; Latorre et al., 2015). The dominant iron-uptake system in *Chlamydomonas* (based on mRNA and proteins levels) comprises of a multicopper ferroxidase and Cu-limitation inevitably affects the successful maturation of the oxidase (La Fontaine et al., 2002). Another example from *Chlamydomonas* is the accumulation of intracellular Cu during Zn-deficiency (Malasarn et al., 2013; Hong-Hermesdorf et al., 2014).

### 1.2.1 The Ionome

The ionome is defined as the mineral nutrient and trace element composition of an organism and represents the inorganic component of cellular and organismal systems. Ionomics involves the quantitative and simultaneous measurement of the elemental composition of organisms and changes in this composition in response to physiological stimuli, developmental state, and genetic modifications. Ionomics studies have now been performed in many plant species, including rice, maize and many others. The concept of the ionome has also been applied to *Saccharomyces cerevisiae* with an ionomic analysis of knockout and overexpression alleles of all identified genes in the yeast genome (Eide et al., 2005; Yu et al., 2012). Recently, ionomic studies in humans (Sun et al., 2012; Malinouski et al., 2014) and other animals (Yoshida et al., 2014) have been reported, with a large interest in cancer and neuro-degenerative research. Once characterized, the ionome can be used as a tool to assess factors affecting specific parts of the elemental profile.

Inductively coupled plasma-mass spectrometry (ICP-MS) is a hard ionization mass spectrometry technique generating ions in a high temperature argon plasma. The low detection limits (ppt range) for most elements, combined with multielement capabilities, a large dynamic range over several orders of magnitude and the possibility of online coupling to different separation techniques (e.g. HPLC) has brought ICP-MS to the method of choice for studying the ionome in different biological systems (Salt et al., 2008). Acid-digested aqueous samples are pumped into a nebulizer where an incoming argon flow provides the pneumatic force to dispersing the liquid sample into a fine aerosol. The liquid droplets then enter the spray chamber where they become subject to either centrifugal or gravitational



## 1. Introduction

---

forces in order to discard the largest droplets. The whole sample introduction is a critical step as only a small fraction of the sample will be brought into the argon plasma (Thomas, 2013). Temperatures between 6000 and 10 000 K dry, vaporize, atomize and ionize the sample. Due to the high temperatures and the total decomposition of the sample, molecular information is lost during the process but enables the total quantification of elements regardless of their speciation. Two cones (sample and skimmer cone) represent the interface region where the transition from atmospheric pressure of the ICP to the MS high vacuum takes place. In order to remove neutral species, photons and negatively charged ions, the particles emerging from the plasma are subjected to several electrostatic lenses. The ions of interest are then focused into the MS where they are separated based on their mass-to-charge ( $m/z$ ) ratios. Three different types of mass analyzers (quadrupole, sector field and TOF) have been employed in ICP-MS, whereas quadrupole is the most common one. By rapidly switching RF/DC voltages on the quadrupole rods (allowing a stable central trajectory only for a certain  $m/z$  ratio through the mass analyzer), a ‘quasi-simultaneous’ determination of several analytes is possible (Thomas, 2013). After passing the mass analyzer, the ions are collected by an electron multiplier and the signal intensities are integrated with the provided software. When dealing with a specific chemical element, one major challenge in ICP-MS analysis is represented by the presence of interferences. Ions possessing the same  $m/z$  ratio as the analyte are called interferences, leading to an elevated background and false positives. Interferences can be polyatomic ions (e.g.  $^{40}\text{Ar}^{16}\text{O}^+$  interferes with  $^{56}\text{Fe}^+$ ), doubly charged ions (e.g.  $^{140}\text{Ce}^{2+}$  interferes with  $^{70}\text{Zn}^+$ ) or elemental isobaric interferences (e.g.  $^{87}\text{Rb}^+$  on  $^{87}\text{Sr}^+$ ). Polyatomic interferences and doubly charged species are caused by components of the argon plasma, atmospheric gases or matrix components whereas elemental interferences originate from the sample. In order to avoid an analytical bias caused by interferences, the measured isotope must be carefully selected and/or mathematical corrections have to be applied, in some cases a low abundant isotope can give more accurate results due to the lack of interferences at a particular mass (Thomas, 2013). Most commercially available ICP-MS devices are quadruple-featured instruments and in many cases, they are additionally equipped with a collision/reaction cell (usually an octopole) (Figure 4).

In collision mode, an inert gas (e.g. He) can reduce the kinetic energy of the interfering species, thereby permitting only the analyte’s detection. In reaction mode, a reactive gas (e.g.  $\text{O}_2$ ,  $\text{H}_2$ ) is introduced into the cell so that upon reaction the mass of either the analyte

## 1. Introduction

or the interfering species is shifted to another mass. In case of sulfur as analyte, the most abundant isotope  $^{32}\text{S}^+$  (high abundance interference of  $^{16}\text{O}^{2+}$ ) reacts with  $\text{O}_2$  in the reaction cell forming the corresponding oxide ( $^{32}\text{S}^{16}\text{O}^+$ ), which is detected at  $m/z$  48 instead of 32, without the interference. For  $^{56}\text{Fe}^+$ , the interfering species ( $^{40}\text{Ar}^{16}\text{O}^+$ ) reacts e.g. with  $\text{H}_2$ , whereas the analyte remains unaffected (Bandura et al., 2002).

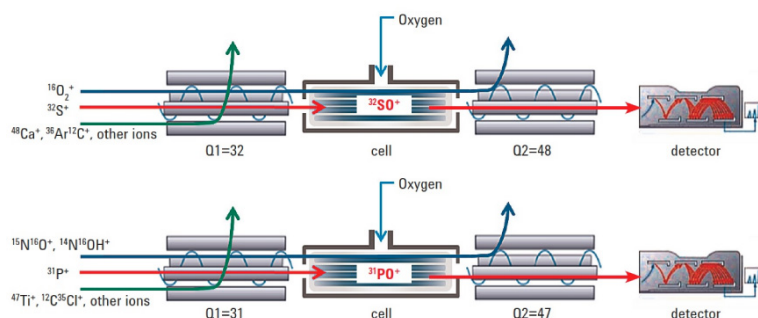


**Figure 4. ICP-QQQ MS/MS reaction/collision cell.** Interference removal in the reaction cell with  $\text{O}_2$  as reaction gas for the analysis of S (top) and (P) in mass-shift mode. (Figure from Agilent)

In recent years, a tandem ICP-MS instrument (e.g. 8800 ICP-QQQ, Agilent) was introduced to the market as a promise of better control interference removal. The Triple Quadrupole ICP-MS is equipped with an octopole that can be operated as collision or reaction cell, situated between two quadrupole mass filters enabling two separate mass selection steps (Figure 4). The first quadrupole transfers only ions with a defined mass-to-charge ratio into the collision/reaction cell. Upon reaction or collision, the second quadrupole selects the ions of interest to be detected. This approach improves challenging spectral overlaps that were present when diverse species enter the reaction or collision cell. Especially the analyses of S, P and Fe from complex matrixes have largely benefited from this approach (Balcaen et al., 2015).

### 1.2.2 Iron Homeostasis

Iron is one of the most abundant elements on Earth and the most abundant transition metal in biology, making it a key nutrient that limits global primary productivity, especially in the oceans (Martin et al., 1990). Fe is required for the synthesis of the building blocks of photosynthesis and many other pathways. Both mitochondria and chloroplasts house

## 1. Introduction

numerous iron-dependent proteins whose functions are essential in the electron transfer pathways of the bioenergetic membranes in those compartments. Even though chloroplast and mitochondria are the major sinks for cellular iron, it is also a significant component of many proteins involved in other essential processes such as reactive oxygen detoxification, fatty acid metabolism and amino acid biosynthesis.

The photosynthetic electron transport pathway likely evolved in the Proterozoic ocean, which was rich in  $\text{Fe}^{2+}$  (Anbar et al., 2008). The subsequent rise in oxygen has drastically decreased the amount of bioavailable  $\text{Fe}^{2+}$  (Figure 5). Although it is relatively abundant in the Earth's crust, in aerobic environments the bioavailability of iron is limited due to poorly soluble  $\text{Fe}^{3+}$ -complexes, chronically limiting terrestrial and aquatic photosynthesis (Guerinot and Yi, 1994; Staiger, 2002).

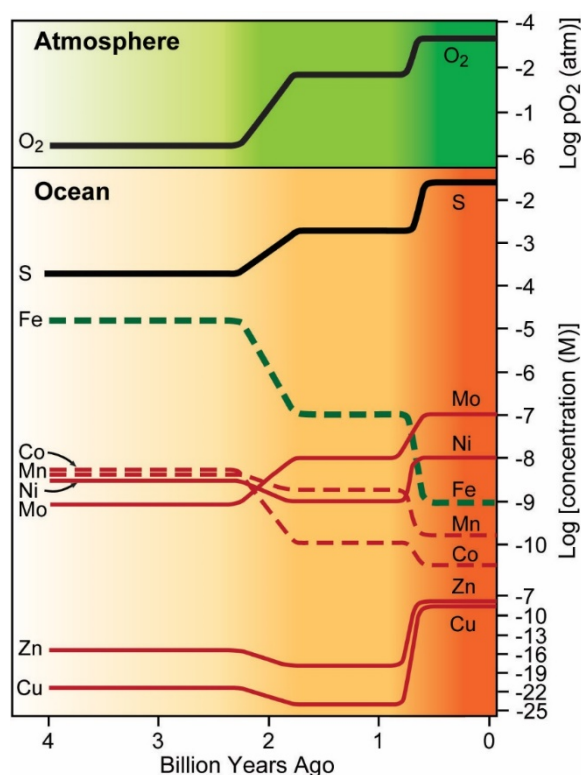


**Figure 5. Changes in element abundance in the ocean through time.** Black line on top shown the increase in dissolved oxygen, the green dashed line the decrease in iron. Modified from Anbar (2008).

Estimated 30% of arable land and 40% of ocean waters are affected by iron malnutrition (Chen and Barak, 1982; Moore et al., 2002), a large quantity of the human population is

thought to exhibit iron deficiency (the actual reported numbers vary based on the region and the source of data). This suggests that poor iron bioavailability causes consequential impacts on food chains, global health, carbon sequestration and oxygen production and limits global primary productivity. Also making it necessary for organisms to adapt to iron-poor conditions to maintain sufficient cellular iron levels, even under constant changing environmental nutrient supply. Accordingly, iron acquisition evolved to include transport systems involving chelation and redox chemistry followed by intracellular usage of iron, for example for the biosynthesis of heme or inorganic Fe/S clusters (Theil, 2004; Lill and Mühlhoff, 2008; Philpott and Prochenko, 2008; Kosman, 2010a), and eukaryotic cells have to deal with the additional obstacle of subcellular compartmentation (Jeong and Guerinot, 2009). The investigation and discovery of these regulatory mechanisms is important as photosynthesis in nature occurs in sub-optimal environments of nutrient deficiency and constantly changing supply of carbon sources.

Roughly 80% of the cellular iron found in green leaves is located in the chloroplasts (Jacobson 1945; Noack and Jiebich, 1941). The contribution of iron-dependent proteins in other cellular compartments to the cellular iron quota may be relatively small, but they are also essential for fitness or survival. These enzymes participate in DNA synthesis and repair, metabolite synthesis, molybdopterin synthesis, fatty acid metabolism and reactive oxygen species detoxification, just to name a few. Therefore, a delicate balance exists to ensure an appropriate amount of iron or iron-bound cofactor such as heme is present throughout the cell for the maturation of each iron-dependent protein. Responses to iron-deficiency in plants have focused on iron-uptake pathways, leading to the discovery of transport, distribution and storage mechanisms, while the details concerning intracellular iron homeostasis are just now being dissected.

### 1.3 Iron Homeostasis in *C. reinhardtii*

Like land plants, algae have two especially iron-rich organelles, the chloroplast and the mitochondrion. Both organelles house numerous iron-dependent proteins whose functions are essential in the electron transfer pathways of the bioenergetic membranes in those compartments. Assuming a 1:1 stoichiometry of the electron transfer complexes (dimers for PSII and the Cyt *b<sub>6</sub>f* complex and a monomer for PSI), linear electron flow from PSII to ferredoxin is estimated to require 30 iron ions (Blaby-Haas and Merchant, 2013). Again assuming 1:1 stoichiometry (monomers for complexes I, II, and IV, and a dimer for

## 1. Introduction

---

complex III), mitochondrial electron transport requires 50 iron atoms, over half contained within complex I (Xu et al., 2013). Although electron transfer in respiration appears to require more iron than photosynthesis, due to the higher abundance, the chloroplast is the dominant sink for iron in the oxygen-evolving plant cell, where this cofactor is concentrated in the abundant iron-dependent proteins of the thylakoid membrane. Microalgae present a unique system for investigating how photosynthetic organisms respond to and cope with suboptimal iron nutrition and *C. reinhardtii* specifically, has been used as a eukaryotic model for studying metal homeostasis in the context of chloroplast functions. Routinely grown in chemically defined liquid cultures, algal cell population and exposure to nutrients can be more homogenous, compared to plants, and in which individual metal concentrations can be easily altered (Kropat et al., 2011).

Iron-deficient *Chlamydomonas* cells assimilate iron from the environment primarily by using a high-affinity uptake machinery that is similar to the iron-uptake in non-graminaceous plants (strategy I, reduction strategy). This high-affinity reduction iron-uptake system in *C. reinhardtii* comprises a ferric reductase (FRE1) and a multicopper ferroxidase (FOX1) that provides the iron in the right oxidation state to be imported into the cells by the FTR1 permease (Figure 6) (La Fontaine et al. 2002; Kosman 2003; Philpott 2006; Allen et al. 2007). Two additional ZIP family members (*IRT1* and *IRT2*) and a putative transporter from the NRAMP family (*NRAMP4*) that showed an increased expression specifically in iron-deficient cells (Allen et al. 2007; Hanikenne 2008) might be involved in low-affinity uptake of ferrous iron. In the high-affinity iron assimilation pathway, FRE1 is reducing the ferric iron ( $\text{Fe}^{3+}$ ) to ferrous iron ( $\text{Fe}^{2+}$ ). The soluble  $\text{Fe}^{2+}$  produced by the FRE1 ferric reductase is re-oxidized by the plasma membrane ferroxidase (FOX1), and the  $\text{Fe}^{3+}$  produced by FOX1 serves as a substrate for the ferric permease FTR1. An important feature of this high-affinity iron acquisition system is that  $\text{Fe}^{3+}$  alone cannot serve as a substrate for uptake by FTR1. It has been shown in yeast that the permeation of iron is coupled to ferroxidation via a substrate channeling mechanism in which the  $\text{Fe}^{3+}$  substrate of Ftr1p is handed off directly from the ferroxidase Fet3p (Terzulli and Kosman 2009, 2010). Residues involved in iron channeling from Fet3p to Ftr1p have been identified in both proteins. It is most likely that the same mechanism is taking place also in the green alga *C. reinhardtii* (Chen et al. 2008). *FEA1* and *FEA2* encode for secreted protein located in the extracellular space, which function as periplasmic substrate binding

## 1. Introduction

proteins to concentrate substrates in the vicinity of assimilatory transporters (Allen et al., 2007).

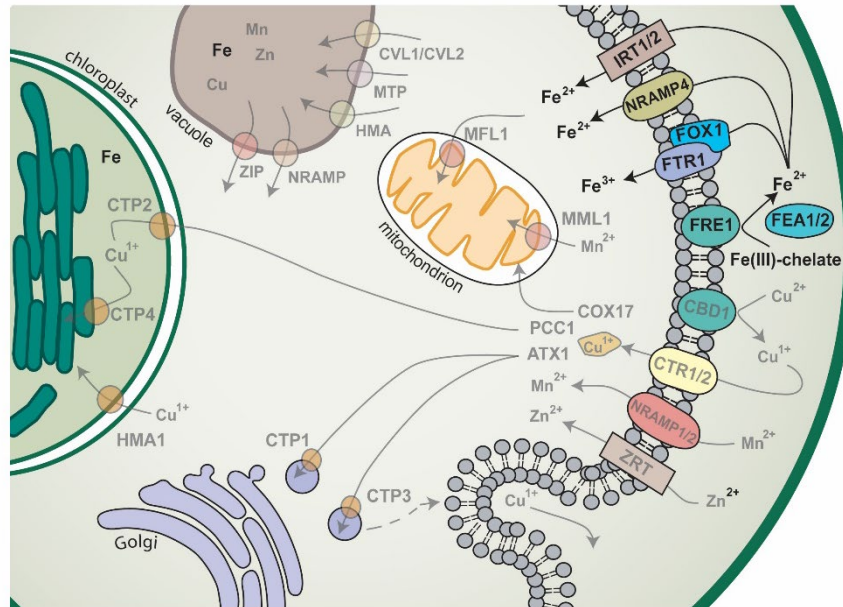


**Figure 6. Assimilative and distributive metal transport in *Chlamydomonas*.** For details of the iron uptake components see text. Adapted from Blaby-Haas and Merchant (2012).

The study of photoheterotrophic iron homeostasis in *C. reinhardtii* is routinely performed in the context of four graded stages of Fe nutrition: excess, replete, deficient and limited. These states were defined by the evaluation of phenotype and iron-responsive gene expression in response to controlled medium iron concentrations. Components of the iron-uptake pathway are routinely used as sentinel genes for iron status. *FOX1* expression responds quickly to changes in iron availability ahead of any observable effects on physiology and thus provides a convenient and robust marker for iron status.

The standard growth medium for *C. reinhardtii* contains 20  $\mu\text{M}$  Fe-EDTA (or 18  $\mu\text{M}$  Fe if Hutner's trace metal composition is used) (Hutner et al., 1950; Kropat et al., 2011). In both trace mixes, iron is supplied as an EDTA chelate, which is used to maintain iron in solution, thereby facilitating uptake. The revised trace metal composition was adjusted to supply a 3-fold excess of each required nutrient and was calculated based on the elemental composition in replete condition and the amount a culture uses throughout a complete growth phase ( $\sim 2 \times 10^4$  to  $1 \times 10^7$  cells  $\cdot$  ml<sup>-1</sup>). Cells grown with the revised trace metal

composition have an increased growth rate, the supplement composition is more stable with regard to bioavailable micronutrients and is less time consuming to prepare (Kropat et al., 2011). It is important to note that the interaction between the cell culture and the nutrient content is dynamic. The cell density and the rate of population growth will affect the intracellular concentration. This Fe-replete stage is characterized by basal low-level expression of the genes encoding the high-affinity FOX1/FTR1 ferric iron transporter and negligible expression of the putative secondary iron transporters NRAMP4, IRT1, and IRT2 (Urzica et al., 2012).

### 1.3.1 Iron-deficient and Fe-limited *C. reinhardtii*

As the iron content of acetate-containing medium is reduced from 20  $\mu\text{M}$  to 1–3  $\mu\text{M}$ , the cells begin to experience iron deficiency. As a consequence, the expression of the iron uptake pathways, including *FOX1/FTR1*, are dramatically induced. At this concentration of iron supply, the cells are usually not chlorotic and photosynthetic complex abundance is generally not affected (Moseley et al., 2002). Depending on genotype, the lower end of this concentration range may result already in symptoms of limitation, such as marginal chlorosis and a mild impact on abundance of photosynthetic complexes. Especially cell wall-deficient strains are more sensitive to reduced extracellular iron concentrations, as the assimilatory proteins FEA1 and FEA2 are lost into the medium and as a result cells are less able to scavenge sparse Fe from the medium.

Despite the absence of chlorosis in the iron-deficient state, spectroscopic measurements reveal changes within the chloroplast. Specifically, fluorescence rise- and decay-kinetics (Kautsky curves) indicate that re-oxidation of the plastoquinone pool is slower in the iron-deficiency situation (Moseley et al., 2002). This has been attributed to some loss-of-function of iron-containing electron transfer complexes downstream of the PQ pool, such as the cytochrome *b<sub>6</sub>f* complex, PSI or ferredoxin. The relatively exposed [4Fe-4S] clusters of PSI are prime candidates. Structural changes in the PSI-LHCI complex accompany iron deficiency, presumably to compensate for reduced PSI function. These modifications to the complex result in reduced energy transfer from the accessory antenna to the reaction center (Moseley et al., 2002). This results both from dissociation of PsaK, a connector between PSI and LHCI, from PSI and proteolysis of individual Lhca subunits in LHCI (Ben-Shem et al., 2003; Naumann et al., 2005).

## 1. Introduction

---

Based on genome-wide expression profiling using RNA-Seq methodology, 78 genes displayed at least a 2-fold difference in transcript abundance between this stage (1  $\mu$  M Fe) and the replete stage (Urzica et al., 2012). Since many organisms occupy a niche that allows them to survive in just barely sufficient iron, the transcriptome of this state is clearly relevant to the impact of marginal iron nutrition on crop yields and primary productivity. The two largest functional groups represented in the iron-deficient stage encode proteins with known or predicted function in metal transport (17%) and the redox/stress response (25%). This includes the upregulation of genes involved in iron transport, like the ferric reductase *FRE1*, the high-affinity iron-uptake system *FOX1/FTR1*, the transcripts for the algal-specific proteins FEA1 and FEA2, and the putative secondary iron transporters NRAMP4 and IRT2. The expression of a Mn-dependent superoxide dismutase is also highly induced. The transcripts of only four genes were significantly reduced in abundance during this condition. One of these is FDX5, an anaerobically induced chloroplast-targeted ferredoxin which contains a [2Fe-2S] cluster (Jacobs et al., 2009). The reduction of FDX5 transcript abundance may serve to spare iron. The large proportion of redox/stress-related transcripts at this stage of iron nutrition, which is visually asymptomatic, may reflect an anticipatory response to incipient stress associated with changes in light harvesting and reduced rate of electron transfer downstream of the PQ pool.

Expression of the two ferritin genes in *Chlamydomonas* is induced during iron deficiency. The ferritins localize to the chloroplast, but only Fer1 appears to increase in abundance in response to iron-deficiency (Busch et al., 2008; Long et al., 2008). Although ferritins are typically regarded as iron storage complexes, neither of the two *Chlamydomonas* complexes appears to contain significant amounts of iron when cells were grown in iron-deficient medium, leading to the conclusion that ferritin buffers instead of stores iron liberated within the chloroplast.

As the iron content of the medium is reduced below  $\sim 0.5 \mu$ M, cells enter the iron-limited stage, where cell growth is inhibited due to limiting nutritional supply of iron. Although the iron transport pathways are still highly expressed, and at a higher level than in the deficiency stage, the cells are markedly chlorotic, corresponding to a decrease in chlorophyll of about 2- to 4-fold. Concurrently, multiple iron-containing proteins in the chloroplast are reduced in abundance. These include PSI (12 iron atoms), the cytochrome *b<sub>6</sub>f* complex (12 iron atoms) and ferredoxin (2 iron atoms), and as a result, iron-limited



cells exhibit a severe block in photosynthesis (Moseley et al., 2002; Page et al., 2012; Urzica et al., 2012).

Genome-wide expression profiling uncovered a large number of genes with increased transcript abundance (at least 2-fold difference; 2050 genes) during this stage (0.25  $\mu$  M) relative to iron replete (Urzica et al., 2012), underscoring the stress induced by iron limitation. As seen in the iron-deficient dataset, the most dramatically increased transcripts are those involved in iron transport and those encoding Mn-dependent superoxide dismutase (Urzica et al., 2012). The large number of differentially abundant transcripts during this condition also highlights the value of studying the transcriptome of the iron-deficient state, where only 78 RNAs are significantly changed in abundance. It is more likely that these 78 RNAs include the direct targets of iron nutrition acclimation rather than secondary stress responses.

### 1.3.2 Excess Iron

In addition to Fe-deficient and Fe-limiting conditions, *Chlamydomonas* can grow in the presence of excess Fe in the medium (200  $\mu$ M Fe). In this condition, cells will over-accumulate iron 2- to 5-fold higher than in Fe-replete cells (Long and Merchant, 2008; Terauchi et al., 2010). Although the cultures do not display any visible phenotype associated with excess iron, the cells are unable to grow at high photon flux density (500  $\mu\text{mol}\cdot\text{m}^{-2}\cdot\text{s}^{-1}$  at the surface of a petri dish) (Long and Merchant, 2008). This result suggests that the higher iron content exacerbates damage caused by photo-oxidative stress and that there may be a pool of reactive iron in the chloroplast.

There are no known mechanisms for iron export in *Chlamydomonas*, presumably because this high iron concentration is not typically experienced in nature and there is no need to establish pathways to export excess iron ions. Because iron is found predominantly in insoluble chelates in an oxidized environment, thereby hindering the ability of cells to acquire iron, deficiency is generally a more pronounced problem for life than iron overload. In contrast to mammals and higher plants, iron excess does not affect the abundance of ferritin in *Chlamydomonas* (Busch et al., 2008; Long et al., 2008). Fe-replete *Chlamydomonas* cells contain a high amount of ferrous ( $\text{Fe}^{2+}$ ) iron, suggesting that the iron is stored in vacuoles and not in typical storage proteins such as ferritin, which would bind ferric ( $\text{Fe}^{3+}$ ) iron (Semin et al., 2003). Ferritin does not seem to be the pre-dominant iron

storage molecule in *Chlamydomonas*. Another candidate for Fe storage is the acidocalcisome, an acidic, calcium- and polyphosphate-rich, membrane-bound, lysosome-related organelle (Ruiz et al., 2001; Docampo et al., 2005; Lander et al., 2016). Indeed, intracellular iron is found in acidic vacuoles in the green alga *Dunaliella salina* and the red alga *Cyanidium caldarium* (Paz et al., 2007; Nagasaka and Yoshimura, 2008) and *Chlamydomonas* acidocalcisomes are sites of transition metal sequestration, so far shown for Cu and Mn (Hong-Hermesdorf et al., 2014; Tsednee et al., 2019). Yet not much is known where the extra accumulated iron is located in the *Chlamydomonas* cell and how it is stored.

### 1.3.3 The Impact of Carbon Source on Iron Homeostasis

As a facultative photoheterotroph, *Chlamydomonas* can generate ATP from either photosynthesis or respiration depending on the presence of light and carbon source. This characteristic provides a unique and powerful experimental system to explore the effect of iron status on bioenergetic metabolism and vice versa. In particular, during the two major trophic states, photoautotrophic and photoheterotrophic, *Chlamydomonas* cells respond to the iron stages with acutely different physiologies (Terauchi et al., 2010; Urzica et al., 2012). During the photoheterotrophic state, the cells are provided with light, CO<sub>2</sub>, and acetate. When iron becomes a limiting resource, competition for iron acquisition between the chloroplast and the mitochondria ensues. In response, the cell maintains respiration while decreasing the dispensable photosynthetic contribution to the bioenergetics of the cell, a phenomenon that may rely on preferential allocation of iron to the mitochondrion or recycling of iron from the chloroplast to the mitochondrion (Moseley et al., 2002; Terauchi et al., 2010).

The iron-dependent bioenergetic complexes in both the photosynthetic and respiratory ETCs are assembled in the chloroplast or mitochondrion, respectively. In the absence of an iron source (iron-chelate or heme), the complexes fail to accumulate, generally because of thermodynamic instability and protease susceptibility of individual apoproteins. It is evident that when iron availability is insufficient to maintain the cellular iron quota for a particular growth condition, there is likely to be competition between the chloroplast and the mitochondrion. When the environmental supply cannot meet the cellular demand, prevailing dogma is that mechanisms for economizing, prioritizing and recycling the

limiting metal nutrient are initiated (Merchant and Helmann, 2012). This is driven by maintenance of more essential biochemical functions over dispensable ones where possible and by priming macromolecular metabolism so that upon metal resupply, proteins in key pathways are prioritized for cofactor loading. When a reduced carbon source is supplied, the photosynthetic apparatus becomes dispensable and is sacrificed during Fe-limitation. During photoautotrophic growth, when the photosynthetic apparatus is required for growth and cellular maintenance, photosynthetic capacity will be retained longer, despite low Fe-availability (Harris, 2009; Terauchi et al., 2010; Urzica et al., 2012).

The same stages of iron nutrition described above can be applied for photoautotrophic *Chlamydomonas* cells, but cellular response to extracellular concentrations and iron concentration thresholds are distinct. These stages are also likely distinct for cells grown purely heterotrophically (dark and acetate), but this phenomenon has not yet been systematically studied.

### 1.4 Aim of This Thesis

The general aim of this thesis was to use *C. reinhardtii* as a model organism to further the understanding of dynamic iron homeostasis in the context of photosynthesis. Specifically, to study the Fe-dependent acclimation during the transition from photoautotrophic to photoheterotrophic conditions, to characterize cells exposed to excess extracellular iron and to define the spectrum of phenotypic variabilities between different wild-type strains. To achieve these goals, different techniques were applied, including the assessment of photosynthetic parameters, elemental composition, whole-genome transcriptome analysis and the comparison of a knock-out mutant.

The first aim was to establish the elemental profile as a useful tool for *Chlamydomonas*, using inductively coupled plasma tandem mass spectrometry (ICP-MS/MS). As the second aim I wanted to verify the published characterization of Fe-deficient and Fe-limited cultures (with Hutner's trace elements, Hutner et al., 1950) with the revised micronutrient composition (Kropat et al., 2011), to add excess extracellular iron concentrations to the assessment and to examine the dynamic response of cells exposed to rapid changes in extracellular iron, from very little available iron to excess and vice versa, including a mutant defective in a compartment believed to be involved in the storage of trace metals. The goal of the third aim was the characterization of the cellular acclimation from photoautotrophic-focused metabolism to the availability of an additional, reduced, carbon

## 1. Introduction

---

source and how this transition is affected by Fe-deficiency. To achieve this goal, photoautotrophic cultures of *Chlamydomonas* will be grown with replete, deficient and limiting amounts of Fe provided, adding acetate to the growth medium to induce the metabolic changes, followed by evaluating the physiology combined with a genome-wide transcriptome analysis to assess the overall coping with the treatment.

Lastly, one aim was the overall description of variability in transcript abundance and physiological parameters between different wild-type strains to assess which aspects exhibit large differences between strains and which are more stable.

The individual aims will be combined into one large result and one discussion section, followed by Materials and Methods, Literature and an Appendix comprised of supplemental figures and tables.

## 2 Results

### 2.1 Elemental Profile of *Chlamydomonas reinhardtii*

Since my thesis was centered around perturbations made to specifically alter the elemental composition, I first wanted to assess the variability of the elemental makeup of *Chlamydomonas* in general, across multiple experiments. The elemental composition, specifically phosphorus (P), sulfur (S), magnesium (Mg), potassium (K), sodium (Na), calcium (Ca), iron (Fe), manganese (Mn), zinc (Zn) and copper (Cu) content, was determined by inductively coupled plasma tandem mass spectrometry (ICP-MS/MS) of nitric acid-hydrolyzed cells against defined calibration solutions and related to the number of cells analyzed. The elements analyzed and displayed here are only a fraction of all elements present in a cell but were the ones most relevant with respect to the research questions. The elements of interest are spanning a range from  $10^7$  to  $10^{10}$  atoms·cell<sup>-1</sup>. Cellular abundance of other elements, less prevalent ones with more specialized functions (e.g. cobalt, molybdenum) or more ubiquitous ones, responsible for assembling the building blocks (e.g. carbon, nitrogen, oxygen) would extend that range further.

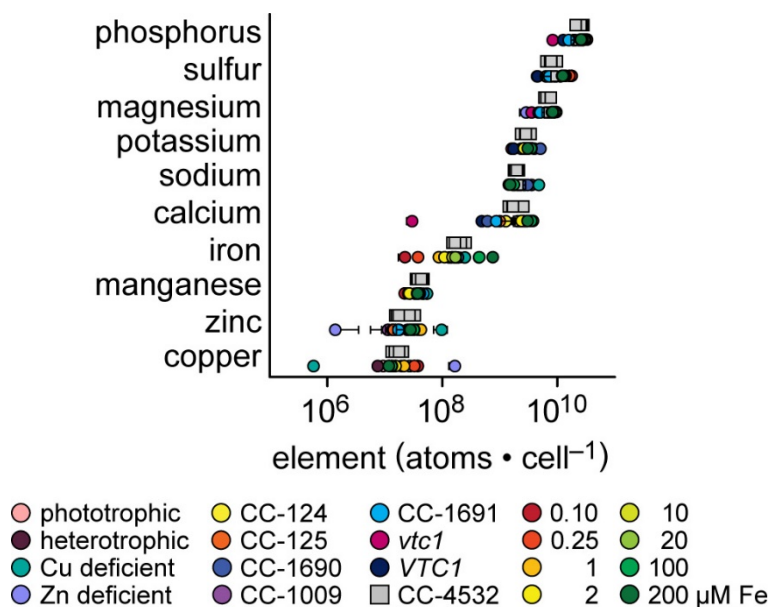


**Figure 7. Elemental composition of *C. reinhardtii*.** Cells were grown in the conditions indicated and the elemental composition was determined by inductively coupled plasma tandem mass spectrometry (ICP-MS/MS) from cell lysates and related to the number of cells analyzed. The mean of three to four (colored) or 26 (grey) replicates is shown, error bars represent SD.

## 2. Results

---

The elemental composition was constant when cells of the same genotype were grown in standard photoheterotrophic growth conditions in replete media (Figure 7), as best demonstrated by the variation of CC-4532 (grey squares) sampled and analyzed over the course of 14 months from 26 independent replicate cultures. Overall, the ratio of the elements to each other was also similar between different strains, with minor changes to the overall abundance. Manipulations, especially changes in the extracellular availability of micronutrients, result in very specific alterations of individual elements that were not aligned with the abundance of the element in replete conditions, moving abundances away from the bulk of the data. Examples include a reduced Ca-content in a *vtc1*-mutant, the large spectrum of cellular Fe content in response to variations in extracellular Fe concentrations, increased Zn- and decreased Cu-content in Cu-deficiency as well as decreased Zn- and increased Cu-content in Zn-deficiency. This indicates cross-talk in metal homeostasis pathways.

### 2.2 Steady State Photoheterotrophic Iron Homeostasis in the Green Alga *Chlamydomonas reinhardtii*.

#### 2.2.1 Extracellular Fe Availability Affects Fe, Cu and Mn Levels.

In order to analyze the effect of extracellular Fe abundance on intracellular trace metal pools, cells of *C. reinhardtii* CC-4532 were grown in illuminated batch cultures with acetate in four iron nutritional states, two concentrations each. Since Tris-Acetate-Phosphate (TAP) medium, utilizing the modified trace metal composition (Kropat et al., 2011), contains 20  $\mu\text{M}$  Fe, I selected 10 and 20  $\mu\text{M}$  Fe for Fe-replete conditions. Based on results from previous studies (Urzica et al., 2012), 0.10 and 0.25  $\mu\text{M}$  were chosen for iron-limited, and 1.0 and 2.0  $\mu\text{M}$  for iron-deficient conditions. In order to investigate the effect of higher extracellular Fe concentrations, 100 and 200  $\mu\text{M}$  were chosen for iron-excess conditions (5-10 $\times$  standard TAP medium). In general, iron concentrations indicated in this thesis refer to EDTA-chelated Fe added to iron-free medium before inoculation, the actual concentration of (bio-) available iron decreases naturally during growth of the cultures when biomass consumes the iron. Therefore, in order to obtain highly reproducible results, cultures were grown in comparable conditions, inoculated from comparative pre-cultures, at the same initial cell density and were sampled at comparable final cell densities (mid-

## 2. Results

---

logarithmic, between  $1-4 \times 10^6$  cells·ml<sup>-1</sup>, if not stated otherwise). For the investigation of iron-dependent elemental composition, cells were grown for one round in pre-cultures with the respective extracellular iron concentrations, except for iron-limited conditions, which were grown in iron-deficient pre-cultures containing 1 μM Fe. Previous and preliminary experiments have shown that cultures grown for longer periods in Fe-limitation showed severe symptoms of iron starvation, including complete growth arrest when repeatedly transferred to Fe-limited medium, which documents the essential nature of Fe and the fact that it can be a growth-limiting nutrient. Growth in the Fe-deficient environment for one round pre-depleted the stored iron pools resulting from luxurious growth to create severe, and highly reproducible, iron limitation within four to five doublings during the experiment, from inoculation at  $1-2 \times 10^4$  cells·ml<sup>-1</sup> to sampling at mid-logarithmic growth phase ( $2 \times 10^6$  cells·ml<sup>-1</sup>). In contrast, cultures in iron-deficient conditions containing 1 μM Fe maintain necessary iron pools and cultures can be inoculated for subsequent growth phases without significant impact. Variations in the growth conditions, like extracellular iron concentrations, cause specific acclimations to the elemental composition (colored circles, Figure 8A). To better illustrate the details of the relationship between extracellular and intracellular iron it was also plotted double-logarithmic in the left panel of Figure 8B. Replete cultures during mid-logarithmic growth maintained a steady state iron pool of  $16.7 \pm 0.6 \times 10^7$  atoms·cell<sup>-1</sup> (mean ± standard deviation), comparable to the concentrations observed throughout the thesis (Figure 7).

The intracellular iron pool was significantly altered between all eight extracellular iron concentrations. In this thesis, a difference between two values was considered significant, when the *p*-value calculated from an unpaired, two-tailed Student's *t*-test passed a significance threshold of  $\alpha = 0.05$ , individual *p*-values between the conditions are listed in Supplemental Table 1. When iron was limiting, cells survived with as little as  $2.2 \pm 0.5 \times 10^7$  atoms·cell<sup>-1</sup>, which correlates to 7.5% of replete levels (0.10 μM compared to 20 μM in the growth medium at inoculation). When cells were repeatedly exposed to excess iron, cells increased the cellular pool to  $74.3 \pm 2.7 \times 10^7$  Fe atoms·cell<sup>-1</sup>, correlating to a more than four-fold change (20 μM compared to 200 μM). From limiting to excess concentrations, cells experience a 2000-fold change in extracellular Fe, whereas cellular steady state iron pools only varied an overall 34-fold. Intra- and extracellular iron content displayed a good linear relationship with a correlation coefficient, calculated from a linear regression over the entire concentration range, of  $R^2 = 0.9825$  (Supplemental Figure 1). A

## 2. Results

slightly better fit can be obtained with two separate regressions, one for iron concentrations below replete (0.10 to 20  $\mu\text{M}$  Fe), with a logarithmic regression and a correlation coefficient of  $R^2 = 0.9946$ , and a second for iron concentrations above replete (10 to 200  $\mu\text{M}$  Fe), with a linear regression and  $R^2 = 0.9965$ . This may speak to two pathways of Fe uptake, high affinity at low extracellular Fe and low affinity at high extracellular Fe. Unsurprisingly, cellular iron content showed the most dramatic change in response to extracellular Fe nutrition, Mn and Cu content however, was also adjusted to extracellular iron concentrations (white and grey circles, right panel Figure 8B) as well.

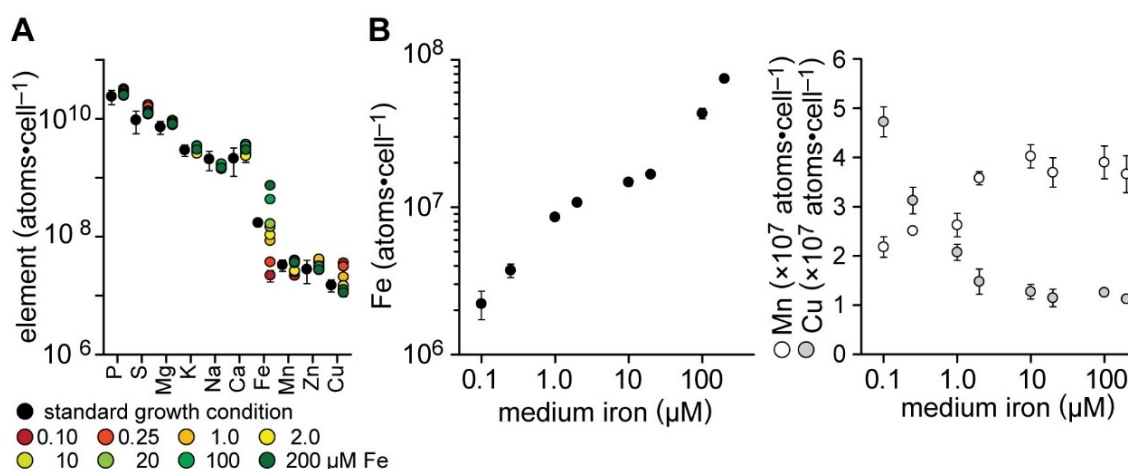


**Figure 8. Fe-dependent elemental composition.** Cells of strain CC-4532 were grown in standard growth conditions (**A**) and in eight different concentrations of extracellular iron (**A**, **B**) in two independent experiments. Elemental composition was analyzed by inductively coupled plasms tandem mass spectromtry (ICP-MS/MS) from cell lysates and related to the number of cells analyzed. The mean of 26 (standard growth conditions in **A**) or four replicates (iron concentrations in **A** and **B**) is shown, error bars represent SD.

Manganese pools were only affected in low Fe-deficient and in Fe-limiting conditions, the cellular content was reduced 41%, from  $3.7 \pm 0.3$  in Fe-replete to  $2.5 \pm 0.1$ ,  $2.6 \pm 0.2$  and  $2.2 \pm 0.2 \times 10^7$  Fe atoms·cell<sup>-1</sup> (at 1.0, 0.25, and 0.10  $\mu\text{M}$  Fe, respectively). Copper pools changed in lower Fe-deficient and Fe-limiting conditions, an increase of up to 411% was observed, from  $1.2 \pm 0.2$  in Fe-replete to  $2.1 \pm 0.2$ ,  $3.1 \pm 0.3$ , and  $4.7 \pm 0.3 \times 10^7$  atoms·cell<sup>-1</sup> (at 1.0, 0.25, and 0.10  $\mu\text{M}$  Fe, respectively), perhaps reflecting increased demand for Cu for the synthesis of high affinity Fe uptake components. Individual *p*-values between the samples are listed in Supplemental Table 2. No significant change in the Mn or Cu pool were observed in excess conditions. The content of Mg, K, Na Ca, and Zn remained largely unchanged in response to iron nutrition compared to standard growth conditions (individually displayed against extracellular iron concentration in Supplemental Figure 2).



### 2.2.2 Iron Accumulation Does Not Impact Micronutrient Content.

While Mn and Cu content only differed in lower extracellular Fe concentrations, and most other elements did not change (Mg, K, Na, Ca, Zn) at all, I did not observe a change of the elemental composition at elevated Fe levels outside of increased Fe amounts. I therefore analyzed the abundance of the macro nutrients carbon (C), nitrogen (N), P and S, often seen as indicators or equivalents for biomass, in response to changes to the extracellular iron concentrations (Figure 9A). Cultures were grown in the same way as described above (2.2.1), P and S were analyzed by ICP-MS/MS from the same cellular samples shown in Figure 8B. Cellular C and N content were examined independently by total organic carbon and total nitrogen analysis (TOC-TN) from intact cells hydrolyzed by hydrochloric acid and quantified against defined reference solutions. The cellular N content in replete conditions amounted to  $22.0 \pm 1.4 \times 10^{10}$  atoms $\cdot$ cell $^{-1}$  and increased by 27% to  $28.0 \pm 1.9 \times 10^{10}$  atoms cell $^{-1}$  at 0.10  $\mu$ M Fe. Phosphorus content was significantly increased by 30% and 23% to  $34.1 \pm 3.0$  and  $32.3 \pm 2.3 \times 10^8$  cells $\cdot$ ml $^{-1}$  at 0.10 and 0.25  $\mu$ M Fe, respectively (compared to  $26.2 \pm 2.0 \times 10^8$  cells $\cdot$ ml $^{-1}$  in replete conditions). The cellular S content showed the same trend as N and P content, increased by 47% and 34% to  $17.5 \pm 1.1$  and  $16.0 \pm 1.1 \times 10^8$  cells $\cdot$ ml $^{-1}$  at 0.10 and 0.25  $\mu$ M Fe, respectively (compared to  $11.9 \pm 0.8 \times 10^8$  cells $\cdot$ ml $^{-1}$  in replete conditions). Individual *p*-values for C, N, P and S content between the conditions are listed in Supplemental Tables 3 and 4.

Cells increased in volume when limited for extracellular iron (Figure 9B, Terauchi et al., 2010). The macro-nutrient content, especially C content, is often regarded as a marker for biomass, the Fe-dependent cell size was estimated as volume calculated from the median of the diameter distribution.

The cell volume changed gradually with reduced extracellular iron, increasing from  $\sim 315 \mu\text{m}^3$  (between 2 and 200  $\mu$ M Fe) to  $345 \pm 19 \mu\text{m}^3$  at 1.0  $\mu$ M Fe (10% increase),  $383 \pm 24$  at 0.25, and  $411 \pm 20 \mu\text{m}^3$  at 0.10  $\mu$ M Fe (increase of 22% and 30%, respectively). Individual *p*-values between the samples are listed in Supplemental Table 5. In order to study the effect of the biomass increase at low Fe concentrations on the elemental composition, in addition to relating the abundance to the number of cells analyzed, I analyzed N, P and S content related to cell volume. When related to cell volume, the gradual increase observed in absolute amounts of N, P and S in low Fe (Figure 9C) were more significantly different to replete conditions, indicating that these increases resulted

## 2. Results

from an increase in cell volume. The carbon content however showed a distinctly different behavior from N, P and S to extracellular iron (Figure 9D). Carbon pools increased in iron-limitation beyond the volume-related increase, 3- and 2-fold, from  $\sim 120$  to  $353 \pm 12$  and  $248 \pm 12 \times 10^{10}$  cells $\cdot$ ml $^{-1}$  (at 0.10 and 0.25  $\mu$ M Fe).

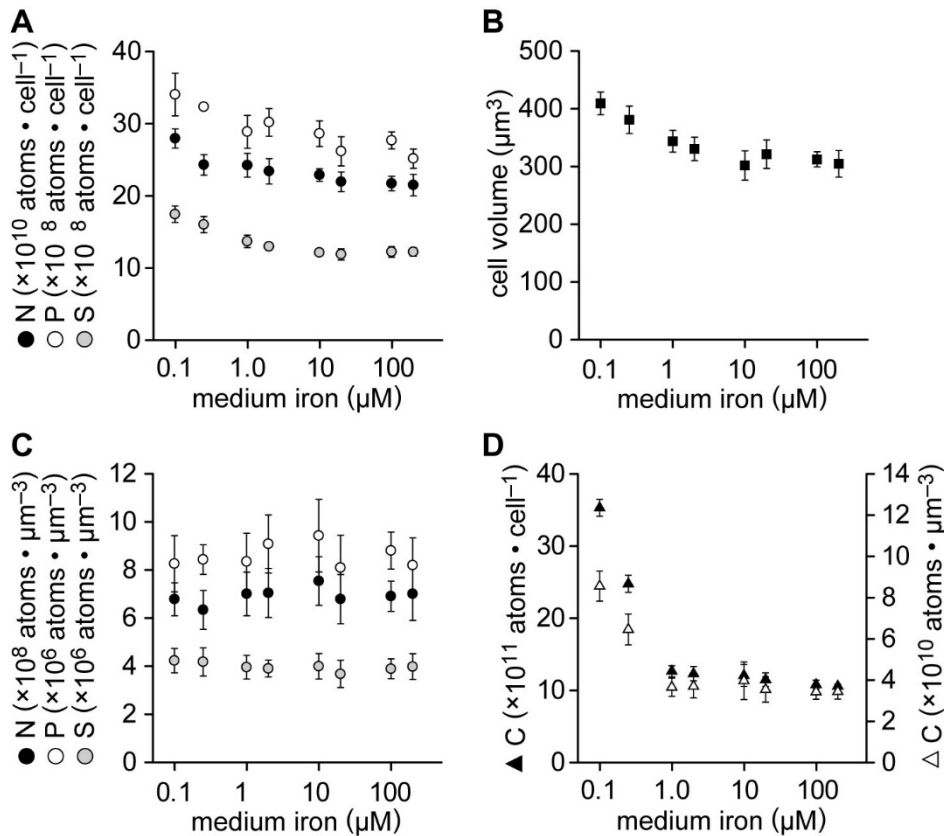


**Figure 9. C, N, P, and S content as a function of medium iron concentrations.** Photoheterotrophic cultures containing the indicated concentrations of Fe were grown to a density of  $2\text{-}3 \times 10^6$  cells $\cdot$ ml $^{-1}$  for elemental analysis by TOC-TN (nitrogen and carbon) and ICP-MS/MS (phosphorus and sulfur). A: Nitrogen (black circles), phosphorus (white circles) and sulfur (grey circles) content was related to the number of cells analyzed. B: Average cell volume was calculated from the median cell diameter of each culture. C: Nitrogen (black circles), phosphorus (white circles) and sulfur (grey circles) content were related to the average cell volume for each extracellular iron concentration. D: Cellular carbon content was related to the number of cells analyzed (black triangle) as well as to the average cell volume (white triangle). The mean of four replicates is shown, error bars represent SD.

Cellular Mg, K, Na, Ca, Fe, Mn, Zn and Cu expressed as atoms per volume instead of cell number are shown in Supplemental Figure 3 and while this normalization method removed the variability from the increased cell volume during iron-limitation, the increase in Cu and decrease in Mn were still found to be significant, which is unsurprising, given the degree of change (Cu) and the direction (Mn).

### 2.2.3 Excess Intracellular Iron Offers a Growth Advantage.

In excess conditions, only internal iron pools were increased, the cellular content of the other elements remained unchanged. In order to analyze the effect of excess Fe accumulation on culture health, I first analyzed growth rates. Figure 10A shows average growth curves of CC-4532 at all eight extracellular iron concentrations. Excess iron in the growth medium led to faster growth in the mid-logarithmic phase at 3.5, 4 and 4.5 d after inoculation, replete cultures grew from  $1.0 \pm 0.1$  to  $2.2 \pm 0.1$ ,  $4.8 \pm 0.4$ ,  $7.2 \pm 0.2$  and  $10.9 \pm 0.9$  cells·ml<sup>-1</sup>, cultures containing 200 μM Fe grew from  $1.1 \pm 0.1$  to  $3.0 \pm 0.1$ ,  $5.2 \pm 0.5$ ,  $8.7 \pm 0.5$  and  $11.8 \pm 0.9 \times 10^6$  cells·ml<sup>-1</sup> at 3, 3.5, 4, 4.5 and 5 d, respectively.

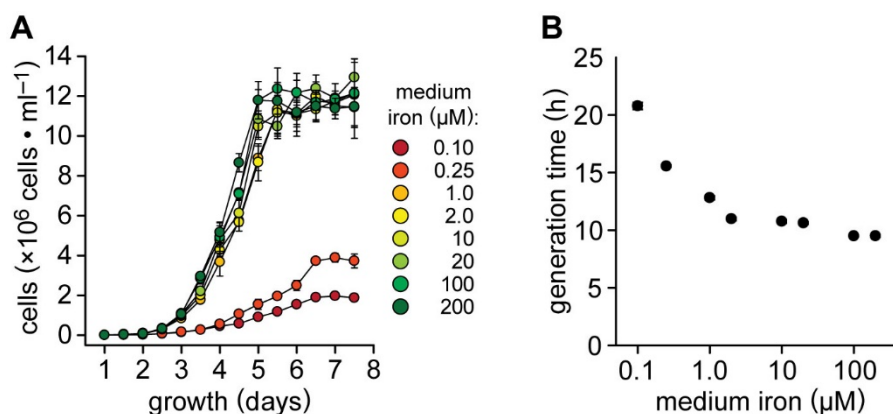


**Figure 10. Iron-dependent growth of *C. reinhardtii*.** Photoheterotrophic cultures containing 0.1, 0.25, 0.5, 1.0, 2.0, 10, 20, 100 and 200 μM Fe-EDTA were inoculated from pre-cultures containing 1.0, 1.0, 1.0, 1.0, 2.0, 10, 20, 100, and 200 μM medium iron, respectively. A: Growth was monitored from inoculation to stationary phase and the cell number was determined every 12h by manual counting. The mean of four replicates is shown, error bars represent SD. B: Generation time was calculated from the growth curves shown in A, when each culture reached  $1 \times 10^5$  cells·ml<sup>-1</sup> up to the first time point of stationary growth phase. The mean of the generation time calculated for each replicate individually is shown, error bars represent SD.

The faster doubling time during the mid-logarithmic phase in excess iron was also visible when expressed as generation time of the entire logarithmic growth phase (from  $1 \times 10^5$  cells·ml<sup>-1</sup> to the first time point of stationary phase) (Figure 10B). The generation time decreased by 1.4h per generation, from  $10.8 \pm 0.1$ h in replete to  $9.4 \pm 0.1$ h of cultures grown in 200 μM Fe. The growth rates of cultures containing 100 μM Fe in the medium were between the rates of cultures with 20 and 200 μM. Individual *p*-values comparing generation time between the samples are listed in Supplemental Table 6.

### 2.2.4 Over-accumulated Iron Did Not Impact Photosynthetic Activity.

Growth rate is a good indicator of culture health. However, *C. reinhardtii* grown in excess iron resulted in an increase in accumulated iron which could have other detrimental effects in combination with light and photosynthetic reactions (Long and Merchant, 2008). In order to evaluate the fitness of cultures grown iron-dependently more generally, I therefore additionally analyzed the photosynthetic activity, cellular chlorophyll content, the maximum quantum efficiency of PSII ( $F_v/F_m$ ) and fluorescence transients (also known as Kautsky effect), which should allow for a more complete evaluation of detrimental effects especially in high Fe conditions.

The chlorophyll content is unchanged over a wide range of extracellular iron concentrations and was not affected in Fe-excess conditions (Figure 11A). In Fe-limited cultures, the cellular chlorophyll content is decreased by 84 and 76%, consistent with the dogma of Fe-deficiency chlorosis. Individual *p*-values comparing the chlorophyll content between the samples are listed in Supplemental Table 7.  $F_v/F_m$  values in the range of 0.78 to 0.84 for plant leaves or 0.75 to 0.80 for algae (Maxwell and Johnson, 2000) show the optimal quantum efficiency of PSII and decreased values indicate stress that impacts the electron flow through the photosynthetic electron transfer chain.

Because this chlorophyll fluorescence measurement relies on a saturating light flash to reduce all reaction centers of PSII and determine the maximum fluorescence  $F_{max}$ , dark-adaptation time and the saturating character of the light flash were established in initial experiments (detailed in section 4.2) and, as an additional control, fractions of the experimental cultures were treated with an irreversible inhibitor of PSII electron flow and analyzed in parallel with the experimental samples to confirm the analytical arrangement. For this experiment, saturating light conditions were verified using cells from photoheterotrophic Fe-replete cultures treated with 20  $\mu$ M DCMU (3-(3,4-dichlorophenyl)-1,1-dimethylurea, in ethanol) on  $2 \times 10^6$  cells·ml<sup>-1</sup> or 20  $\mu$ M ethanol as control 2 min before immobilization and dark-adaptation, fluorescence was captured before ( $F_0$ ) as well as after the light flash ( $F_{max}$ ) (Supplemental Figure 4).

Cells after the light flash showed the same level of fluorescence as dark-adapted cells in the presence of DCMU, indicating interrupted electron flow through the photosynthetic electron transfer chain (ETC) due to the reduction of most PSII reaction centers by the light flash. As observed with the chlorophyll content, the maximum quantum efficiency of PSII

## 2. Results

is only affected in iron-limitation ( $F_v/F_m$  of  $0.38 \pm 0.04$  and  $0.49 \pm 0.03$  at 0.10 and 0.25  $\mu\text{M}$  Fe, respectively) and unchanged in iron-deficient to -excess cultures (average  $F_v/F_m$  of  $\sim 0.77$  between 1.0 and 200  $\mu\text{M}$  Fe) (Figure 11B). Individual  $p$ -values comparing the maximum quantum efficiency between the conditions are listed in Supplemental Table 8.

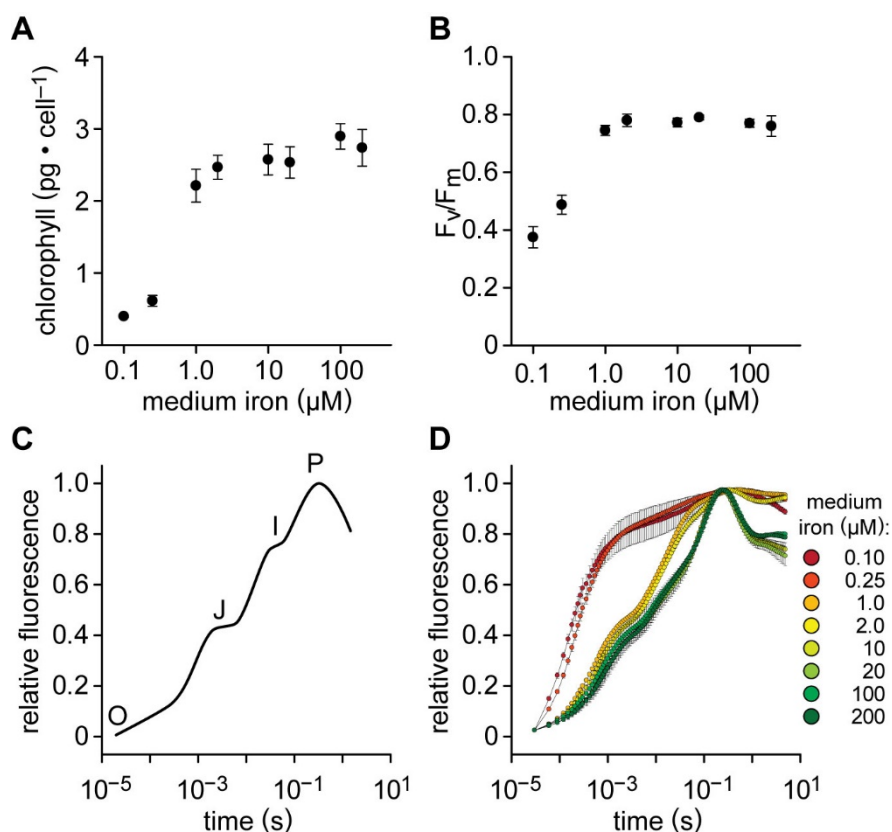


**Figure 11. Photosynthetic parameters as a function of medium iron concentration.** Photoheterotrophic cultures containing 0.10, 0.25, 1.0, 2.0, 10, 20, 100 and 200  $\mu\text{M}$  Fe were grown to a density of  $2\text{-}3 \times 10^6$  cells·ml<sup>-1</sup> for analysis. **A:** Total chlorophyll was extracted from  $\sim 4 \times 10^6$  intact cells with a mixture of 80% acetone/20% methanol (v/v) and absorption of the extract measured spectrophotometrically against a solvent blank. The mean of four replicates is shown, error bars represent SD. **B:** Maximum quantum efficiency of PSII ( $F_v/F_m$ ) was determined from  $\sim 2 \times 10^6$  cells immobilized onto 15 mm round filters after dark-adaptation for 12-15 min using saturating light. The mean of four replicates is shown, error bars represent SD. **C:** A cartoon of a typical fluorescence transient curve showing the characteristic O-J-I-P sections of the curve. **D:** Measured fluorescence, corrected for background, was normalized to 1 for comparison. The mean of three replicates is shown, error bars represent SD.

When dark-adapted samples are continuously illuminated, and fluorescence changes recorded with millisecond-resolution, the fluorescence intensity shows characteristic changes, called fluorescence transient or Kautsky curve, with a fast-increasing induction

## 2. Results

---

phase of less than a second, and a slower decreasing phase of up to a few minutes. The induction curve has characteristic inflection points, named OJIP. Where O is the origin and gives the lowest measured fluorescence  $F_0$ , J and I are intermediate levels and P is the peak fluorescence level, similar to  $F_{max}$  (Figure 11C). The induction phase can be largely linked to the events taking place during successive reduction of the electron acceptors of the ETC, whereas the slow part, due to an increasing number of different processes involved, is more difficult to interpret, and is not included in this analysis.

The iron-dependent fluorescence transient curves were normalized for fluorescence in the O phase and expressed relative to the maximum fluorescence at the P phase. The resulting fluorescence curves can be grouped into three distinct patterns. The first group consisted of the Fe-limited cells (0.10 and 0.25  $\mu\text{M}$  Fe) and showed a distinct fluorescence induction pattern without distinguishable J or I phases (Figure 11D) and were very similar to the fluorescence levels of cells treated with DCMU (Supplemental Figure 5). A second group consisted of the Fe-deficient cultures (1.0 and 2.0  $\mu\text{M}$  Fe), with slightly increased fluorescence levels in the J phase (the trend is noticeable, but the difference did not meet the significance threshold applied in this thesis for most time points around this section of the curve) and a significant increase in the fluorescence induction in the I phase was observed. The third group contained Fe-replete and -excess cells (10, 20, 100, and 200  $\mu\text{M}$  Fe) and showed the expected J and I sections of the curve.

### 2.2.5 Identification of Candidate Genes Facilitating Iron Accumulation.

Growth in 10-fold excess iron led to significant intracellular iron accumulation, did not negatively impact fitness and even allows for a small growth advantage. In order to characterize the underlying molecular changes of cells to accommodate these changes, we used an RNA-Seq analysis comparing transcript abundance in steady state Fe-replete and -excess conditions (Figure 12). Cells were grown in Fe-replete and -excess pre-cultures to late-logarithmic phase and used to inoculate three replicate experimental cultures containing 20 or 200  $\mu\text{M}$  Fe at a starting density of  $1-2 \times 10^4$  cells $\cdot\text{ml}^{-1}$ , grown to  $2 \times 10^6$  cells $\cdot\text{ml}^{-1}$  and  $3 \times 10^6$  cells were sampled for RNA extraction. In parallel to sampling for RNA, additional cells were collected from the same cultures for elemental analysis by ICP-MS/MS to ensure the accumulation of iron in Fe-excess conditions (Supplemental Figure 6). The transcriptome in each sample was determined by RNA-Seq on the Illumina

## 2. Results

platform, the sequenced reads were aligned to the Au111.6 gene models and expression estimates calculated as FPKM (fragments per kilobase of transcript per million fragments mapped). The between-sample variation of the three replicate samples is small for both conditions (Supplemental Figure 7) and thus the average expression was used for further analysis unless stated otherwise. A maximum expression cutoff of  $\geq 1$  FPKM across all conditions was applied to all 17 741 gene models to remove genes with low expression within the data set and resulted in 13 823 detected transcripts (Supplemental Figure 8). Genes were classified as differentially expressed using a false discovery rate of  $< 5\%$  and a minimum of 2-fold regulation. Using these criteria, a small number of 46 genes (0.33% of detected transcripts) were identified whose transcripts accumulated differentially in response to excess iron (Figure 12A).

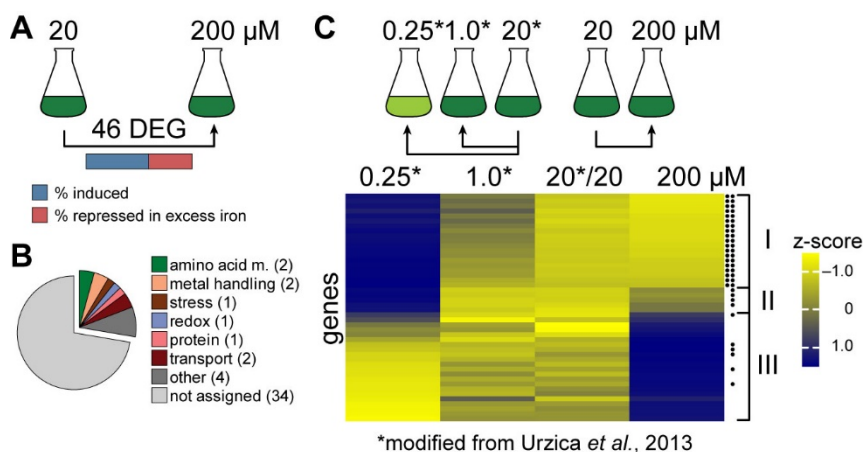


**Figure 12. Transcriptome analysis of cultures exposed to excess Fe.** Photoheterotrophic cultures containing 20 and 200  $\mu\text{M}$  Fe-EDTA were inoculated from pre-cultures with 20 and 200  $\mu\text{M}$  Fe-EDTA, respectively, and grown to a density of  $2 \times 10^6$  cells·ml<sup>-1</sup>. RNA was extracted and purified, mRNA selected, and cDNA generated for RNA-seq analysis. Replicate expression estimates of the Phytozome v5.5 gene models were averaged and reported in FPKM for each gene. **A:** Differentially expressed genes (DEG) were extracted from the Cuffdiff output using additional selection ( $> 1$  FPKM in at least one of the two samples, FDR  $< 5\%$ , fold change  $\geq 2$ ). **B:** DE genes were grouped by the functional annotation of their predicted protein sequence according to the MapMan annotation. The category ‘other’ includes several small annotation groups. The number of genes in each category is noted in parentheses behind each group. **C:** Comparison of DE genes in excess iron to the expression levels in iron deficiency and limitation (modified from Urzica et al., 2012). The first filled circle next to the heatmap marks genes that are differentially expressed between iron-deficient and -replete conditions, the second circle DE genes between iron-limited and -replete conditions. Three groups of coordinated expression patterns are labeled with I, II and III.

## 2. Results

---

Of these 46 genes, 19 had reduced and 27 increased transcript abundance in excess iron. For a functional characterization of the transcriptome response, the differentially expressed (DE) genes were grouped according to the functional annotation of their predicted protein sequence according to the MapMan ontology (Figure 12B) (Thimm et al., 2004). Of all detected transcripts in this dataset, 39% have been assigned functional annotations (35% of all gene models). The number of genes in each category are summarized in Supplemental Figure 9. Of the DE genes in excess Fe only 12, or 26%, have an annotation, the number of genes is displayed in parentheses next to each group. Even though only a fraction of the genes has annotations, a much larger fraction, consisting of 29 genes, or 63%, are also differentially expressed the Fe-deficiency RNA-Seq dataset. For the Fe-deficiency RNA-Seq dataset, cells of CC-4532 were grown in photoheterotrophic batch cultures containing 0.25, 1.0 and 20  $\mu\text{M}$  Fe (Urzica et al., 2012), Fe-deficient cells had 78 and Fe-limited 2050 differentially expressed genes when compared to Fe-replete cells. The expression profiles of the 46 DE genes in Fe-excess conditions were plotted as a clustered heatmap (Figure 12C), where each dataset was separately normalized to the respective Fe-replete sample.

Three groups of expression patterns can be observed in the heatmap, marked I, II, and III. The first group consisted of all 19 genes that showed repressed transcript abundance in excess iron, and interestingly, all of them show increased transcript abundance in both Fe-deficiency and Fe-limitation, highlighted by the two dots on the right side of the heatmap, and are among the genes with the largest fold increase in the Fe-deficiency dataset. This group includes components of the assimilatory iron uptake (*FTR1*, *FEA1*, *FEA2*, *IRT2*, *FOX1*), other intracellular components of iron homeostasis (*NRAMP4*, *FRE1*, *FER1*, *MSD3*) and genes with preliminary or predicted function in iron homeostasis (Cre12.g546500 *TEF22*, Cre05.g241400 a ferric-chelate reductase, Cre03.g146447 a protein containing a kelch-repeat domain). The second group contains genes with decreased transcript abundance in Fe-excess conditions and 4 of the 5 genes showed induced abundance only in Fe-limitation (0.25  $\mu\text{M}$  Fe), highlighted by one dot on the right side of the heatmap, but are not responding in the primary iron-deficiency response (1  $\mu\text{M}$  Fe). Most interestingly, the third group consisted of 22 genes that are induced in Fe-excess and are repressed or not responsive to Fe-deficiency (6 of 22 genes are repressed in Fe-limitation). This group consisted of mostly uncharacterized genes and most likely contains



genes that are involved in the storage and handling of the additional accumulated iron, presenting excellent targets for detailed follow-up studies.

### 2.2.6 Effect of Pre-culture Iron Status on Iron Accumulation.

Over the course of the thesis, I observed that not all cultures and experiments in excess Fe conditions over-accumulated iron to the same extent, which led, on the one hand, to the development of more stringently-controlled growth protocols for the experiments presented here, but secondly, left me curious for the underlying reason of the inconsistency. Therefore, I introduced additional perturbations in the experimental setup to identify conditions affecting the extent of iron accumulation in excess conditions in order to increase the detailed understanding of iron overaccumulation.

Focusing on the pre-culture, in a first experiment, cultures containing 0.10, 0.25, 1.0, 2.0, 10, 20, 100, and 200  $\mu\text{M}$  Fe were inoculated directly from replete pre-cultures (20  $\mu\text{M}$  Fe) and analyzed for elemental composition by ICP-MS/MS at mid-logarithmic growth phase ( $2\text{-}3 \times 10^6$  cells $\cdot\text{ml}^{-1}$ ). In a parallel experiment, the cultures were inoculated from pre-cultures containing more matching Fe concentrations (1.0, 1.0, 1.0, 2.0, 10, 20, 100, and 200  $\mu\text{M}$  Fe-EDTA, respectively, Figure 13A, left). These cultures were sampled at mid-logarithmic growth ( $2 \times 10^6$  cells $\cdot\text{ml}^{-1}$ ), like the directly inoculated cultures, but additionally also in stationary growth phase ( $10 \times 10^6$  cells $\cdot\text{ml}^{-1}$ ).

In addition to cells, fractions of growth medium were taken from this experiment before inoculation and at both cell sampling points. Both, the iron status of the pre-culture and the sampling point within the growth curve, have significant impact on the elemental profile, specifically the cellular iron content (Figure 13A). First, looking at the impact of pre-culture Fe-status, mid-logarithmic iron content of cultures inoculated from replete (white) or iron pre-cultures (black circles, Figure 13A) does not differ at 2.0, 10, or 20  $\mu\text{M}$  Fe, cells contain between 10 and  $17 \times 10^7$  Fe atoms $\cdot\text{cell}^{-1}$ . When inoculated from Fe-depleted pre-cultures, Fe-limited cells have lower iron content than cells inoculated from replete cultures,  $2.2 \pm 0.5$  vs.  $4.8 \pm 0.4$ ,  $3.7 \pm 0.4$  vs.  $6.4 \pm 0.4$  and  $8.6 \pm 0.4$  vs.  $10.6 \pm 1.4 \times 10^7$  Fe atoms $\cdot\text{cell}^{-1}$  at 0.10, 0.25 and 1  $\mu\text{M}$  Fe, respectively. The cellular iron content of the pre-culture is already reduced compared to replete cultures, equal to 1.0  $\mu\text{M}$  inoculated from replete. Iron-excess cultures started from replete pre-cultures accumulate 1.8- and 2.4-fold more iron at 100 and 200  $\mu\text{M}$  than at 20  $\mu\text{M}$  Fe,  $27.9 \pm 2.5$ ,  $37.5 \pm 5.1$ , and  $15.8 \pm 2.0 \times 10^7$

## 2. Results

Fe atoms·cell<sup>-1</sup>, respectively. When inoculated from already over-accumulating pre-cultures (equal to 200 μM Fe inoculated from replete pre-cultures), cells accumulate 2.6- and 4.5-fold more iron than in replete conditions,  $43.3 \pm 3.5$ ,  $74.3 \pm 2.7$ , and  $16.7 \pm 0.6 \times 10^7$  Fe atoms·cell<sup>-1</sup>, respectively.

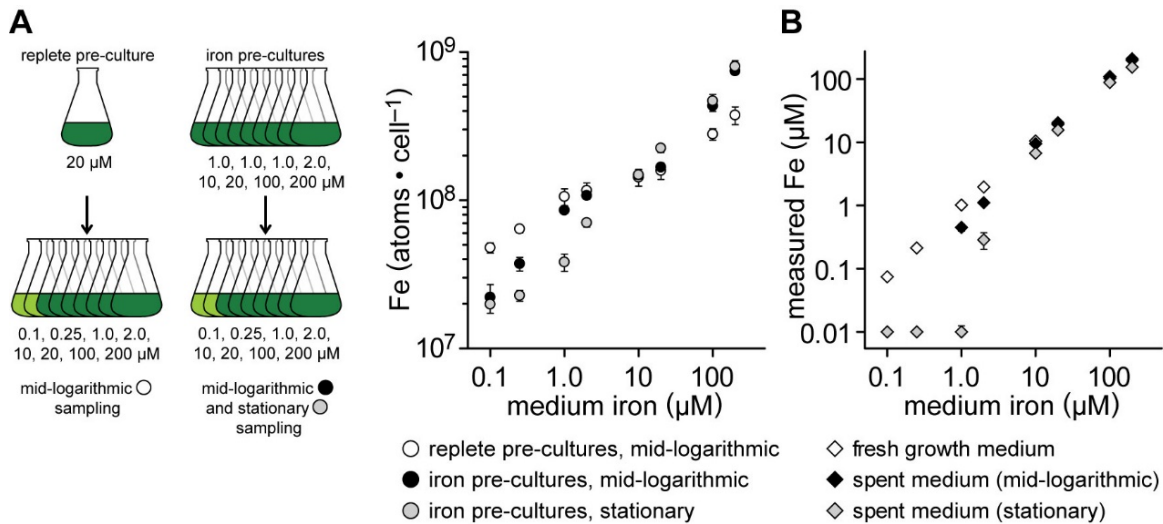


**Figure 13. Iron content as a function of pre-culture condition and growth phase. A:** In one experiment, photoheterotrophic cultures containing 0.10, 0.25, 1.0, 2.0, 10, 20, 100 and 200 μM Fe were inoculated from replete cultures and grown to a density of  $2-3 \times 10^6$  cells·ml<sup>-1</sup> (white circles). In a second experimental setup, photoheterotrophic cultures containing 0.10, 0.25, 1.0, 2.0, 10, 20, 100 and 200 μM Fe were inoculated from pre-cultures containing 1.0, 1.0, 1.0, 2.0, 10, 20, 100, and 200 μM iron, respectively, and grown to a density of  $2-3 \times 10^6$  cells·ml<sup>-1</sup> for mid-logarithmic sampling (black circles) and  $10 \times 10^6$  cells·ml<sup>-1</sup> for stationary sampling (grey circles). Iron content was analyzed by ICP-MS/MS from cell lysates and related to the number of cells analyzed. The mean of three (white circles, replete pre-cultures) or four (black and grey circles, iron pre-cultures) replicates are shown, error bars represent SD. **B:** Iron concentrations of freshly prepared growth medium (white diamonds), cell-free spent medium at  $2-3 \times 10^6$  cells·ml<sup>-1</sup> for mid-logarithmic (black diamonds) and at  $10 \times 10^6$  cells·ml<sup>-1</sup> for stationary growth phase (grey diamonds) were determined by ICP-MS/MS and expressed as micromolar concentration. The mean of four replicates is shown, error bars represent SD.

Comparing cultures at mid-logarithmic and stationary growth phase (black and grey circles, Figure 13A), only cultures grown at 10 μM Fe exhibited no significant difference in cellular iron content. At 2.0, 1.0, and 0.25 μM, the iron content is significantly reduced at stationary compared to mid-logarithmic growth phase. Cells from cultures started with 0.10 μM Fe in the growth medium had already used up the measurable extracellular iron early in the growth curve. At mid-logarithmic phase, the cells contained already the lowest tolerable iron content and soon after, growth stopped entirely. The steady state iron content was at the lowest possible value for photoheterotrophic cultures and did not decrease further. At 20 μM the cellular content was increased by  $5.8 \times 10^7$ , from  $16.7 \pm 0.6$  to  $22.4$

## 2. Results

---

$\pm 1.4 \times 10^7$  atoms $\cdot$ cell $^{-1}$ . Reaching a steadier equilibrium once in stationary growth phase did not increase the iron content of excess cultures further, cells contained  $43.3 \pm 3.5$  and  $46.7 \pm 5.0$  at 100  $\mu$ M, or  $74.3 \pm 2.7$  and  $79.8 \pm 7.5 \times 10^7$  Fe atoms $\cdot$ cell $^{-1}$  at 200  $\mu$ M Fe, respectively. Individual *p*-values comparing the iron content between the conditions are listed in Supplemental Table 9. Other than iron, the cellular Mn content decreased, and the Cu content increased in low extracellular iron as expected and described before, and there were no major changes in the other elements (Supplemental Figure 10).

Figure 13B shows the measured iron concentration in the growth medium before inoculation as well as at mid-logarithmic and stationary growth phase. In mid-logarithmic growth phase ( $2 \times 10^6$  cells $\cdot$ ml $^{-1}$ ), cells had doubled seven to eight times since inoculation. In the stationary phase, cells had doubled between nine and eleven times. The extracellular iron concentration was at or below detection limit in Fe-limited conditions (0.10 and 0.25  $\mu$ M Fe), because the cells had consumed all the Fe. Cultures containing 1.0 and 2.0  $\mu$ M Fe at inoculation had used up 0.57  $\mu$ M (46%) and 0.85  $\mu$ M (58%) of their available extracellular iron. Cultures containing 10 and 20  $\mu$ M Fe had used up 1  $\mu$ M, cultures containing 100 and 200  $\mu$ M Fe had used up 6 and 10  $\mu$ M Fe, respectively. At stationary growth phase, cultures inoculated at 1  $\mu$ M Fe had also used up all detectable iron. All other cells used up 1.7, 3.8, 4.7, 21.7, and 54.1  $\mu$ M Fe (or 84, 36, 23, 20, and 10% of the available iron of 2, 10, 20, 100, and 200  $\mu$ M Fe cultures). Individual *p*-values comparing the extracellular iron concentrations between the samples are listed in Supplemental Table 10. There were no major decreases in the extracellular concentrations of P, S, Mg, K, Ca and Cu in fresh or spent medium (Supplemental Figure 11), Mn and Zn concentrations were reduced slightly in some samples, but not more than 30%.

In order to analyze the impact of cells exposed to an extended stationary growth phase on the overaccumulation of iron (Figure 14A), I performed an additional experiment, comparing the elemental composition of replete (20  $\mu$ M) and excess (200  $\mu$ M) Fe cultures, inoculated from replete pre-cultures for the first four days in stationary growth phase. Before stationary, when coming from replete pre-cultures, excess extracellular iron led to an accumulation of about two-fold ( $16.0 \pm 1.7$  and  $37.0 \pm 2.3 \times 10^7$  atoms $\cdot$ cell $^{-1}$ ) when cells were in late logarithmic growth phase, the iron accumulation increased to four-fold after 4 days in stationary ( $19.59 \pm 0.83$  and  $90.75 \pm 4.75 \times 10^7$  Fe atoms $\cdot$ cell $^{-1}$ ).

## 2. Results

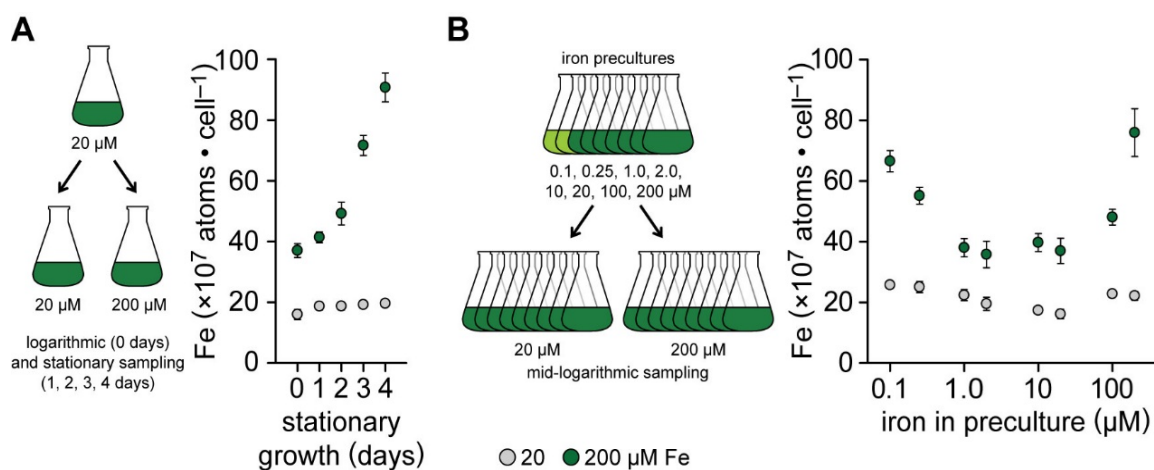


**Figure 14. Iron accumulation during stationary growth.** **A:** Photoheterotrophic cultures containing 20 and 200  $\mu\text{M}$  Fe were inoculated from replete cultures and the elemental composition was analyzed once the cultures reached  $10 \times 10^6$  cells $\cdot\text{ml}^{-1}$  (0 d) and every 24h following (1-4 d) by ICP-MS/MS from cell lysates. The mean of three replicates is shown, error bars represent SD. **B:** Photoheterotrophic cultures containing 0.10, 0.25, 1.0, 2.0, 10, 20, 100 and 200  $\mu\text{M}$  Fe were grown from inoculation to a density of  $2 \times 10^6$  (0.10 and 0.25  $\mu\text{M}$ ) or  $\sim 8 \times 10^6$  cells $\cdot\text{ml}^{-1}$  (all other), used to start cultures containing 20 and 200  $\mu\text{M}$  Fe at an initial cell density of  $1-2 \times 10^4$  cells $\cdot\text{ml}^{-1}$  and grown to  $2-3 \times 10^6$  cells $\cdot\text{ml}^{-1}$  for analysis by ICP-MS/MS. The mean of three replicates is shown, error bars represent SD.

In iron replete conditions, the iron content increased by a small amount between  $10 \times 10^6$  cells  $\text{ml}^{-1}$  (day 0) and one day of stationary (comparable to mid-log versus stationary before) and did not change further in prolonged stationary growth phase. Every day of stationary growth in excess conditions added more iron to the pool of accumulated Fe, from  $37.04 \pm 2.27$  to  $90.75 \pm 4.74 \times 10^7$  atoms $\cdot\text{cell}^{-1}$ . Individual *p*-values comparing the iron content between the samples are listed in Supplemental Table 11. P, S, Mg, K, Na, Ca, Mn, Zn, and Cu contents were not significantly changed during extended stationary growth phase (Supplemental Figure 12). This means that cells can accumulate Fe even when they are not growing, perhaps as a reservoir for the future.

In an additional experimental variation, medium containing 20 and 200  $\mu\text{M}$  Fe was inoculated from pre-cultures containing 0.10, 0.25, 1.0, 2.0, 10, 20, 100 and 200  $\mu\text{M}$  Fe-EDTA (Figure 14B) and cultures were analyzed for their elemental composition at mid-logarithmic growth phase. Excess cultures (200  $\mu\text{M}$ ) inoculated from iron limited (0.10 and 0.25  $\mu\text{M}$ ) or iron excess (100 and 200  $\mu\text{M}$ ) pre-cultures accumulated more iron than cultures inoculated from deficient or replete (1, 2, 10, 20  $\mu\text{M}$ ) pre-cultures. All had higher iron content than cultures in 20  $\mu\text{M}$  Fe, but the extent of hyperaccumulation was different. Fe-deficient and -replete pre-cultures led to the previously observed 2-fold increase in

## 2. Results

---

accumulated iron in excess from  $\sim 20$  to  $40 \times 10^7$  atoms $\cdot$ cell $^{-1}$ . Even replete cultures inoculated from Fe-limited or -excess cultures showed increased iron levels ( $25.7 \pm 1.0$ ,  $25.0 \pm 1.8$ ,  $22.3 \pm 1.8$ ,  $19.5 \pm 2.2$ ,  $18.3 \pm 0.9$ ,  $16.1 \pm 1.6$ ,  $22.8 \pm 1.0$ ,  $22.1 \pm 1.5 \times 10^7$  atoms $\cdot$ cell $^{-1}$  of replete cultures inoculated from pre-cultures containing 0.10, 0.25, 1.0, 2.0, 10, 20, 100, and 200  $\mu$ M Fe). Individual *p*-values comparing the iron content between the samples are listed in Supplemental Table 12. No major changes in the cellular composition of P, S, Mg, K, Na, Ca, Mn, Zn or Co were observed when replete and excess cultures were inoculated from pre-cultures with various extracellular iron concentrations (Supplemental Figure 13).

### 2.2.7 Influence of C-source on Fe-status-dependent Elemental Profiles.

It was reported before, that photoautotrophic iron deficiency/limitation exhibits unique differences to photoheterotrophic (Terauchi et al., 2010, Urzica et al., 2012). In an additional set of experiments, I systematically examined phenotypic parameters of trophic-dependent iron homeostasis over the whole range of concentrations and extending the analysis to heterotrophic growth conditions. Cells of strain CC-4532 were grown in photoheterotrophic, photoautotrophic and heterotrophic conditions, with one (instead of two, as before) concentration per defined state in the iron homeostasis: 0.25  $\mu$ M for Fe-limited, 1.0  $\mu$ M for -deficient, 20  $\mu$ M for -replete and 200  $\mu$ M for -excess. Figure 15 summarizes the results, analyses included cellular Fe, Mn and C content, generation time, chlorophyll content and  $F_v/F_m$  as a function of both iron nutrition and trophic status. The cellular iron content displayed small, but significant, alterations in the Fe-dependent iron pools (Figure 15A). In Fe-limiting conditions (0.25  $\mu$ M), photoautotrophic cultures were able to maintain a larger intracellular Fe pool than photoheterotrophic cultures, ( $4.5 \pm 0.7$  vs.  $3.3 \pm 0.3 \times 10^7$  atoms $\cdot$ cell $^{-1}$ ), and no significant alteration was observed in heterotrophic conditions compared to photoheterotrophic ( $3.4 \pm 0.4 \times 10^7$  atoms $\cdot$ cell $^{-1}$ ). In Fe-deficient conditions, this larger photoautotrophic iron pool was even more distinct ( $12.4 \pm 1.5$  vs.  $8.6 \pm 0.5 \times 10^7$  atoms $\cdot$ cell $^{-1}$ ), the heterotrophic iron pool was reduced compared to photoheterotrophic conditions ( $6.7 \pm 0.3 \times 10^7$  atoms $\cdot$ cell $^{-1}$ ). In Fe-replete conditions, the photoheterotrophic and photoautotrophic iron pools were comparable, the photoheterotrophic iron content was increased by  $\sim 7.5 \times 10^7$  Fe atoms $\cdot$ cell $^{-1}$  ( $17.0 \pm 1.7$ ,  $17.2 \pm 1.7$ , and  $24.8 \pm 2.0 \times 10^7$  atoms $\cdot$ cell $^{-1}$ ). When grown in the presence of excess

## 2. Results

extracellular iron, all three trophic states led to an over-accumulation of iron, photoautotrophic cultures displayed a 3.4-fold increase ( $57.4 \pm 5.2 \times 10^7$  atoms $\cdot$ cell $^{-1}$ ), photoheterotrophic a 4.2-fold increase ( $71.5 \pm 4.8 \times 10^7$  atoms $\cdot$ cell $^{-1}$ ) and heterotrophic a 3.5-fold increase ( $87.0 \pm 10.0 \times 10^7$  atoms $\cdot$ cell $^{-1}$ ). Individual *p*-values comparing the iron content between the samples are listed in Supplemental Table 13.

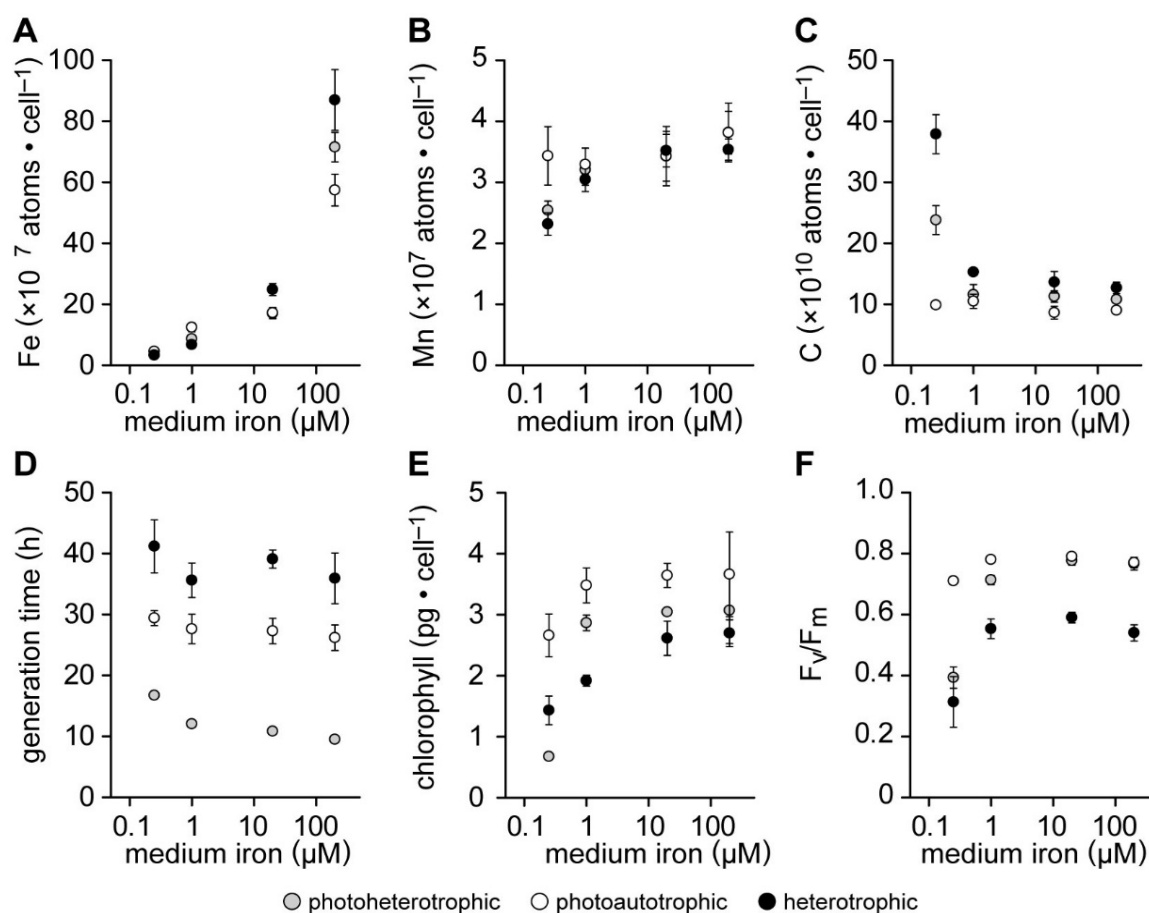


**Figure 15. Phenotypic description of Fe nutrition and trophic state.** Cultures containing 0.25, 1.0, 1.0, 20 and 200  $\mu$ M Fe-EDTA were inoculated from pre-cultures containing 1.0, 1.0, 20 and 200  $\mu$ M extracellular iron, respectively, and were grown in the presence of acetate and light (photoheterotrophic), air and light (photoautotrophic), or acetate (heterotrophic) to a density of  $2-3 \times 10^6$  cells $\cdot$ ml $^{-1}$  for analysis. **A:** Intracellular iron and **B:** manganese content were analyzed by ICP-MS/MS and related to the number of cells analyzed. **C:** Cellular carbon content was analyzed by TOC-TN. **D:** Growth was monitored from inoculation to stationary phase and the cell density was determined every 24h by manual counting (Hemocytometer). Generation time was calculated from the point when the culture reached  $1 \times 10^5$  cells $\cdot$ ml $^{-1}$  up to the first time point when the culture reached stationary growth phase. **E:** Total chlorophyll was extracted from  $4 \times 10^6$  cells with a mixture of 80% acetone/20% methanol (v/v) and absorption of the extract measured spectrophotometrically against a solvent blank. **F:** Maximum quantum efficiency of PSII ( $F_v/F_m$ ) was determined from  $2 \times 10^6$  cells immobilized onto a 15 mm round filter after dark-adaptation for 10-14 min using saturating light. The means of three replicates are shown, error bars represent sd.

## 2. Results

---

The cellular manganese content was responding differently between the trophic states in Fe-limiting conditions (Figure 15B), decreasing in photoheterotrophic and heterotrophic, but not in photoautotrophic conditions ( $2.5 \pm 0.2$ ,  $2.3 \pm 0.2$ , and  $3.4 \pm 0.5 \times 10^7$  atoms·cell<sup>-1</sup>, respectively;  $3.4 \times 10^7$  atoms·cell<sup>-1</sup> in photoheterotrophic replete conditions). Individual *p*-values comparing the Mn content between the samples are listed in Supplemental Table 14.

No major differences in P, S, Mg, K, and Ca content were found, Na content increased in heterotrophic Fe-limitation but by less than 2-fold (Supplemental Figure 14). The carbon content showed large differences between the trophic states in Fe-limitation, a 2.8-fold increase in heterotrophic conditions ( $37.9 \pm 3.2$  and  $13.6 \pm 1.8 \times 10^{10}$  atoms·cell<sup>-1</sup> in replete), a 2.1-fold in photoheterotrophic ( $23.8 \pm 2.4$  and  $11.3 \pm 0.9 \times 10^{10}$  atoms·cell<sup>-1</sup> in replete), and a small increase in photoautotrophic conditions ( $9.9 \pm 0.4$  and  $8.6 \pm 1.1 \times 10^{10}$  atoms·cell<sup>-1</sup> in replete) (Figure 15 C). Individual *p*-values comparing the carbon content between the samples are listed in Supplemental Table 15. The minor variations in Fe-deficient, -replete and -excess conditions between the three trophic conditions were mainly due to the difference in cell size (Supplemental Figure 15). Photoautotrophic cultures had decreased nitrogen content and cell volume compared to photoheterotrophic cultures (smaller cells) and were increased in heterotrophic conditions (larger cells) with only small Fe-dependent differences (cells are a little bigger in cultures with 0.25  $\mu$ M Fe, in all three trophic states).

In photoheterotrophic conditions, the generation time increased with lower extracellular iron, decreased in excess conditions (grey, Figure 15 D and Figure 4) and exceeded photoautotrophic and heterotrophic growth (single-trophic) in all iron concentrations. No significant differences between the iron states were found in photoautotrophic or heterotrophic growth. The individual growth curves used for the calculation of the generation times are shown in Supplemental Figure 16. Individual *p*-values comparing the growth rates between the samples are listed in Supplemental Table 16.

The cellular chlorophyll content displayed both Fe- and trophic-dependent behavior (Figure 15 E). Photoheterotrophic chlorophyll levels remained unchanged in Fe-deficient, -replete, and -excess conditions ( $2.9 \pm 0.1$ ,  $3.0 \pm 0.1$ , and  $3.1 \pm 0.5$  pg·cell<sup>-1</sup>, respectively) and were reduced by 78% ( $0.7 \pm 0.1$  pg·cell<sup>-1</sup>) in Fe-limitation. Photoautotrophic chlorophyll content was generally higher than photoheterotrophic, also remained unchanged in Fe-deficient, -replete, and -excess conditions ( $3.5 \pm 0.3$ ,  $3.6 \pm 0.2$ , and  $3.7 \pm$

## 2. Results

---

0.7 pg·cell<sup>-1</sup>, respectively) and exhibited a much smaller, but still significant reduction in Fe-limited chlorophyll content by 27% ( $2.7 \pm 0.4$  pg·cell<sup>-1</sup>). Without exposure to light, the chlorophyll content was generally reduced, but cells still maintained chlorophyll. Chlorophyll in heterotrophic cells was unchanged in Fe-replete, and -excess conditions ( $2.6 \pm 0.3$  and  $2.7 \pm 0.2$  pg·cell<sup>-1</sup>), was already reduced to  $1.9 \pm 0.1$  pg·cell<sup>-1</sup> in Fe-deficiency and further reduced to  $1.4 \pm 0.2$  pg·cell<sup>-1</sup> in -limitation. Individual *p*-values comparing the chlorophyll content between the samples are listed in Supplemental Table 17. Similarly, the maximum quantum efficiency of PSII ( $F_v/F_m$ ) displayed both Fe- and trophic-dependent behavior (Figure 15 F). Photoheterotrophic  $F_v/F_m$  remained unchanged in Fe-deficient, -replete, and -excess conditions ( $0.71 \pm 0.02$ ,  $0.78 \pm 0.02$ , and  $0.77 \pm 0.02$ , respectively) and was reduced in Fe-limitation ( $0.39 \pm 0.04$ ). Photoautotrophic  $F_v/F_m$  remained unchanged in Fe-deficient, -replete, and -excess conditions ( $0.78 \pm 0.01$ ,  $0.79 \pm 0.01$ , and  $0.77 \pm 0.02$ , respectively) and was reduced in Fe-limitation ( $0.71 \pm 0.01$ ). Heterotrophic cells exhibited a general reduction in  $F_v/F_m$  compared to photoheterotrophic and -autotrophic conditions, remained unchanged Fe-deficient, -replete, and -excess conditions ( $0.50 \pm 0.06$ ,  $0.56 \pm 0.04$ , and  $0.57 \pm 0.07$ , respectively) and was reduced in Fe-limitation ( $0.31 \pm 0.08$ ). Individual *p*-values comparing  $F_v/F_m$  between the samples are listed in Supplemental Table 18. Since the differences in trophic status cause differences in the composition of photosynthetic complexes, DCMU-treated controls of all three trophic states were performed prior to the experimental samples (Supplemental Figure 17).

### 2.2.8 Iron Accumulation in Excess Fe Conditions is Affected in *vtc1*.

In order to study the effect of mutations to potential iron storage sites, I analyzed the iron accumulation in *vtc1*, which is deficient in correct acidocalcisome formation. This mutant, with altered ability to acclimate to S-deficiency was isolated by Aksoy et al. (2014) from a forward genetic screen for strains with impacted ability to acclimate to medium without added S. The gene effective in complementing the observed phenotype encodes the putative VTC1 subunit of the polyphosphate polymerase complex, which has also been called the vacuolar transporter chaperone complex (VTC). Transmission electron microscopy (TEM) analysis showed a lower number of electron dense acidocalcisomes (vacuoles containing polyphosphate granules) during S-starvation in the mutant and cells were more susceptible to other nutrient deprivations, including P-deficiency, but not the



## 2. Results

complemented strain. We received the *vtc1* mutant and *VTC1*-complemented strain as a kind gift from Arthur Grossman to test if in addition to the micronutrients S and P the homeostasis of micronutrients is affected by the lack of properly functioning acidocalcisomes. Genes directly affected by the insertional mutation and the complementation were verified by genome sequencing, in addition to the *VTC1* gene (Cre12.g510250), the neighboring gene (Cre12.g510252) was truncated by the transgene insertion in *vtc1* and the gene construct for complementation for *VTC1* inserted into a gene on Chromosome 14 (Cre14.g531250) (Supplemental Table 19). Only one allele of *vtc1* (CC-5321) and *VTC1* (CC-5324) were available at the time of the analysis, strain CC-4532 was included for comparison to other experiments performed in this thesis. Growth and photosynthetic parameters were verified in all three strains and did not show altered behavior compared to CC-4532 (Supplemental Figure 18, growth is shown as an example). For the elemental characterization of the mutant, cells of *vtc1*, *VTC1* and CC-4532 were grown in photoheterotrophic batch cultures in Fe-replete and -excess conditions and analyzed for the elemental composition by ICP-MS/MS.

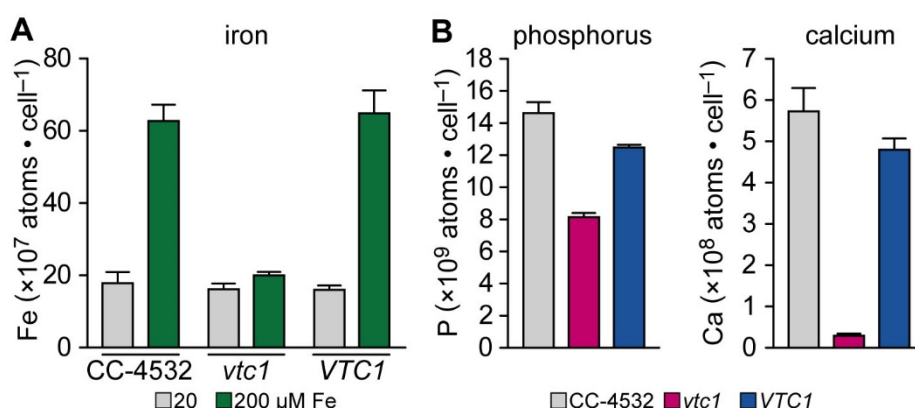


**Figure 16. Fe, P and Ca content of CC-45321, *vtc1* and *VTC1*.** Photoheterotrophic cultures containing 20 and 200  $\mu$ M Fe were inoculated with CC-4532, *vtc1* or *VTC1* from pre-cultures containing 20 and 200  $\mu$ M Fe, respectively, and grown to a density of  $2-3 \times 10^6$  cells  $\cdot$  ml $^{-1}$  for analysis by ICP-MS/MS of cell lysates and related to the number of cells analyzed. **A:** Cellular iron content comparing iron replete and iron excess conditions. **B:** Phosphorus and calcium content of strains CC-4532, *vtc1* and *VTC1* in iron replete growth conditions. The mean of four replicates is shown, error bars represent SD.

In replete conditions, the iron content was similar in all three strains. In excess conditions, CC-4532 and *VTC1* displayed a 3.5- and 4-fold Fe-accumulation, respectively, and the *vtc1* mutant exhibited a much lower, but still significant, accumulation by 1.2-fold (Figure

## 2. Results

---

16A). Individual *p*-values comparing the iron content between the samples are listed in Supplemental Table 20. In addition to the difference in iron composition, P and Ca showed specific alterations between the strains (Figure 16B). Compared to CC-4532, the P content of *VTC1* was reduced by 15% (CC-4532:  $14.6 \pm 0.7$  and *VTC1*:  $12.5 \pm 0.2 \times 10^9$  atoms·cell<sup>-1</sup>) and by 44% in the mutant ( $8.2 \pm 0.3 \times 10^9$  atoms·cell<sup>-1</sup>). Cellular Ca was reduced by 16% (CC-4532:  $5.7 \pm 0.6$  and *VTC1*:  $4.8 \pm 0.3 \times 10^8$  atoms·cell<sup>-1</sup>) and the most dramatic reduction was observed in the mutant, where only ~ 5% of wild-type levels were detected ( $0.29 \pm 0.05 \times 10^8$  atoms·cell<sup>-1</sup>). Individual *p*-values comparing the elemental content between the samples are listed in Supplemental Table 21. The Mg content is reduced by 24% in *vtc1*, all other elements exhibited similar levels between the three strains (Supplemental Figure 19).

### 2.2.9 Comparative Transcriptome Analysis of the *vtc1* Mutant.

In order to get a better understanding of the underlying mechanisms that result in differential iron accumulation in Fe excess conditions in the *vtc1* mutant, in addition to the Fe-excess transcriptome analysis of wild-type strain CC-4532, the mRNA abundance in the mutant strain *vtc1* and its corresponding complemented strain *VTC1* were analyzed between iron-replete and iron-excess conditions (Figure 17). Cells of both strains were grown in Fe-replete and -excess pre-cultures to late-logarithmic phase and used to inoculate three replicate experimental cultures containing 20 or 200  $\mu$ M Fe at a starting density of  $1-2 \times 10^4$  cells·ml<sup>-1</sup>, grown to  $2 \times 10^6$  cells·ml<sup>-1</sup>. In parallel to sampling for RNA, cells were collected from the same cultures for elemental analysis by ICP-MS/MS to verify the observed iron accumulation phenotype (Supplemental Figure 20).

The transcriptome in each sample was determined by RNA-Seq on the Illumina platform, together with the samples from strain CC-4532 (see Figure 6), the sequenced reads were aligned to the Au111.6 gene models and expression estimates calculated as FPKM (fragments per kilobase of transcript per million fragments mapped) using Cuffdiff. The between-sample variation of the three biological replicates is small for all four conditions (Supplemental Figure 21 and 22) and therefore the average expression was used for further analysis unless stated otherwise.

A minimum expression cutoff of  $\geq 1$  FPKM in at least one of the four conditions was applied to remove genes with low expression and resulted in 13'823 detected transcripts

## 2. Results

(Supplemental Figure 23). Genes were classified as differentially expressed using a false discovery rate of  $< 5\%$  and a minimum of 2-fold regulation. Applying these criteria, 1025 genes were identified whose transcripts accumulated differentially in the *vtc1* mutant compared to the complemented strain in standard growth conditions (Figure 17A).

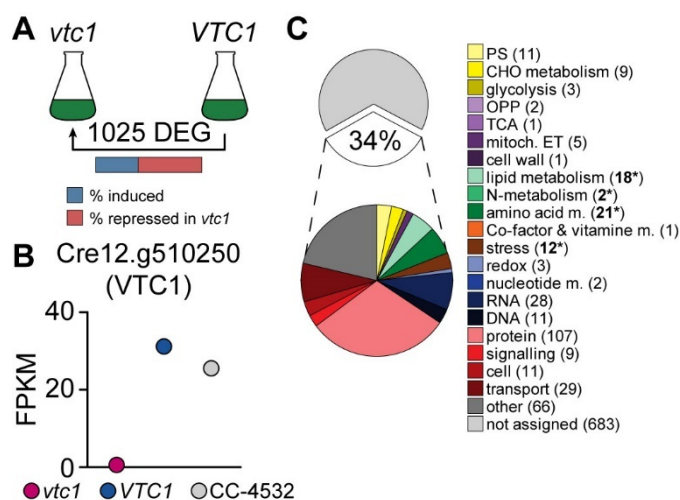


**Figure 17. Differentially expressed genes between *vtc1* and *VTC1*.** Cells of strains *vtc1* and *VTC1* were grown in iron-replete and -excess conditions, collected at  $2 \times 10^6$  cells·ml<sup>-1</sup>, mRNA was extracted, purified, and cDNA was generated for RNA-seq analysis. Replicate expression estimates of the Phytozome v5.5 gene models were averaged and are reported in FPKM for each gene. **A:** Differentially expressed genes (DEG) between *vtc1* and *VTC1* were extracted from the Cuffdiff output using additional selection ( $> 1$  FPKM in at least one on the samples,  $FDR < 5\%$ , fold change  $\geq 2$ ) as described before. **B:** Expression of gene Cre12.g510250 (*VTC1*) in the mutant (*vtc1*) and complemented strain (*VTC1*). **C:** DE genes were grouped according to the functional annotation of their protein sequence according to the MapMan annotation. The number of genes in each category is stated behind each group in parentheses and groups that are significantly ( $p$ -value  $> 0.05$ ) enriched against a group of randomly assigned genes are labeled with \* and highlighted in bold.

Of the 1025 transcripts, 615 genes had increased (60%), and 410 reduced transcript abundance in the mutant. One of the genes with the largest fold-change repression in the mutant was the *VTC1* gene, Cre12.g510250. The expression of *VTC1* was non-existent ( $< 0.1$  FPKM) and at about intrinsic levels in the complemented strain (31.2 FPKM in *VTC1*, 35.8 FPKM in CC-4532) (Figure 17B). For most neighboring genes, the expression

## 2. Results

---

was not affected by the mutation or complementation (Supplemental Figure 24). One neighboring gene, that is also partially disrupted by the insertion showed diminished expression in the mutant, as well as in the complemented strain (not rescued by the complementation).

For a functional characterization of the transcriptome response, the differentially expressed (DE) genes were grouped according to the annotation of their predicted protein sequence based on the MapMan ontology (Figure 17C). Of all detected transcripts in this comparison, 34% have been assigned functional annotations. Genes of all annotation groups were regulated. Genes in classes lipid, nitrogen and amino acid metabolism were enriched within the DE genes, as well as stress-related genes. The functional annotation groups of both induced and repressed gene models are summarized in Supplemental Figures 25. Genes involved in amino acid metabolism were enriched in both induced and repressed genes, compared to randomly assigned genes. Transport was enriched among the induced genes and genes without annotation were enriched among the repressed genes.

In addition to replete conditions, the *vtc1* mutant with its complemented strain were exposed to excess extracellular iron and the transcriptome assessed by RNAseq. Applying the selection criteria described above resulted in 3513 DE genes among all four VTC-samples (Figure 18). The number of differentially expressed genes between any two samples was not evenly distributed, the lowest number of DE genes was observed between Fe-replete and -excess conditions in the *vtc1* mutant (421 genes), followed by Fe-excess *vtc1* versus Fe-replete *VTC1* (553 genes), and Fe-replete versus -excess *VTC1* (867 genes). The number of excess iron-dependent differentially expressed genes was much larger compared to CC-4532 (46 DE genes, Figure 12).

Genes encoding proteins and complexes in multiple energy conversion pathways and general housekeeping functions were enriched among the DE genes, including photosynthesis, glycolysis, gluconeogenesis, TCA cycle, lipid, amino acid and sulfur metabolism, as well as general stress response (Supplemental Figure 26). The expression profile of the 3513 differentially expressed genes were plotted as a z-score normalized, clustered heatmap (Figure 18C). A large proportion of the 3513 DE genes showed a gradual response from Fe-replete *vtc1* cells to the Fe-excess *VTC1* as indicated by the two large blocks in the heatmap converging from yellow to blue and blue to yellow (from left to right).

## 2. Results

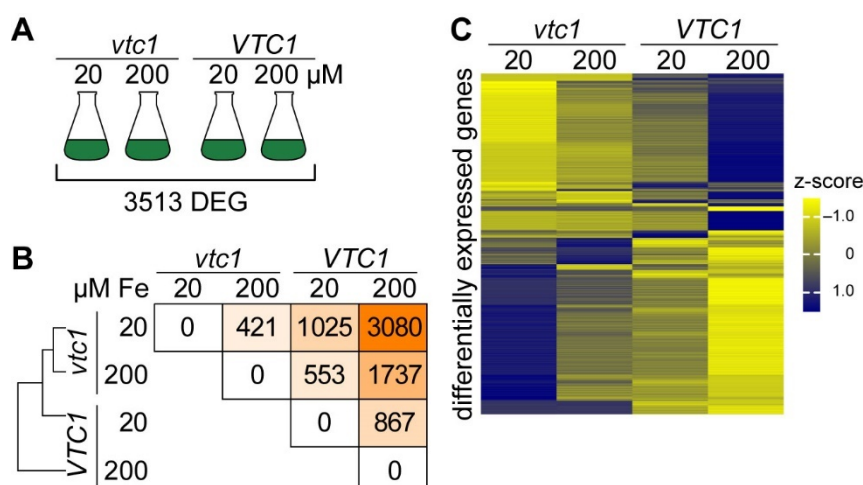


**Figure 18. Whole transcriptome analysis of *vtc1* and *VTC1*.** Cells of strains *vtc1* and *VTC1* were grown in iron-replete and -excess conditions and collected at a density of  $2 \times 10^6$  cells·ml<sup>-1</sup>. RNA was extracted and purified, mRNA selected, and cDNA generated for RNA-seq analysis. Replicate expression estimates of the Phytozome v5.5 gene models were averaged and are reported in FPKM for each gene. **A:** Differentially expressed (DE) genes were extracted from the Cuffdiff output using additional selection ( $> 1$  FPKM in at least one of the samples, FDR  $< 5\%$ , fold change  $\geq 2$ ). **B:** DE genes between individual samples are shown, the color gradient from white to orange indicates the number of DEG from minimum to maximum. The distance tree left of the matrix was calculated based on the number of differentially expressed genes between the strains and iron concentrations. **C:** A heatmap containing the z-score normalized expression of all 3513 DE genes.

### 2.2.10 Common transcriptomic response to excess iron.

The excess iron response in the wild-type strain CC-4532 was much more limited than in both the *vtc1* mutant and its complemented strain, pointing to potential differences in between individual Chlamydomonas strains to accommodate elevated iron concentrations. In order to identify the similarities and differences in between the strains, I analyzed the response of the transcriptome in between iron-replete and iron-excess conditions in the three different strains more detailed (Figure 19A). CC-4532 and *vtc1* had both about same percentage of induced versus repressed genes (59 and 61% induced in excess Fe, respectively), *VTC1* complemented had not only a larger overall number of DE genes but also the percentage of induced and repressed genes was shifted (only 31% induced in Fe-excess conditions).

Most of the genes regulated in the wild-type strain (25 of 46) were found to be similarly regulated in *vtc1* and the complemented strain (Figure 19B). In between *vtc1* and *VTC1*,

## 2. Results

119 genes showed a shared reaction, this group includes many genes identified as low iron-responsive genes, while the majority of genes changing were uniquely regulated in either *vtc1* or the complemented strain. When comparing the overlap between *vtc1* and the complemented strains to the published low Fe transcriptome response (Urzica et al., 2012), these were mostly genes that were DE between 1 and 20 Fe.

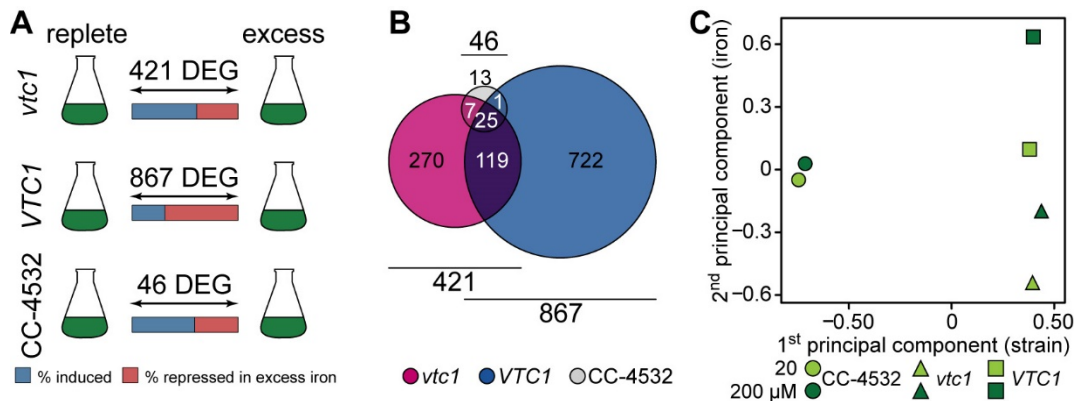


**Figure 19. Differentially expressed genes at excess conditions.** **A:** DE genes between iron-replete and -excess conditions in the strains *vtc1*, *VTC1* and CC-4532 were extracted from the Cuffdiff output using additional selection as described above. **B:** Venn diagram displaying the number of shared and unique DEG in iron-excess conditions between the three strains. **C:** A principal component analysis was generated from all six samples using cummeRbund (detailed in section 4.2). The first principal component refers to the variation due to the different strain backgrounds, The second is the extracellular iron concentration.

To display the overall relationship of all six Fe-excess samples, a principal component analysis was performed to determine what fraction of the dataset's variations is caused by which variable (Figure 19C). The first component recapitulated variation due to the different strain backgrounds, showing large differences between CC-4532 on the left side and the VTC-strains on the right side. The *vtc1* mutant (triangle) and *VTC1* complemented (square) grouped together with regard to the strain background. The second principal component was separating the external iron concentration, which accounted for a smaller fraction of the variation than the difference between strains CC-4532 and *vtc1/VTC1*. The variation between replete and excess iron in strain CC-4532 was small compared to *vtc1/VTC1*. It is interesting to note, that *vtc1* in Fe-excess conditions clustered closest to Fe-replete CC-4532 with regard to iron, *VTC1* Fe-replete closest to CC-4532 in Fe-excess; and *vtc1* in Fe-excess closest to *VTC1* Fe-replete. PCA of the individual replicates in Supplemental Figure 27.

## 2. Results

### 2.2.11 *vtc1* is More Sensitive to Oxidative Stress Fe-excess Conditions.

Excess Fe contributes to the production of ROS, Chlamydomonas cells grown in excess extracellular iron are more sensitive to photooxidative stress (Long and Merchant, 2008), high photon flux densities of  $500 \mu\text{mol}\cdot\text{m}^{-2}\cdot\text{s}^{-1}$  were shown to be lethal to cells of CC-4532 in the presence of  $200 \mu\text{M}$  Fe. Since the characterization of the *vtc1* mutant showed alterations in iron homeostasis compared to the complemented and wild-type strain but those differences did not lead to an impact on growth at standard growth conditions, I wondered if the many changes in the transcriptome of the mutant in response to excess iron were able to successfully mediate some of the detrimental effects resulting from the absence of functional acidocalcisomes in *vtc1*. I therefore analyzed the sensitivity to photooxidative stress dependent on the amount of iron present in the media as an additional marker to test the fitness of *vtc1* (Figure 20).

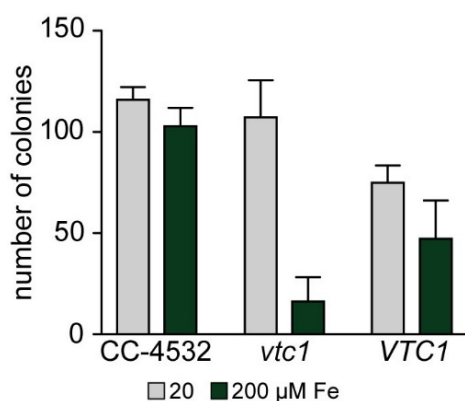


**Figure 20. Growth at high light conditions.** Photoheterotrophic cultures containing 20 and  $200 \mu\text{M}$  Fe were inoculated with CC-4532, *vtc1* and *VTC1* from pre-cultures containing 20 and  $200 \mu\text{M}$  Fe, respectively, and grown to a density of  $2-3 \times 10^6$  cells $\cdot\text{ml}^{-1}$ . An aliquot of  $1 \times 10^4$  cells was spread evenly onto dishes containing TAP-agar with 20 or  $200 \mu\text{M}$  Fe. Dishes were either exposed to standard ( $60 \mu\text{mol}\cdot\text{m}^{-2}\cdot\text{s}^{-1}$ ) or medium-high ( $350 \mu\text{mol}\cdot\text{m}^{-2}\cdot\text{s}^{-1}$ ) photon flux density for 7 d until the number of colonies was determined. The mean colonie number from three individual plates is shown for each condition, error bars represent SD.

The sensitivity was reproduced and verified for CC-4532 and in an initial pre-experiment, recovery at different photon flux densities was tested. A light intensity of  $350 \mu\text{mol}\cdot\text{m}^{-2}\cdot\text{s}^{-1}$  was chosen, where cells of CC-4532 were able to recover even when grown on plates with  $200 \mu\text{M}$  Fe. Cells of the three strains CC-4532, *vtc1* and *VTC1* were grown in replete liquid pre-cultures to a density of  $2-3 \times 10^6$  cells $\cdot\text{ml}^{-1}$  and  $1 \times 10^4$  cells were spread evenly onto dishes containing TAP-agar with 20 or  $200 \mu\text{M}$  Fe. Plates were either exposed to standard ( $60 \mu\text{mol}\cdot\text{m}^{-2}\cdot\text{s}^{-1}$ ) or medium-high ( $350 \mu\text{mol}\cdot\text{m}^{-2}\cdot\text{s}^{-1}$ ) photon flux density and the number of colonies were determined after 7 d of growth. All three replicate plates for each condition were grown in parallel, the plates were rotated occasionally, and condensation removed when necessary. For strain CC-4532, the increased photon flux density did not

## 2. Results

---

alter the viability at 20 or 200  $\mu\text{M}$  Fe ( $116 \pm 6$  and  $103 \pm 9$  colonies, respectively). The *vtc1* mutant however showed a significant decrease in the number of recovered colonies by 85% when grown in iron excess conditions ( $16 \pm 12$  colonies, and  $107 \pm 18$  in replete). Cells of the complemented strain *VTC1* exhibited an overall lower number of viable colonies but showed no significant difference between Fe-replete and -excess conditions ( $75 \pm 9$  and  $47 \pm 19$  colonies). Individual *p*-values comparing the number of colonies between the samples are listed in Supplemental Table 22.

### 2.3 Dynamic acclimations to Changes in Extracellular Iron.

#### 2.3.1 Over-accumulated Iron Can Be Remobilized When Necessary.

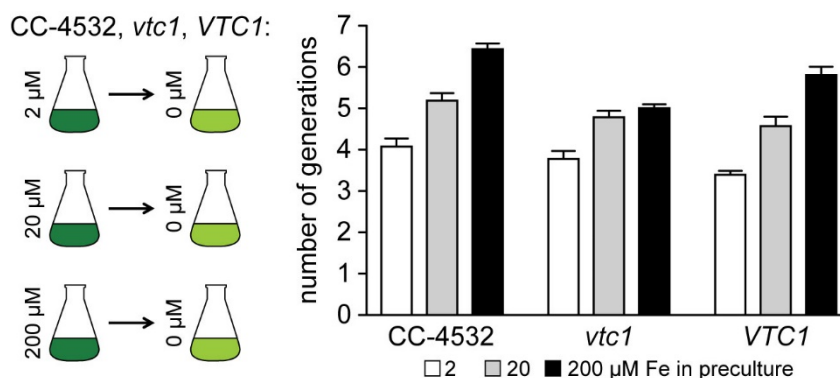
In order to assess the potential function of the additional intracellular iron accumulated in iron-excess conditions, specifically to distinguish sequestration to prevent damage versus a potential role in storage for anticipated iron shortage periods, I aimed first to identify if the additional iron stored is bioavailable. Cells of CC-4532, *vtc1* and *VTC1* were entrained in photoheterotrophic pre-cultures containing 2, 20, and 200  $\mu\text{M}$  Fe for multiple rounds, before cultures were grown to mid-logarithmic growth ( $5 \times 10^6$  cells·ml<sup>-1</sup>) before being transferred to medium without added iron at a starting density of  $1 \times 10^6$  cells·ml<sup>-1</sup>. To minimize iron carry-over, cells were washed with EDTA and fresh TAP medium without added iron before the transfer to iron-free medium. The number of doublings each culture was able to achieve with the initially provided iron within 9 days (12h after inoculation, removing noise from the initial lag-phase or the transfer procedure) was monitored for four replicates.

Figure 21 shows that the accumulated iron in CC-4532 and the complemented strain gave a growth advantage when extracellular Fe became unavailable. The *vtc1* mutant showed similar iron content as CC-4532 in replete conditions but did not accumulate excess iron to the same extent (Figure 10) and in relation to this facilitated additional growth between 2 and 20  $\mu\text{M}$  Fe in the pre-culture, but no additional growth when coming from excess ( $3.8 \pm 0.2$ ,  $4.8 \pm 0.2$  and  $5.0 \pm 0.1$  doublings, respectively). In strain CC-4532, replete cells contain about  $6 \times 10^7$  Fe atoms·cell<sup>-1</sup> more than mildly Fe-deficient cells at 2  $\mu\text{M}$  Fe ( $10.7 \pm 0.6$  vs.  $16.7 \pm 0.6 \times 10^7$  atoms·cell<sup>-1</sup>, see Figure 12). This additional intracellular iron facilitated longer growth:  $4.08 \pm 0.20$ ,  $5.19 \pm 0.18$ , and  $6.44 \pm 0.14$  doublings after transfer to iron-



## 2. Results

free medium (mean  $\pm$  standard deviation, from Fe-deficient, -replete, and -excess cultures, respectively).



**Figure 21. Growth after the transition to iron-free growth medium.** Photoheterotrophic cultures containing 2, 20 and 200  $\mu\text{M}$  Fe-EDTA were inoculated with CC-4532, *vtc1* or *VTC1* from pre-cultures containing 2, 20 or 200  $\mu\text{M}$  Fe, respectively, and grown to a density of  $2\text{--}3 \times 10^6$  cells $\cdot\text{ml}^{-1}$ . Cells were washed twice with 1 mM Na-EDTA and once with purified water and transferred to fresh photoheterotrophic growth medium without added iron to an initial cell density of  $1 \times 10^5$  cells $\cdot\text{ml}^{-1}$ . Growth was monitored from inoculation to stationary phase, the cell number was determined every 24h by manual counting (Hemocytometer) and the number of generations until stationary phase for each independent culture was calculated. The mean of four replicate cultures is shown for each condition, error bars represent SD.

The *VTC1* complemented strain showed similar iron content as CC-4532 in both replete and excess Fe and exhibited the same iron salvaging behavior, cultures inoculated from 2, 20 and 200  $\mu\text{M}$  Fe doubled  $3.4 \pm 0.1$ ,  $4.6 \pm 0.2$ , and  $5.8 \pm 0.2$  times when extracellular iron became unavailable. This shows that the *VTC1* required for Fe storage is beneficial for cells that encounter Fe starvation. Individual *p*-values of doublings between the conditions are listed in Supplemental Table 23. The individual growth curves used for the calculation of doublings after transfer to iron-free medium are shown in Supplemental Figure 28.

### 2.3.2 Iron Re-supply to Fe-starved *vtc1* Cultures.

The accumulated iron in wild-type *Chlamydomonas* strains gave a growth advantage when iron became unavailable, and this gain was proportional to the quantity of accumulated iron, pointing to a role of the acidocalcisome in facilitating the accumulation of extra iron. Additionally, storage compartments facilitate intracellular buffering of (temporary) fluctuations in intracellular iron concentrations, e.g. when iron becomes suddenly available

## 2. Results

---

to starved cells, due to external, environmental changes or internally during transition between individual metabolic states with different iron requirements.

To test a role of the acidocalcisomes in this aspect of storage compartment, cells of CC-4532, *vtc1* and *VTCl* were grown in iron-deficient pre-cultures with 1  $\mu\text{M}$  Fe from inoculation to late-logarithmic phase ( $1\text{-}2 \times 10^4$  to  $9 \times 10^6$  cells $\cdot\text{ml}^{-1}$ ) to deplete the iron pools resulting from luxurious growth, before being transferred to medium without added iron at a density of  $1 \times 10^4$  cells $\cdot\text{ml}^{-1}$  and grown for 3 (CC-4532) or 3.5 d (*vtc1* and *VTCl*) until the cultures reached  $\sim 1 \times 10^6$  cells $\cdot\text{ml}^{-1}$  (Figure 22A). Fe-EDTA was added at the indicated concentrations (2, 20 and 200  $\mu\text{M}$ ) and the cultures were analyzed 0, 2, 4, 6, 12, 24 and 48h after the addition of iron for growth (viability) and elemental composition by inductively coupled plasma tandem mass spectrometry (ICP-MS/MS).

Growth curves of CC-4532 (grey), *vtc1* (pink), and *VTCl* (blue) after the addition of Fe at 0h were grouped by the concentration of iron added. Starting two hours after the addition of 2  $\mu\text{M}$  Fe, strains CC-4532 and *VTCl* picked up growth again, whereas the *vtc1* mutant showed a significant lag in growth after iron became available again. Twelve hours after the iron re-supply, the *vtc1* mutant's growth caught up with the other two, and all strains reached late logarithmic phase at 48h (Figure 22B).

Adding 20 or 200  $\mu\text{M}$  Fe to starved cultures lead to a longer and more severe growth lag in the *vtc1* mutant (Figure 22C and D). After 12 h, the cell number of the *vtc1* mutant increased to  $1.8 \pm 0.3$ ,  $1.2 \pm 0.2$ , and  $1.2 \pm 0.1 \times 10^6$  cells $\cdot\text{ml}^{-1}$  when 2, 20, or 200  $\mu\text{M}$  Fe was added, and to  $3.7 \pm 0.6$ ,  $2.7 \pm 0.3$ , and  $2.8 \pm 0.4 \times 10^6$  cells $\cdot\text{ml}^{-1}$  after 24 h, respectively. CC-4532 and *VTCl* did not exhibited a significant delay in growth in response to the iron re-supply. Individual *p*-values of cell number between the conditions are listed in Supplemental Table 24.

In addition to the sensitivity to iron re-supply to starved cells assessed through growth, changes in the elemental composition were examined. All three strains, including the *vtc1* mutant, temporarily took up large amounts of iron when 20 or 200  $\mu\text{M}$  were added to iron starved cultures (Figure 23). At the beginning of the time course, all cultures exhibited low intracellular iron pools of  $\sim 2.5 \times 10^7$  atoms $\cdot\text{cell}^{-1}$ . The cellular iron content is grouped by strain, and the iron content of steady state cultures (Figure 10) is displayed as dashed lines for reference. When a lower-than replete iron concentration was added (2  $\mu\text{M}$ , white circles), all three strains reached their maximum iron accumulation of  $\sim 15\text{-}20 \times 10^7$  atoms cell $^{-1}$  after 6h and maintained this content up to late logarithmic growth phase (48 h).

## 2. Results

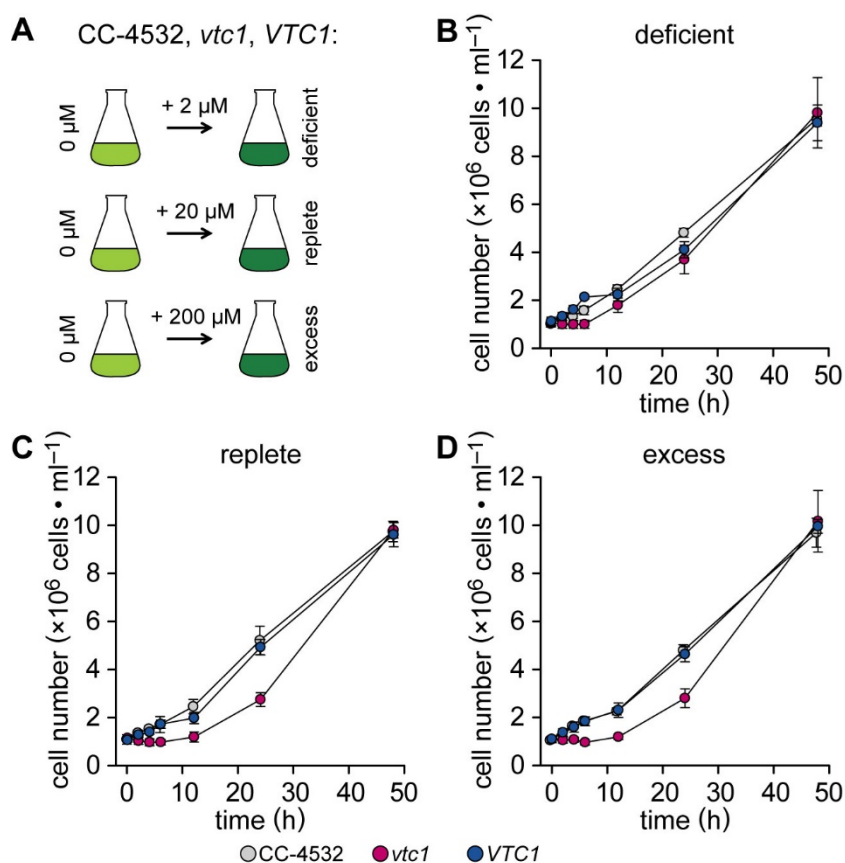


**Figure 22. Growth after the re-supply of iron.** **A:** Photoheterotrophic cultures containing no added iron were inoculated with CC-4532, *vtc1* and *VTC1* from pre-cultures containing 1  $\mu\text{M}$  Fe, grown to a density of  $1 \times 10^6$  cells $\cdot$ ml $^{-1}$  and Fe was added to the cultures at the indicated concentrations. Growth of **B:** iron deficient, **C:** replete, and **D:** excess cultures was assessed by monitoring the cell density at 0, 2, 4, 6, 12, 24, and 48h after the addition of Fe by manual counting (Hemocytometer). The mean of four replicates is shown for each condition, error bars represent SD.

When 20 or 200  $\mu\text{M}$  Fe were added, the intracellular iron content increased more than 50-fold during the first 12h to maximum levels of  $147.0 \pm 25.2$  and  $146.2 \pm 30.0$ ,  $154.5 \pm 14.6$  and  $198.7 \pm 29.7$ , and  $122.0 \pm 7.2$  and  $170.4 \pm 38.2 \times 10^7$  atoms $\cdot$ cell $^{-1}$  (20 and 200  $\mu\text{M}$  Fe, in CC-4532, *vtc1* and *VTC1*, respectively) correlating to 2.3-, 9.9- and 2.6-fold higher levels than observed in steady state Fe-excess. The highest uptake rate was observed in the first 2 h, increases of 13- and 13-, 13- and 34-, and 19- and 22-fold of intracellular iron in 20 and 200  $\mu\text{M}$  Fe of CC-4532, *vtc1* and *VTC1*, respectively, followed by rates less than 2-fold of the prior sampling time point. Even though the *vtc1* mutant did not accumulate iron to the same extent as *VTC1* or CC-4532 in steady state, the cells temporarily took up large amounts of iron. The largest increase of 112-fold (Fe-starved to 6h at 200  $\mu\text{M}$  Fe) as

## 2. Results

well as the highest content of  $198.7 \pm 29.7 \times 10^7$  cells $\cdot$ ml $^{-1}$  at 6h in excess conditions was observed in the mutant, representing an almost 10-fold increase over steady state excess conditions. In strain CC-4532, the only difference in iron content observed between 20 and 200  $\mu$ M iron was 24h after the addition, where cells exposed to 20  $\mu$ M Fe showed a 30% reduction of maximum iron content, whereas cells exposed to 200  $\mu$ M Fe displayed maximum levels. Both *vtc1* and *VTC1* displayed a bigger difference in maximum iron of up to 28% additional accumulated atoms in excess conditions. After the maximum content at 6 or 12h was reached, the cellular iron content decreased again to levels similar to Fe-excess steady state pools (CC-4532:  $45.5 \pm 9.4$  and  $45.9 \pm 4.8$ , *vtc1*:  $25.5 \pm 2.2$  and  $31.7 \pm 3.1$ , and *VTC1*:  $38.0 \pm 4.4$  and  $50.2 \pm 3.7 \times 10^7$  atoms $\cdot$ cell $^{-1}$  in 20 and 200  $\mu$ M Fe). Individual *p*-values comparing the iron content between the samples are listed in Supplemental Table 25. When normalizing the Fe- to the S-content of the same sample, *vtc1* and *VTC1c* accumulated almost 2-times more iron than CC-4532 (Supplemental Figure 29). Fluctuations in the cellular P, S, and Mg, K, Na, and Ca, and Mn, Zn and Cu content in response to the iron supply are shown in Supplemental Figures 30, 31, and 32.

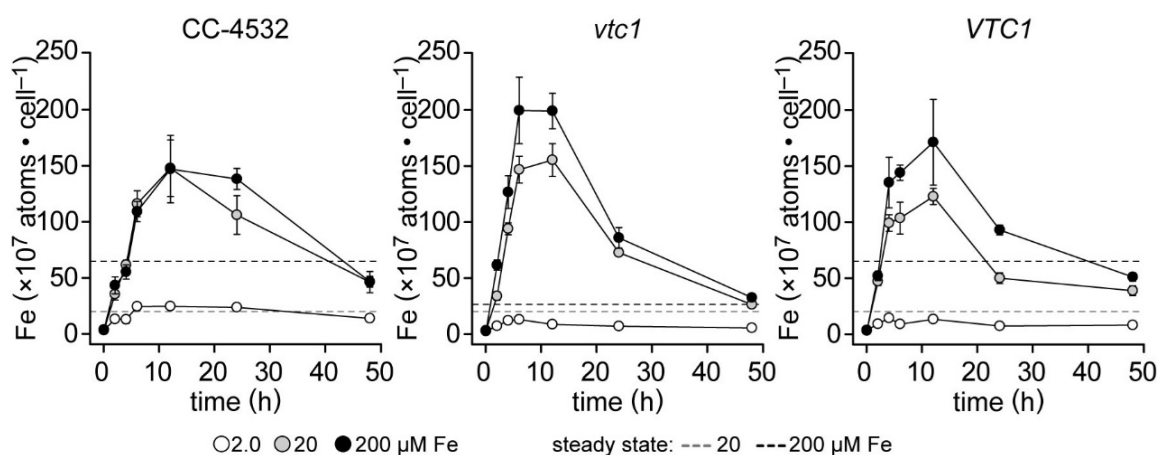


**Figure 23. Iron content after re-supply of iron to starved cultures.** Photoheterotrophic cultures containing no added iron were inoculated with CC-4532, *vtc1* and *VTC1* from pre-cultures containing 1  $\mu$ M Fe to a density of  $1 \times 10^6$  cells $\cdot$ ml $^{-1}$  and Fe was added to the cultures at the indicated concentrations. Cellular iron content was assessed by ICP-MS/MS analysis of cell lysates at 0, 2, 4, 6, 12, 24, and 48h after the addition of Fe to the cultures and was related to the number of cells analyzed. The mean of four replicates is shown, error bars represent SD. Dashed lines show the cellular iron content of steady state cultures of the strains containing 20 (grey) or 200  $\mu$ M (black) Fe in the growth medium.

### 2.4 Acclimation to Heterotrophic Carbon During Iron Starvation.

Iron limitation has severe cellular effects, including decreased cellular iron content, reduced photosynthetic capacity and inhibited growth. Photoheterotrophically-grown *C. reinhardtii* cells sacrifice the photosynthetic apparatus in Fe-limited growth conditions, while photoautotrophically-grown cells do not (Terauchi et al., 2010; Urzica et al., 2012). The rationale is that the photosynthetic apparatus is a major Fe sink, which is dispensable when acetate is available as an additional carbon and energy source but is essential in its absence. In this chapter, I will examine the changes in *Chlamydomonas* cells during the immediate transition from photoautotrophic to photoheterotrophic growth under different iron nutritional conditions in more detail, time-dependent, at the levels of transcript abundance as well as physiological responses, including assessing functionality of photosynthetic and respiratory electron transport chains.

Significant differences in cellular chlorophyll content in response to limiting Fe were observed between cells grown with or without acetate in steady state. As a first experiment, I verified this finding as starting point for this project. Iron limited, photoheterotrophic cultures grown in steady state batch cultures showed a reduction in chlorophyll content to 30% of replete levels ( $0.8 \pm 0.1 \text{ pg}\cdot\text{cell}^{-1}$  in iron limitation versus  $2.6 \pm 0.3 \text{ pg}\cdot\text{cell}^{-1}$  in replete; mean  $\pm$  standard deviation), whereas photoautotrophic cultures maintain chlorophyll content at replete levels ( $2.5 \pm 0.4 \text{ pg}\cdot\text{cell}^{-1}$  in iron limitation versus  $2.7 \pm 0.4 \text{ pg}\cdot\text{cell}^{-1}$  in replete) (Figure 24A). A difference is considered significant when the *p*-value calculated from an unpaired, two-tailed Student's *t*-test passes a significance threshold of  $\alpha=0.05$ , *p*-values calculated between the individual conditions are listed in Supplemental Table 26. As expected, iron-deficient cultures (1  $\mu\text{M}$ ), both photoheterotrophic and photoautotrophic, did not experience a significant loss in cellular chlorophyll content relative to replete ( $2.8 \pm 0.2$  and  $2.5 \pm 0.2 \text{ pg}\cdot\text{cell}^{-1}$ , respectively).

This phenotype, the strategic loss or failure to maintain chlorophyll-levels at low Fe concentrations dependent on the C-source presents a unique opportunity to study the dynamics of the photosynthetic apparatus. I therefore performed a set of experiments investigating the dynamic response of photoautotrophic cultures to provision of acetate, documenting the acclimation of *Chlamydomonas* cultures, Fe- and time-dependently, to changing trophic conditions.

## 2. Results

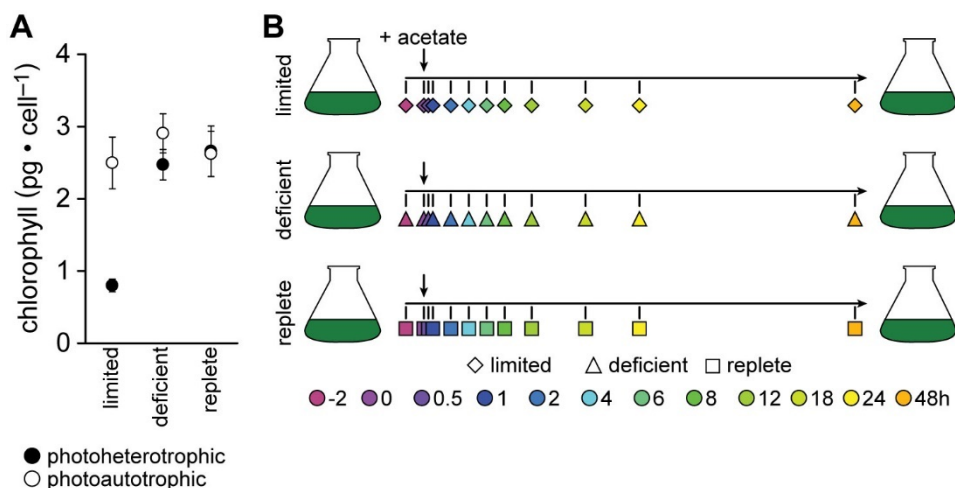


**Figure 24. A Dynamic experimental design to characterize the acclimation response.** **A:** Cultures containing 0.25, 1.0, and 20  $\mu\text{M}$  Fe-EDTA were inoculated from pre-cultures containing 1.0, 1.0, and 20  $\mu\text{M}$  extracellular iron, respectively, and were grown in the presence of acetate and light (photoheterotrophic) or increased air supply and light (photoautotrophic) to a density of  $2\text{--}3 \times 10^6$  cells $\cdot\text{ml}^{-1}$ . Total chlorophyll was extracted from  $\sim 4 \times 10^6$  cells with a mixture of 80% acetone/20% methanol (v/v) and absorption of the extract measured spectrophotometrically against a solvent blank. The mean of three replicates is shown, error bars represent SD. **B:** Experimental design for investigating the acclimation response after the addition of acetate to photoautotrophic cultures.

Physiological parameters during the acclimation to the reduced carbon source were assessed as a framework and physiological context for a whole transcriptome analysis. The experiments were performed in large liquid cultures (1 to 1.2 l) of strain CC-4532 in conditions of iron limitation at 0.25  $\mu\text{M}$ , iron deficiency at 1  $\mu\text{M}$ , and iron replete at 20  $\mu\text{M}$  Fe-EDTA, in order to accommodate a long time course experiment with many sampling points for different materials (RNA, elemental analysis, physiological parameters) originating from the same culture. All experimental cultures were started from photoautotrophic mid- to late-logarithmic precultures containing 1  $\mu\text{M}$  Fe and grown to mid-logarithmic phase for the addition of 17 mM acetate. Unless specifically stated otherwise, only one or two replicates of the three iron concentrations were grown in parallel, and repeated over several weeks to collect replicate samples, due to space restrictions when positioning the large Fernbach-flasks in optimal light conditions in the growth incubators. Samples were stored until processed and analyzed together, where possible. Cells were analyzed 2 hours before the addition of acetate (-2h), directly after (0h) as well as 0.5, 1, 2, 4, 6, 8, 12, 18, 24 and 48h after the addition of acetate (Figure 24B), for details on the experimental setup and sampling, see section 4.2. Cells were grown photoautotrophically on air-level  $\text{CO}_2$  in iron-limited (0.25  $\mu\text{M}$ ), -deficient (1  $\mu\text{M}$ ) and -

## 2. Results

replete (20  $\mu\text{M}$ ) conditions, supplemented with acetate during logarithmic growth phase at time 0 ( $t = 0\text{h}$ ), and sampled for monitoring physiological parameters, including chlorophyll content, oxygen evolution and consumption, fluorescence transients, photosynthetic (PSII) efficiency  $F_v/F_m$ , total organic C and N (for biomass equivalent and C to N ratio), and the elemental profile and compared to “control” cultures maintained under photoautotrophic conditions. As an additional control the experiment was repeated in full in a similar fashion with only water added at time-point 0, instead of acetate, maintaining the cultures under photoautotrophic conditions, but documenting the changes resulting from growth at that period of the growth cycle, eliminating that variable from the analysis.

### 2.4.1.1 Chlorophyll Content of Fe-limited Cells is Reduced Rapidly 6h After Acetate Addition.

After the addition of acetate, the cellular chlorophyll content changed only in iron-limited conditions and remained unchanged in iron-deficient and -replete cultures (black circles, Figure 25). The reduction in chlorophyll content did not occur in cultures where no acetate was added (grey circles).

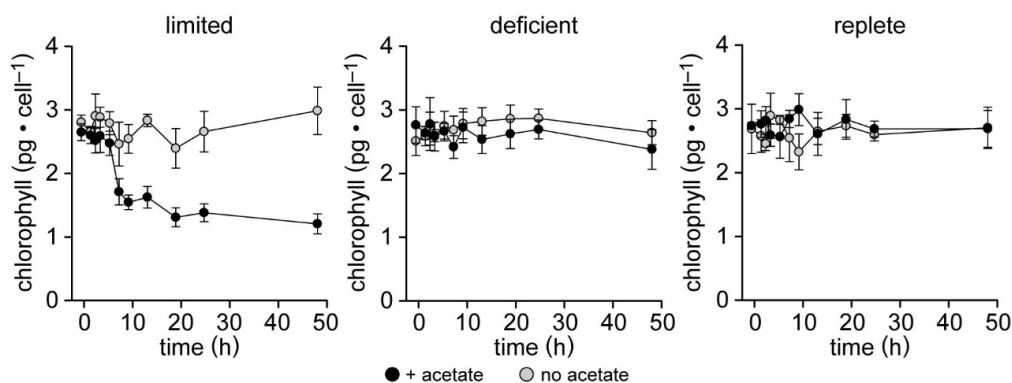


**Figure 25. Cellular chlorophyll content after the addition of acetate.** Cells were grown without acetate (photoautotrophic) for a full growth curve before starting replicate pre-cultures containing 2  $\mu\text{M}$  Fe. Photoautotrophic cultures containing 0.25 (limited), 1.0 (deficient), and 20  $\mu\text{M}$  Fe (replete) were inoculated to an initial cell density of  $2 \times 10^4$  cells · ml<sup>-1</sup>, grown for 6-7 days to a cell density of  $2 \times 10^6$  cells · ml<sup>-1</sup> and each culture was either supplied with 17 mM sterile sodium acetate (black circles) or with the equal volume of sterile purified water as control (grey circles). Total chlorophyll content was assessed before and 0, 1, 2, 4, 6, 8, 12, 18, 24, and 48h after the addition of acetate from  $\sim 4 \times 10^6$  cells with a mixture of 80% acetone and 20% methanol (v/v) and absorption of the extract was measured spectrophotometrically against a blank. The mean of four independent biological replicates is shown, error bars represent SD.

## 2. Results

---

No significant difference in chlorophyll content was observed before the addition of acetate ( $2.7 \pm 0.1$ ,  $2.8 \pm 0.3$  and  $2.7 \pm 0.1$   $\text{pg}\cdot\text{cell}^{-1}$  in Fe-limited, -deficient and -replete, respectively) and for the first 4h. Six hours post-acetate the chlorophyll content, of Fe-limited cultures only, rapidly decreased to 65% and decreased more steadily to as low as 46% after 48h ( $2.5 \pm 0.2$ ,  $1.7 \pm 0.2$  and  $1.2 \pm 0.2$   $\text{pg}\cdot\text{cell}^{-1}$  at 4, 6 and 48h, respectively). The Fe-deficient and -replete cultures with acetate and all control cultures showed no significant difference in cellular chlorophyll content. Individual *p*-values comparing total chlorophyll content between the samples are listed in Supplemental Table 27.

### 2.4.1.2 Decrease in Chl is Not Due to Dilution by Cell Division.

One obvious question arising from the reduction in cellular chlorophyll content is if this reduction might simply be due to dilution of existing chlorophyll molecules by cell division. To address this question, growth rates of iron-limited, -deficient, and -replete cultures were monitored during the transition, and I did not observe a sudden change of cell density between 4 and 6 h after acetate addition. At 6h post-acetate, the cell numbers had not increased significantly (Figure 26, magnified section), from  $2.3 \pm 0.3$  at 0h to  $2.4 \pm 0.3$  at 4h and  $2.5 \pm 0.4 \times 10^6$   $\text{cells}\cdot\text{ml}^{-1}$  at 6h. Cultures did, however, experience temporary growth delays or arrests after acetate became available in all three iron states.

In Fe-limitation (left panel), no significant difference in cell number was observed between acetate and control cultures for the first 18h. Most cells doubled one more time during this time. Control cultures grew more steadily without added acetate and doubled one more time after water addition to reach a stationary cell density of around  $8 \times 10^6$   $\text{cells}\cdot\text{ml}^{-1}$ . After the addition of acetate, Fe-limited cells doubled one more time and reached a stationary cell density of  $\sim 4 \times 10^6$   $\text{cells}\cdot\text{ml}^{-1}$  ( $1.9 \pm 0.2$  and  $3.4 \pm 0.1 \times 10^6$   $\text{cells}\cdot\text{ml}^{-1}$  before and 48h after, respectively). When cells were monitored longer than 48h post-acetate, a maximum cell density of  $4.7 \pm 0.2 \times 10^6$   $\text{cells}\cdot\text{ml}^{-1}$  was observed (Supplemental Figure 33).

Fe-deficient cultures exhibited a delay in growth in response to the acetate for 24h, but then increased dramatically in growth rate and exceeded the photoautotrophic stationary cell density. Fe-deficient and -replete cultures grew to reach final cell density similar to steady state cultures (Supplemental Figure 34). The growth was slightly slower due to the larger culture volumes and resulting small differences in growth conditions. At 20  $\mu\text{M}$  Fe, right panel, growth after addition was slower than control for the first 12 h after the addition, significantly lower cell number in +acetate compared to no-acetate samples at 6,



## 2. Results

8 and 12 h after the addition of acetate. At 18 and 24h the same cell number was observed, even higher cell numbers at 48 h and beyond (up to 96 h, Supplemental) in acetate containing cultures, demonstrating the successful switch to photoheterotrophic conditions. Control cultures in general doubled more consistently over the 24 h after addition of H<sub>2</sub>O, hourly rate is constant over the time span. Acetate-added cultures experienced a growth arrest, many cells doubled at once around 18 to 24 h after the addition of acetate, cultures showed behavior similar to synchronized cultures. higher stationary cell density. Individual *p*-values comparing the cell density between the samples are listed in Supplemental Table 28.

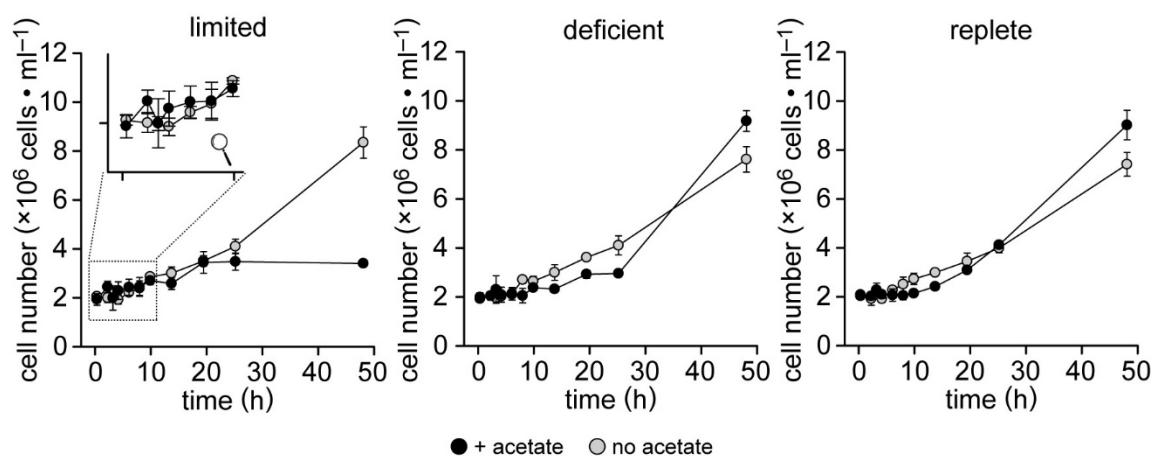


**Figure 26. Growth after the addition of acetate.** Cells were grown without acetate (photoautotrophic) for a full growth curve before starting replicate pre-cultures containing 2  $\mu$ M Fe. Photoautotrophic cultures containing 0.25 (limited), 1.0 (deficient), and 20  $\mu$ M Fe (replete) were inoculated to an initial cell density of  $2 \times 10^4$  cells  $\cdot$  ml $^{-1}$ , grown for 6-7 days to a cell density of  $2 \times 10^6$  cells  $\cdot$  ml $^{-1}$  and each culture was either supplied with 17 mM sterile sodium acetate (black circles) or with the equal volume of sterile purified water as control (grey circles). Growth was monitored 0, 2, 4, 6, 8, 12, 18, 24, and 48h after the addition of acetate by manual counting (Hemocytometer). The mean of four independent replicates is shown, error bars represent SD.

### 2.4.1.3 The Reduction of Chlorophyll depends on Protein Synthesis.

As shown above, the reduction in chlorophyll content in iron limited cultures in response to the availability of a reduced carbon source is not due to dilution by cell division. To assess whether the decrease in chlorophyll is an active or rather a passive process, I added an inhibitor of protein synthesis, cycloheximide, at the same time as the acetate. This does not allow the cell to synthesize new proteins after acetate addition, requiring adjusting to changes in the trophic status on photoautotrophically-optimized protein setup. This experiment was performed using 4 sets of three independent Fe-limited cultures, which

## 2. Results

were either supplied with acetate or not and with either  $10 \mu\text{g}\cdot\text{ml}^{-1}$  cycloheximide or without (Figure 27).

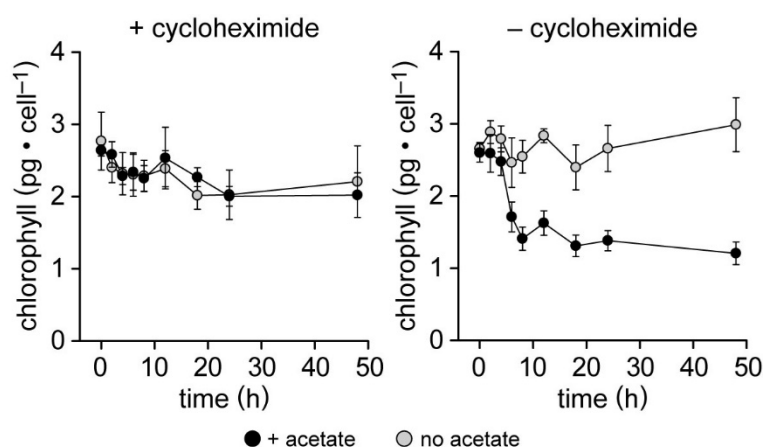


**Figure 27. Chlorophyll content of Fe-limited cultures treated with cycloheximide.** Cells were grown with increased aeration and without acetate (photoautotrophic) for a full growth curve before starting replicate pre-cultures containing  $2 \mu\text{M}$  Fe-EDTA. Photoautotrophic cultures containing  $0.25 \mu\text{M}$  Fe-EDTA (limited) were inoculated to an initial cell density of  $2 \times 10^4$  cells $\cdot\text{ml}^{-1}$ , grown for 6-7 days to a cell density of  $2 \times 10^6$  cells $\cdot\text{ml}^{-1}$  and each culture was either supplied with  $17 \text{ mM}$  sterile sodium acetate (black circles) or with the equal volume of sterile purified water as control (grey circles). Cycloheximide was added at the same time point as acetate or water control to a final concentration of  $10 \mu\text{g}/\text{ml}$ . Total chlorophyll content was assessed before and 0, 1, 2, 4, 6, 8, 12, 18, 24, and 48h after the addition of acetate from  $\sim 4 \times 10^6$  cells with a mixture of 80% acetone and 20% methanol (v/v) and absorption of the extract was measured spectrophotometrically against a blank. Absorption for each extract was measured twice and the mean was used as the individual replicate. The mean of three independent replicates is shown, error bars represent SD.

The observed reduction in chlorophyll content required protein synthesis as seen by the maintained chlorophyll levels in the presence of cycloheximide. The chlorophyll content decreased gradually in both acetate and control cultures; growth and general health of the cells were impacted in the continued presence of cycloheximide for longer periods of time, however independent of acetate and Fe (Supplemental Figure 35). Individual *p*-values comparing the chlorophyll content between the samples are listed in Supplemental Table 29.

### 2.4.2 Untargeted Analysis of Transcript Abundance Changes upon Acetate Addition.

#### 2.4.2.1 A Vast Majority of Transcripts is Differentially Expressed.

For a comparative transcriptome analysis of the Fe-dependent acetate response, RNA-Seq analysis was performed on cultures grown in Fe-replete, -deficient and -limited conditions. Acetate was added to photoautotrophic cultures and RNA for whole transcriptome analysis was taken before, at and up to 48 hours after the addition of acetate. As described before, photoautotrophic cultures were grown in Fe-limited, -deficient and -replete conditions to  $2 \times 10^6$  cells·ml<sup>-1</sup> in mid-logarithmic growth phase, acetate was added to a final concentration of 17 mM and  $5 \times 10^6$  cells collected. mRNAs from two independent experiments were sequenced and expression estimates obtained using pipelines developed for *Chlamydomonas* (for details, see section 4.2). The transcriptome in each sample was determined by RNA-Seq on the Illumina platform, the sequenced reads were aligned to the Au111.6 gene models and expression estimates calculated as FPKM (fragments per kilobase of transcript per million fragments mapped). Expression level distribution for all samples (Supplemental Figure 36) is uniform, no outliers were detected. The between-sample variation of the two replicate samples was small for all conditions and time points (Supplemental Figure 37) and thus the average expression was used for most of the analysis unless stated otherwise. Even though it is not best practice, the average of the 2 replicate samples was used for convenience, because of the large number of samples. Individual FPKM values were compared for most analyses to verify, that the variation between the two values is small. The % deviation of each of the two values from the average was calculated and were smaller than 10% for most expressed genes. Spike-in controls of synthetic RNA molecules were added to a subset of the samples to verify the detected limit and linear range of the expression estimates. Based on the spike-in analysis, the lowest FPKM value detected was around 1 FPKM, or > 10 FPKM with high confidence. Expression estimates were found to be linear between 1 and 100 000 FPKM.

Acetate-addition resulted in changes in transcript abundances of thousands of genes (Figure 28). Most of these changes happened independent of the iron-nutrition state, but for a subset of genes, the program in Fe-limited cells is distinctly different from that in Fe-deficient or -replete cultures. Of the 17 741 predicted genes (v5.5, Merchant 2007, Blaby 2014), 13 885 genes were expressed in this dataset (>1 FPKM in at least two of the 36

## 2. Results

samples). Of those expressed genes, 94%, or 13 035 genes, were differentially expressed between at least two of the 36 samples. A gene is considered differentially expressed between two conditions, when the following criteria are met: a) a p-value of 0.005, b) a false discovery threshold of 0.005 and c) 2-fold  $\log_2$ -change. Within the Fe-limited subset, 12 694 genes were differentially expressed, compared to 12 721 genes within the Fe-deficient and 12 641 genes within Fe-replete subsets. The overlap of differentially expressed genes present in all three Fe-subsets is 11 873 genes. Criteria for the calculation of the number of differentially expressed genes are shown in Supplemental Figure 38.

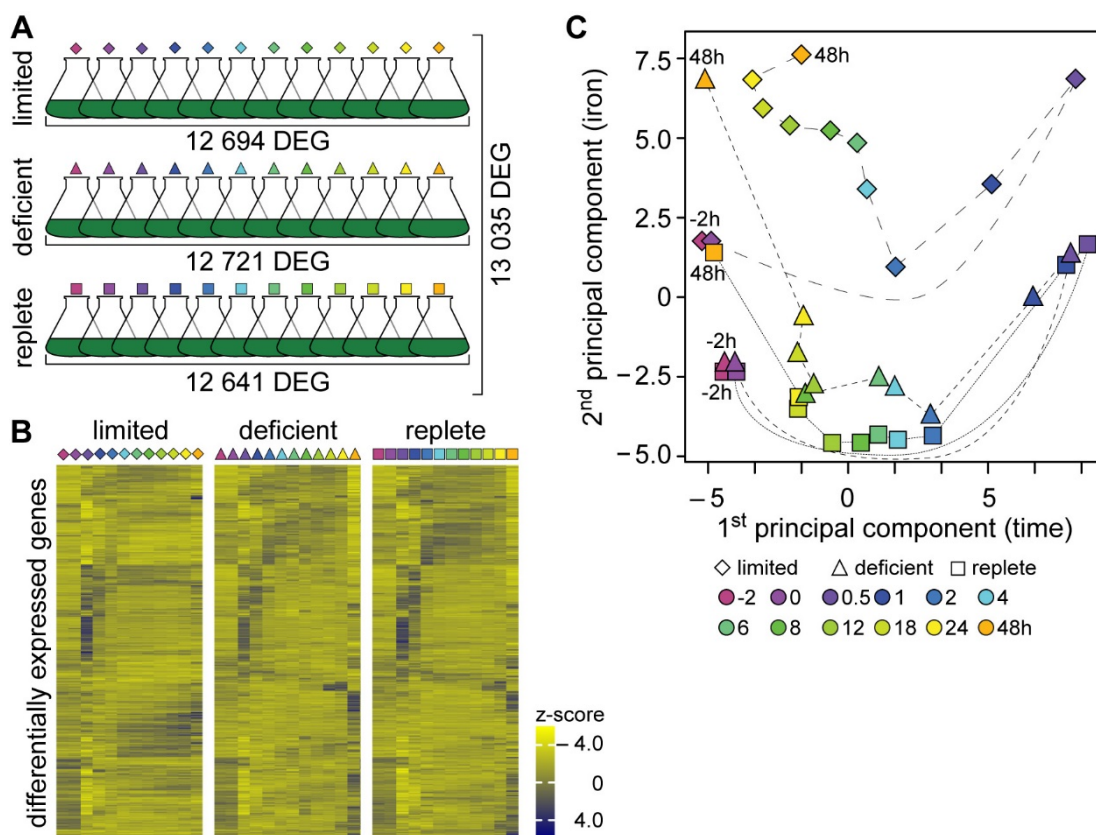


**Figure 28. Transcriptome analysis of Fe-dependent acclimation response to acetate.** Cells were grown without acetate (photoautotrophic) for a full growth curve before starting replicate pre-cultures containing 2  $\mu\text{M}$  Fe. Photoautotrophic cultures containing 0.25 (limited), 1.0 (deficient), and 20  $\mu\text{M}$  Fe (replete) were inoculated to an initial cell density of 2 104 cells ml<sup>-1</sup>, grown for 6-7 days to a cell density of 2 106 cells ml<sup>-1</sup> and each culture was supplied with 17 mM sterile sodium acetate. RNA was extracted and purified, mRNA selected, and cDNA generated for RNA-Seq analysis. Replicate expression estimates of the Phytozome v5.5 gene models were averaged and reported in FPKM for each gene. A: Differentially expressed genes (DEG) were extracted from the Cuffdiff output using additional selection ( $> 1$  FPKM in at least one sample, FDR  $< 5\%$ , fold change  $\geq 2$ ). B: A heatmap containing the z-score normalized expression of all 13 035 DE genes. C: Principal component analysis of the acetate acclimation response. All genes of the 36 samples were analyzed using cummeRbund (for details, see section 4.2) The output was recolored and dashed lines added for visibility.

## 2. Results

---

The expression profile of the 13 035 differentially expressed genes were z-score normalized over the entire set of 36 samples and plotted as a clustered heatmap (Figure 28B). Genes were primarily clustered by the expression of the Fe-replete subset, and genes are in the same order from top to bottom for all three conditions. In general, the heatmap shows very similar expression patterns between the Fe conditions. The -2 and 0h time point had very little change, whereas 30 and 60 minutes after the addition of acetate, many transcripts significantly changed in their abundance, both increases and decreases were observed. A few distinct groups of expression pattern can be distinguished, for example genes that are induced after the addition of acetate, but not to the same extent in Fe-limitation, or genes that are more highly induced in Fe-limitation. For a functional characterization of the transcriptome response, the differentially expressed (DE) genes were grouped according to the annotation of their predicted protein sequence based on the MapMan ontology, and genes from all annotation groups were among the large number of differentially expressed genes, with no clear overrepresentation.

To display the overall relationship of all the transcript changes, I performed a principal component analysis to determine the fraction of variation due to the two different variables, Fe-status and acclimation time to acetate (Figure 28C). The first principal component, and by that the bigger contributor to variances, is the acclimation time to acetate. Regarding this variable, the overall pattern is very similar, with the -2 and 0h time points clustering very close together at the left side of the plot. The 0.5 and 1h time points were most different from the previous time points (at the right side of the plot) and samples gradually moving back to be more similar to the photoautotrophic transcriptome (-2h).

The second principal component is the external iron concentration, which accounts for a smaller, but still relevant fraction of the variation. Fe-replete and -deficient clustered close together for most of the early time points, with specific differences arising 6h post-acetate. The 48h time point displayed Fe-specific differences in all three conditions, even the Fe-replete cultures experienced Fe-related transcript changes at the end of the experiment. Individual replicate samples show same correlation (Supplemental Figure 39)

### 2.4.2.2 Acetate-dependent, but Iron-independent Acclimation

To explore this large dataset in more detail, I first looked at the effect of acetate independent of iron nutrition. When comparing the individual time points of the Fe-replete conditions to -2h, 7620 genes were found to be differentially expressed in at least one of

## 2. Results

---

the time points (Figure 29A). Three genes were differentially expressed between -2 and 0h, none of which had annotations or predicted functions and the expression values were below 3 FKPM, therefore these genes were not analyzed further. For consistency, individual time points were compared to -2h and not 0h, but it I verified that there are no major differences regarding the 0h sample by comparing both sets of differentially expressed genes and “0h versus time points” yielded a > 90% overlap to the genes from “-2h versus time points”. Of the 7620 differentially expressed genes, more than half were rapidly induced or repressed, at 0.5 and 1h post-acetate (4211 and 3781 genes, respectively) (Figure 29 B). The fraction of induced and repressed genes was similar for most time points, between 45 and 55%, except for 48h, where only 42% of the genes showed an increased transcript abundance.

For a functional characterization of the transcriptome response, annotations based on the MapMan ontology were assigned and enrichment of a group was calculated compared to a set of randomly assigned genes. At 0.5h, genes associated with stress, redox homeostasis and transport were enriched among the induced genes, whereas genes without functional annotation were enriched among the repressed genes. 1h post-acetate, a number of major pathways start to be overrepresented among the induced transcripts, including genes encoding enzymes of the tricarboxylic acid (TCA) cycle, lipid and amino acid metabolism, sulfur assimilation, cellular stress response, protein homeostasis, signaling pathways and transport were enriched among the induced genes. Genes induced 2h post-acetate were enriched for TCA cycle, amino acid metabolism, redox homeostasis and tetrapyrrole biosynthesis. Whereas the TCA genes were induced rapidly, the downstream pathways start to be overrepresented at 4 and 6h after acetate, including photosynthesis and respiration.

For the first 8h post-acetate the repressed genes were enriched in genes without functional annotation, whereas after that time point the repressed genes showed an increased number of genes from the photosynthesis, gluconeogenesis, TCA cycle and cell wall biosynthesis groups. At 12 and 18h post-acetate, photosynthetic and central carbon (TCA, glycolysis, gluconeogenesis) genes were enriched among the repressed genes, whereas respiration and transport were overrepresented within the induced genes. 24h after the addition of acetate, cell wall and redox homeostasis were enriched among the induced genes, which coincides with the timing of the first cell division after the growth arrest. At the last time point of this experiment, 48h after extracellular acetate was provided, proportionally more genes were

## 2. Results

reduced in their transcript abundance and were enriched for genes involved in photosynthesis, cell wall and amino acid metabolism and S-assimilation.

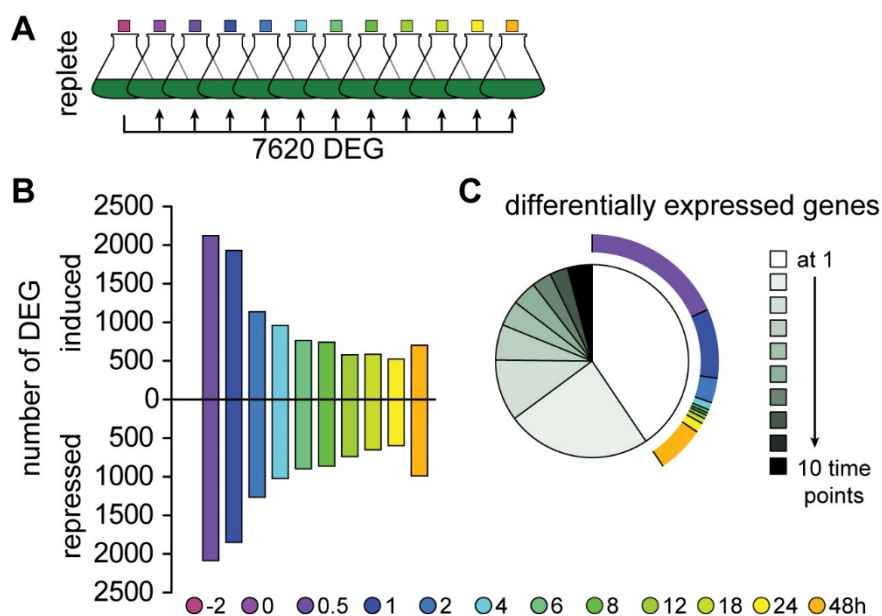


**Figure 29. Transcriptome response of Fe-replete cultures to acetate.**

**A:** Differentially expressed genes between all Fe-replete time points were extracted from the Cuffdiff output using additional selection ( $> 1$  FPKM in at least one of the Fe-replete samples,  $FDR < 5\%$ , fold change  $\geq 2$ ). **B:** Number of DE genes induced (up) and repressed (down) at each time point compared to the time point before acetate addition. **C:** A heatmap containing the z-score normalized expression of the 7620 differentially expressed genes. Eight groups of expression patterns are labeled I to VIII. Averaged z-score normalized expression for each group is shown in the right graph.

Of the 7620 DEG, more than one-third were differentially expressed at one particular time point only (3091 or 40%; white wedge, Figure 29 C). The early time points of 0.5 and 1h are disproportionately in this fast and very transient response, making up more than half of the genes that respond very transiently, as well as the last time point (48h).

A k-mean clustering algorithm was applied to the Fe-replete subset and the mean z-score over the genes in each of the 10 clusters was plotted as a heatmap (Figure 30). Fe-deficient and -limited samples were grouped in the same clusters and showed a good correlation with each cluster, despite the fact, that the clustering was performed using only the Fe-replete subset. Furthermore, it shows that the Fe-independent impact of acetate is the major contributor to the dataset's variability. Clusters 1 and 2 exhibited a large fold-change

## 2. Results

induction at 0.5 and 1h, with expression levels rapidly returning to pre-acetate levels. Both clusters were independent of the Fe-nutritional status of the cultures. Cluster 1 was the largest cluster with 1450 genes and among those, genes involved in the cellular stress response and lipid metabolism were enriched compared to randomly assigned genes. Cluster 2, contrary to cluster 1 showed an increase in transcript abundance 48h post-acetate and did not have specific annotation groups enriched.

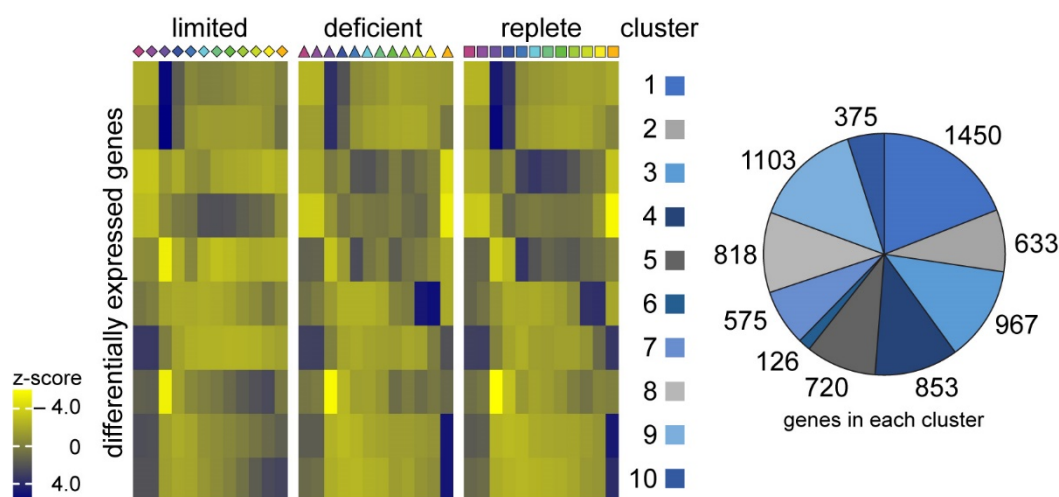


**Figure 30. Cluster analysis of the Fe-replete response to acetate.** The 7620 differentially expressed genes were clustered using a k-mean clustering algorithm. Mean z-score normalized expression of the genes in each cluster were displayed as a heatmap. The number of genes

The third cluster was enriched for genes involved in TCA cycle, photosynthesis, respiration and tetrapyrrole metabolism, with an induction between 4 and 12h post-acetate. Within this group of genes some showed a differential response in both Fe-deficiency and Fe-limitation. Cluster 5 exhibited a similar expression pattern to cluster 3, with the difference that the transcript abundance was reduced faster, with a narrower peak expression around the 2h time point. This cluster is enriched for genes in cellular signaling processes and cofactor biosynthesis.

Cluster 4 showed a transiently, more delayed increased transcript abundance, 4-8h post-acetate, and was also enriched in genes encoding stress, redox related proteins, some of which showed a higher induction in Fe-limiting conditions. Cluster 8 has a similar pattern, but it additionally shows an initial decrease in abundance at 0.5h from which a slow increase in transcript abundance emerges, peaking in the later time points. The degree of induction was different in Fe-limitation, and slightly in Fe-deficiency, while no group of



## 2. Results

---

genes was found to be specifically enriched in this cluster. Cluster 6 included genes that were induced towards the end of the experiment, at 18 and 24h, but this induction was markedly reduced in Fe-limitation conditions. Cluster 6 is the smallest cluster (126 genes), but highly enriched for genes involved in DNA and cell functions.

Cluster 7, 9 and 10 have very similar patterns of expression. High expression in phototrophic conditions (-2 and 0 h), reduction of transcript abundance upon acetate addition, and later (24, 48 h) a recovery of transcript levels to varying degrees. Cluster 7 was highest expressed in phototrophic conditions, expression in response to acetate was reduced very quickly, with only a slight recovery at the very end of the experiment (48 h), most prominently in Fe-replete cultures, with Fe-limited cultures not recovering at all. The cluster is enriched for genes encoding cell, cell wall proteins. Clusters 9 and 10 showed very similar expression patterns, lower expression levels in phototrophic conditions compared to cluster 7, the highest expression of genes in these clusters can be found at 48 h instead of -2/0 h, and all genes were recovering expression levels in all stages of Fe limitation. Cluster 10, compared to cluster 9, showed a more pronounced recovery in Fe-limited cultures. Cluster 9 has no enrichments, while cluster 10 is enriched for genes encoding metal handling proteins.

### 2.4.2.3 Iron- and Acetate-dependent Acclimation.

Next, I looked at the acetate effect on Fe-deficient and -limited cultures. There were only very small numbers of differentially expressed genes between -2 and 0h in both Fe-deficient conditions, and they were also not further analyzed. The overall number of induced and repressed transcripts is comparable to Fe-replete conditions (Figure 31A), even though minor differences can be observed. The rapidly induced and repressed responses were in the same range for all three iron conditions, around 2000 genes at 0.5 and 1h. With reduced number of differentially expressed genes in the middle time points and an increasing response 48h post-acetate.

To visualize the overlap between the respective time points, I added proportion-correct Venn diagrams (Figure 31B) of both the entire time courses (left) and each time point individually (right). The shared response to acetate is large, with proportional sections of genes that are unique to either of the Fe states. The overlap is large at the early time points, with an increase in diversity of the transcriptome response to acetate. The number of genes in each diagram is displayed in Supplemental Figure 40. At 1 and 2h, a few more genes

## 2. Results

unique to Fe-replete were present. Starting at 4h, the fraction of genes unique to Fe-limitation increased steadily and the overlap with Fe-deficient and -replete cultures was decreasing. Fe-deficient cultures started to have an increasing number of unique differentially expressed genes at 18h post-acetate. These unique genes are enriched for genes upregulated in Fe-limitation, indicating that these cultures became more Fe-starved during the progressing growth. The shared Fe-independent response to acetate is rapid, whereas the Fe-dependent acclimation was observed later and more gradual. The extracellular acetate is taken up and metabolized, metabolic intermediates need to accumulate to initiate the Fe-dependent portion of transcript changes.

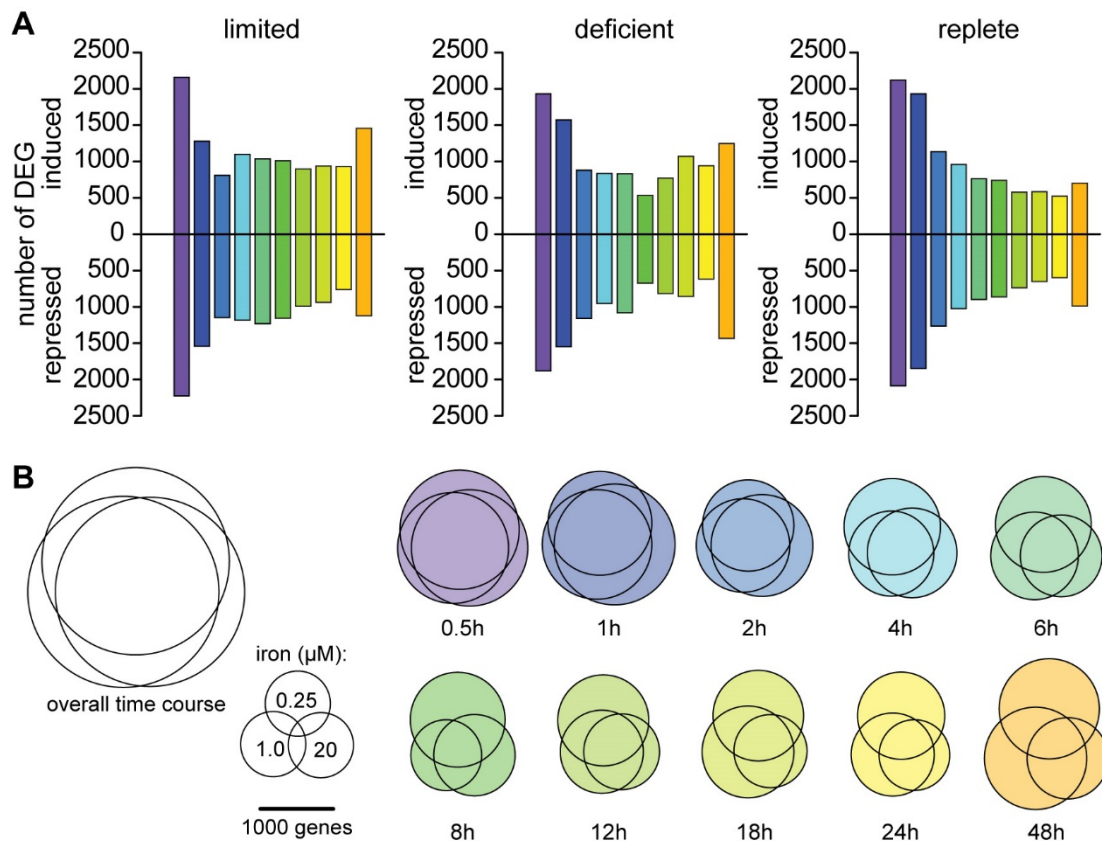


**Figure 31. The iron-dependent transcriptome response to acetate.** Differentially expressed genes between Fe-limited (left), -deficient (middle) and -replete (right) time points compared to -2h were extracted from the Cuffdiff output using additional selection. Number of DE genes induced (up) and repressed (down) at each time point are shown. B: Size-correct Venn diagrams showing the shared response for each time point. The scale bar indicates circle diameter per 1000 genes, Fe-limited is at the top, -deficient at the bottom left and -replete at the bottom right.

## 2. Results

### 2.4.2.4 Primary iron response consists of a small number of transcripts.

The Fe-independent response to acetate is rather large. Removing the acetate portion of the transcriptome, I compared individual time points of Fe limited, or Fe-deficient cultures, to Fe-replete cultures as a reference (Figure 32A). The number of genes differentially expressed in Fe deficiency in at least in one of the time points was lower compared to the acetate-dependent changes, 1099 unique genes that exhibited induced or repressed transcript abundance in Fe-deficiency. Interestingly, the number of differentially expressed genes is small for most of the time course, with transient increases to ~200 DEG 6 and 8h post-acetate. This is followed by a large increase in differentially expressed genes to > 600 genes at 48h, two-thirds of which showed increased transcript abundance in Fe-deficient conditions, when cells become more severely Fe-deficient after cell division.

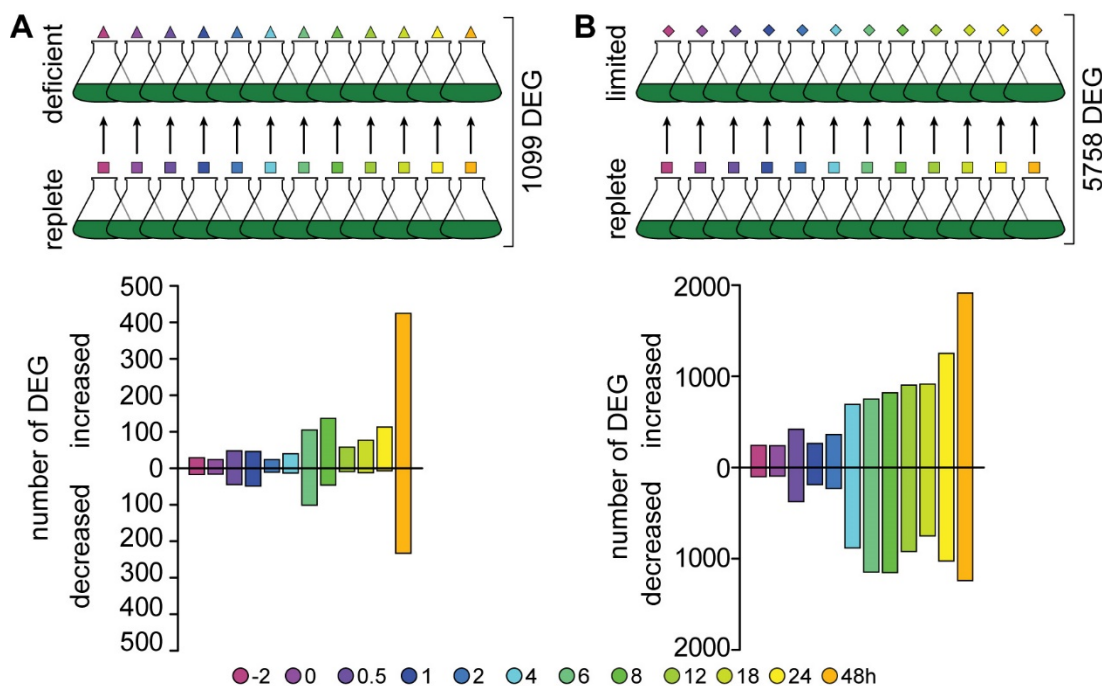


**Figure 32. Comparison of Fe-deficient and -limited transcriptome.** Differentially expressed genes between individual time points of A: Fe-deficient and -replete and B: Fe-limited and -replete conditions were extracted from the Cuffdiff output using additional selection ( $> 1$  FPKM in at least one of the Fe-replete samples,  $FDR < 5\%$ , fold change  $\geq 2$ ).

Iron-limited cultures were significantly different from -replete cultures at all times (Figure 32B). A total of 5758 genes showed differentially accumulated transcripts in Fe-limitation. The impact of Fe-limitation specific transcript changes increases over time, similar to Fe-deficient cultures, but, in each individual time point, expression of more genes was altered throughout. Additionally, there was a marked increase in differentially expressed genes

## 2. Results

---

after 4h to ~600 -1000 transcripts in Fe-limited conditions, that was not observed in Fe-deficient conditions, both compared to the same replete cultures. The additional increase at 48h found in Fe-deficient cultures was also observed in Fe-limited, to a lesser extent since there was already an earlier induction but affecting vastly more genes.

### 2.4.3 Cellular Processes and Pathways Affected by Iron and Acetate.

#### 2.4.3.1 Central carbon conversion pathways are induced by acetate and are mostly Fe-independent.

All major cellular pathways were represented among the many differentially expressed genes in the experiment, and while some pathways were found to be enriched in some clusters, showing a conserved response, a more nuanced analysis is required to uncover the acclimation processes to acetate addition dependent on the Fe status. Therefore, I looked at some of the most interesting pathways in more detail to dissect the underlying mechanisms and responses as acetate becomes available. The expression in each pathway or gene group is displayed as a small heatmap for each gene, circles from left to right indicate the time points, the top row are Fe-limited, middle -deficient and bottom row are -replete expression. FPKM values were z-score normalized over all 36 samples and color-coded from yellow to blue according to the z-score. Only genes within the initial set of 13'035 DE genes are included. To add the differential expression information between the comparisons, filled and open symbols were added: filled diamond/triangle/square on the right of the first/second or third row, respectively, indicate that at least one time point in the time series was significantly differentially expressed compared to the -2h time point. Open symbols indicate that none of the time points were differentially expressed compared to -2h, but, however, could still be differentially expressed between any two time points. The individual comparison was not added mainly due to the large number of genes whose transcripts increase or decrease in abundance within the first hour and many genes were differentially expressed at a given time point when compared to 0.5 or 1h. Filled circles next to the gene name indicate that this gene was differentially expressed between 0.25 and 20  $\mu$ M Fe (left circle) or between 1 and 20  $\mu$ M Fe (right circle), at least at one of the time points. For this comparison, only the same time points were related (e.g. 4h between 1 and 20  $\mu$ M Fe) and not to any other time points (e.g. not 4h 0.25  $\mu$ M Fe and 12h 20  $\mu$ M Fe), similar to what was described before.

## 2. Results

First, I analyzed transcripts involved in metabolizing acetate. All five putative acetate transporter responded to the availability of extracellular acetate (Figure 33A), filled symbols next to the time course. Two of the 5 genes showed the same expression pattern of rapid induction at 0.5h followed by a rapid reduction back to pre-acetate levels, in all 3 Fe-conditions. The other three were initially repressed and slowly induced a few hours after acetate became available, suggesting functional differences of these five related genes.

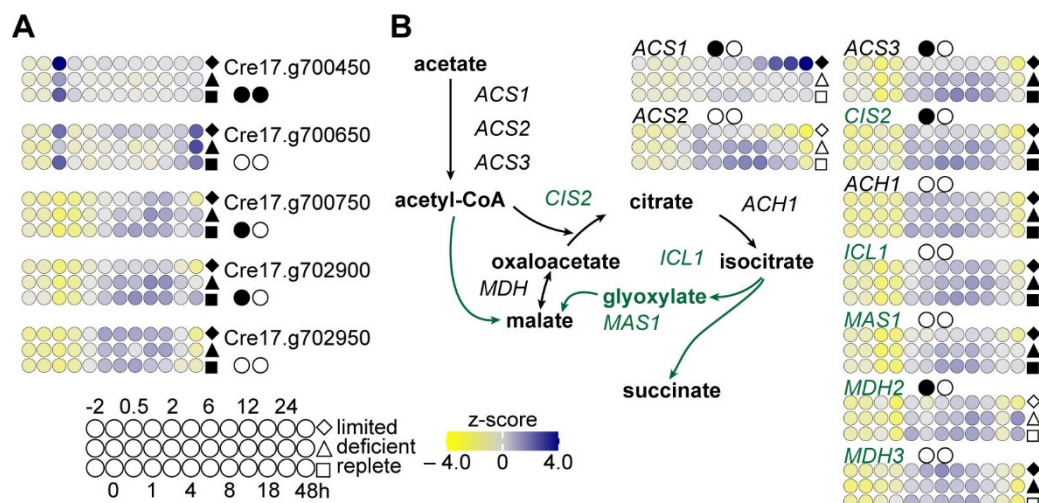


**Figure 33. Expression pattern of genes involved in acetate uptake and metabolic conversion.** Expression pattern of **A**: genes that encode putative acetate uptake transporters and **B**: genes encoding enzymes of acetate conversion and glyoxylate cycle. The enzymatic reactions constituting the pathways are represented by double or single-directional arrows, according to the reversibility of the reactions. Green arrows and gene names indicate glyoxylate cycle-specific components of the pathway. The expression estimates are displayed in colored circles blocks based on z-score normalized expression levels. Fe-limited (diamond), -deficient (triangle) and -replete (square), filled Fe-symbols indicate at least one time point is differentially regulated compared to before the acetate addition in the respective Fe condition. The filled circles next to the gene name indicate indicate differentially expressed time points between Fe-limited and -replete (left circle) or Fe-deficient and -replete (right circle).

The expression of intracellular acetate conversion and the glyoxylate cycle was tightly co-regulated (Figure 33B). Most genes responded to the acetate by an increase in transcript abundance, starting 2h after acetate was added to the growth medium. The acetyl-CoA synthetase *ACS1* showed a distinctly different, Fe-dependent, expression pattern from the other two isoforms and the enzymes of the glyoxylate cycle. The transcript abundance increased in Fe-limited condition, but not in Fe-deficient or -replete cultures. *ACS2* was not differentially expressed. *ACS3*, *CIS2*, *ACH1*, *ICL1* and *MAS1* were tightly co-

## 2. Results

expressed, all responded to acetate by increased transcript abundance between 2 and 18h post-acetate and exhibited only minor differences between the iron concentrations.

Genes with products involved in the tricarboxylic acid cycle were highly co-expressed also and exhibited similar expression pattern to the glyoxylate cycle (Figure 34). The citrate synthase isoform *CIS1* showed an expression pattern distinctive different from *CIS2*, and the tightly co-regulated genes of glyoxylate and tricarboxylate cycle. The other genes involved in the TCA cycle were co-expressed with the acetate conversion and glyoxylate cycle genes, both shared and genes unique to one of the two pathways (increases in both energy and carbon structures). All, except *MDH4*, were acetate-regulated (filled symbols) and had only a minor Fe-dependent component (open circles).

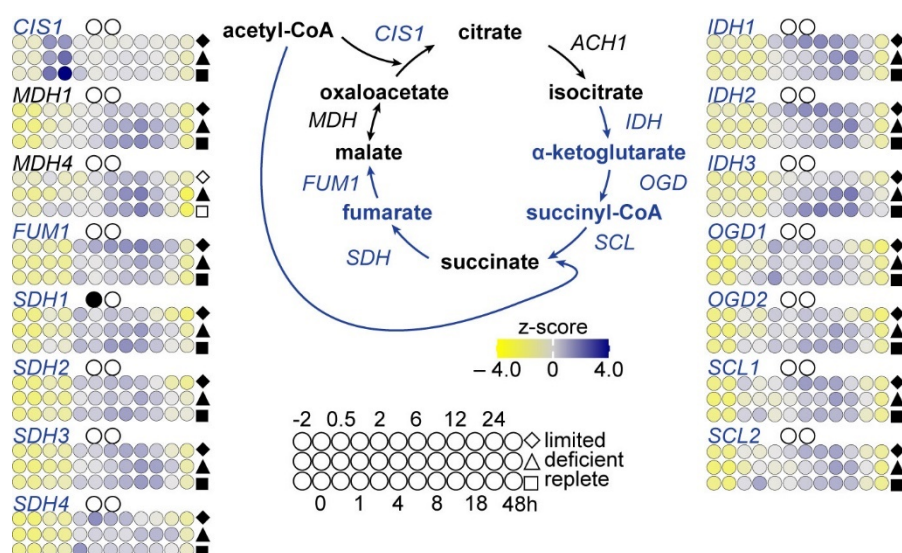


**Figure 34. Expression pattern of genes involved in the TCA cycle.** Expression pattern of genes that encode enzymes of the TCA cycle. The enzymatic reactions constituting the pathways are represented by double or single-directional arrows, according to the reversibility of the reactions. Dark blue arrows and gene names indicate TCA-specific components of the pathway. The expression estimates are displayed in colored circles blocks based on z-score normalized expression levels. Fe-limited (diamond), -deficient (triangle) and -replete (square), filled Fe-symbols indicate at least one time point is differentially regulated compared to before the acetate addition in the respective Fe condition. The filled circles next to the gene name indicate differentially expressed time points between Fe-limited and -replete (left circle) or Fe-deficient and -replete (right circle).

Genes with products involved in the Calvin-Benson cycle and photorespiration were not as tightly co-expressed as glyoxylate and tricarboxylic acid cycle and showed distinctively different expression patterns (Figure 35A). Whereas RBL genes and genes whose products

## 2. Results

catalyze the conversion from 3-phospho-glycerate to glyceraldehyde-3-phosphate were co-expressed with TCA cycle genes, *RBCS1*, *PGK1*, *GAP1* and *GAP2* were differentially expressed in response to Fe and not or barely Fe-dependent, as indicated by the filled symbols and open circles. The peak expression appeared later than that of glyoxylate and tricarboxylic acid cycle, shifted towards 6 to 24h. The following reduction and carbohydrate formation phase were less regulated by acetate and more dependent on the Fe-state, as indicated by open symbols and filled circles. Genes involved in the competing reactions of photorespiration were not co-regulated and most were not differentially expressed.

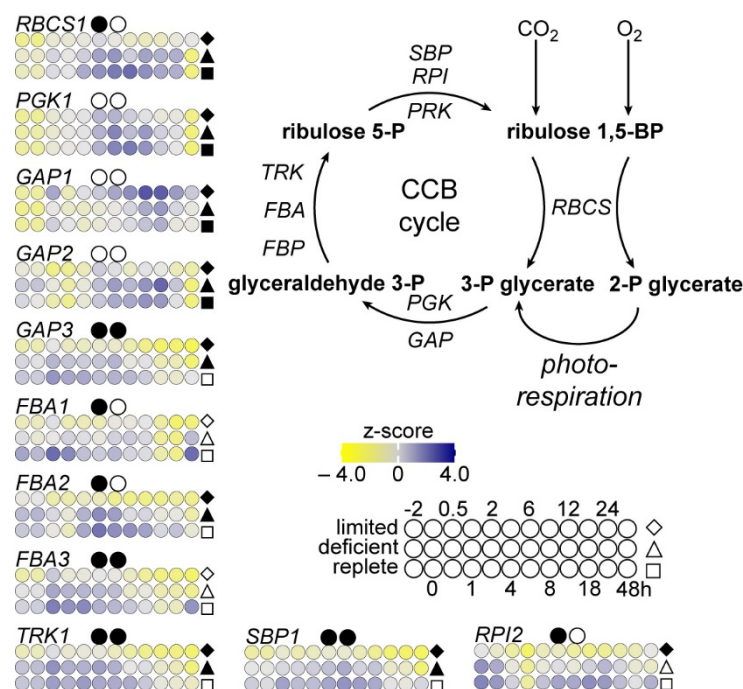


**Figure 35. Expression pattern of genes involved in Calvin-Benson cycle.** Expression pattern of genes that encode enzymes of the Calvin-Benson cycle. The enzymatic reactions constituting the pathways are represented by double or single-directional arrows, according to the reversibility of the reactions. The expression estimates are displayed in colored circles blocks based on z-score normalized expression levels. Fe-limited (diamond), -deficient (triangle) and -replete (square), filled Fe-symbols indicate at least one time point is differentially regulated compared to before the acetate addition in the respective Fe condition. The filled circles next to the gene name indicate indicate differentially expressed time points between Fe-limited and -replete (left circle) or Fe-deficient and -replete (right circle).

## 2. Results

### 2.4.3.2 Energy conversion pathways are induced by acetate and are partially Fe-dependent.

Next, I examined the expression of genes building the energy conversion pathways, photosynthesis (Figure 36) and respiration (Figure 37) because they appeared in the initial untargeted analysis and were overrepresented in the functional annotation groups in several comparisons. The genes were grouped by the complexes their products form. The majority (>80%) of genes in each complex group were among the differentially expressed and showed a high degree of co-regulation, therefore, the average of each complex is shown.

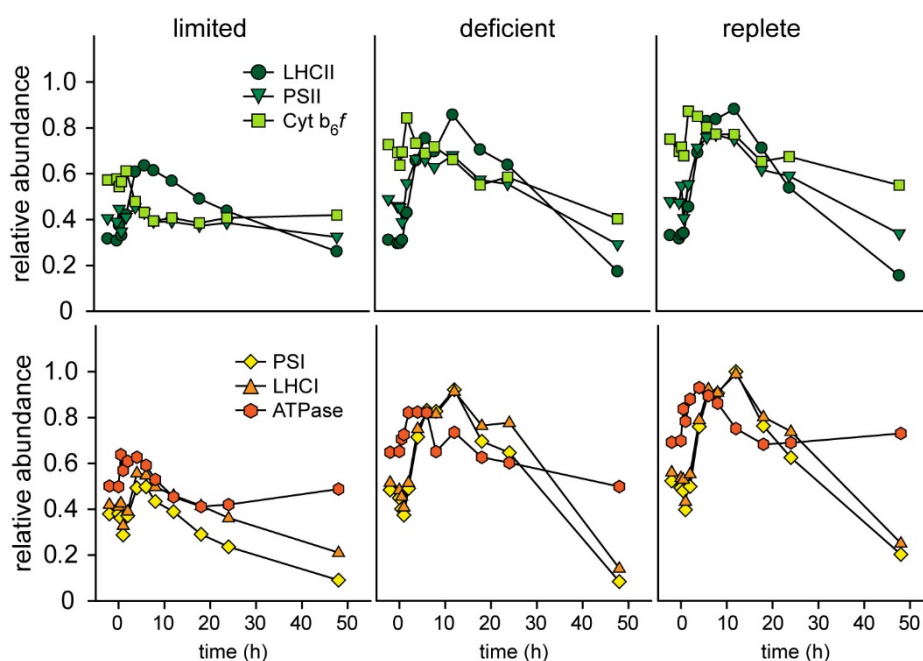


**Figure 36. Expression pattern of genes involved in photosynthesis.** The enzymatic reactions constituting the pathways are represented by double or single-directional arrows, according to the reversibility of the reactions. The expression estimates are displayed in colored circles blocks based on z-score normalized expression levels. Fe-limited (diamond), -deficient (triangle) and -replete (square), filled Fe-symbols indicate at least one time point is differentially regulated compared to before the acetate addition in the respective Fe condition. The filled circles next to the gene name indicate differentially expressed time points between Fe-limited and -replete (left circle) or Fe-deficient and -replete (right circle)..

The display of expression changes of the photosynthetic complexes was split in two panels, LHCII, PSII and b6f versus PSI, LHCI and ATPase, to better distinguish the observed differences between the complexes (Figure 36). In Fe-replete (right panel) and Fe-deficient (middle panel) conditions, transcripts encoding LHCII and PSII complexes increase



## 2. Results

constantly after the addition of acetate, reaching a maximum expression level at 12h, whereas the transcripts encoding Cyt *b<sub>6</sub>f* remain large unchanged. In Fe-limited cells, the transcripts for PSII and LHCII increase as well, but not to the same extent as in Fe-replete conditions and reach the peak expression earlier, at 6h. The expression of *b<sub>6</sub>f* rapidly, starting 2h after acetate was provided and reached the lowest level after 8h. The Fe-replete and Fe-deficient expression of proteins of the PSI and LHCI complexes were nicely co-expressed, showing the same pattern of induction to a maximum expression at 12h. Fe-limited cells showed a brief increase in abundance at 4 and 6h after acetate addition, followed by a steady decrease. The expression of ATPase components preceded the induction of the other complexes. The transcript abundance reached the peak expression earlier, after 1-2h, and decreased faster, starting 6h after the addition of acetate. The pattern of expression in unaffected in Fe-limited cells, only the overall expression level is lower.

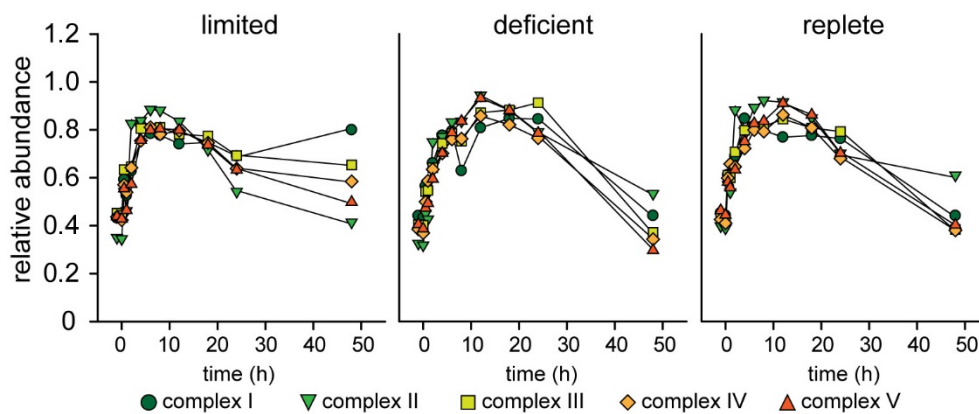


**Figure 37. Expression pattern of genes involved in respiration.** The enzymatic reactions constituting the pathways are represented by double or single-directional arrows, according to the reversibility of the reactions. The expression estimates are displayed in colored circles blocks based on z-score normalized expression levels. Fe-limited (diamond), -deficient (triangle) and -replete (square), filled Fe-symbols indicate at least one time point is differentially regulated compared to before the acetate addition in the respective Fe condition. The filled circles next to the gene name indicate differentially expressed time points between Fe-limited and -replete (left circle) or Fe-deficient and -replete (right circle)..

The respiratory complexes showed a very tight co-expression, within the complexes, but also comparing the complexes with each other (Figure 37). The effect of Fe-nutrition is not as evident as in the photosynthetic complexes. The transcript abundance of all 5 groups increased steadily as soon as acetate became available. The decrease in transcripts was less sharp than the photosynthetic one. Fe-replete and Fe-deficient peak transcript levels remained high between 8 and 24h, only decreasing 48h after acetate became available. The

## 2. Results

transcripts also increase in Fe-limited conditions, to about the same overall levels, but the high abundance was not maintained as long as in Fe-replete cells, decreasing already 18h after acetate addition.

### 2.4.3.3 Only Genes Involved in Chlorophyll Synthesis, But Not Chlorophyll Degradation, Respond to Acetate and Iron-Limitation.

Among the pathways found to be enriched in certain clusters was also co-factor metabolism (Cluster 3), including pathways and gene products involved in chlorophyll synthesis and degradation. Since chlorophyll levels were found to decline rapidly between 4h and 6h of the time course, when cells were not dividing, I wanted to analyze this part of the metabolism in more detail (Figure 38).

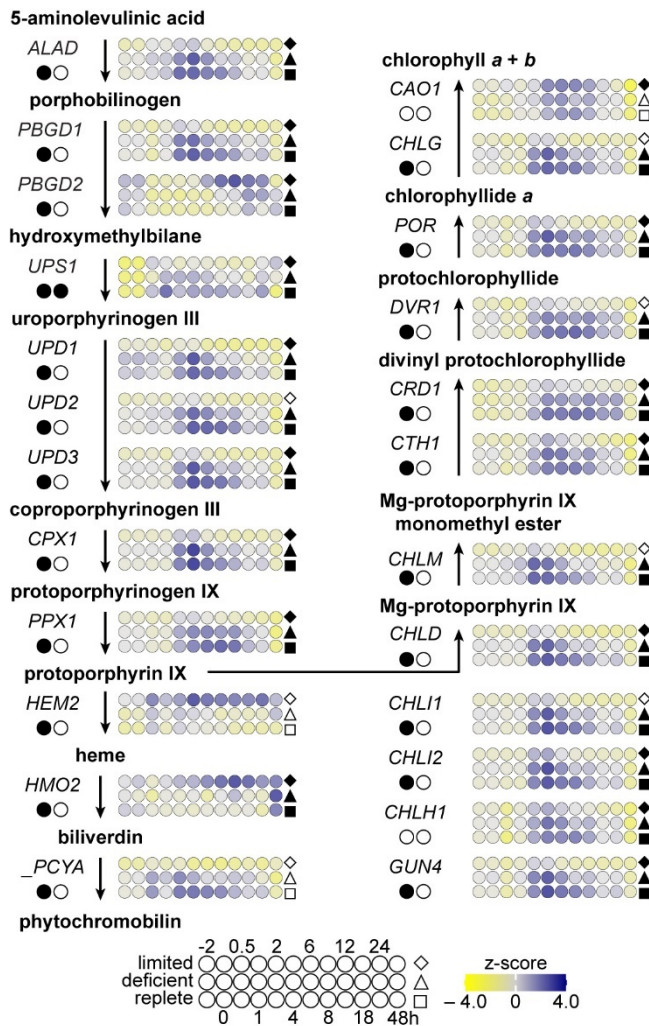


**Figure 38. Expression pattern of genes involved in chlorophyll synthesis.** The enzymatic reactions constituting the pathways are represented by double or single-directional arrows, according to the reversibility of the reactions. The expression estimates are displayed in colored circles blocks based on z-score normalized expression levels. Fe-limited (diamond), -deficient (triangle) and -replete (square), filled Fe-symbols indicate at least one time point is differentially regulated compared to before the acetate addition in the respective Fe condition. The filled circles next to the gene name indicate differentially expressed time points between Fe-limited and -replete (left circle) or Fe-deficient and -replete (right circle)..

## 2. Results

---

Differentially accumulated transcripts were found only in the pathway of chlorophyll synthesis, but not among the genes involved in chlorophyll degradation.

Most genes encoding components of the chlorophyll synthesis pathway were found to be induced in Fe-replete and Fe-deficient conditions, but to a lesser degree if at all in Fe-limitation. The expression was tightly co-regulated, with differentially accumulated transcripts within each Fe condition (filled symbols). The genes also showed distinct expression in Fe-limitation (first filled circle). Fe-limited cultures still exhibited an increase of transcripts at least 2-fold, but the magnitude is much smaller compared to Fe-deficient and -replete conditions. Additionally, the early genes of this pathway, ALAD, PBGD1, PBGD2 and UPS1 exhibited less co-regulated expression from the downstream components, are involved in other cellular processes. The side branch of the conversion of protoporphyrin IX to heme to phytychromobilin, specifically *HEM2* and *HMO2*, were significantly induced in Fe-limitation only.

### 2.4.4 Photosynthetic Parameters Respond to the Addition of Acetate.

#### 2.4.4.1 Oxygen Evolution is Reduced Only in Fe-limited Photoheterotrophic Cultures.

The central metabolic pathways are affected after the addition of acetate, including genes encoding respiratory and photosynthetic complexes change in mRNA abundance in response to acetate, both dependent and independent of iron. To get a quantitative readout of how the transcript changes might translate to physiological effects, I measured the net oxygen consumption in the dark and oxygen evolution during constant illumination during the time course. In photoautotrophic conditions, the Fe-limited, -deficient and -replete oxygen consumption were very similar ( $0.7 \text{ nmol O}_2 \text{ min}^{-1} 10^6 \text{ cells}$  at -2h) (Figure 39). After the addition of acetate, the oxygen consumption rate increased rapidly for the first 4h, independent of the cultures iron status. Whereas the consumption rate increased further in Fe-deficient and -replete cells up to four-fold, reaching the peak oxygen consumption rate 8h after the addition of acetate, the Fe-limited rate reached the peak at 4h, decreasing afterwards and leveling around  $1 \text{ nmol O}_2$ .

For estimating the net oxygen evolution, the decrease in dissolved oxygen in the dark was subtracted from the increase in oxygen concentration during constant illumination for each culture. Photoautotrophic Fe-limited cultures experienced a lower rate in oxygen evolution.

## 2. Results

Even though the cells did not show visible signs of Fe-limitation as in photoheterotrophic conditions, the reduced Fe content caused a slightly reduced rate of photosynthetic oxygen evolution. The post-acetate oxygen evolution displayed even larger differences between Fe-limited and -replete conditions. The Fe-limited evolution rate declined steadily after the addition of acetate and reached its minimum at 12h. More surprisingly, Fe-deficient and -replete cultures exhibited a very similar behavior in response to acetate availability; after a sudden decrease in the first 2h, the rate steadily increased to before-level at 8h and reaching the peak rate 12h after the addition. The increase is slightly delayed in Fe-deficiency at 4 and 6h but catches up to -replete levels at 12h.

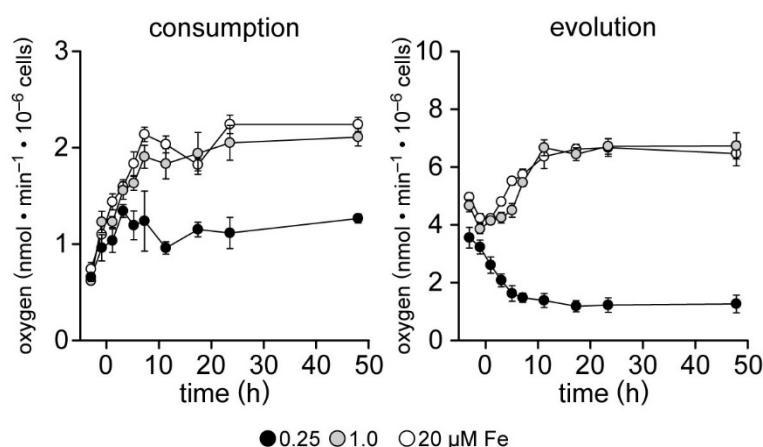


**Figure 39. Net oxygen consumption in the dark and evolution in illumination of iron limited, deficient and replete cultures after the addition of acetate.** Cells of strain CC-4532 were grown with increased aeration and light, without acetate (photoautotrophic) for a full growth curve before starting replicate pre-cultures containing 2  $\mu\text{M}$  Fe-EDTA. Photoautotrophic cultures containing 0.25 (black circles), 1.0 (grey circles), and 20  $\mu\text{M}$  Fe-EDTA (white circles) were inoculated to an initial cell density of  $2 \times 10^4$  cells  $\text{ml}^{-1}$ , grown for 6-7 days to a cell density of  $2 \times 10^6$  cells  $\text{ml}^{-1}$  and each culture was supplied with 17 mM sterile sodium acetate. The rates of net oxygen consumption and evolution were measured from  $\sim 4 \times 10^6$  intact cells. The decrease in dissolved oxygen in the dark and the increase during constant illumination with  $100 \mu\text{mol m}^{-2} \text{s}^{-1}$  was monitored for five minutes each and the resulting rate was related to the number of cells analyzed. The mean of three independent replicates is shown, error bars represent SD.

Individual *p*-values comparing the oxygen consumption and evolution between the samples are listed in Supplemental Table 30 and 31, respectively. Net oxygen consumption and evolution during the control time course did not change significantly (Supplemental

## 2. Results

Figure 41), consumption in the dark was between 0.58 and 0.75  $\text{nmol O}_2 \cdot \text{min}^{-1} \cdot 10^{-6}$  cells over all time points and Fe conditions. Net oxygen evolution was between 3.5 and 4.1  $\text{nmol O}_2 \cdot \text{min}^{-1} \cdot 10^{-6}$  cells in Fe-limited and between 4.0 and 4.8  $\text{nmol O}_2 \cdot \text{min}^{-1} \cdot 10^{-6}$  cells in Fe-deficient and -replete conditions.

### 2.4.4.2 $F_v/F_m$ is Reduced Hours After the Chlorophyll Content.

In addition to cellular chlorophyll content, net oxygen consumption and evolution, I monitored the maximum fluorescence efficiency of PSII ( $F_v/F_m$ ) during the time course (Figure 40).

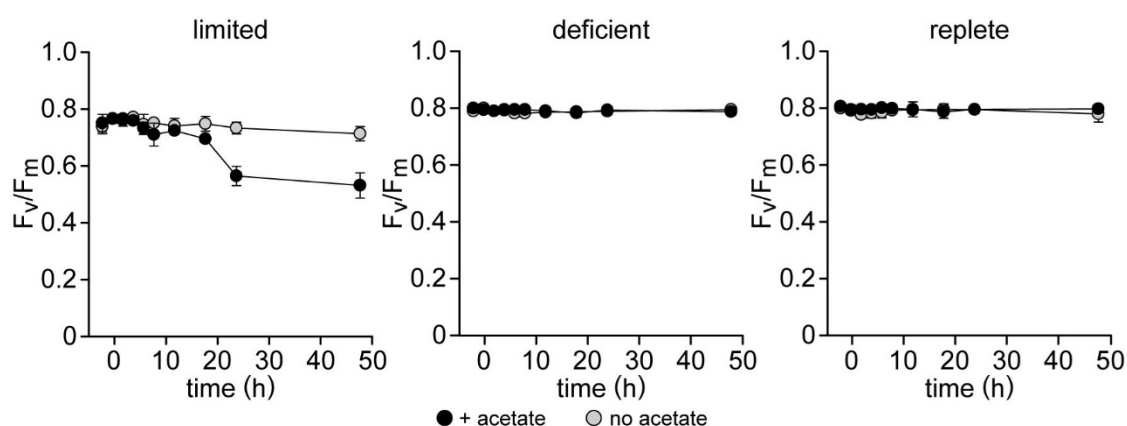


**Figure 40. Maximum quantum efficiency of PSII ( $F_v/F_m$ ).** Cells of strain CC-4532 were grown with increased aeration and light, without acetate (photoautotrophic) for a full growth curve before starting replicate pre-cultures containing 2  $\mu\text{M}$  Fe-EDTA. Photoautotrophic cultures containing 0.25, 1.0, and 20  $\mu\text{M}$  Fe-EDTA were inoculated to an initial cell density of  $2 \times 10^4$  cells  $\text{ml}^{-1}$ , grown for 6-7 days to a cell density of  $2 \times 10^6$  cells  $\text{ml}^{-1}$  and each culture was either supplied with 17 mM sterile sodium acetate (black circles) or with the equal volume of sterile purified water as control (grey circles). Maximum quantum efficiency of PSII ( $F_v/F_m$ ) was determined from  $\sim 2 \times 10^6$  cells immobilized onto a 15 mm round filter after dark-adaptation for 12 – 15 min using saturating light. The mean of four independent replicates is shown, error bars represent SD.

Compared to photoautotrophic control cultures, only Fe-limited cultures displayed a significant reduction in  $F_v/F_m$  starting surprisingly late, 18h after the addition of acetate. It is interesting to note that the reduction in  $F_v/F_m$  occurred much later than the reduction in chlorophyll content in iron limited cultures, or the reduction in net  $\text{O}_2$  evolution. Both  $F_0$  and  $F_{\text{max}}$  increased at about the same rate, so that  $F_v/F_m$  remained relatively constant.  $F_0$  and  $F_{\text{max}}$  of the time course (two replicates) are shown in Supplemental Figure 42. Both these values, however, need to be considered very carefully, because normalization and comparison of absolute fluorescence can be difficult. Individual  $p$ -values comparing  $F_v/F_m$

## 2. Results

---

between the samples are listed in Supplemental Table 32. DCMU addition was used to test that saturating light is indeed saturating during the time course. All three iron concentrations were chosen, and cells at 0, 12 and 48h were treated with DCMU, and fluorescence was measured (Supplemental Figure 43).

### 2.4.5 Acetate- and Fe-specific changes to the ionome.

#### 2.4.5.1 Macronutrients Temporarily Increase Post-acetate.

Cultures experienced growth arrest in response to suddenly available extracellular acetate and during the analysis I noticed an increase in cellular mass. In order to examine the changes in the ionome after the addition of acetate, I analyzed Fe-limited, Fe-deficient and Fe-replete cells for changes in macro- and micronutrients by total carbon and total nitrogen (TOC/TN) analysis and ICP-MS/MS. The cellular composition of the macro-nutrients C, N, P, and S displayed distinct patterns after the addition of acetate (Figure 41).

The carbon content increased by 2.5-fold until the Fe-deficient and Fe-replete cells divided after 24h. Cultures experiencing Fe-limitation accumulated more carbon and maintained a higher C content even after cell division, which is most likely due to increased starch and lipid accumulation, as observed before during Fe-limitation (Urzica et al., 2013).

For Fe-replete and -deficient conditions, the nitrogen content mirrors the increase and decrease in cellular carbon. Fe-limited cultures accumulated cellular nitrogen to a lower rate and extent than Fe-replete and compared to carbon. The C/N ratio increased gradually in Fe-limitation only (Supplemental Figure 44). Individual *p*-values comparing the carbon to nitrogen ratio between the samples are listed in Supplemental Table 33. Phosphorus and sulfur levels did not exhibit the same time resolved pattern as carbon and nitrogen. P and S levels only slowly increase and decrease a little earlier than C and N. Whereas C and N content were reduced to ~50% around the time the cells divide, both P and N content were reduced to 30%, which is more than the passive dilution by cell division. Control cultures did not show the acetate-induced increase in C, N, P or S over time (Supplemental Figure 45). Individual *p*-values comparing the carbon, nitrogen, phosphorus and sulfur content between the samples are listed in Supplemental Table 34-37, respectively.

## 2. Results

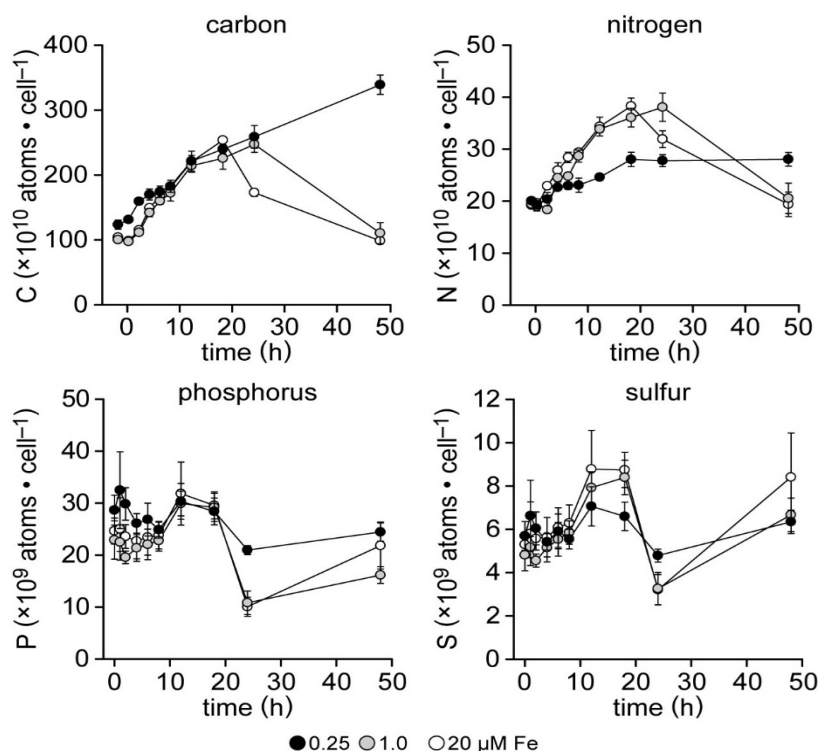


**Figure 41. C, N, P and S content after the addition of acetate.** Cells of strain CC-4532 were grown with increased aeration and light, without acetate (photoautotrophic) for a full growth curve before starting replicate pre-cultures containing 2  $\mu\text{M}$  Fe-EDTA. Photoautotrophic cultures containing 0.25 (black circles), 1.0 (grey circles), and 20  $\mu\text{M}$  Fe-EDTA (white circles) were inoculated to an initial cell density of  $2 \times 10^4$  cells  $\text{ml}^{-1}$ , grown for 6-7 days to a cell density of  $2 \times 10^6$  cells  $\text{ml}^{-1}$ , each culture was supplied with 17 mM sodium acetate and cells for elemental analysis by TOC (nitrogen and carbon) and ICP-MS/MS (phosphorus and sulfur) were taken at each time point and the content related to the number of cells analyzed. The mean of four independent replicates is shown, error bars represent one standard deviation of the mean.

The cell volume changes specifically after the addition of acetate (Figure 42). Cell volume increased steadily in response to acetate, decreasing rapidly after Fe-deficient and -replete cultures divided after 24h but remained increased in Fe-limitation. Even though Fe-limited control cultures had a slightly increased volume compared to Fe-deficient and Fe-replete conditions, the volume did not change systematically during the time course.

The median cell diameter used for calculating the cell volume is shown in Supplemental Figure 46. Individual *p*-values comparing the median cell volume between the samples are listed in Supplemental Table 38. Not all variation in C, N, P and S can be explained by cell volume increase during the growth arrest. Specifically, the N content stayed elevated at 24h, when the cell volume already decreased due to division. Between 18 and 24h, when

## 2. Results

the cells prepare for division, they appear to accumulate N for amino acid and protein synthesis required for biomass increase and subsequent division.

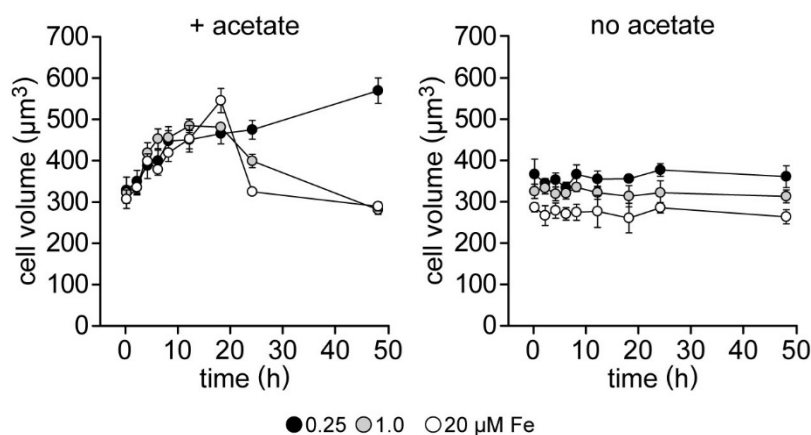


**Figure 42. Cell volume changes in response to acetate.** Cells of strain CC-4532 were grown with increased aeration and light, without acetate (photoautotrophic) for a full growth curve before starting replicate pre-cultures containing 2 µM Fe-EDTA. Photoautotrophic cultures containing 0.25 (black circles), 1.0 (grey circles), and 20 µM Fe-EDTA (white circles) were inoculated to an initial cell density of  $2 \times 10^4$  cells ml<sup>-1</sup>, grown for 6-7 days to a cell density of  $2 \times 10^6$  cells ml<sup>-1</sup> and each culture was either supplied with 17 mM sterile sodium acetate or with the equal volume of sterile purified water as control. Average cell volume was calculated from the median cell diameter of 500 to 600 (+ acetate) or 200 to 300 (no acetate) cells of each culture. The mean of four independent replicates is shown, error bars represent one standard deviation of the mean.

### 2.4.5.2 Micronutrients Display Distinct Response to Both Acetate and Iron

Among the differentially expressed genes that are expressed in iron-dependent patterns are the known iron regulon genes. Iron-deficiency marker transcripts, like *FOX1*, *FTR1*, *FRE1*, *IRT1* and *IRT2*, are increased in abundance 48h after the addition of acetate, specifically in Fe-deficient cultures. To investigate, if this correlates with decreased iron pools and cells turning more Fe-limited, I analyzed the elemental profile during the acclimation time course.

The iron content of photoautotrophic cultures (-2h) showed the expected levels of Fe-limited ( $6 \times 10^7$  atoms·cell<sup>-1</sup>), Fe-deficient ( $10 \times 10^7$  atoms·cell<sup>-1</sup>) and Fe-replete ( $16 \times 10^7$  atoms·cell<sup>-1</sup>) cultures. Following the availability of extracellular acetate, the Fe level of Fe-limited cultures remained unchanged, until after the final cell division around 24h, when the cellular Fe pool reduced to  $3 \times 10^7$  atoms·cell<sup>-1</sup> (Figure 43A). A very similar behavior of cellular Fe was observed in the control time course without added acetate, for Fe-limited,



## 2. Results

Fe-deficient and Fe-replete cultures. Both Fe-deficient and Fe-replete cultures experienced an increase in cellular Fe levels, starting 8h post-acetate with a maximum 1.5-fold increase at 12 and 18h.

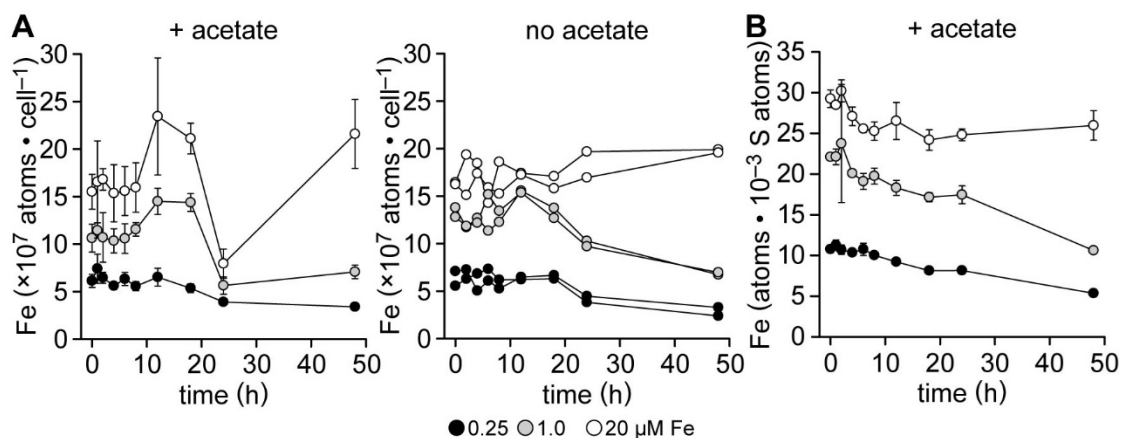


**Figure 43. Iron content after the addition of acetate.** Cells were grown with increased aeration and light, without acetate (photoautotrophic) for a full growth curve before starting replicate pre-cultures containing 2  $\mu$ M Fe-EDTA. Photoautotrophic cultures containing 0.25 (black circles), 1.0 (grey circles), and 20  $\mu$ M Fe-EDTA (white circles) were inoculated to an initial cell density of  $2 \times 10^4$  cells  $\text{ml}^{-1}$ , grown for 6-7 days to a cell density of  $2 \times 10^6$  cells  $\text{ml}^{-1}$ , each culture was either supplied with 17 mM sterile sodium acetate (left) or with the equal volume of sterile purified water as control (right) and cells for elemental analysis by ICP-MS/MS were taken at each time point. **A:** Cellular iron content was related to the number of cells analyzed as well as **B:** to the sulfur content of the same sample. The mean of four independent replicates is shown for the acetate addition experiment, error bars represent SD. Two independent replicates of the control experiment are shown as individual line graphs.

The various normalization options become useful in the context of the biology here. temporary synchronization/cell size increase effect from acetate addition, different normalizations to decipher what the underlying cause of the changes in the individual elements is. what the short-term and the long-term adjustment to the change in trophic status are, no changes in no-acetate control time course; and for all element's differences between acetate and no-acetate time course, change in trophic status has major effect on metal homeostasis; but the fluctuations in the elemental contents are different from each other (so not a general affect, but probably specific). most elements show an increase at 12 and 18h after addition of acetate as well as 48h when normalized to cell number, also present in S. Normalization to sulfur works well to reduce this increase at 12, 18 and 48h (due to cell size changes when normalized to /cell); Fe/S looks similar to Fe/cell of the no-acetate ctrl time course (S fluctuates a lot in ctrl time course); 1  $\mu$ M has a gradual decrease in iron content, becomes more like 0.25  $\mu$ M at 48h (they get Fe limited at the end).

## 2. Results

Individual *p*-values comparing the iron content between the samples are listed in Supplemental Table 39.

Cellular magnesium and calcium levels, normalized to the number of sulfur atoms, gradually decreased during the acclimation to acetate, showing little or no effect between the iron conditions (Figure 44). Mg levels decreased to less than 45% of photoautotrophic levels, whereas Fe-limited cells only exhibiting a milder reduction by 25%.

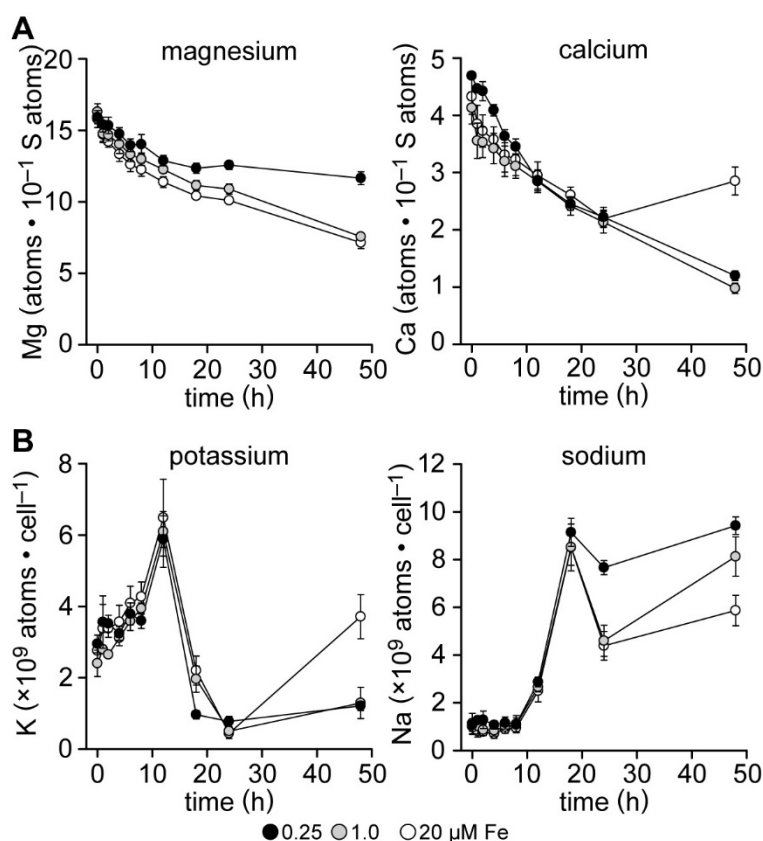


**Figure 44. Mg and Ca content.** Cells of strain CC-4532 were grown with increased aeration and light, without acetate (photoautotrophic) for a full growth curve before starting replicate pre-cultures containing 2  $\mu$ M Fe-EDTA. Photoautotrophic cultures containing 0.25 (black circles), 1.0 (grey circles), and 20  $\mu$ M Fe-EDTA (white circles) were inoculated to an initial cell density of  $2 \times 10^4$  cells  $\text{ml}^{-1}$ , grown for 6-7 days to a cell density of  $2 \times 10^6$  cells  $\text{ml}^{-1}$ , each culture was either supplied with 17 mM sterile sodium acetate. Cells for elemental analysis by ICP-MS/MS were taken at each time point. **A:** Cellular Mg and Ca content was related to the sulfur content of the same sample. **B:** Cellular K and Na content was related to the number of cells analyzed. The mean of four independent replicates is shown, error bars represent one standard deviation of the mean.

## 2. Results

Potassium and sodium pools displayed distinctly different behavior from the other elements. Both experienced large increases in the cellular quota, 2-fold increase in K pools at 12h and a 6-fold reduction from  $6$  to  $1 \times 10^9$  atoms $\cdot$ cell $^{-1}$  within four hours. The Na content increased almost 10-fold between 8 and 18h post-acetate. This could be influenced by the increased extracellular Na level, because the acetate was added with Na as the counter ion. But even though the extracellular Na increased rapidly by more than 170-fold, the intracellular content did not increase until 8h after the addition. Whereas the reduction in Na content by  $\sim 50\%$  coincides with cell division and a passive dilution of cellular Na levels, K is excreted before cells divide and to a more dramatic extent, suggesting an active export. Na and K did not exhibit dramatic changes in control cultures without acetate (Supplemental Figure 47). Individual  $p$ -values comparing the Mg, Ca, K and Na content between the samples are listed in Supplemental Table 40-43.

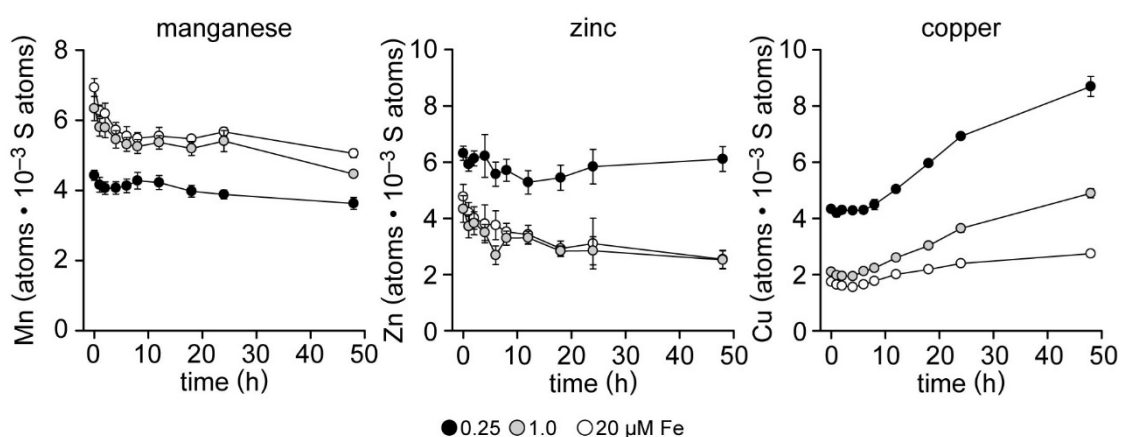


**Figure 45. Sulfur-normalized Mn, Zn, and Cu content.** Cells of strain CC-4532 were grown with increased aeration and light, without acetate (photoautotrophic) for a full growth curve before starting replicate pre-cultures containing 2  $\mu$ M Fe-EDTA. Photoautotrophic cultures containing 0.25 (black circles), 1.0 (grey circles), and 20  $\mu$ M Fe-EDTA (white circles) were inoculated to an initial cell density of  $2 \times 10^4$  cells ml $^{-1}$ , grown for 6-7 d to a cell density of  $2 \times 10^6$  cells ml $^{-1}$ , each culture was supplied with 17 mM sterile sodium acetate and cells for elemental analysis by ICP-MS/MS were taken at each time point. Cellular content was related to the sulfur content of the same sample. The mean of four independent replicates is shown, error bars represent one standard deviation of the mean.

Mn, Zn and Cu represent elements of the ionome with an Fe-dependent quota and only minor variation during the acclimation to acetate (Figure 45). The manganese pool is one-third lower during Fe-limitation and remained largely unchanged during the time course. The zinc and copper pool are large during Fe-limitation, zinc was increased by 50% in Fe-limitation and cellular levels remained unchanged during the acclimation to acetate. The

## 2. Results

---

Fe-limited Cu content was 2.2-fold increase compared to replete conditions and increased 2-fold during the time course. Cu increased in correlation with Fe starvation, Fe limited cultures became more Fe-starved during the time course and Fe-deficient cells experienced Fe-limitation at the end of the experiment, both indicated by increasing cellular Cu levels. Individual *p*-values comparing the Mg, Zn and Cu content between the samples are listed in Supplemental Table 44-46.

### 2.4.6 Variations in the Experimental Procedure.

The experimental results presented in the previous section were obtained from large flasks in large cultural volume, it has been observed before, that flask size and culture volume can influence the phenotype to a substantial extent (factors can include aeration rate, turbulences, illumination profile of the culture). To start further characterization of specific details of the trophic switch and what affects the pathway(s) responsible for the acclimation, four variations of the experimental setup were analyzed. Chlorophyll content was examined as marker for the trophic modification. The experiment resulted the same characteristic loss in chlorophyll content in a small culture volume (100 ml TP-medium in 250 ml-Erlenmeyer flasks, Figure 46A). In addition to the replicated conditions, Fe-excess was included and showed no deviation in chlorophyll content from replete cultures. Individual *p*-values comparing the chlorophyll content between the samples are listed in Supplemental Table 47.

When adding acetate to Fe-limited photoautotrophic cultures at  $2 \times 10^6$  cells·ml<sup>-1</sup>, cells doubled one more time and the cultures reached  $\sim 4 \times 10^6$  cells·ml<sup>-1</sup>, even though control cultures were able to sustain more doublings. This is the same final stationary phase density observed in Fe-limited cultures during steady state photoheterotrophic growth. To test whether cells double one more time after the addition of acetate or if rather the density of  $4 \times 10^6$  cells·ml<sup>-1</sup> is critical, acetate was added to cultures at 0.5, 1.0 and  $4 \times 10^6$  cells·ml<sup>-1</sup> (Figure 46B). The final cell density was the same as in the initial experiment. The chlorophyll content showed the same characteristic behavior, the reduction six hours after addition of acetate was observed independent of the cell density at the time of acetate supply. Individual *p*-values comparing the chlorophyll content between the samples are listed in Supplemental Table 48.

## 2. Results

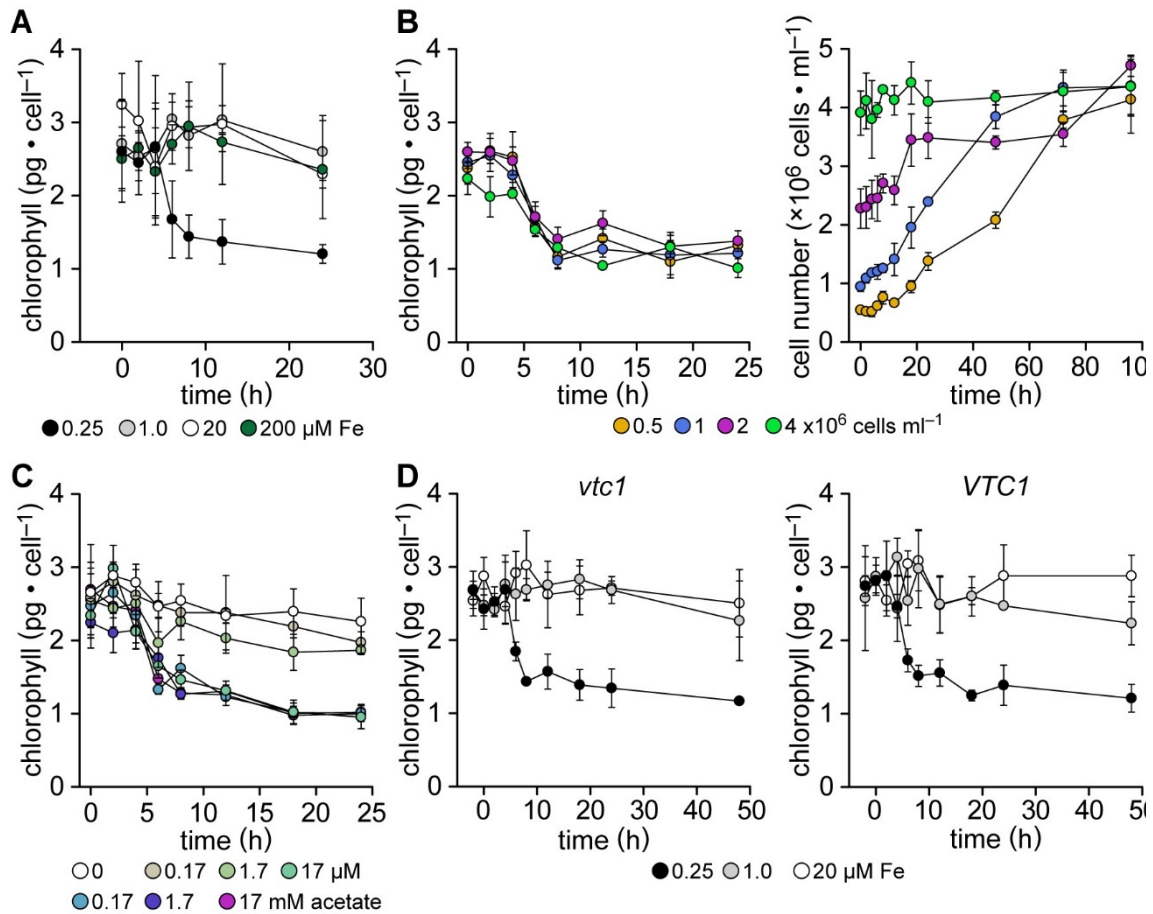


**Figure 46. Variations in the Experimental Setup.** Cells were grown with light and increased aeration, without acetate (photoautotrophic) in pre-cultures containing 2  $\mu\text{M}$  Fe. Photoautotrophic cultures containing 0.25, 1.0, and 20  $\mu\text{M}$  Fe were inoculated to an initial cell density of  $2 \times 10^4$  cells  $\text{ml}^{-1}$ , grown to a density of  $2 \times 10^6$  cells  $\text{ml}^{-1}$  (except C) and each culture was supplied with 17 mM sterile sodium acetate. Total chlorophyll content was assessed before and 0, 2, 4, 6, 8, 12, 18, and 24 hours after the addition of acetate from  $\sim 4 \times 10^6$  cells with a mixture of 80% acetone and 20% methanol (v/v) and absorption of the extract was measured spectrophotometrically against a solvent blank. The mean of three independent replicates is shown, error bars represent SD. **A:** Cultures grown in small flasks and including the excess iron condition. **B:** Variations in acetate concentration. **C:** Variation in cell density at acetate addition **D:** Wild-type strain CC-4533 and **E:** *vtc1* mutant and VTC1 complemented strain.

To dissect if the addition of acetate acts as carbon source, metabolic signal or both, a serial dilution of acetate was performed (Figure 46C). Acetate at a concentration as little as 17  $\mu\text{M}$  still lead to the characteristic reduction in chlorophyll content. Addition of 1.7  $\mu\text{M}$  acetate caused a chlorophyll phenotype situated in between control and the reduced chlorophyll content. Individual *p*-values comparing the chlorophyll content between the samples are listed in Supplemental Table 49. Growth curves of the acetate dilutions show the same behavior as the chlorophyll content, reduced concentrations up to 17  $\mu\text{M}$  lead to acetate-characteristic growth arrest at lower stationary cell density (Supplemental Figure

48), whereas lower concentrations maintain photoautotrophic characteristics. The VTC1 complemented strain, which can also be viewed as additional wild-type strain, displayed the chlorophyll reduction (Figure 46E) and the characteristic behavior was not affected in the *vtc1* mutant. Both strains showed no significant difference compared to wild-type strain CC-4532, the timing and extent of chlorophyll are comparable. Individual *p*-values comparing the samples are listed in Supplemental Table 50.

### 2.5 Examining the Range of Phenotypical Deviation in Wild-type Strains of *Chlamydomonas reinhardtii*.

#### 2.5.1 Chlorophyll content is a Prominent and Easily Visible Difference Observed Between *C. reinhardtii* Wild-type Strains.

Despite the recent common ancestry of the standard laboratory strains, there are many readily observable phenotypic differences between standard wild-type strains. These differences affect a wide range of cellular functions, including photosynthetic parameters, like the presence or absence of non-photochemical quenching (NPQ) mechanisms (personal communication by F.A. Wollman, Paris), maintenance or loss of chlorophyll in the dark (Sager, 1955), the presence or absence of a well wall (Pazour et al., 1995); the ability to utilize macro- and micronutrients, like the loss of the ability to use nitrate as a N source (Fernández et al., 1989) and the effectiveness of utilization of sparse metal ions from the growth medium (Gallaher et al., 2015). It is likely that those factors contribute to controversially discussed experimental outcomes between different laboratories. One observation that is especially relevant to the metal-deficiency work of the Merchant laboratory, is chlorosis during copper-deficiency. Due to the correlation between Fe and Cu homeostasis and the reported differences in iron requirements, we propose that the reduction in chlorophyll content during Cu-deficiency in some, but not all, strains is due to secondary iron-deficiency. To assess this, cells of CC-4532, the strain used for most trace metal research in the Merchant laboratory and CC-4402, the strain more sensitive to Fe-limitation (Gallaher et al., 2015), were compared. Cultures were grown in illuminated batch cultures in the presence of acetate in three different conditions: a) replete TAP medium containing 20  $\mu$ M Fe and 2.5  $\mu$ M Cu, b) Cu-deficient medium with 20  $\mu$ M Fe and no added Cu and c) Fe-excess and Cu-deficient medium containing 200  $\mu$ M Fe and no

## 2. Results

added Cu (Figure 47A). Cu-deficient cultures of CC-4532 show replete chlorophyll levels (light grey, left) at both regular (white, left) and excess (dark grey, left) iron concentrations in the growth medium:  $3.1 \pm 0.3 \text{ pg}\cdot\text{cell}^{-1}$  in replete,  $3.1 \pm 0.3 \text{ pg}\cdot\text{cell}^{-1}$  in Cu-deficient and  $3.7 \pm 0.2 \text{ pg}\cdot\text{cell}^{-1}$  in Cu-deficient/Fe-excess conditions.

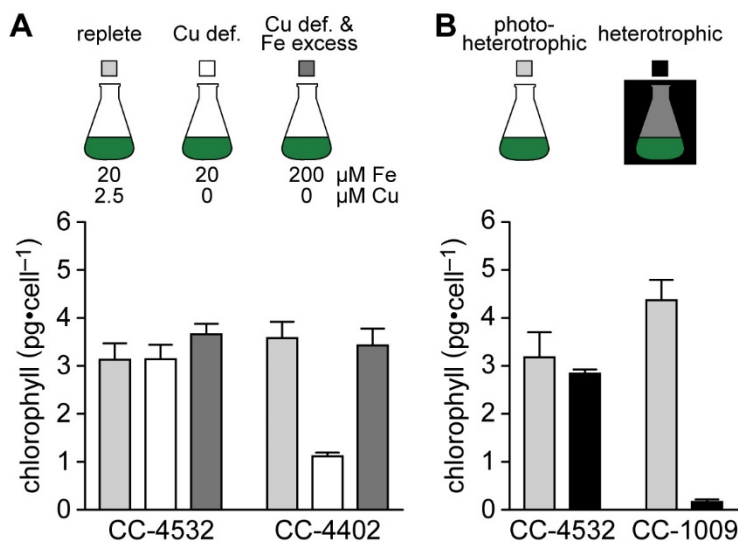


**Figure 47. Chlorophyll content between different strains. A:** Replicate cultures of strains CC-4532 and CC-4402 were grown three times from inoculation to stationary growth phase in photoheterotrophic growth medium without added Cu. From this, cultures containing replete or no Cu, with and without excess Fe were inoculated at an initial cell density of  $1-2 \times 10^4 \text{ cells}\cdot\text{ml}^{-1}$  and grown to a density of  $4-5 \times 10^6 \text{ cells}\cdot\text{ml}^{-1}$ . **B:** Cells from replete cultures of CC-4532 and CC-1009 were grown in the presence of acetate and light (photoheterotrophic, grey) or acetate without light (heterotrophic, black) for a full growth curve before starting replicate pre-cultures. Cultures were inoculated to an initial density of  $1-2 \times 10^4 \text{ cells}\cdot\text{ml}^{-1}$  and grown to a density of  $2-3 \times 10^6 \text{ cells}\cdot\text{ml}^{-1}$  for analysis. Total chlorophyll content was assessed from  $\sim 4 \times 10^6$  intact cells with a mixture of 80% acetone and 20% methanol (v/v) and absorption of the extract was measured spectrophotometrically against a blank. The mean of three (A) or four (B) replicates is shown for each condition, error bars represent SD.

In contrast, Cu-deficient cultures of strain CC-4402 displayed a significant reduction in chlorophyll content by 69%, from  $3.6 \pm 0.3 \text{ pg}\cdot\text{cell}^{-1}$  in replete (light grey, right) to  $1.12 \pm 0.07 \text{ pg}\cdot\text{cell}^{-1}$  in Cu-deficient (white, right) cultures. A difference is considered significant when the *p*-value calculated from an unpaired, two-tailed Student's *t*-test passes a significance threshold of  $\alpha = 0.05$ , individual *p*-values of chlorophyll content between the conditions are displayed in Supplemental Table 51. The presence of excess iron in the growth medium (dark grey, right) prevented the reduction in chlorophyll content ( $3.4 \pm 0.4$

## 2. Results

---

pg·cell<sup>-1</sup>). Only the chlorophyll content, but not the growth rate, were affected by Cu-deficient and Fe-excess conditions.

Another variation is the maintenance of chlorophyll in the dark (Figure 47B). In heterotrophic conditions, it is not obligatory for this alga to maintain phototrophic levels of chlorophyll for optimal growth, yet most strains invest energy to sustain chlorophyll molecules, even for long periods of heterotrophic growth spanning many rounds of doubling. Replete cultures of strains CC-4532 and CC-1009 were grown in the presence of acetate with and without illumination in batch cultures for a full growth curve before starting replicate pre-cultures. Three experimental cultures for each strain and condition were inoculated to an initial density of  $1-2 \times 10^4$  cells·ml<sup>-1</sup> and grown for 3 d with, or 9 d without illumination, to a density of  $2-3 \times 10^6$  cells·ml<sup>-1</sup>. Cells of strain CC-4532 maintain chlorophyll levels in the dark,  $3.2 \pm 0.5$  pg·cell<sup>-1</sup> with, and  $2.8 \pm 0.1$  pg·cell<sup>-1</sup> without illumination. In contrast, cultures of CC-1009 exhibited a significant loss of chlorophyll down to only 4% of photoheterotrophic levels ( $4.4 \pm 0.4$  pg·cell<sup>-1</sup> with, and  $0.2 \pm 0.1$  pg·cell<sup>-1</sup> without illumination). Individual *p*-values are listed in Supplemental Table 52. In order to investigate observed changes between wildtype strains, we generated transcriptomics data for all 5 wildtype strains. This will allow us to investigate which genes might be responsible for the observed phenotypic changes between the different strains.

### 2.5.2 Variability in the Transcriptome of Different Wildtype Strains

Genome sequencing of wildtype strains showed some differences between genome sequences in the range of around 2%. These differences are not randomly distributed over the genome, but rather falling in one of two haplotypes (Gallaher et al., 2015). One question arising from this observation was whether or how this affects the expression of the genome. To get an idea of how large this general background variability is, I compared basal expression levels of several standard laboratory strains, grown in standard growth conditions, in well documented experimental conditions. Based on the haplotype blocks described before (Gallaher et al., 2015), I chose five representative strains, that have a wide distribution over the different haplotype combinations and are broadly used in *Chlamydomonas* laboratories (Figure 48A). Cells of strains CC-124, CC-4532, CC-1690, CC1009 and CC-1691 were grown to mid-logarithmic growth in replete TAP medium and cells from 4 individual cultures per strain were collected for mRNA extraction. The



## 2. Results

transcriptome in each sample was determined by Illumina RNA-Seq and the sequenced reads were aligned to the Au111.6 gene models. Expression estimates were calculated as FPKM (fragments per kilobase of transcript per million fragments mapped). The between-sample variation of the four replicate samples is small (Supplemental Figure 49) and the average expression was used for further analysis unless stated otherwise. A minimum expression cutoff of  $\geq 1$  FPKM across all strains was applied and resulted in 14038 detected transcripts (Supplemental Figure 50).

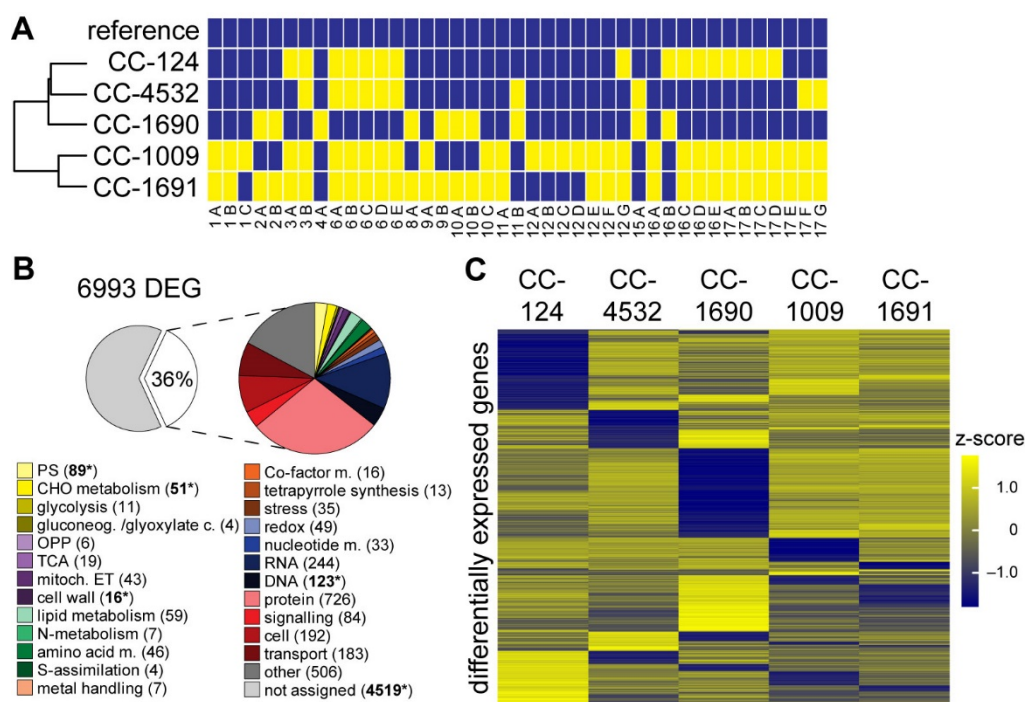


**Figure 48. Transcriptome analysis of five different wild-type strains.** Photoheterotrophic cultures were grown to a density of  $2 \times 10^6$  cells·ml<sup>-1</sup> for analysis by RNA-Seq. **A:** Haplotype block distribution modified from (Gallaher et al., 2015). The distance tree was calculated based on the differences in genome sequences and haplotype block distribution. **B:** Differentially expressed genes (DEG) between the wild-type strains were extracted from Cuffdiff output using additional selection (FDR < 5%, fold change  $\geq 2$ ) and grouped by functional annotation of their predicted protein sequence according to the MapMan annotation. The number of genes in each category is noted in parentheses behind each group, an asterisk (\*) marks groups that are significantly enriched ( $\alpha=0.005$ ) compared to randomly assigned gene groups. **C:** Clustered heatmap containing the z-score normalized expression of all 6993 differentially expressed genes.

The reference refers to strain CC-503, which is the strain used as the reference genome at JGI and the standard genome sequence for mapping transcriptome reads. Genes were classified as differentially expressed using a confidence level of  $\alpha=0.005$ , a false discovery rate of < 5% and a minimum of 2-fold regulation. Using these criteria, 6993 genes (39%

## 2. Results

of all transcripts or 50% of expressed transcripts) were identified (Figure 48B) with differential expression between at least two of the strains.

For a functional characterization of the transcriptome changes, the differentially expressed (DE) genes were grouped by the functional annotation of their predicted protein sequence according to the MapMan ontology. The number of genes in each group is displayed in parentheses next to the group. Overrepresented groups include photosynthesis, major and minor carbohydrate metabolism and DNA metabolism. Genes without assigned annotation are overrepresented as well, compared to randomly assigned genes. The z-score normalized expression profiles of the 6993 DE genes were plotted as a clustered heatmap (Figure 48C).

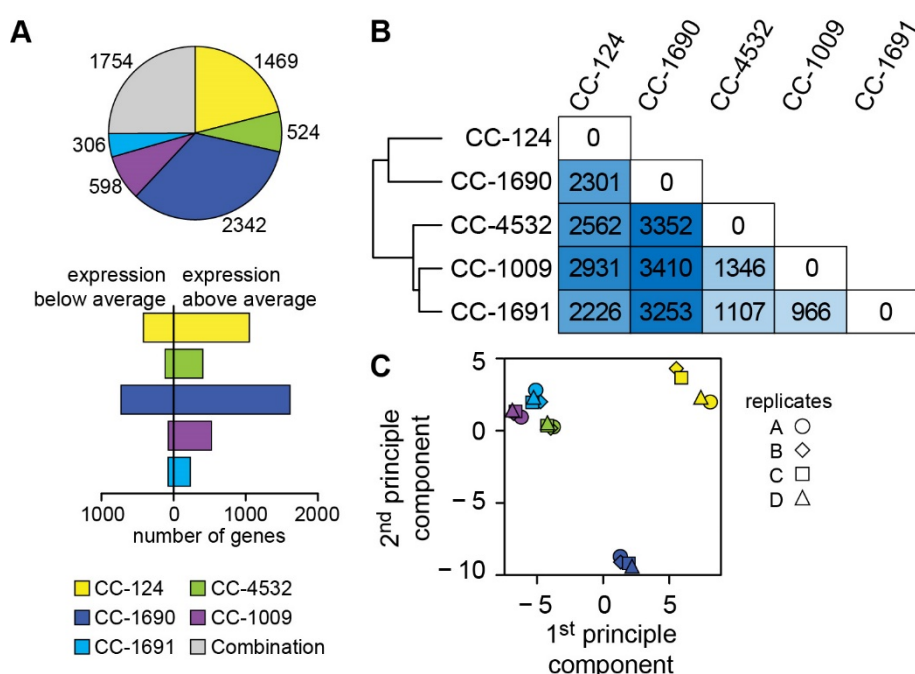


**Figure 49. Transcriptome analysis.** **A:** Proportion of DE genes that are only different from average in one of the five strains (top) and how the proportion of genes with expression above or below average (bottom). **B:** DE genes between individual samples are shown, the color gradient from white to blue indicates the number of DEGs from minimum to maximum. The distance tree left of the matrix was calculated based on the number of differentially expressed between the strains. **C:** A principal component analysis was generated from the individual replicates of the 5 strains using cummeRbund (details in section 4.2).

The distribution of DE genes was not evenly dispersed between the strains with large blocks of genes in the heatmap that are above (yellow) or below (blue) average in only one of the strains. Of the 6693 DE genes, around  $\frac{3}{4}$  of genes were significantly different in only one of the 5 strains (Figure 49). The pie chart shows the distribution of genes uniquely

## 2. Results

---

different in only one of the strains. The number was highest in CC-1690 and lowest in CC-1691. Of the deviating genes, the majority exhibited expression levels above the mean. The distance tree was calculated based on the expression of the 6993 DE genes and turned out to be slightly different from the distance calculated from the genome (Figure 49B and Figure 48A).

The general relationship is the same, only CC-4532 clusters differently between the two major groups, now closer related to the transcriptome of CC-1009 and CC-1691, instead of CC-124 and CC-1690. Genes from all major annotation groups are represented in the differentially expressed genes, and genes without annotation are overrepresented in all comparisons (Supplemental Figure 51). To display the overall relationship between the strains, a principal component analysis was performed (Figure 49C). CC-4532, CC-1009 and CC-1691 cluster close together, whereas both CC-1690 and CC-124 are more diverse from the other strains and also from each other.

### 2.5.3 Examples of Differentially Expressed Genes Between the Strains

The expression patterns of several genes are illustrated to show the range of variation observed between the five strains. The 15 genes on the left (Figure 50A) are all amongst the 18 most highly expressed genes in every strain. The genes were sorted by FPKM expression in strain CC-124. The highest expressed genes are the same in all strains, even though the absolute expression levels were quite different. Nine of the genes are ribosomal subunits (genes 4, 5, 7, 9, 10, 11, 12, 13 and 14), 3 genes encode chlorophyll binding subunits of the light harvesting complex II (genes 1, 8 and 15), *PCY1*, encoding plastocyanin (2.), the RuBisCo subunit *RBCS2* (6.) and *LCl3*, a low CO<sub>2</sub>-inducible gene (3.). The absolute expression level of all 15 genes was highest in CC-1690. This strain exhibited a higher expression in a large number of genes, but not systematically over the entire dataset that would indicate a technical bias or general issue, but rather a strain-specific expression effect.

Next, I picked 15 genes with large fold change differences and interesting expression patterns (Figure 50B). This group includes genes that are only expressed in a subset of strains, therefore low expression values were included, and the green dashed line indicates the  $\leq 1$  FPKM cutoff that was applied to determine differentially expressed genes. Of the 15 genes, only 7 have a predicted functional annotation and 5 of the genes without

## 2. Results

annotation also do not have any orthologs in *Chlamydomonas* or other organisms. This group of genes with predicted function include an extracellular polypeptide (2.), a peptidyl-prolyl cis-trans isomerase (3.), an L-arabinitol 4-dehydrogenase (4.), a gene associated with flagella (5.), a gene with a methyltransferase domain (6.), and a gene encoding a protein involved thylakoid curvature (13.). Two genes with largest fold-change between strains were Cre18.g748297 (11.) and Cre24.g755997, a predicted cell wall protein pherophorin (15.) with an estimated difference in expression of 200 to 400-fold. Both genes showed lowest expression levels in CC-1690 and highest expression in CC-4532.

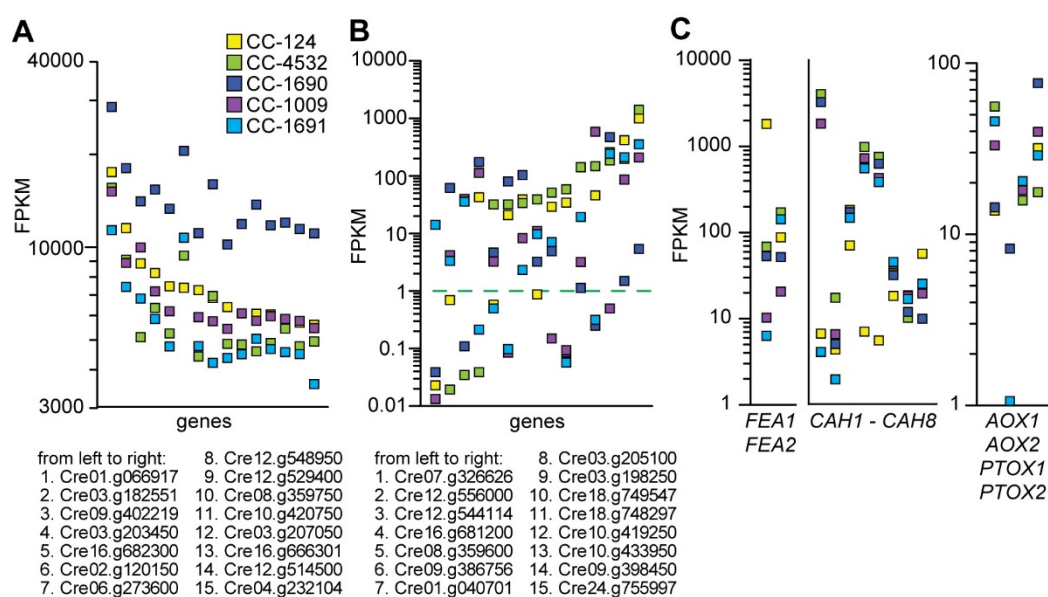


**Figure 50. Expression of exemplary genes with distinct expression pattern between strains.** **A:** 15 genes that exhibited the highest expression. **B:** 15 genes with specific expression patterns. The dashed line indicates the  $\leq 1$  FPKM cut off. **C:** Expression of FEA1 and FEA2, the carbonic anhydrases, and alternative alternative oxidases.

A few specific genes that stood out were *FEA1* and *FEA2*, the carbonic anhydrases and alternative oxidases (Figure 50C). *FEA1* and *FEA2* are excreted proteins that are involved in cellular Fe uptake, *FEA1* had an 8-fold and *FEA2* a 3-fold expression difference between the strains. Of the carbonic anhydrases, enzymes catalyzing the conversions between  $\text{CO}_2$  and  $\text{HCO}_3^{1-}$ , CAH7 is the only one whose gene is not differentially expressed between any of the strains. The spectrum varies for CA, the strains seem to utilize the various isoforms differently, maybe depending on the carbonate requirements of the compartments of the respective isoform. Mitochondrial alternative oxidases were both differentially expressed between strains; CC-1690 for example had lowest *AOX1*, but highest *AOX2* expression

## 2. Results

amongst the strains, whereas CC-1691 showed second highest *AOX1* expression, but without notable *AOX2* transcript abundance. The *Chlamydomonas* genome encodes two chloroplast localized alternative oxidases, *PTOX1* and *PTOX2*, with *PTOX2* being mainly responsible for alternative oxidase activity in the chloroplast (Houille-Vernes et al., 2011). As expected, *PTOX1* was not differentially expressed between any of the strains, but *PTOX2* showed up to 4-fold change in transcript abundance between CC-4532 and CC-1690.

All major pathways are represented in the differentially expressed genes between the strains, including central carbon metabolism and energy conversion. As an additional illustration of the variability within certain pathways, the normalized expression of genes involved in photosynthesis and respiration were plotted (Figure 51). The expression of each gene was normalized to the maximum expression among the 5 samples, the expression of individual genes within the larger complexes were staggered and arranged by strain and only genes matching the criteria for differential expression were included. Some complexes of both photosynthesis and respiration are more variable than others. Even though there is a lot of variation, PSI and LHCI genes are very similar in their relative expression, both showed variation between the strains but tight relative expression within a strain. CC-1690 had the highest expression levels for most, but not all complexes, whereas CC-1691 was often at the lower end of the expression levels.

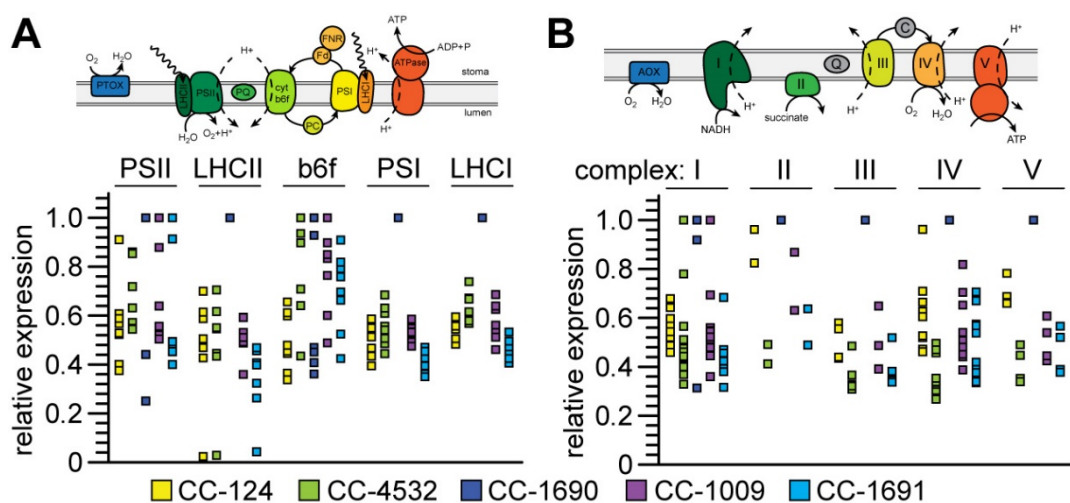


**Figure 51. Expression of photosynthetic and respiratory genes.** Relative expression of genes encoding **A:** photosynthetic and **B:** respiratory complexes. Differentially expressed genes were normalized, grouped and stacked by complex and arranged by strain.

## 2. Results

---

When using whole transcriptome analysis to investigate scientific questions, comparisons between conditions are commonly used. If differences in the strain background already lead to a rather large number of differentially expressed genes even in the same standard growth conditions, wrong conclusions may be drawn. Another approach may be to look at the same strain in many different experiments. Therefore, I used the large pool of transcriptome datasets in *Chlamydomonas* to compare the transcriptome of CC-4532 in standard replete conditions between individual replicate samples and various experiments for the overall variability in expression estimates.

First, I looked at the 4 independent samples from the strain comparison dataset (Figure 52A). A specific replication strategy was used to analyze the variability within independent biological replicates. Cultures A and B were grown and sampled in parallel, as well as cultures C and D, about 3 weeks apart. A bias between these two groups of cultures would show in higher Spearman's correlation coefficients of the A-B and C-D comparison and lower coefficients of the other cross-comparisons. The correlation between replicates was very good ( $\rho > 0.980$ ) but a bias was not observed. The degree of correlation between replicates was more depending on strain background, CC-4532 with the lowest and CC-124 with the largest differences in correlation coefficients.

Next, I compared the transcriptome of CC-4532 from several experiments (Figure 52B). "Dataset 1" is CC-4532 from this strain comparison, "Dataset 2" is replete CC-4532 from the Fe-excess experiment (Figure 12). Both were prepared by the same person, in the same laboratory, grown in the same conditions, about 6 months apart. "Dataset 3" is CC-4532 before treatment, taken from an unpublished dataset from the Merchant Lab (Castruita et al., in preparation), prepared by a different person, but grown in the same conditions. "Dataset 4" and "Dataset 5" are replete CC-4532 sets from published experiments from the Merchant group [Dataset 4: Kropat et al., 2011; Dataset 5: Urzica et al., 2012], both were prepared in the same laboratory, but by different researchers and cells were grown in Hutner's trace metals, instead of the revised trace metal composition used in more recent experiments. All three additional datasets were re-analyzed (mapped to the same genome version and with the same parameters) to match the datasets in this thesis. The best correlation was observed between Dataset 1 and 2, which were prepared by the same researcher, followed by Dataset 3, which had the same trace metal composition in the growth medium. If the criteria for differentially expressed genes were applied, these three datasets will have between 10 and 100 differentially expressed genes. The number would

## 2. Results

increase up to 5000 DE genes when comparing to Datasets 4 and 5. This gives an indication for the importance of external parameters in determining DE genes from these types of experiments.

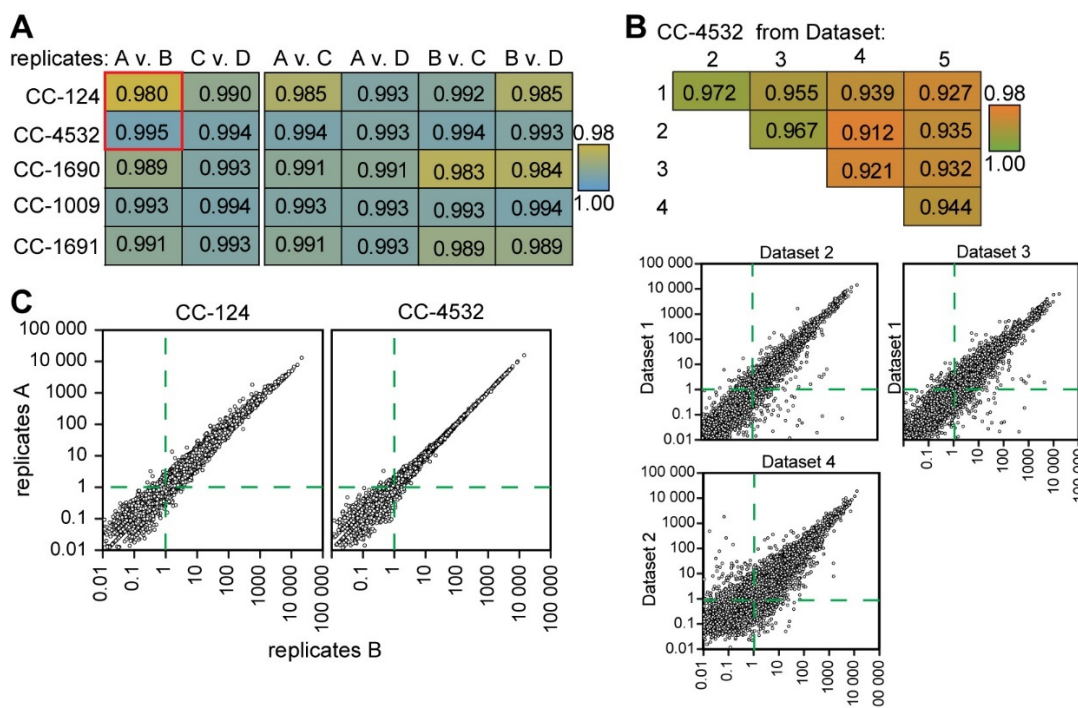


**Figure 52. Variance between independent samples.** The Spearman's rank correlation coefficient ( $\rho$ ) was calculated between the **A**: independent biological replicates for each of the strains and **B**: between CC-4532 from different experiments. Expression of all 17 741 genes were expressed as scatter plots to display the extent of variance between individual datasets (**B** and **C**).

### 2.5.4 Phenotypic Variability in Different Wild-type Strains.

#### 2.5.4.1 Conditions in which even small differences matter: a case study.

The transcriptome analysis revealed a large number of differentially expressed genes between the wild-type strains, almost all major pathways and cellular processes are affected and despite the substantial variation, no clear correlation between genotype and genes expression was observed. Do these differences in the transcriptome translate to phenotypic differences and how severe are they? To add some more general phenotypic characterization, I examined some basic features, including growth, photosynthetic parameters and elemental composition. Photoheterotrophic growth rates are very similar between the strains, with generation times between 9.3 and 9.6h (grey bars,  $9.4 \pm 0.3$ ,  $9.3 \pm 0.2$ ,  $9.6 \pm 0.2$ ,  $9.5 \pm 0.2$ , and  $9.5 \pm 0.1$ h in CC-124, CC-4532, CC-1690, CC-1009, and

## 2. Results

CC-1691, respectively) and get more divergent when the cells are grown photoautotrophic or heterotrophic (Figure 53). All five strains have significantly longer generation times in single-trophic (photoautotrophic or heterotrophic) than in double-trophic growth (photoheterotrophic). Based on the photoautotrophic growth, the strains can be distinguished into two groups: first, strains CC-124, CC-4532 and CC-1691 with a similar generation time of  $\sim 31$ h (white bars,  $31.0 \pm 1.9$ ,  $31.8 \pm 2.0$ , and  $29.1 \pm 1.1$ h in CC-124, CC-4532, and CC-1691, respectively) and strains CC-1690 and CC-1009 in a second group with a similar generation time of  $\sim 24$ h ( $24.9 \pm 2.2$ ,  $23.5 \pm 1.6$ h, respectively) which is 7h faster than the first groups growth without acetate. Heterotrophic growth is similar in all five strains, with generation times between 36 and 49h (black bars,  $36.4 \pm 2.6$ ,  $39.4 \pm 2.3$ ,  $49.6 \pm 9.2$ ,  $38.7 \pm 1.8$ , and  $36.5 \pm 2.0$ h in CC-124, CC-4532, CC-1690, CC-1009, and CC-1691, respectively). Growth on acetate alone permitted the slowest doubling times in all five strains (black, Figure 53). Individual *p*-values comparing the growth rates between the samples are listed in Supplemental Table 53. Photoautotrophic cultures reached stationary growth phase at a lower final cell density than photoheterotrophic cultures ( $9.5$  or  $12 \times 10^6$  cells $\cdot$ ml $^{-1}$ ), and heterotrophic cultures exhibited a prolonged lag-phase after inoculation. The growth curves used for calculating the generation time are displayed in Supplemental Figure 52.

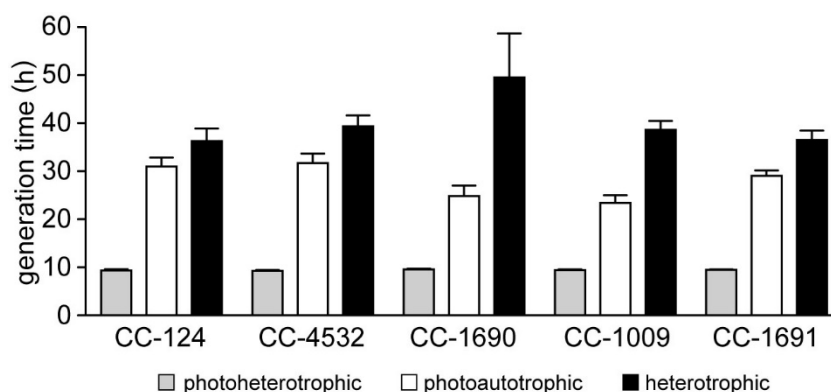


**Figure 53. Generation time of wild-type strains.** Cultures were grown in the presence of acetate and light (photoheterotrophic), increased air flow and light (photoautotrophic), or acetate (heterotrophic). Growth was monitored from inoculation to stationary phase and the cell number was determined every 24h by manual counting (Hemocytometer). The generation time was calculated from the resulting growth curves, starting when each culture reached  $1 \times 10^5$  cells $\cdot$ ml $^{-1}$  up to the first time point of stationary phase. The mean of the generation time calculated for each replicate individually is shown, error bars represent SD.



### 2.5.4.2 Strain-specific Variations in Photosynthetic Parameters.

Chlorophyll content was observed to be different in copper deficiency and can vary between strains and growth conditions. Genes encoding photosynthetic complexes are among the enriched groups in the differential expressed genes between the strains. To assess how this translates to potential physiological impacts, I compared the cellular chlorophyll content, the maximum quantum efficiency of PSII ( $F_v/F_m$ ) and the net oxygen consumption and evolution of steady state photoheterotrophic cultures in replete conditions. The cellular chlorophyll content varied significantly between the strains (Figure 54A), with CC-124, CC-4532 and CC-1690 at around  $3 \text{ pg}\cdot\text{cell}^{-1}$  ( $3.2 \pm 0.1$ ,  $3.2 \pm 0.5$ , and  $3.0 \pm 0.3 \text{ pg}\cdot\text{cell}^{-1}$ , respectively) and CC-1690 and CC-1009 with increased cellular content of  $5.5 \pm 0.6$  and  $4.4 \pm 0.4 \text{ pg}\cdot\text{cell}^{-1}$ . The maximum quantum efficiency of PSII ( $F_v/F_m$ ) is only significantly reduced from optimal values in strain CC-1009 ( $0.73 \pm 0.03$ ), all other strains exhibited a ratio between 0.78 and 0.8 (Figure 54B). Individual  $p$ -values comparing the chlorophyll and  $F_v/F_m$  between the strains are listed in Supplemental Tables 54 and 55.

The net oxygen consumption in the dark and evolution in constant illumination showed a larger range of variation between the strains (Figure 54C and D). When comparing individual rates to the spectrum observed in these five strains, CC-124 had a medium consumption rate and a medium evolution rate ( $2.2 \pm 0.2$  and  $4.2 \pm 0.5 \text{ nmol}\cdot\text{min}^{-1}\cdot 10^{-6}$  cells, respectively). CC-4532 exhibited a medium consumption and high evolution rate ( $2.3 \pm 0.2$  and  $6.4 \pm 0.55 \text{ nmol}\cdot\text{min}^{-1}\cdot 10^{-6}$  cells) and CC1690 with the highest consumption and lowest evolution rate ( $2.9 \pm 0.3$  and  $2.6 \pm 0.65 \text{ nmol}\cdot\text{min}^{-1}\cdot 10^{-6}$  cells). Strain CC-1009 had the lowest consumption and highest evolution rates ( $0.8 \pm 0.1$  and  $7.9 \pm 0.35 \text{ nmol}\cdot\text{min}^{-1}\cdot 10^{-6}$  cells) and CC-1691 showed medium consumption and high evolution rates ( $1.6 \pm 0.1$  and  $6.3 \pm 0.45 \text{ nmol}\cdot\text{min}^{-1}\cdot 10^{-6}$  cells). Except for the consumption rates between CC-124 and CC-4532 (same) and CC-4532 and CC-1690 (large error), all other rates differ significantly between the strains. Individual  $p$ -values comparing oxygen consumption and evolution between the strains are listed in Supplemental Table 56. Based on oxygen consumption and evolution, strains CC-124, CC-4532 and CC-1691 cluster together in a medium range, and CC-1690 and CC-1009 outside this range. In this case in opposite characteristics, CC-1690 with a large proportion of oxygen consumption and CC-1009 with a large proportion of oxygen evolution. This correlates well with the overall lower transcript abundance in ETC in CC-1009.

## 2. Results

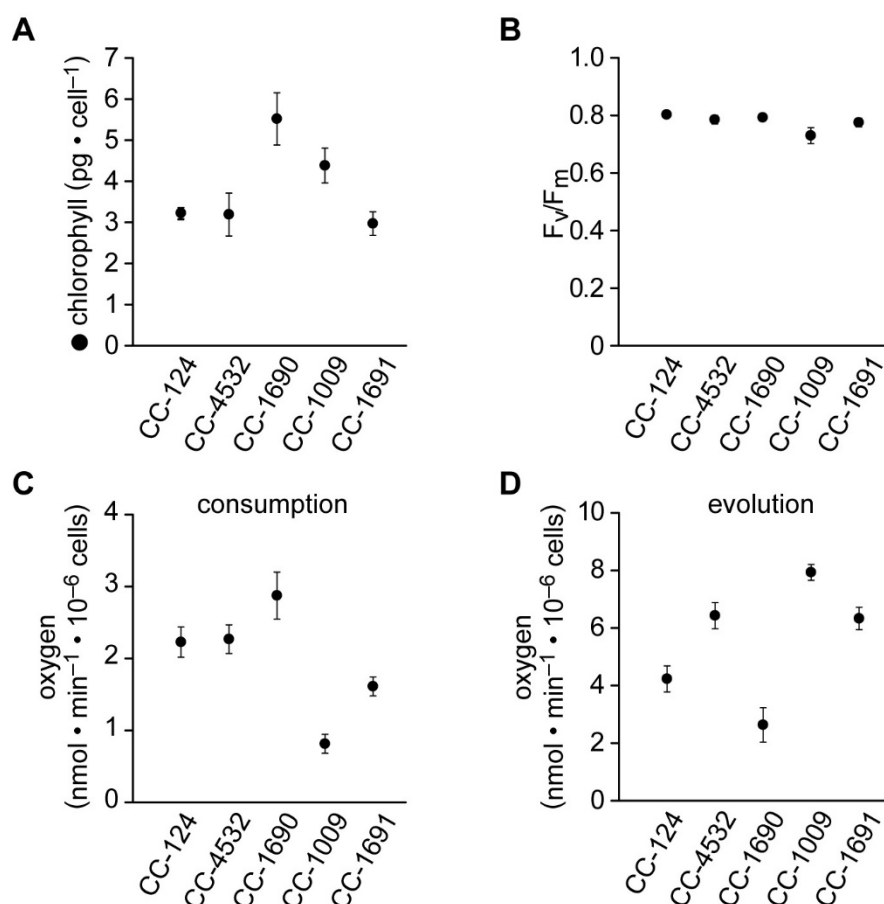


**Figure 54. Photosynthetic parameters of different wild-type strains.**

Photoheterotrophic cultures were grown to a density of  $2 \times 10^6$  cells·ml<sup>-1</sup> for analysis. **A:** Total chlorophyll was extracted from  $\sim 4 \times 10^6$  cells with a mixture of 80% acetone/20% methanol (v/v) and absorption of the extract measured spectrophotometrically against a solvent blank. Chlorophyll content was related to the number of cells analyzed. **B:** Maximum quantum efficiency of PSII ( $F_v/F_m$ ) was determined from  $\sim 2 \times 10^6$  cells immobilized onto 15 mm round filters after dark-adaptation for 12-15 min using saturating light. The rates of **C:** net oxygen consumption and **D:** net oxygen evolution was measured from  $\sim 4 \times 10^6$  intact cells. The decrease in dissolved oxygen in the dark and the increase during constant illumination with  $100 \mu\text{mol m}^{-2} \text{s}^{-1}$  was monitored for five minutes each and the resulting rate was related to the number of cells analyzed. The mean of four replicates is shown, error bars represent SD.

### 2.5.4.3 Macro Nutrient Dissimilarities Largely Due to Cell Volume.

One observation during the work with various *Chlamydomonas* strains was the variability in cell size in some of the strains. Particularly, cells of CC-1690 appeared larger and in some instances tended to form clusters of 3 to 4 cells when stressed. To quantify this observation, the cell diameter distribution of healthy mid-logarithmic cells was determined

## 2. Results

using a cell counter and the median diameter of at least 500 individual cells was used to calculate the median volume of 4 independent cultures for each strain. CC-124, CC-4532, and CC-1691 had a very similar cell volume of  $353 \pm 38$ ,  $328 \pm 49$ , and  $315 \pm 42 \mu\text{m}^3$ , respectively (Figure 55A). CC-1690 had a significantly increased cell volume by 134%, to  $439 \pm 69 \mu\text{m}^3$  compared to CC-4532. In addition, cells of the same cultures were examined using a hemocytometer under a light microscope to estimate the proportion of clustered cells, which were below 5% in all strains. In contrast, CC-1009 displayed a significantly smaller cell volume of  $227 \pm 25 \mu\text{m}^3$ , 69% of CC-4532's volume.

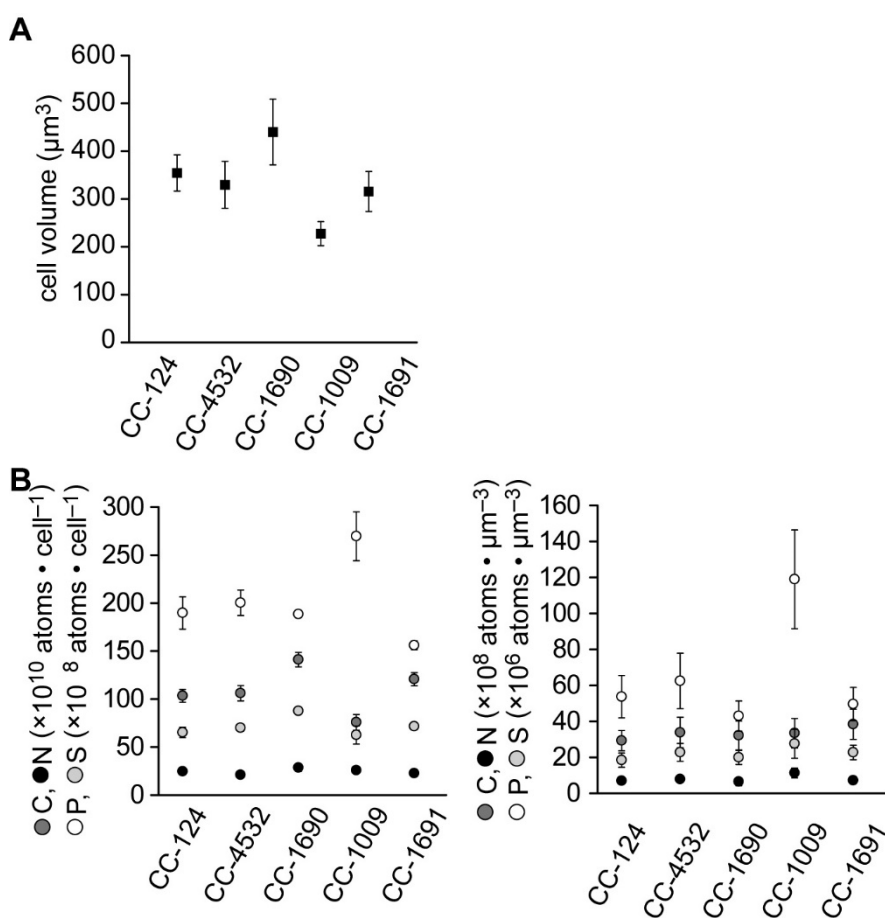


**Figure 55. Cellular C, N, P, and S content.** Cells were grown in the presence of acetate and light (photoheterotrophic), increased air flow and light (photoautotrophic), or acetate (heterotrophic) to a density of  $2 \times 10^6$  cells  $\cdot$  ml $^{-1}$ . **A:** Average cell volume was calculated from the median cell diameter of 4 cultures of each strain. **B:** C (dark grey), N (black), P (white) and S (light grey) content were analyzed by TOC-TN analysis and related to the number of cells analyzed (left) and the average cell volume (right). The mean of four replicates is shown, error bars represent SD.

## 2. Results

---

The cellular content of the macro nutrients carbon, nitrogen, phosphorus and sulfur is often considered as an indicator or equivalent for biomass, but only very little systematic characterization has been published on these parameters. To check if there are specific ratios or differences in the macro-nutrients and how they correlate to the cellular volume, I analyzed the five strains for their cellular content of C, N, P and S (Figure 55B).

Strains CC-124, CC-4532, and CC-1691 exhibited a similar composition of C, N, P, and S. Again, deviating behavior was observed in strains CC-1690 and CC-1009. CC-1690 showed reduced P content, both per cell and when related to cell volume. Carbon per cell appears higher compared to the other strains but falls in the same range when normalized to the cell volume. The cellular phosphorus content is significantly increased in CC-1009, both when normalized to the number of cells analyzed or the cellular volume, 2-fold increase of phosphorus compared to strain CC-4532 ( $119.0 \pm 27.4$  and  $61.0 \pm 15.4 \times 10^6$  atoms $\cdot\mu\text{m}^{-3}$ ) and even a 3-fold increase compared to CC-1690 ( $43.0 \pm 8.4 \times 10^6$  atoms $\cdot\mu\text{m}^{-3}$ ). The lower carbon content of CC-1009 can be related to the smaller cell volume and is not significant anymore, when normalized to the volume. Individual *p*-values comparing the C, N, P, S content and cell volume between the samples are listed in Supplemental Tables 57 and 58.

### 2.5.4.4 Micronutrient Composition of Wild-type Strains.

In addition to the macronutrients C, N, S and P, also the so-called micronutrients show distinct variabilities between the strains. While micronutrients are in general much lower in abundance in eukaryotic cells as compared to macronutrients, they have critical roles as co-factors for many enzymes. Cultures were grown in replete conditions to their mid-logarithmic growth phase, analyzed by ICP-MS/MS and normalized to cell number and the S content (Figure 56). ICP-MS/MS data were normalized to the S content instead of the cellular volume, because the sulfur content showed a good correlation to cellular biomass and is measured from the same cell lysate by the same analytical method, and by this allowing for the most accurate comparison and smallest errors. Both normalizations, content per cell (filled) and atoms per S (open symbols) are compared.

CC-124 and CC-4532 had the same cellular content of K, Na, Mg and Ca. K content of CC-1691 was the same as CC-124/CC-4532, whereas Na, Mg and Ca were significantly lower compared to CC-124/CC-4532. CC-1690 exhibited significantly higher potassium content, slightly higher Na, slightly lower Mg content and significantly lower Ca content

## 2. Results

compared to CC-124/CC-4532. Which can be seen by the even higher content of all four elements when normalized to S.

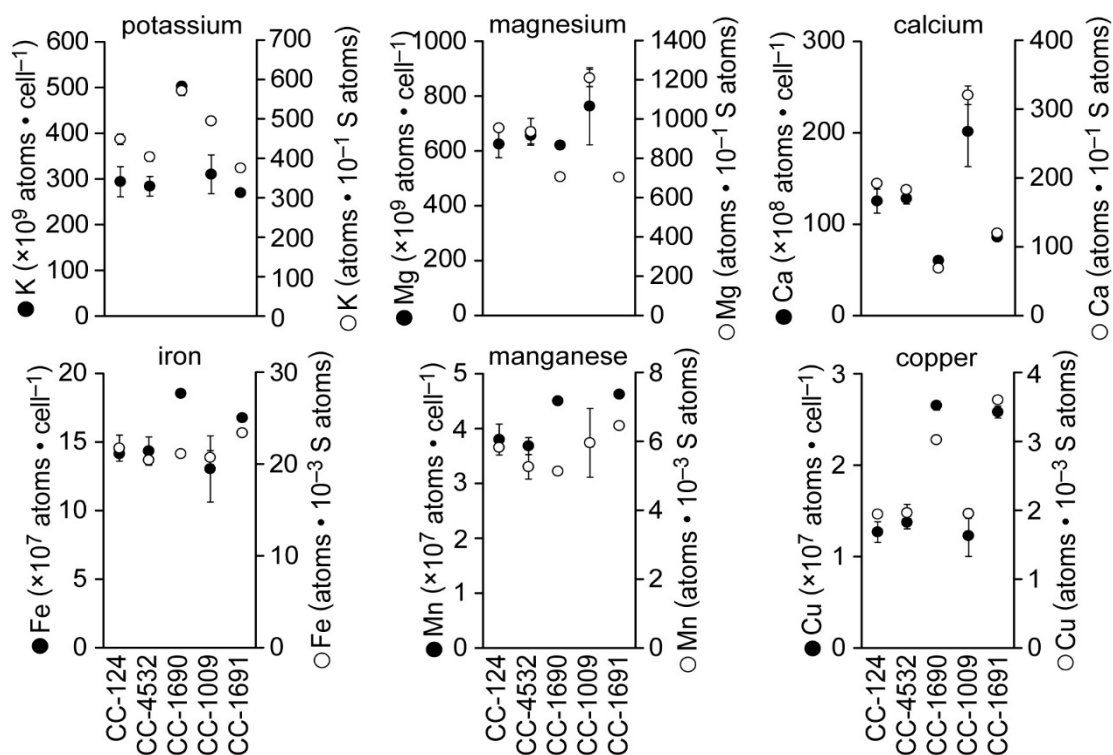


**Figure 56. Micro nutrient content.** Photoheterotrophic cultures were grown to a density of  $2 \times 10^6$  cells  $\cdot$  ml $^{-1}$  for analysis by ICP-MS/MS. Cellular K, Mg, Ca, Fe, Mn and Cu content was related to the number of cells analyzed (black circles) and to the cell volume (white circles). The mean of four replicates is shown, error bars represent SD.

The difference in Ca content between CC-1690 and CC-1009 is more than 4-fold. Again, CC-124, CC-4532 and CC-1691 group closely, whereas CC-1690 and CC-1009 are distinctly different. Individual *p*-values comparing the micronutrient content between the samples are listed in Supplemental Table 59. Cellular iron and manganese levels were similar in strains CC-124, CC-4532 and CC-1009 and slightly elevated in CC-1691. CC-1690 showed again higher cellular content of both Fe and Mn, but this difference disappears, when the larger cell volume is taken into account. The cellular copper levels were similar in CC-124, CC-4532 and CC1009, CC-1690 and CC-1691 about double of CC-4532 levels.

## 2. Results

### 2.5.4.5 Strain-dependent Variation in Iron Homeostasis.

Minor differences in the elemental composition in standard conditions were observed between the five wild-type strains. To test if such variation is also observed for iron homeostasis, cells of the wild-type strains were grown in pre-cultures containing 1  $\mu\text{M}$  Fe and transferred to experimental cultures containing 0.1, 0.25, 1.0, 20 and 200  $\mu\text{M}$  Fe and grown to stationary growth phase. Cultures were photographed 4 days after inoculation, when most cultures were between mid- and late-logarithmic growth phase (Figure 57A) and the generation time was calculated from the linear section of the growth curves for each strain and condition (between days 2 and 4 for most cultures).

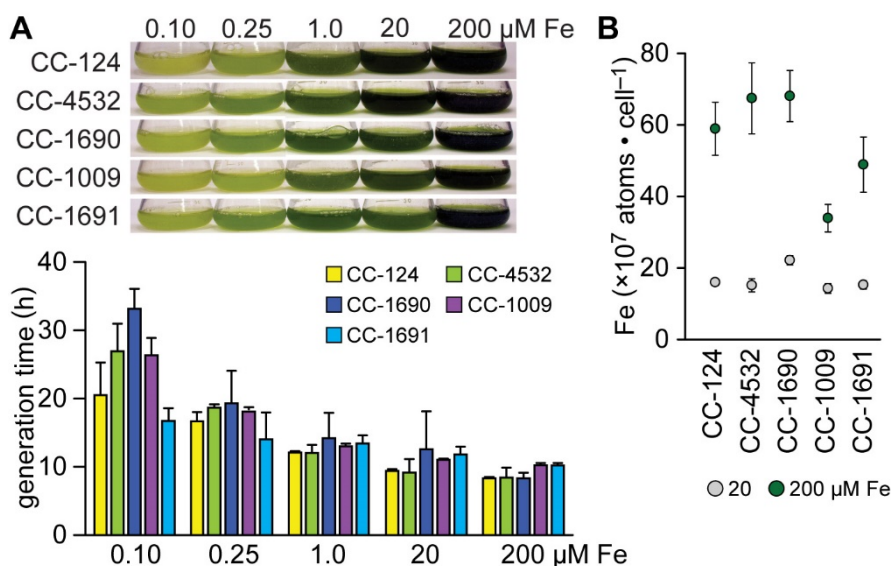


**Figure 57. Iron homeostasis in wildtype strains.** **A:** Photoheterotrophic cultures containing 0.10, 0.25, 1.0, 2.0, **B:** Iron accumulation in excess conditions. Photoheterotrophic cultures containing 20 and 200  $\mu\text{M}$  Fe were inoculated from pre-cultures containing 20 and 200  $\mu\text{M}$  Fe, grown to  $2 \times 10^6$  cells $\cdot\text{ml}^{-1}$  and analyzed by ICP-MS/MS. The mean of three replicates is shown, error bars represent SD.

To characterize the ability to accumulate excess Fe, all strains were grown in both Fe-replete and -excess precultures and transferred into the respective experimental cultures. Cellular iron content was analyzed by ICP-MS/MS of three independent cultures each. All strains tested hyper-accumulated iron in excess conditions, but to a different extent (Figure 57B). CC-124 showed very similar iron accumulation levels as strain CC-4532. Both Fe-replete levels were comparable ( $16.0 \pm 0.9$  in CC-124 and  $15.2 \pm 1.9 \times 10^7$  atoms $\cdot\text{cell}^{-1}$  in CC-4532) and the cellular iron content increased 3.7 and 4.4-fold in excess ( $59.1 \pm 7.4$  in

## 2. Results

---

CC-124 and  $67.7 \pm 10.0 \times 10^7$  atoms·cell<sup>-1</sup> in CC-4532). Strain CC-1690 has been shown to have a slightly larger volume than the other strains. Replete Fe-levels on a cell basis are elevated by 47% to  $22.2 \pm 1.3 \times 10^7$  atoms·cell<sup>-1</sup>, which compared well to the increased cell volume.

The accumulated level is in the same range as CC-4532,  $68.3 \pm 7.2 \times 10^7$  atoms·cell<sup>-1</sup>, but due to the elevated iron content in replete conditions, this only amounts to a 3.0-fold increase. Strain CC-1691 exhibited same replete levels and the hyper-accumulation amounted to a 2.5-fold increase ( $15.3 \pm 1.2$  and  $49.0 \pm 7.8 \times 10^7$  atoms·cell<sup>-1</sup>) of intracellular iron. Strain CC-1009 exhibited the lowest increase, by 2-fold, of the five strains compared ( $14.3 \pm 1.4$  and  $34.0 \pm 3.9 \times 10^7$  atoms·cell<sup>-1</sup>). Individual *p*-values comparing the iron content between the samples are listed in Supplemental Table 60. Cellular P, S, Mg, K, Na, Ca, Mn, Zn and Cu did not change significantly between the strains in response to Fe-excess growth condition (Supplemental Figure 53).





## 3 Discussion

### 3.1 Elemental Profile of *Chlamydomonas reinhardtii*

Ionomics, or elemental profiling, is the quantitative and simultaneous measurement of the total elemental composition of an organism to address biological questions (Lahner et al., 2003; Salt 2004; Eide et al., 2005). The elemental composition changes in response to physiological stimuli, developmental state, and genetic modifications. Once characterized, the ionome can be used as a tool to assess factors affecting specific parts of the elemental profile, and high-throughput elemental profiling combined with genetics is used to identify the genes that control the ionome (Danku et al., 2013). The total elemental composition of an organism is still rarely determined on a routine basis. The number and type of elements measured are limited by the available instrumentation, the assumed concentration of the element and the respective detection limit, the biological question, and the added cost of measuring each additional element (even though elements can be analyzed simultaneously, adding more elements to the analysis either increases the instrument run time, consumable costs, the quantity of the biological material or any combination of these factors).

Since the first key ionome (Lahner et al., 2003), studies have been performed in many plant species, including rice (Norton et al., 2010, Zhang et al., 2014, Pinson et al., 2015), maize (Baxter et al., 2013, Baxter et al., 2014, Mascher et al., 2014, Gu et al., 2015), barley (Wu et al., 2013), lotus (Chen et al., 2009), potato (Chaparro et al., 2018) and others (Watanabe et al., 2007; Parent et al., 2013; Pilon et al., 2019). Large interest has been in agricultural research and nutrition, to increase beneficial nutritional values of crops or life-stock or to reduce the incorporation of heavy metals. Studies in humans (Sun et al., 2012, Malinouski et al., 2014; Ying and Zhang, 2019) and animals (Yoshida et al., 2014) have been reported and suggest a link between disruptions of the cell-specific homeostasis and diseases, including cancer and neuro-degenerative disorders. The first *Chlamydomonas* elemental profile was published 2011 by Kropat et al. to determine the cellular needs for the nutrients supplied in the growth medium. So far, the trace metal content in *Chlamydomonas* has been analyzed in several studies, mostly with very specific questions and looking at one element of interest in response to a treatment (Terauchi et al., 2010; Kropat et al., 2011; Malasarn et al., 2013; Hong-Hermesdorf et al., 2014; Kropat et al., 2015; Tsednee et al., 2019). In addition to trace metal nutrition, several studies investigate

### 3. Discussion

---

The elemental composition of *Chlamydomonas* cells grown in standard photoheterotrophic conditions is constant and tightly regulated. The between-sample variation of the elements was different, specifically Na and Zn were very sensitive to fluctuations. Zinc is a common contaminant in the air, dust and sweat. Sodium is a common environmental contaminant as well, but was also used in the sample preparation, where cells are washed with Na<sub>2</sub>-EDTA, followed by water prior to ICP-MS/MS analysis, and minor changes in the sample preparation can cause different levels of Na to remain in the sample. Calcium showed higher variability between batches, but usually exhibited a low variability in an experimental set of samples. Calcium may be more sensitive, or mobile, because as a secondary messenger molecule, the content may respond fast to small differences in handling of cells and stress of sample preparation between independent experiments. The fine-tuned and tight homeostasis can be disrupted by changed conditions, often leading to specific and reproducible shifts in a subset of elements. Different growth conditions can require a different set of elements in different concentrations, or the conditions imposes a stress on the cell which leads to mis-regulation (Sunda et al., 2005; Merchant et al., 2006).

By coupling genetics with high-throughput elemental profiling, ionomics has led to the identification of numerous genes controlling the ionome. Furthermore, ionomics has allowed the discovery of genes controlling natural variation in the plant ionome (Buescher et al., 2010; Campos et al., 2017). The concept of the ionome has also been applied to *Saccharomyces cerevisiae* with an analysis of knockout and overexpression alleles of all identified genes in the yeast genome (Eide et al., 2005, Yu et al., 2012).

The availability of a large mutant collection in *C. reinhardtii* (Li et al., 2016) and recent improvements in ICP-MS/MS method developments will allow for large scale elemental analysis soon. A newer version of the ICP-MS/MS allows the measure *Chlamydomonas* samples of less than 0.5ml, which relates to a reduction in required cell material from  $1 \times 10^8$  to  $5 \times 10^6$  cells. Preliminary protocol development looks promising to soon be able to analyze *Chlamydomonas* cells grown in very small volume (< 10 ml) or 96-well microtiter plates to facilitate high throughput analysis of a large number of strains and conditions, including mutants. The defined elemental composition as well as a handful of defined conditions create the framework for future discoveries.

## 3.2 Steady State Photoheterotrophic Iron Homeostasis in the Green Alga *Chlamydomonas reinhardtii*.

Unicellular algae such as *C. reinhardtii* offer high signal-to-noise ratios during experiments due to the ease of growth in controlled environments (defined growth medium, temperature and light regimes) and the homogenous nature of the cultures. Numerous studies have characterized the low-iron stages, Fe-deficient and Fe-limited, in *Chlamydomonas* (Moseley et al., 2000; Urzica et al., 2012; Höhner et al., 2013), including specific impacts of the trophic status (Terauchi et al., 2010, Urzica et al., 2012). Whereas iron starved conditions have been well studied, the state of cells exposed to excess extracellular Fe is not as well described (Long and Merchant, 2008). Since the studies of iron homeostasis described above were all performed in growth medium containing trace nutrients based on Hutner's recipe (Hutner et al., 1950), I verified the findings using the revised trace metal composition (Kropat et al., 2011), that is now routinely used by the *Chlamydomonas* community. Comparing a wide range of extracellular iron concentrations allowed me to verify the phenotypes of iron starvation and extending the knowledge towards the characterization of excess iron, in a large, systematic, and comparable approach.

No differences in the low-iron response was found between cells grown with Hutner's trace metals or with the revised recipe. The intracellular iron content changes with the extracellular availability, and no significant differences in the content were observed, compared to what Terauchi et al. (2010) reported. The iron quota of a cell changes with variations in the growth conditions, depending on the sinks and requirements for iron-containing proteins. Cells face a constant balance between taking up enough iron to meet the most necessary needs, scavenging sparse extracellular iron, recycling intracellular iron and storing spare iron for times of limitation.

The extra accumulated iron did not impact photosynthetic activity, assessed through chlorophyll content,  $F_v/F_m$  and Kautsky chlorophyll transients, indicating that the iron is stored in a way that prevents direct contact of the O<sub>2</sub>-producing photosynthetic apparatus and free Fe. The transcriptome analysis revealed only a limited response to the excess iron. The known iron regulon, particularly the uptake machinery, are further repressed and only a small number of genes responded with increased transcript abundance. These gene products most likely help the cell handle the excess Fe, making them prime candidates for

### 3. Discussion

---

further analyses. Many of the genes are available as knock-out mutant strains in the mutant collection (Li et al., 2016), thus allowing further characterization of the iron storage in *Chlamydomonas*.

In logarithmic photoheterotrophic growth, the cells divide so fast, that iron is a limiting factor, as seen by the almost linear correlation of generation time and extracellular iron concentration and the fact, that increased concentration of extracellular iron led to an increased growth rate. The growth advantage was especially well distinguishable in the mid-logarithmic growth phase. As cells divide fast, they transiently experience symptoms of iron deficiency, even though plenty of extracellular is available ( $16$  versus  $20 \times 10^7$  atoms $\cdot$ cell $^{-1}$ , Figure 13 and Page et al., 2012). Because of multiple redox steps involved in the iron metabolism, its uptake and distribution often cannot keep up with growth (Hoffman et al., 1995). *Chlamydomonas* cells compromise between fully charged iron pools and fast growth when all other nutrients are available and only take up the iron that is necessary for maintenance and growth. This correlates well with the difference in iron content between mid-logarithmic and stationary growth phase and an increase in iron content in extended stationary phase. In single-trophic (photoautotrophic or heterotrophic) growth, the iron is not the limiting factor anymore. Growth is generally slower, even slower than Fe-limited photoheterotrophic growth.

The *vtc1* mutant, lacking fully functional acidocalcisomes (Aksoy et al., 2014) did not accumulate additional iron during steady state growth, suggesting a role of the acidocalcisome in the storage of the iron, which is lacking in this mutant. Even though the cells did not store additional iron, they exhibited increased sensitivity to increased photon flux densities. This is probably caused by the generous iron pool that is already present at replete conditions. On the other hand, the cells took up large amounts of iron during the fast transition. This process was involuntary, due to the large abundance of the high affinity iron uptake system due to the preceding Fe-limitation and the mutant cells indicated stress, assessed by slower growth, due to the lack of fully functioning acidocalcisomes. A larger transcriptome response to excess iron in the *vtc1* mutant indicates an increased overall stress level these cells experienced, increased transcript levels were already observed in Fe-replete conditions, also pointing to a general elevated stress experience. Excess light generates oxidative stress in chloroplasts when the absorbed light energy is greater than

the capacity of metabolism to use the reducing equivalents that are generated. While there is substantial research on the protective (such as activation of genes in anti-oxidant pathways) and preventative mechanisms (such as movement away, remodeling of antennae) used by *Chlamydomonas* to avoid oxidative injury in this situation, the question of how metal homeostasis, re-allocation and storage respond to light intensity is another unexplored area.

### 3.3 Dynamic acclimations to Changes in Extracellular Iron.

After the characterization of extra iron accumulation in excess conditions, I asked, how this iron, potential harmful to the cell, can be beneficial. The cells were able to re-mobilize the accumulated iron when necessary, which gave a growth advantage when external Fe became unavailable. This shows that the iron is bio-available to the cell and can be utilized when needed. Assuming  $\sim 10 \times 10^7$  atom $\cdot$ cell $^{-1}$  in cultures with 2  $\mu$ M Fe,  $\sim 20 \times 10^7$  atom $\cdot$ cell $^{-1}$  for 20  $\mu$ M and  $\sim 60 \times 10^7$  atom $\cdot$ cell $^{-1}$  for 200  $\mu$ M cultures, this correlates well with the observed phenotype of one more division between 2 and 20 ( $10$  vs  $20 \times 10^7$  atom $\cdot$ cell $^{-1}$ ) and 1-2 more doublings between 20 and 200 ( $20$  vs  $60 \times 10^7$  atom $\cdot$ cell $^{-1}$ ). The observed growth advantage was proportional to the accumulated iron. The *vtc1* mutant, lacking a fully functional acidocalcisome, did not show the same growth advantage, due to the lack in additional iron storage.

When Fe-starved cells were exposed to excess extracellular Fe, they temporarily took up large quantities of Fe, exceeding the accumulation observed in steady state conditions. The accumulation of iron was observed for 12h, up to more than a 50-fold increase. The differences between the addition of 20 and 200  $\mu$ M Fe was mainly during the decrease phase, where cultures exposed to 200  $\mu$ M Fe showed a slower loss of iron.

The reduction in cellular iron content starting 12h after iron was provided, coincides with cell division. Whereas the iron content remains higher than dilution by division in CC-4532, both *VTC1* and *vtc1* reduce the cellular iron content faster and maintain a lower level during divisions. Strains CC-4532 and *VTC1* did not exhibit a growth impact, whereas the *vtc1* mutant exhibited delayed growth in response to high concentrations of iron (20 and 200  $\mu$ M) compared to low concentration of iron (2  $\mu$ M) added. The *vtc1* mutant was more sensitive to iron overload, presumably due to the lack of the acidocalcisome. It is interesting to note, that the steady state iron accumulation was lower than the temporary

### 3. Discussion

---

overload during the fast iron transition (60 compared to  $200 \times 10^7$  atoms·cell<sup>-1</sup>). Even cells of strain CC-4532, that accumulate Fe in steady state, did not maintain the high iron amounts experienced during the fast transition, but return to an equilibrium closer to replete levels.

The rapid increase in cellular iron is probably involuntary, as Fe-starved cells exhibit a high abundance of the high affinity Fe uptake system as a response to the sparse extracellular Fe (Terauchi et al., 2010; Urzica et al., 2012; Hsieh et al., 2013), and suddenly available Fe in the growth medium will be taken up rapidly by the vast amount of transport capacity, suddenly flooding the cell with iron. The fact, that the *vtc1* mutant did not accumulate extra iron in steady state conditions, but temporarily took up large amounts during the fast transition from no iron to overload, indicates that the acidocalcisome is more important for the long-term storage of iron. Even though *vtc1* did take up a lot of iron, the lack of the acidocalcisome caused a growth defect, suggesting some involvement in the short-term overload.

In most eukaryotic cells, ferritin is the major iron storage protein which binds the iron in a non-toxic way and acts as buffer for intracellular iron concentration. The *Chlamydomonas* genome encodes for two ferritin genes, *FER1* and *FER2*, which are localized to the chloroplast. Contrary to many other organisms, expression of *Chlamydomonas FER1* and *FER2* are increased in iron-deficient and iron-limited cells relative to iron-replete cells (Urzica et al., 2012) and did not increase in excess conditions (this study). One possibility is that the increase is important to chelate the iron that is released from the programmed degradation of PSI and ferredoxin in iron-limited cells. This is preceded by the finding that ferritin expression is increased also in senescing leaves engaged in programmed destruction of the photosynthetic apparatus (Gepstein et al., 2003). It may also be important to increase the iron chelating potential of the chloroplast in an iron-limited situation because of the potential for generating reactive oxygen species in a membrane with a compromised electron transfer chain. In this situation, ferritin would be providing a cytoprotective antioxidant role. While there are enzymes to de-toxify hydrogen peroxide and superoxide, the only defense mechanism to combat hydroxyl radical is removal of reactive iron.

Even though the exact mechanism is not understood yet, both the acidic vacuole and ferritin complexes are playing a critical, though distinct, roles in the storage of Fe in *Chlamydomonas*. Furthering the understanding of the iron storage will remain a key goal

for future research. Growing cells in the presence of a clean Fe-isotope, for example  $^{56}\text{Fe}$ , before starvation, then supplying  $^{57}\text{Fe}$  for the overload, combined with subcellular fractionation and detection of the respective isotopes could be a key experiment in dissecting the mechanisms of iron storage and the interplay of the different components.

#### 3.4 Acclimation to Heterotrophic Carbon During Iron Starvation.

Research published previously showed that acetate-grown *C. reinhardtii* cells sacrifice the photosynthetic apparatus in Fe-limited growth conditions, but  $\text{CO}_2$ -grown cells do not (Terauchi et al., 2010; Urzica et al., 2012). The rationale is that photosynthesis, a major Fe sink, is dispensable when acetate is available as carbon and energy source but is essential in its absence. Iron limitation has diverse cellular effects, including decreased cellular iron content, reduced photosynthetic capacity and inhibited growth. Using comparative transcriptomics and physiological characterization to discover components of the acetate-signaling pathway to reveal the pathway for dis-assembly of the thylakoid membrane and understanding the interaction of iron nutrition signaling with the status of central carbon metabolism. A first step was to define the physiology of the transition from photoautotrophic to photoheterotrophic growth. Cells were grown photoautotrophically on air-level  $\text{CO}_2$  in Fe-limited, Fe-deficient and Fe-replete conditions, supplemented with acetate in mid-logarithmic to induce the shift to photoheterotrophic conditions and analyzed using a variety of techniques.

Fe-limited exhibited a reduction in chlorophyll content 6h after acetate supply and this reduction was not due to a dilution by cell division but was rather an active process. Protein synthesis is required for the reduction to take place, as the presence of cycloheximide, an inhibitor of ribosomal protein synthesis prevents the chlorophyll phenotype. In addition, control cultures were analyzed, where sterile water was added instead of Fe-EDTA to account for changes caused by the experimental setup.

In general, I observed two main aspects with regard of the acclimation to acetate. First is the cellular acclimation to acetate, independent of the cellular iron status, and secondly the deviating response during Fe-limitation. The availability of acetate has a large impact on the cell, accompanied by major remodeling of many, if not all, cellular processes and pathways to utilize the additional carbon and energy source. Both transcriptome analysis and physiological parameters showed an increase in photosynthetic as well as respiratory

### 3. Discussion

---

capacity in Fe-replete and Fe-deficient conditions, and to a lesser extent in Fe-limited cells. Acetate signaling caused a fast induction of pathways utilizing acetate to produce energy and carbon intermediate further down the line. Genes involved in components of the tricarboxylic acid (TCA) and glyoxylate cycle, are the first steps in assimilating acetate and are among the first pathways to increase transcript abundances in response to acetate to increase the throughput of acetate through both pathways. The glyoxylate cycle bypasses the two oxidative decarboxylation steps of the TCA cycle and directly convert isocitrate through isocitrate lyase and malate synthase into malate and succinate. The induction of acetate utilizing components was partially Fe-dependent, the general time-dependent pattern of expression was the same in Fe-limitation, but usually to a lesser extent. Pathways of the central carbon conversion pathways, including gluconeogenesis and both energy conversion pathways, photosynthesis and respiration, were induced in response to acetate and were mostly Fe-independent. The individual pathways were induced in a timely pattern, with TCA cycle reaching peak expression fast, around 2h after acetate became available, followed by the pathways further downstream. Photosynthesis, respiration and gluconeogenesis transcript abundances were peaking between 4, 6, 8 and 12h. Genes involved in the tetrapyrrole biosynthesis were overrepresented among the induced genes at 2, 4, and 6h post-acetate in Fe-replete conditions. This induction pattern was also observed in Fe-limited conditions, but to a lesser extent. Photosynthetic and respiratory capacity increased with the availability of acetate, as assessed by net oxygen evolution and consumption. The Fe-limited oxygen consumption increased slightly, whereas the evolution rate was reduced rapidly, even before the cellular Chl content was reduced. The maximum quantum efficiency of PSII was reduced hours after the chlorophyll content was reduced. Taken together, this indicates that the cells preemptively decrease the oxygen evolution before photosynthetic complexes were degraded and that the remaining chlorophyll is fully functionally bound to the respective light harvesting complexes. Interestingly, even though the chlorophyll content was decreasing, the genes involved in chlorophyll synthesis, but not chlorophyll degradation, respond to acetate and iron-limitation. This points to the possibility, that the reduction in chlorophyll content may be induced in response to acetate independent of the iron status, but that Fe-replete and Fe-deficient cells were able to rebuild the chlorophyll pool, whereas Fe-limited cells less so.



The proportion of the iron-independent response to acetate was observed fast whereas the proportion of iron-dependent transcript changes increased over time. Suggesting that even in Fe-limited cells, acetate is taken up rapidly and metabolized to increase the energetic status of the cell and due to the increased metabolic activity, the cells become more limited for iron.

The observed response was very robust, as variations did not change the phenotypical characteristics, it was observed in other wild-type strains and in the *vtc1* mutant. No dose-response of acetate was observed, concentrations as low as 17  $\mu\text{M}$  (1:1000 of the original TAP content and used in the main experiments) still caused the chlorophyll loss, suggesting acetate is perceived as carbon source as well as signaling component. The cell density at acetate supply did not affect the extend or timing of the chlorophyll reduction, suggesting the program to reduce the chlorophyll content is independent of the exact number of Fe atoms per cell left, as a little more Fe is left at  $0.5 \times 10^6$  compared to 2 or  $4 \times 10^6$  cells $\cdot\text{ml}^{-1}$ .

The timing of 4-6h was observed in many aspects of the analysis, from chlorophyll loss, to transcript changes in several pathways, including chlorophyll synthesis, photosynthesis, respiration and is a prime target for follow up investigations using protein analysis, ribosome profiling and characterization of mutant strains deleted for genes of interest.

#### 3.5 Examining the Range of Phenotypical Deviation in Wild-type Strains of *Chlamydomonas reinhardtii*.

Several different *C. reinhardtii* strains are used as the favorite go-to “wild-type” by the Chlamydomonas community. Despite their recent common ancestry, there are many readily observable phenotypic differences between the common laboratory strains. Important indicators such as the presence or absence of a cell wall, the ability to utilize different nutrient sources, and maintenance or sacrifice of metabolic pathways under specific environmental conditions suggest that Chlamydomonas may harbor intraspecific diversity for important cellular and metabolic traits. Some of these phenotypes have been traced to specific mutations (e.g. NIT mutations or arginine auxotrophy). and have been characterized to varying extents (Sager, 1955; Fernández et al., 1989; Pazour et al., 1995). But a larger fraction of the observed, or still to be examined, differences are due to the

### 3. Discussion

---

interplay of multiple genetic loci. At present, there is little systematic information on phenotypic variation among the strains, especially regarding complex or nuanced observations (e.g. triacylglycerol formation upon stress, effectiveness of micronutrient utilization), especially those expected to be affected by multiple gene products. To systematically characterize the variance between common laboratory strains, Gallaher et al. (2015) re-sequenced the genomes of 39 strains revealed genetic diversity not evenly distributed but condensed in discrete blocks of either of two types, with 2% sequence variance between them, called haplotype 1 and 2. Many variants were identified, that are predicted to have some effect on gene coding sequences (Flowers et al., 2015; Gallaher et al., 2015). However, given that both haplotypes are present in fully functional, wild-type strains, complete loss-of-function should account only for a rather small fraction of the variants. On the other hand, complete loss-of-function might be more likely to be sustained in genes that are only required or beneficial under specific environmental conditions and thus have no major fitness impact on strains that are routinely grown in replete growth conditions under ideal laboratory conditions. Another study on the genome variance between laboratory strains observed that mutations were biased toward those that are less deleterious to gene expression (Flowers et al., 2015).

Examples of varying phenotypes between strains were also observed by the Merchant group, including maintenance versus loss of chlorophyll (Figure 47). The findings, that some strains are able to maintain chlorophyll levels during Cu-deficiency, whereas others experience chlorosis, fits the hypothesis that the reduced chlorophyll content in Cu-deficiency is caused by secondary iron deficiency. Strain CC-4402, but not CC-4532, displayed this behavior, which can be rescued by excess extracellular Fe, relating well to the initial characterization of strain-specific nuances in iron homeostasis reported by Gallaher et al (2015). The Cu-dependent ferroxidase FOX1, together with the iron permease FTR1, is an integral part of the high-affinity iron uptake system (Blaby-Haas and Merchant, 2012). This strain showed Cu-dependent Fe-deficiency, probably due to reduced efficiency to allocate the scarce Cu to FOX1 in strain CC-4402, compared to CC-4532, though the cause or correlation to a specific protein has not been identified yet. Even though both *FOX1* and *FRT1* were among the differentially expressed genes between the 5 strains compared in this thesis, the overall FPKM levels were much lower than in Fe-deficiency (Urzica et al., 2012) and none of the strains in this comparison exhibited the

### 3. Discussion

---

Cu-deficient chlorosis. These analyses underscore the importance of documenting strain genotype, culture history and specific growth parameters in each study, especially for complex setups (like nutritional iron signaling) involving multiple redundant pathways. For future analysis of this aspect, a first experiment should include the determination of the cellular Cu and Fe quota of strain CC-4402 and potentially other strains with this shared phenotype to determine whether cells experienced altered overall cellular levels or if the sub-cellular allocation is affected.

In order to assess the effects of the genome variants on the transcriptome, I compared the basal level transcript abundance of 5 strains in replete growth conditions. Strains CC-124, CC-4532, CC-1690, CC1009 and CC-1691 were chosen based on the distribution of haplotype blocks and broad usage as frequently used wild-type strains. It is generally understood that Smith distributed *Chlamydomonas* strains to the community as three different lineages and that each of these lineages is distinct from the others. To evaluate if this background has a prevalent effect on the variability, I included strains that are the direct descendants of those original strains: CC-1690 and CC-1691 for the Sager, CC-1009 for the Cambridge and CC-124 for Ebersold-Levine lineage. Strain CC-4532, the strain used for most trace metal research in the Merchant laboratory, was included for comparison, and because many experimental datasets already existed prior to or were generated in parallel to my Ph.D. research. I found a large number of genes to be differentially expressed between the wild-type strains by criteria commonly used in comparative transcriptomics analyses. Between the 5 strains, 6993 transcripts met the criteria of differential expression between at least two of the strains (Figure 48). A large fraction of those genes however was only significantly altered in transcript abundance in one of the strains compared to the other four (Figure 49). Genes of all functional annotation groups were found to be amongst the differentially expressed genes. A small subset of genes was found to be expressed in a subset of strains, but not expressed at all in others and those gene would be considered to fall in the category of deleterious mutations, but only a fraction of the affected genes is located in the haplotype blocks of the genome. The group of genes was enriched for genes without functional annotation, suggesting a large fraction of genes without critical function or that are niche-specific for sub-optimal growth conditions.

### 3. Discussion

---

Interestingly, more than half of the differentially expressed genes between the strains were not located in either of the two haplotype blocks but in the more conserved regions between blocks, suggesting that the haplotype variances may play a part in the observed transcriptome and phenotypic variance, but is certainly not the complete picture.

Gene expression is sensitive to many factors, leading to variations in expression level of the exact same strain between laboratories, between individual researchers in the same laboratory, between experiments by the same or different researchers. Deviating conditions with potentially significant impact on gene expression can include differences in light quality and quantity, aeration rate, and nutrient availability, to name just a few. Over the past decade an increasing number of high-quality RNA-Seq datasets from *Chlamydomonas* have become available, inviting larger cross-experiment comparisons. Taking advantage of the large collection of datasets, I compared the transcript abundances between strains and experiments to assess the range of transcript changes in what should be the same condition, to be able to better extract the biologically relevant differences in future analyses.

For the immediate future, one analysis that has not been finished yet is the system-wide comparison of the transcriptome with reads mapped to the reference genome (CC-503) compared to the custom genomes for each strain. As suggested in Gallaher et al. (2015), we expect that the expression estimates of a subset of genes found in the haplotype areas will be affected in their transcript abundance. Haplotype-accurate, strain specific “custom” genomes were generated and mapping the RNA-Seq reads of all five strains to both genomes (reference and respective custom genome) and the following comparison are still underway. An initial comparison was done by Gallaher et al. (2015) for strains CC-4348 and CC-4349 (a dataset from Blaby et al., 2013) and a number of reads aligning to regions affected by the haplotype blocks between the two strains were mapped to both haplotypes for the regions, resulting in decreased number of mismatches and an increase in mappable reads. Most genes were unaffected in their expression estimates, but a handful of genes showed significant differences. This dataset will allow for a more systematic comparison, not only of the reads aligned to the haplotype blocks but the entire custom genome from resequencing as opposed to the reference genome. Even though a majority of the variances

### 3. Discussion

---

was found to be in either of the haplotype blocks, there were still a number of variances outside those defined regions.

The initial selection of strains for this thesis included CC-125, which has the same haplotype block distribution as the reference strain CC-503. During data analysis, based on RNA-Seq reads compared to the strain-specific genome sequences, this strain did not match the genome of CC-125, but probably was CC-124. As it is impossible to determine when or how the mixed-up occurred, the entire subset of CC-125 was excluded from transcriptome analysis and physiological characterization. A hypothetical data analysis comparing the transcriptome of “CC-125” to the other strains, revealed a much lower number of differentially expressed genes between CC-124 and “CC-125”, ~ 10 genes, compared to the several hundred among the other strains. In this case, the interpretation would have been, that CC-124 and “CC-125” exhibited a much more similar transcriptome than the genome haplotype blocks would suggest. This shows that the comparison to the individual genome or the haplotype sequences can be a useful tool to include in the transcriptomics data analysis to reduce the changes of overinterpretation.

In addition to the variances in the transcriptome, I characterized commonly used physiological parameters to create a framework for the overall variability of phenotypes. For example, differences in growth emerged at less than ideal conditions. The difference in the macro and micronutrient content was largely due to variations in cell volume. All elements analyzed showed the same range of variability overall, with small, but significant changes in certain strains, which were highly reproducible, thus indicating differences in the trace metal quota. The biological relevance of these differences in metal quota are an interesting question to pursue for future characterizations of niche specific differences.

One major variation observed was the strain-specific proportions of photosynthesis versus respiration contributing to the overall energetics of the cell. Both CC-1690 and CC-1009 showed higher transcript abundance of the genes encoding for the photosynthetic complexes and had higher oxygen evolution rates, which translated to faster generation time in photoautotrophic conditions.

A good example of a more complex interplay is metal homeostasis. The intracellular concentration of iron is tightly regulated by *Chlamydomonas* via the action of a host of

### 3. Discussion

---

transporters and scavenging proteins (Glaesener et al., 2013). As the available iron becomes limited, these proteins engage in a coordinated process to import needed iron. When strains of *Chlamydomonas* are grown in limiting concentrations of iron, the effectiveness of these iron-harvesting mechanisms becomes readily observable as reduced growth and, in extreme cases, as chlorosis. The overall ironome is constant and changes only in specific conditions. Iron accumulation during excess availability is conserved between the strains and thus can be considered rather beneficial for the cells, as all strains compared shared this preparative mechanism for future Fe-starvation. Interestingly, the strain with the lowest iron accumulation, CC-1009, is also the strain with the lowest oxygen consumption and highest oxygen evolution rate, suggesting a regulation of iron stores depending on the predominant energetic pathways. A highly active photosynthetic machinery, where the combination of O<sub>2</sub> and high concentrations of Fe increase the detrimental accumulation of reactive oxygen species, could create conditions where the disadvantage of extra stored iron outweighs the benefits. This finding fits well with the lower Fe accumulation observed in photoautotrophic growth conditions (Terauchi et al., 2010 and Figure 15), where photosynthesis is the major energy source and increased Fe accumulation in heterotrophic conditions without light and thus without photosynthetic activity. In this context, it would be interesting to evaluate the correlation of iron accumulation with oxygen consumption and evolution rates and to test whether cells decrease oxygen evolution during acute iron overload (e.g. during the transition of 0  $\mu$ M Fe to 200  $\mu$ M Fe, as described in Figure 23).

## 4 Materials and Methods

### 4.1 Materials

#### 4.1.1 *Chlamydomonas reinhardtii* Strains

For most experiments in this thesis and when not further specified, *C. reinhardtii* wild-type strain CC-4532 (mt<sup>-</sup>, also known as 2137) was used. In experiments in which the variance between different wild-type strains was analyzed, strains CC-4402, CC-124, CC-1690, CC-1691, and CC-1009 were also utilized. To analyze the contribution of acidocalcisomes to iron storage, mutant strain CC-5321 (*vtc1*) and its complemented strain CC-5324 (*VTCl*) were used. The mutant and complemented strain were a kind gift from Arthur Grossmann (Aksoy et al., 2014, CC-5165 and CC-5166) and were submitted to the Chlamydomonas Resource Center after genome sequencing, where they were assigned CC-5321 and CC-5324. All strains used in this thesis are available at the Chlamydomonas Resource Center (<http://www.chlamycollection.org>). Strains will be referred to by their CC number, except for *vtc1* and *VTCl*, to make it more intuitive to distinguish the mutant from the complemented background.

#### 4.1.2 Chemicals

General chemicals used in this work were purchased from Acros Organics (Geel, Belgium), Alfa Aesar (Haverhill, MA, USA), Agilent (Santa Clara, CA, USA), Bethesda Research Laboratories Inc. (Gaithersburg, MD, USA), Calbiochem/EMD Chemicals Inc. (San Diego, CA, USA), EMD Millipore (Burlington, MA, USA), Fisher Scientific (Hampton, NH, USA), Fluka (now Honeywell Specialty Chemicals, Morris Plains, NJ, USA), Gold Shield Chemical Co. (Hayward, CA, USA), Inorganic Ventures (Christiansburg, VA, USA), Invitrogen (Carlsbad, CA, USA), J.T. Baker Chemical (Avantor Performance Materials, LLC., Center Valley, PA, USA), Mallinckrodt (St. Louis, MI, USA), Qiagen Inc. (Germantown, MD, USA), Riedel-de Haën (now Honeywell Specialty Chemicals), Sigma-Aldrich (St. Louis, MI, USA), TraceSELECT and TraceSELECT ULTRA (now Honeywell Specialty Chemicals). Ultra-pure chemicals with Certificates of Analysis were purchased from Acros Organics (nickel(II) chloride), Calbiochem/EMD (sodium acetate), EMD Milipore (ammonium chloride, potassium dihydrogen phosphate), Fisher Scientific (nitric acid, ferric chloride), Fluka (sodium

## 4. Materials and Methods

---

carbonate), Inorganic Ventures (single-element calibration standards phosphorus, scandium, sulfur, yttrium), and Sigma-Aldrich (ammonium molybdate, cobalt(II) chloride, magnesium chloride, magnesium sulfate, manganese(II) chloride, potassium chloride, sodium chloride, sodium phosphate dibasic, sodium phosphate monobasic, sodium selenite, boric acid, cobalt(II) nitrate, copper(II) chloride, disodium ethylenediaminetetraacetic acid, manganese(II) chloride, potassium hydroxide, sodium nitrate, triethylenetetramine dihydrochloride, zinc sulfate).

Proteinase K was purchased from Fisher Scientific, 3-(2-(3,5-Dimethyl-2-oxocyclohexyl)-2-hydroxyethyl)glutarimide (cycloheximide) and 3-(3,4-Dichlorophenyl)-1,1-dimethylurea (DCMU) from Sigma-Aldrich. Purified water was prepared when needed with a Milli-Q A10 purification system (EMD Millipore, Burlington, MA, USA). Specific instruments are listed with the respective method, standard laboratory equipment, for example balances, is not listed.

### 4.1.3 Software, Computer Programs and Other Resources

Calculations, data processing, general data analysis and figure design were performed using Excel (Microsoft Office 2016), SigmaPlot 12.0 (Systat Software), Origin Pro 9.1 (OriginLab Corp.), and Illustrator CS4 (Adobe). Instrument-specific software is listed with the respective method. Phytozome (version 12.1, <http://www.phytozome.jgi.doe.gov>) (Goodstein et al., 2012) was used as source for genomics information and gene annotation, gene identifiers (e.g. Cre09.g393150) or names (e.g. *FOX1*) used in this thesis refer to the *C. reinhardtii* JGI v5.0 genome assembly with v5.5 (Augustus 111.6) gene annotations. Functional annotation of large gene lists was performed with the Algal Functional Annotation Tool (<http://www.pathways.mcdb.ucla.edu/algal>) (Lopez et al., 2011). Prediction of subcellular localization of translated protein sequences was performed with PredAlgo (<https://www.giavap-genomes.ibpc.fr/predalgo>) (Tardif et al., 2012). Area-proportional Venn diagrams were created with BioVenn (<http://www.biovenn.nl>) (Hulsen et al., 2008) and modified in Illustrator.



### 4.2 Methods

#### 4.2.1 *Chlamydomonas reinhardtii* Growth Conditions

##### 4.2.1.1 Standard Growth Medium

If not stated otherwise, cultures were grown photoheterotrophically in standard Tris-acetate-phosphate (TAP) medium (7.5 mM NH<sub>4</sub>Cl, 0.34 mM CaCl<sub>2</sub>, 0.4 mM MgSO<sub>4</sub>, 1.13 mM KH<sub>2</sub>PO<sub>4</sub>, 20 mM Tris(tris(hydroxymethyl)aminomethane, 17 mM sodium acetate) (Harris, 2009) containing the revised micro-nutrient composition (57.75 μM EDTA, 0.2 μM (NH<sub>4</sub>)<sub>6</sub>Mo<sub>7</sub>O<sub>24</sub>, 0.1 μM Na<sub>2</sub>SeO<sub>3</sub>, 2.5 μM ZnSO<sub>4</sub>, 6 μM MnCl<sub>2</sub>, 20 μM FeCl<sub>3</sub>, 22 μM Na<sub>2</sub>CO<sub>3</sub>, 2 μM CuCl<sub>2</sub>) (Kropat et al., 2011). Cells were grown in 100 ml liquid medium in 250 ml-Erlenmeyer flasks at 24°C with 180 rpm agitation (Innova 44R orbital incubator shakers, New Brunswick Scientific, Edison, NJ, USA) and 70-80 μmol·m<sup>-2</sup>·s<sup>-1</sup> continuous illumination (2:1 ratio of 4100 K cool white and 3000 K warm white fluorescence bulbs). Light intensities were determined using a light meter with sensors for either air or liquid suspension (LI-COR LI-250A, Biosciences, Lincoln, NE, USA) and are expressed as Photosynthetic Photon Flux Density (PPFD).

All strains were maintained on slants containing TAP agar at 20-30 μmol·m<sup>-2</sup>·s<sup>-1</sup> (16h light and 8h dark, 2:1 ratio of 4100 K cool white and 3000 K warm white fluorescence bulbs) and 18°C. Cells were stored for four to eight weeks before transfer to fresh slants. Liquid cultures were started from slant and grown at least once from inoculation to stationary growth phase before starting pre-cultures. Liquid cultures were maintained in replete growth conditions and transferred to fresh medium every week for several weeks, before starting fresh from slant. Detergents from manufacturing, impurities in the agar and batch differences can impact growth or can create variance in agar-grown cultures. To ensure consistent starting material, the agar (SELECT agar, Invitrogen) was thoroughly washed before preparing solid growth medium. A 2-l flask was filled with deionized water to the desired final volume of medium, the fill-level noted with a permanent marker and agar added. The agar was washed four times by gently swirling the flask in a small volume of water, bringing to flask volume with deionized water, letting settle by gravity (90 min or longer) and carefully removing most of the liquid. The treated agar was used to prepare Tris-acetate phosphate (TAP) medium in the flask by using the volume mark. Round deep plates (100 × 20 mm) were filled with ~ 50 ml TAP-agar (1.5% w/v) after autoclaving,

glass tubes with screwed lids for slants (100 × 10 mm) were filled with 3 ml melted TAP-agar (1.2% w/v) and autoclaved.

### 4.2.1.2 Replication Strategies.

Replicates were analyzed for each experiment; the exact number of independent cultures are given with each figure. Four replicates were grown as follows: replicates A and B were inoculated from pre-culture I, grown and sampled in parallel and replicates C and D were inoculated from pre-culture II and treated together, but independent of replicates A and B, usually 1 to 4 weeks later (Figure 58 A). If three replicates were analyzed, all three replicate cultures were inoculated from one pre-culture and grown and sampled in parallel. There was no significant correlation of variance between the four replicates and thus they were considered to be independent, biological replicate cultures and were used equally to calculate mean and standard deviation.

### 4.2.1.3 Trace Metal-deficient Growth Conditions.

To consistently reproduce trace metal-deficient and -limited growth conditions, clean labware was used. Routinely, all glass- and reusable plasticware was rinsed three times with 6 N hydrochloric acid (~19% HCl) to displace residual metal ions and six times with purified water to remove the acid prior to use. Chemicals for the preparation of metal-deficient solutions and growth medium were of special purity (trace metal grade, low contaminations were ensured for each batch from the Certificate of Analysis), designated to allow the preparation of metal-deficient solutions; stock solutions were stored in acid-cleaned plasticware. Contact with surfaces in general, and especially such that cannot be made “metal-free”, like metal spatulas or skin, was avoided as much as possible. Metal-deficient growth medium was prepared freshly before each experiment and was not stored for more than two days prior to inoculation. Iron-free medium was prepared by omitting Fe-EDTA (Kropat et al., 2011), copper-free medium by omitting CuCl<sub>2</sub>. Medium containing various concentrations of iron was prepared from Fe-free medium and Fe-EDTA at the indicated concentrations was added to each flask prior to sterilization.

To achieve copper-deficiency, replete cultures were grown three time in copper-free medium from inoculation ( $1-2 \times 10^4$  cells·ml<sup>-1</sup>) to late-logarithmic ( $8 \times 10^6$  cells·ml<sup>-1</sup>) growth phase in three independent cultures each before starting experimental cultures. Each independent pre-culture was transferred to experimental cultures containing Cu-

## 4. Materials and Methods

replete, Cu-free and Cu-free/Fe-excess growth medium at a cell density of  $1-2 \times 10^4$  cells·ml<sup>-1</sup> and were grown to  $5 \times 10^6$  cells·ml<sup>-1</sup> for the analysis of chlorophyll content, growth was monitored from inoculation to stationary growth phase.

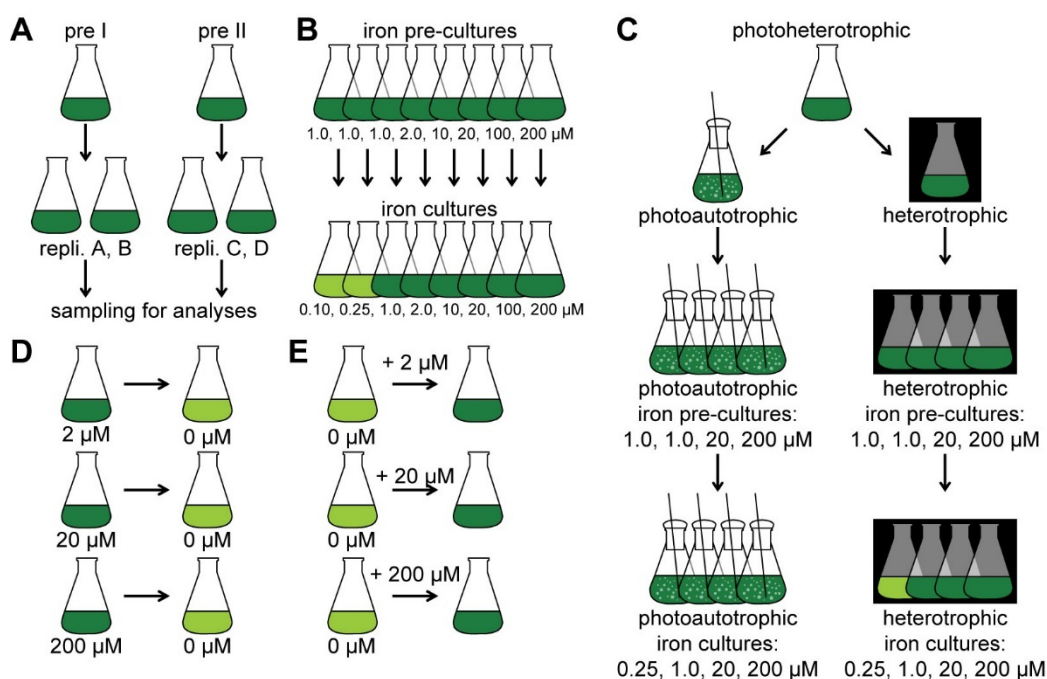


**Figure 58. Pre-culture and replication strategies.** **A:** A photoheterotrophic pre-culture I was inoculated from a maintenance culture and grown to a density of  $\sim 6-8 \times 10^6$  cells·ml<sup>-1</sup> for inoculation of two replicate cultures A and B to an initial cell density of  $1-2 \times 10^4$  cells·ml<sup>-1</sup> and grown to the desired cell density for analysis. **B:** Iron pre-cultures containing 1.0, 1.0, 1.0, 2.0, 10, 20, 100, and 200  $\mu$ M Fe-EDTA were inoculated from a replete culture, grown to a density of  $\sim 6-8 \times 10^6$  cells·ml<sup>-1</sup> and used for inoculation of two replicate cultures A and B containing 0.10, 0.25, 1.0, 2.0, 10, 20, 100 and 200  $\mu$ M Fe, respectively. Cultures were started at an initial cell density of  $1-2 \times 10^4$  cells·ml<sup>-1</sup> and grown to the desired cell density for analysis. **C:** Photoautotrophic or heterotrophic cultures were inoculated from a maintenance culture, grown for one growth phase before inoculation of iron pre-cultures containing 1.0, 1.0, 20 and 200  $\mu$ M Fe. **D:** Photoheterotrophic cultures containing 2, 20 and 200  $\mu$ M Fe were inoculated with CC-4532, *vtc1* or *VTc1* from pre-cultures containing 2, 20 or 200  $\mu$ M Fe, respectively, and grown to a density of  $2-3 \times 10^6$  cells·ml<sup>-1</sup>. Cells were washed twice with 1 mM Na-EDTA and once with purified water and transferred to fresh photoheterotrophic growth medium without added iron to an initial cell density of  $1 \times 10^5$  cells·ml<sup>-1</sup>. **E:** Photoheterotrophic cultures containing no added iron were inoculated with CC-4532, *vtc1* and *VTc1* from pre-cultures containing 1  $\mu$ M Fe, grown to a density of  $1 \times 10^6$  cells·ml<sup>-1</sup> and Fe was added to the cultures at the indicated concentrations.

For growth in various iron concentrations, medium was prepared as described above, and pre-cultures containing 1.0, 1.0, 1.0, 2.0, 10, 20, 100, and 200  $\mu$ M extracellular iron were started from replete cultures. Pre-cultures were grown from  $1-2 \times 10^4$  cells·ml<sup>-1</sup> to  $\sim 8 \times 10^6$  cells·ml<sup>-1</sup> and used to inoculate experimental cultures containing 0.10, 0.25, 1.0, 2.0, 10,

## 4. Materials and Methods

---

20, 100 and 200  $\mu\text{M}$  Fe, respectively (Figure 58 B). After contact with solutions containing excess iron (100 and 200  $\mu\text{M}$  Fe), glass- and reusable plasticware used during the experiment was rinsed with 6 N HCl after the end of the experiment before cleaning and general reuse to replace the embedded iron ions from the material and not contaminate the cleaning process.

### 4.2.1.4 Different Growth Modes

For photoautotrophic growth, acetate was omitted from the medium (TP) and the pH adjusted to 7.4 with hydrochloric acid (HCl). Unless noted otherwise, cultures were grown in 100 ml TP medium in 250 ml-Erlenmeyer flasks at 24°C with 180 rpm agitation and 70-80  $\mu\text{mol}\cdot\text{m}^{-2}\cdot\text{sec}^{-1}$  continuous illumination (2:1 ratio of 4100 K cool white and 3000 K warm white fluorescence bulbs) and were bubbled with air at a rate of 0.5-1  $\text{l}\cdot\text{min}^{-1}\cdot\text{l}^{-1}$  culture volume (Figure 58 C). Sterile air was supplied to the cultures with an aquarium pump (Whisper 20, Tetra, Melle, DE) through a filter (Millex Sterile Syringe Filters Durapore, PVFD membrane, 0.45  $\mu\text{m}$  pore size, EMD Millipore), attached with a sterile 1 cm-piece of flexible tubing to a single-use plastic pipette (1 ml Sterile Disposable Standard Serological Pipets, Fisher Scientific) which was threaded through the center of a sterile tight-fitting foam plug into the culture medium. Incubators were fitted with a stationary bubbling setup, containing the aquarium pump, a 12-way air flow divider and 12 flexible tubes of 15-30 cm length with male Luer-Lok connector. Each culture was connected to one air tube and spare tubes were closed with female Luer-Lok plugs. Air flow rates were checked occasionally using a rotameter-style gas flow meter. Cells from a replete culture were grown in photoautotrophic conditions for a full growth curve before starting pre-cultures for experiments. If not stated otherwise, pre-cultures were grown to late-logarithmic phase ( $\sim 8 \times 10^6$  cells $\cdot\text{ml}^{-1}$ ) to inoculate pre- and experimental cultures to an initial density of  $1\text{-}2 \times 10^4$  cells $\cdot\text{ml}^{-1}$ . Large cultures of 1-1.2 l medium in 2.8-l Fernbach flasks (without baffles) were grown with a larger air pump (Whisper 40, Tetra) and two 1 ml plastic pipettes into the medium, creating air flow rates of 0.3-0.5  $\text{l}\cdot\text{min}^{-1}\cdot\text{l}^{-1}$  culture volume.

For heterotrophic growth, flasks were wrapped in aluminum foil, inoculated from heterotrophic pre-cultures and grown in incubators without illumination (internal illumination turned off and front glass window covered with cardboard and foil) at 24°C with 180 rpm agitation. During handling of cultures and sampling, illumination was kept

## 4. Materials and Methods

---

to a minimum ( $< 1 \mu\text{mol}\cdot\text{m}^{-2}\cdot\text{s}^{-1}$ ). Cells from a replete culture were grown in heterotrophic conditions for a full growth curve before starting pre-cultures for experiments.

For growth in medium-high light conditions,  $2 \times 10^3$  cells each were gently spread on agar plates, allowed to dry, sealed with Parafilm and illuminated at  $350\text{-}400 \mu\text{mol}\cdot\text{m}^{-2}\cdot\text{s}^{-1}$  (Sylvania Metalarc M1000/U/BT37, 3800 K). Transparent water-filled plastic bags were placed between light source and plates to reduce IR and UV radiation. The temperature was maintained at  $20^\circ\text{C}$  (air-conditioned room), condensation was removed from the lids if necessary and the position of the plates was alternated regularly.

### 4.2.1.5 Dynamic Growth Conditions

For the dynamic examination of Fe-excess conditions, cells of CC-4532, *vtc1* and *VTCl* were grown in 2, 20, and 200  $\mu\text{M}$  Fe and transferred to Fe-free medium or in Fe-free conditions and supplied with 2, 20, and 200  $\mu\text{M}$  Fe. For the transfer from iron-containing to iron-free conditions, cells grown in photoheterotrophic pre-cultures containing 2, 20, and 200  $\mu\text{M}$  Fe were used to inoculate experimental cultures with 2, 20, and 200  $\mu\text{M}$  Fe, respectively (Figure 58 D). Cultures were grown to  $5 \times 10^6 \text{ cells}\cdot\text{ml}^{-1}$ , a fraction of the cells pelleted ( $\sim 1.2 \text{ ml}$ , 20 s, 16 420 g,  $20^\circ\text{C}$ ), resuspended in 1 ml Fe-free TAP medium, washed in the same way with 1 ml 1 mM EDTA, and 1 ml Fe-free medium, resuspended in 1.2 ml Fe-free TAP and used to inoculate 100 ml TAP containing 2, 20, or 200  $\mu\text{M}$  Fe to a starting density of  $1 \times 10^6 \text{ cells}\cdot\text{ml}^{-1}$ . For the re-supply of iron to starved cultures, cells of CC-4532, *vtc1* and *VTCl* were grown in pre-cultures containing 1  $\mu\text{M}$  Fe from inoculation to late-logarithmic phase ( $1\text{-}2 \times 10^4$  to  $9 \times 10^6 \text{ cells}\cdot\text{ml}^{-1}$ ) to deplete the luxurious iron pools, transferred to medium without added iron at a density of  $1 \times 10^4 \text{ cells}\cdot\text{ml}^{-1}$  and grown for 3 (CC-4532) or 3.5 d (*vtc1* and *VTCl*) until the cultures reached  $\sim 1 \times 10^6 \text{ cells}\cdot\text{ml}^{-1}$  (Figure 58 E). 2, 20 and 200  $\mu\text{M}$  Fe-EDTA was added and cultures were analyzed at 0, 2, 4, 6, 12, 24 and 48 h.

### 4.2.1.6 Acetate addition

For the assessment of dynamic acclimation of photoautotrophic cultures to organic carbon, cells of strain CC-4532 were grown in 1.2 l TP medium with 1  $\mu\text{M}$  Fe. One replicate culture of 0.25, 1.0, and 20  $\mu\text{M}$  Fe each were inoculated to an initial density of  $1 \times 10^4 \text{ cells}\cdot\text{ml}^{-1}$  and grown in parallel for 6-7 days, until they reached  $2 \times 10^6 \text{ cells}\cdot\text{ml}^{-1}$ . A sample for the -2h or 'before' time point was taken, and 12 ml sterile 1.7 M  $\text{Na}_2\text{-EDTA}$ , pH 7.2, was added

## 4. Materials and Methods

---

to each culture at 0 h. Cells for the time point 0h were taken immediately after the addition, cultures were mixed with the acetate by letting the cultures shake for 5 rounds (about 15 seconds) using a setup that allowed to add acetate to shaking flasks in the incubator. A cycloheximide stock solution of  $2 \text{ mg}\cdot\text{ml}^{-1}$  in MilliQ water was prepared fresh before use and 0.5 ml was added to small Fe-limited (100 ml,  $0.25 \text{ }\mu\text{M Fe}$ ) cultures to obtain a final concentration of  $10 \text{ }\mu\text{g}\cdot\text{ml}^{-1}$ .

### 4.2.2 Cell Density, Generation Time and Cell Volume

Cells were counted by light microscopy using a hemocytometer (Improved Neubauer, Hausser Scientific, Horsham, PA, USA). 1-ml samples of culture was removed under sterile conditions with single-use pipettes in a laminar flow hood, before diluting cultures or during experiments every 12 or 24 h, to calculate growth rates and visually inspect cultures for contaminations or phenotypic changes. Cell samples were diluted with TAP medium or 10 mM phosphate buffer if necessary and immobilized by adding iodine (0.25% w/v in ethanol,  $10 \text{ }\mu\text{l}\cdot\text{ml}^{-1}$  cell suspension). The generation time was calculated as the time each culture needed for a full doubling of the cell number during logarithmic growth ( $\sim 1 \times 10^5$  to  $\sim 5 \times 10^6 \text{ cells}\cdot\text{ml}^{-1}$ ). Cell diameter and volume were determined from at least 200 individual cells using an automated cell counter (Cellometer Auto T4, Nexcelome, Lawrence, MA, USA). Cells were sampled, diluted and immobilized as described above and loaded into the counting chambers (SD100 Disposable Counting Chambers, Nexcelome) with a minimum and maximum diameter cut-off of 3 and 30  $\mu\text{m}$ , respectively. The median of the diameter distribution was used to calculate the cell volume.

### 4.2.3 Photosynthetic Parameters

#### 4.2.3.1 Chlorophyll Content

$1\text{-}4 \times 10^6$  cells were collected in a 1.5 ml test tube in duplicates from each biological replicate sample by centrifugation (2 min, 16 200 g,  $4^\circ\text{C}$ ) in the tabletop centrifuge (5415R with rotor FA-45-24-11, Eppendorf, Hauppauge, NY, USA). The medium was removed by aspiration and the pellet dissolved vigorously in 1 ml 80% acetone/20% methanol (v/v). Cell debris was pelleted (10 min, 16 200 g,  $4^\circ\text{C}$ , 5415R) and absorption (A) of the cleared extract measured spectrophotometrically (Lambda 25, PerkinElmer, Waltham, MA, USA)

## 4. Materials and Methods

---

against a solvent blank at 663.6 and 646.6 as well as 750.0 nm for reference. The chlorophyll content was calculated according to Porra et al. (1989) and related to the number of cells analyzed (Equation 1).

Equation 1: Calculation of total cellular chlorophyll content.

$$\text{chl (pg} \cdot \text{cell}^{-1}) = \frac{(17.76 * (A_{646.6} - A_{750})) + (7.34 * (A_{663.6} - A_{750}))}{\text{number of cells}}$$

### 4.2.3.2 In Vivo Chlorophyll Fluorescence

In vivo chlorophyll fluorescence analysis included measurement of maximum quantum efficiency of PSII ( $F_v/F_m$ ) and OJIP fluorescence transients. Photochemical efficiency was measured at room temperature from  $\sim 2 \times 10^6$  intact cells using an IMAGING PAM (with IMAG-K7 camera, IMAG-MAX/1 LED field and ImagingWin v2.46i software, Heinz Walz GmbH, Eifeltrich, DE). Cells were immobilized and concentrated onto 15 mm round filters by gentle, vacuum-assisted suction, placed in the instrument chamber and the instrument set up (measuring light intensity 1, measuring light frequency 8, damping 2, saturating pulse intensity 8; camera focus was adjusted, and gain set to a value between 4 and 6 manually for every measurement). After dark-adaptation on wet filters inside the instrument for 12-15 min, initial fluorescence ( $F_0$ ) and maximum fluorescence ( $F_{\max}$ ) after a saturating light pulse were recorded and  $F_v/F_m$  was calculated as  $(F_{\max} - F_0)/F_{\max}$ .

Fluorescence measurements, like  $F_v/F_m$  and OJIP, rely on light that saturates all photosynthetic reaction centers. In initial experiments, dark-adaptation time and inhibitor concentration were optimized and verified to catch as many reaction centers open (dark-adapted) or closed (DCMU or saturating light flash) as possible. Replete photoheterotrophic cells were immobilized onto 15 mm round filters, placed in plastic dishes and kept in the dark for 1, 2, 3, 4, 5, 7.5, 10, 12.5, 15, 17.5, 20 or 25 min.  $F_0$  was recorded as described before and the lowest  $F_0$  was observed between 10 and 15 min. The concentration of the inhibitor 3-(3,4-dichlorophenyl)-1,1-dimethylurea (DCMU, dissolved in ethanol) was determined using a dose-response-curve. Replete photoheterotrophic cells were transferred into a 96-well plate, gently mixed with 0, 0.5, 1, 2, 5, 10, 15, 20, 50, and 100  $\mu\text{M}$  DCMU, and  $F_0$  and  $F_{\max}$  were determined as described above (gain was set to 10).  $F_0$  in the presence of DCMU increased with increasing inhibitor concentrations and

## 4. Materials and Methods

---

reached a maximum between 15 and 50  $\mu\text{M}$  at similar fluorescence levels as  $F_{\text{max}}$  after a saturating light pulse.

The fast fluorescence transients (OJIP) were measured at room temperature of  $\sim 2 \times 10^6$  intact cells with a Joliot-type spectrophotometer (JTS-10 with Fluo\_59 accessory, Bio-Logic SAS, Seyssinet-Pariset/Claix, FR). Cells were immobilized and concentrated onto 15 mm filters, dark adapted for 10-15 min, placed in the leaf holder of the instrument and fluorescence changes recorded. Initial fluorescence ( $F_0$ ) and fluorescence ( $F$ ) during continuous illumination at 520 nm were recorded using a modified sequence for OJIP measurements (sequence: “20(5msD) 300 $\mu\text{sG}$  10(30 $\mu\text{sD}$ ) 10(60 $\mu\text{sD}$ ) {100 $\mu\text{s}$ ,100,5s,D} 100 $\mu\text{sH}$ ”; illumination: L7113 green Fluo (GH) = 1650  $\mu\text{mol m}^{-2} \text{s}^{-1}$ ). As a control, filters soaked in growth medium were measured in the same way. Fluorescence transients were normalized to  $F_0$  and subsequently normalized to the maximum value for comparison.

To verify that the light intensity applied was saturating for the different experimental cultures, a fraction of the samples was additionally treated with 20  $\mu\text{M}$  DCMU 2 min prior immobilization and measured in the same way as non-treated cells.

### 4.2.3.3 Oxygen Consumption and Evolution.

Net oxygen consumption and evolution were measured using a standard Clarke-type polarographic oxygen electrode (Chlorolab 2 System, Hansatech, Norfolk, UK). Oxygen concentrations were recorded and analyzed with the Hansatech OxyLab software. The Chlorolab 2 was calibrated with oxygen-saturated and -depleted water before every run. Oxygen-saturated water was prepared by blowing air into water; oxygen-depleted water was prepared by adding 0.2 g sodium sulfite ( $\text{Na}_2\text{SO}_3$ ) to 2 ml water. Measurements were carried out using  $2\text{-}4 \times 10^6$  cells in a total volume of 2 ml (cell number and volume were adjusted with 10 mM sterile phosphate buffer if necessary) at room temperature (18-20°C), in the presence of 10 mM  $\text{KHCO}_3$  (to avoid substrate limitation). The cell suspension was stirred at a rate of 100 rpm to avoid cells settling and ensure homogeneous distribution of nutrients and gases. Changes in oxygen concentration were monitored for  $\sim 20$  min, using a programmed sequence of 9 min darkness and 6 min illumination at setting 100 (203  $\mu\text{mol}\cdot\text{m}^{-2}\cdot\text{s}^{-1}$ ), followed by darkness. The light intensity was chosen based on a light-response-curve performed for strain CC-4532 in iron-limited and -replete photoheterotrophic and photoautotrophic conditions. The rate of oxygen consumption in the dark was calculated from the change in oxygen concentration between four and nine



## 4. Materials and Methods

---

minutes. Net oxygen evolution was calculated from the rate of change in oxygen concentration between minutes 10 and 15, subtracted by the calculated rate of oxygen consumption in the dark. Oxygen consumption and evolution rates were related to the number of cells analyzed, which were counted in parallel, as described above.

### 4.2.4 Elemental Analysis

#### 4.2.4.1 Analysis by Inductively Coupled Plasma (ICP)-MS/MS

To obtain reproducible data from elemental analysis by ICP-MS/MS, timely sample processing is crucial. To that end, not more than eight samples were collected and processed in parallel to avoid pausing periods for individual samples and to reduce the risk of cell lysis. If not indicated otherwise,  $1 \times 10^8$  cells were collected in 50-ml Falcon tubes by centrifugation (2 min, 2 500 g, 20°C, 5810R), washed twice with 50 ml 1 mM Na<sub>2</sub>-EDTA, pH 8.0, quantitatively transferred to 15-ml Falcon tubes and rinsed twice with 15 ml purified water. Pelleted cells without any remaining supernatant were frozen and stored at -20°C until further processing. One or two days before analysis by ICP-MS/MS, up to 80 samples were thawed and the intact pellets carefully overlaid with 286 µl nitric acid (~70% v/v, Fisher Sci. Optima). Two additional tubes containing 120 µl purified water instead of cells were prepared as blank controls for every batch and treated and digested the same as the cellular samples. All samples were lysed at room temperature for 20-24 h, followed by 1-2h at 65°C to completely dissolve the biomass, resulting in clear, homogenous solutions which were mixed by vortex shaker for 20 seconds, briefly spun to collect droplets in the lid and diluted with 9.6 ml deionized water to a final nitric acid concentration of 2%. During the acetate-addition time course experiment,  $5 \times 10^7$  cells were collected to allow for a denser sampling scheme, washed as described above, digested in 143 µl nitric acid and diluted with 4.8 ml purified water. For the analysis of fresh or spent growth medium, cells were pelleted as described above, a fraction of the first supernatant was carefully transferred into fresh 15-ml Falcon tubes, centrifuged again (5 min, 2 500 g, 20°C, 5810R) and 2 ml transferred into clean 15-ml Falcon tubes. Samples were mixed with 200 µl nitric acid, digested for 2-3h at room temperature and diluted with 4.8 ml purified water. Two blank controls containing 2 ml purified water instead of (spent) medium were treated the same way.

#### 4. Materials and Methods

---

Inductively coupled plasma mass spectrometry on an Agilent 8800 triple quadrupole ICP-MS/MS instrument with autosampler and standard sample introduction system, consisting of a concentric nebulizer, quartz spray chamber, and nickel interface cones, was used to determine sodium (Na), magnesium (Mg), phosphorus (P), sulfur (S), potassium (K), calcium (Ca), manganese (Mn), iron (Fe), copper (Cu), and zinc (Zn) content. For some experiments, cobalt (Co), nickel (Ni), selenium (Se) and molybdenum (Mo) were analyzed as well but are not shown in this thesis. Plasma settings and lens voltages were fine-tuned before every analysis according to manufacturer's instructions, the MassHunter software (v1.0, Agilent) was used to control the instrument and for initial data analysis.

The concentrations of the analytes were determined in MS/MS mode, Na, Mg, Mn, Co, Ni, Cu, Zn and Mo were analyzed directly with helium (He) in collision mode, K, Ca, Fe, and Se were analyzed directly with hydrogen (H<sub>2</sub>) in reaction mode, P and S were analyzed with oxygen (O<sub>2</sub>) in reaction mode and detected as mass-shifted ions ( $Q2 = Q1 + 16$ ). The average of five technical replicates was used for each individual biological sample, the variation between the technical replicates never exceeded 5% for an individual sample.

An internal standard (ISTD) containing scandium (Sc) and yttrium (Y) (MSSC-100PPM and MSY-100PPM, Inorganic Ventures), which are not present in algae, at low concentrations of  $\sim 2 \text{ ng}\cdot\text{ml}^{-1}$  was added "in-line" to the analyte flow for normalization purposes. Recovery rates of both internal standards were monitored over the entire analysis and stayed within 80 to 120% of ion counts from the first calibration sample. Analyte ion counts were normalized to Sc using the MassHunter software. Calibration solutions and calibration verification samples were prepared from a multi-element environmental calibration standard (#5183-4688, Agilent) containing  $1000 \text{ }\mu\text{g}\cdot\text{ml}^{-1}$  each of Fe, K, Ca, Na, Mg and  $10 \text{ }\mu\text{g}\cdot\text{ml}^{-1}$  each of Ag, Al, As, Ba, Be, Cd, Co, Cr, Cu, Mn, Mo, Ni, Pb, Sb, Se, Th, Tl, U, V and Zn and single element standards containing  $1 \text{ mg}\cdot\text{ml}^{-1}$  each of S and P (CGS1 and CGP1, Inorganic Ventures). A set of calibration solutions prepared in the background of cell matrix was analyzed as unknown samples and showed a good linear fit and a constant shift in counts. The complex matrix in the cellular samples did not alter the linearity of retrieved ion counts of the calibration solutions. A serial dilution of an exemplary cellular sample showed good linear relationship and confirmed quantitative signal recovery over a wide range of concentrations. In addition, cellular samples spiked with known concentrations of calibration solution were analyzed to verify quantitative recovery. All solutions for elemental analysis by ICP-MS/MS were prepared with

## 4. Materials and Methods

---

deionized water in HCl-cleaned laboratory glass and plastic ware and stored in HCl-cleaned bottles and containers. A typical elemental analysis consisted of twelve calibration samples (level 1-12, Supplemental Table 61), calibration verification samples (level 1, 5 and 8) to monitor signal intensity drifts over time, a calibration sample exceeding the concentration range of the calibration (level 13), up to 80 analytical samples with blank check samples containing 2% nitric acid every 6 to 12 analytical samples to ensure effectiveness of the rinse protocol, and calibration verification samples at the end of the analysis. During longer queues, calibration verification samples were analyzed periodically between unknown samples to ensure enduring linearity of calibration.

### 4.2.4.2 Analysis of Total Organic Carbon and Total Nitrogen (TOC-TN)

If not stated otherwise,  $3 \times 10^7$  cells were collected by centrifugation (5 min, 2 500 g, 4°C, 5810R), washed twice with 50 ml purified water, resuspended in 3 M HCl to a final volume of 540  $\mu$ l and incubated for 16h at 65°C with constant agitation. Samples containing large amounts of complex carbon compounds (like starch and lipids) were incubated for up to 36h for proper break down. Fractions of the cell lysate were diluted to  $1 \times 10^5$  cells·ml<sup>-1</sup> with deionized water (180  $\mu$ l cell lysate and 19.82 ml water) and analyzed for non-purgeable organic carbon (C) and total nitrogen (N) content using a TOC-1 CSH with TNM-1 unit and autosampler (Shimadzu Corp., Kyoto, JP). In the instrument, a fraction of the sample (200  $\mu$ l) is acidified with H<sub>3</sub>PO<sub>4</sub>, purged of inorganic carbon by sparging with purified air, and the remaining non-purgeable organic carbon oxidized to CO<sub>2</sub> at 720°C in the presence of a catalyst. The resulting CO<sub>2</sub> concentration was measured in technical triplicates with a non-dispersive infrared (NDIR) gas analyzer. Nitrogen oxide from the oxidized total nitrogen was analyzed in triplicates on a chemiluminescence gas analyzer. Separate C and N calibration solutions containing 25 mg C·l<sup>-1</sup> (potassium hydrogen phthalate) and 25 mg N·l<sup>-1</sup> (potassium nitrate), respectively, were prepared fresh from 1000 mg·l<sup>-1</sup> stock solution. Calibrations for C and N were generated separately, calibration check samples contained 5 mg·l<sup>-1</sup> C, 5 mg·l<sup>-1</sup> N or 10 mg·l<sup>-1</sup> of both, spike-in samples contained both carbon and nitrogen at concentrations of 10 mg·l<sup>-1</sup> and 5 mg·l<sup>-1</sup>, respectively. A typical sequence of calibration, quality control and analytical samples comprised of water blank samples to check on instrument and general C or N contaminations, calibration samples (the seven calibration concentrations 0, 0.5, 1.0, 2.5, 5.0, 10 and 25 mg·l<sup>-1</sup> were obtained by auto-dilution of 25 mg·l<sup>-1</sup>), calibration check samples (5 mg·l<sup>-1</sup> and 10 mg·l<sup>-1</sup>) to check

## 4. Materials and Methods

---

accuracy of the calibration samples, up to 60 analytical samples with water blank samples every four to ten analytical samples, a spiked sample (5 mg·l<sup>-1</sup> and 10 mg·l<sup>-1</sup> added to an additional analytical sample) to test recovery in the sample matrix and calibration check samples to verify that the calibration linearity did not drift during the analysis. When more than 40 analytical samples were analyzed at a time, additional calibration check samples were placed between the analytical samples. Initially, a calibration in the background of cellular sample was performed to verify quantitative recovery of both C and N from the complex sample matrix over a wide range of concentration. A serial dilution of a small subset of analytical samples was performed to verify that the recovery of carbon and nitrogen is quantitative over a wide range of concentrations and ratios of carbon to nitrogen. The peak area was calculated and compared to the calibration curves using the TOC-Control software (version 1.0) to determine the concentration of non-purgeable carbon and total nitrogen of the analytical samples. Measured concentrations did not exceed the range of 2-25 mg·l<sup>-1</sup> for C and 1-5 mg·l<sup>-1</sup> for N. Samples with carbon content outside the linear range were additionally analyzed as a 1:200 dilution (photoheterotrophic cultures with 0.10 and 0.25 μM Fe and heterotrophic cultures with 0.25 μM Fe)

### 4.2.5 Transcriptome Analysis

If not stated otherwise,  $3 \times 10^6$  cells were collected by centrifugation (5 min, 2 500 g, 4°C, 5810R) and resuspended in RNase free water to an exact volume of 0.5 ml. Not more than four samples were collected and processed in parallel to avoid pausing periods for individual samples. The resuspended cells were combined with 0.5 ml of fresh 2x lysis buffer (final concentrations: 50 mM Tris-HCl pH 7.5, 150 mM NaCl, 15 mM EDTA, 2% SDS, and 40 ng·ml<sup>-1</sup> Proteinase K), mixed by gently pipetting up and down five times and inversion of the tube for 30 s. Cellular starch was pelleted by centrifugation (3 min, 600 g, 20°C, 5810R), the lysate transferred to a fresh 15-ml tube, flash-frozen in liquid N<sub>2</sub>, and stored at -80°C. RNA from four to six frozen samples was extracted in parallel, samples were kept on ice and solutions were pre-cooled when possible. At room temperature, 10 ml TRIzol (Thermo Fisher Scientific) was added to each frozen pellet and samples were gently inverted until thawed. Nucleic acids were extracted by adding 2 ml chloroform/isoamylalcohol (24:1, v/v), and vigorously shaken for 30 s. Phases were separated by centrifugation (5 min, 1500 g, 20°C, 5810R), the aqueous phase carefully

#### 4. Materials and Methods

---

transferred to a fresh tube without contaminations from the protein-containing interphase and mixed with ~10 ml ethanol (RNase-free, 100%, 200 proof). The mixture was transferred onto RNeasy mini columns (QIAGEN, Venlo, NL) using a vacuum manifold, washed according to manufacturer's instructions (but with buffer RWT instead of RW1), DNase treated on the column, washed with buffer RWT and RPE and eluted into 90  $\mu$ l purified water. In an additional step, the RNA is further purified by precipitation with 10% (v/v) 3M sodium acetate pH 7.0 and 2.5 volumes ethanol (30 min,  $-20^{\circ}\text{C}$ , followed by centrifugation for 30 min, 16 200 g,  $4^{\circ}\text{C}$ , 5415R), the resulting pellets were washed with 70% ethanol (v/v) and resuspended in 60  $\mu$ l RNase-free water. Concentration of total RNA was determined using a NanoDrop 2000 (Thermo Fisher Scientific, Waltham, MA, USA), concentrations were  $>100 \text{ ng}\cdot\text{ml}^{-1}$ , and the quality was assessed by the ratios of  $A_{260}/A_{280} \sim 2.05\text{-}2.20$ , and  $A_{260}/A_{230} >2.00$  (NanoDrop), and on a bioanalyzer according to manufacturer's instructions (2100 Bioanalyzer, Agilent).

A spike-in kit was used on a subset of sample of the acetate addition experiment (ERCC RNA Spike-In, Ambion, Thermo Fisher Scientific). The spike-in kit consists of a collection of in vitro generated poly-A mRNA molecules of known size and quantity and is used to determine the dynamic range and limit of detection. It is not necessary to include the spike-in control in all samples and the samples supplied with spike-in were chosen at random across the time course and iron conditions. The spike-in kit contains two different mixtures with RNAs in different concentrations and ratios. Four samples were spiked with mixture A and four samples with mixture B after RNA purification (1  $\mu$ l diluted spike-in per 5  $\mu$ g RNA) to validate the library preparation and sequencing steps and four were spiked with mixture A and four with mixture B prior to TRIzol extraction (2  $\mu$ l diluted spike-in per lysate) to also validate the RNA purification steps. For all three RNA-Seq experiments, "excess iron", "acetate addition" and "strains", RNA extraction, sequencing and initial data analysis were performed in the same manner. Differences between the experiments and resulting data sets are highlighted below. Strand-specific libraries were prepared from mRNA (KAPA stranded mRNA-Seq Kit for Illumina Platforms, KAPABiosystems, Wilmington, MA, USA), multiplexed for 12 libraries per lane and sequenced in 50-nt, single end reads on an Illumina HiSeq 4000. RNA-Seq libraries were prepared by the Clinical Microarray Core Facility (DGSOM, Department of Pathology and Laboratory Medicine, UCLA) and RNA-Sequencing was performed. Libraries were sequenced using a HiSeq 1000 sequencer (Illumina) and single end 50-bp sequences were generated. The

## 4. Materials and Methods

---

resulting sequencing data were filtered to remove the 3' adaptor sequence and low-quality nucleotide calls. Reads were aligned to the *C. reinhardtii* genome (genome assembly v5, gene annotations v5.5, Phytozome v10.3, phytozome.jgi.doe.gov) using RNA-STAR (version 2.4.1d) (Dobin et al, 2013) with default settings for aligning reads with multiple hits. For each sample and gene, expression estimates were obtained using Cuffdiff (version 2.2.1) after normalizing the counts by the mappable length of the gene and the sample's sequencing depth and are given in units of FPKM (fragments per kilobase of transcript per million fragments mapped) (Trapnell et al., 2012). Data visualization was performed using the R package cummeRbund (version 2.20.0; R version 3.3.2) (Goff et al., 2013) and standard software (Excel, SigmaPlot, Adobe Illustrator). A minimum expression cutoff of 1 FPKM across all samples (average expression of the replicates) was subsequently applied to remove genes with low expression within each of the three data sets. Genes were classified as differentially expressed using a minimum of 2-fold regulation and a false discovery rate (FDR) of < 5% for the "excess iron" and "acetate addition" data sets and FDR < 0.5% for the "strains" data set.

### 4.2.6 Calculations and Statistics

Data from individual biological replicates are assumed to be samples of a population, but do not represent the entire population. Normal distribution of arguments and equal variance between conditions are assumed for statistical calculations and were tested for a random fraction of experiments and datasets. Mean and standard deviation are used to report normally distributed data. For skewed datasets, for example cell diameter distributions, median and inter-percentile range were used. Fractions of time are given in hundredths, not raw fractions, with 0.5h or 9.4h corresponding to 30 min or 9h and 24 min, respectively. Common calculations for computing the standard deviation of values obtained from calculations of values that contain standard deviations were applied. Cohen's *d*-value was computed as a measure of effect size, or practical significance, between the individual conditions and were reported as absolute values with larger numbers indicating a larger difference or effect between the conditions. Statistical significance was calculated using an unpaired, two-tailed Student's *t*-test, if not specifically stated otherwise. A difference between two average values is considered significant when the *p*-value passes a

#### 4. Materials and Methods

---

significance threshold of  $\alpha = 0.05$ . Individual  $d$ - and  $p$ -values are presented in Supplemental Tables.

---

## 5 References

- Aksoy M, Pootakham W, Grossman AR.** (2014). Critical function of a *Chlamydomonas reinhardtii* putative polyphosphate polymerase subunit during nutrient deprivation. *Plant Cell*. 10: 4214-29.
- Allen MD, del Campo JA, Kropat J, Merchant SS.** (2007) FEA1, FEA2, and FRE1, encoding two homologous secreted proteins and a candidate ferrireductase, are expressed coordinately with FOX1 and FTR1 in iron-deficient *Chlamydomonas reinhardtii*. *Eukaryot Cell*. 6(10): 1841-52.
- Anbar AD.** (2008) Oceans. Elements and evolution. *Science*. 322(5907): 1481-3.
- Andreini C, Bertini I, Cavallaro G, Holliday GL, Thornton JM.** (2008) Metal ions in biological catalysis: from enzyme databases to general principles. *J Biol Inorg Chem* 13: 1205.
- Arnon DI.** (1959). Conversion of light into chemical energy in photosynthesis. *Nature* 184: 10-12.
- Asada K.** (2000) The water-water cycle as alternative photon and electron sinks. *Philos Trans R Soc Lond B Biol Sci* 355 (1402): 1419–1431.
- Baker NR.** (2008) Chlorophyll fluorescence: a probe of photosynthesis in vivo. *Annu Rev Plant Biol*.59: 89-113.
- Balcaen L, Bolea-Fernandez E, Resano M, Vanhaecke F.** (2015) Inductively coupled plasma - Tandem mass spectrometry (ICP-MS/MS): A powerful and universal tool for the interference-free determination of (ultra)trace elements – A tutorial review. *Anal Chim Acta*. 24: 894:7-19.
- Bandura DR, Baranov VI, Tanner SD.** (2002) Inductively coupled plasma mass spectrometer with axial field in a quadrupole reaction cell. *J Am Soc Mass Spectrom*. 10: 1176-85.
- Baxter IR, Gustin JL, Settles AM, Hoekenga OA.** (2103) Ionomics characterization of maize kernels in the intermated B73× Mo17 population. *Crop Science*. 53(1): 208-20.
- Baxter IR, Ziegler G, Lahner B, Mickelbart MV, Foley R, Danku J, Armstrong P, Salt DE, Hoekenga OA.** (2014) Single-kernel ionomic profiles are highly heritable indicators of genetic and environmental influences on elemental accumulation in maize grain (*Zea mays*). *PLoS One*. 9(1): e87628.



## 5. References

---

- Ben-Shem A, Frolow F, Nelson N.** (2003) Crystal structure of plant photosystem I. *Nature*. 426(6967): 630-5.
- Blaby IK, Blaby-Haas CE, Tourasse N, Hom EF, Lopez D, Aksoy M, Grossman A, Umen J, Dutcher S, Porter M, King S, Witman GB, Stanke M, Harris EH, Goodstein D, Grimwood J, Schmutz J, Vallon O, Merchant SS, Prochnik S.** (2014) The *Chlamydomonas* genome project: a decade on. *Trends Plant Sci*. 10: 672-80.
- Blaby-Haas CE, Merchant SS.** (2012) The ins and outs of algal metal transport. *Biochim Biophys Acta*. 1823(9): 1531-52.
- Blaby-Haas CE, Merchant SS.** (2013) Iron sparing and recycling in a compartmentalized cell. *Curr Opin Microbiol*. 6: 677-85.
- Blaby-Haas CE, Merchant SS.** (2014) Lysosome-related organelles as mediators of metal homeostasis. *J Biol Chem*. 289(41): 28129-36.
- Blaby-Haas CE, Merchant SS.** (2019) Comparative and Functional Algal Genomics. *Annu Rev Plant Biol*. 70: 605-638.
- Boal AK, Rosenzweig AC.** (2009) Structural biology of copper trafficking. *Chem Rev*. 109(10): 4760-79.
- Bowsher C, Steer MW, Tobin AK** (2008). *Plant biochemistry* (New York, NY: Garland Science).
- Buescher E, Achberger T, Amusan I, Giannini A, Ochsenfeld C, Rus A, Lahner B, Hoekenga O, Yakubova E, Harper JF, Guerinot ML, Zhang M, Salt DE, Baxter IR.** (2010) Natural genetic variation in selected populations of *Arabidopsis thaliana* is associated with ionic differences. *PLoS One*. 5(6): e11081.
- Busch A, Rimbauld B, Naumann B, Rensch S, Hippler M.** (2008) Ferritin is required for rapid remodeling of the photosynthetic apparatus and minimizes photo-oxidative stress in response to iron availability in *Chlamydomonas reinhardtii*. *Plant J*. 55(2): 201-11.
- Calvin M, Benson A.** (1948) The path of carbon in photosynthesis. *Science*. 107(2784): 476-80.
- Campos ACAL, Kruijer W, Alexander R1, Akkers RC, Danku J, Salt DE, Aarts MGM.** (2017) Natural variation in *Arabidopsis thaliana* reveals shoot ionome, biomass, and gene expression changes as biomarkers for zinc deficiency tolerance. *J Exp Bot*. 68(13): 3643-3656.

## 5. References

---

- Cao J, Govindjee.** (1990) Chlorophyll a fluorescence transient as an indicator of active and inactive Photosystem II in thylakoid membranes. *Biochim Biophys Acta.* 1015(2): 180-8.
- Castruita M.** (in preparation) Cadmium-toxicity in *Chlamydomonas reinhardtii*.
- Chaparro JM, Holm DG, Broeckling CD, Prenni JE, Heuberger AL.** (2018) Metabolomics and ionomics of potato tuber reveals an influence of cultivar and market class on human nutrients and bioactive compounds. *Frontiers in nutrition.* 5:36.
- Chen Y, Barak P.** (1982). Iron nutrition of plants in calcareous soils. *Adv. Agron.* 35, 217–240.
- Chen JC, Hsieh SI, Kropat J, Merchant SS.** (2008) A ferroxidase encoded by *FOX1* contributes to iron assimilation under conditions of poor iron nutrition in *Chlamydomonas*. *Eukaryotic cell.* 7(3): 541-5.
- Chen Z, Watanabe T, Shinano T, Okazaki K, Osaki M.** (2009) Rapid characterization of plant mutants with an altered ion-profile: a case study using *Lotus japonicus*. *New Phytologist.* 181(4): 795-801.
- Cole DG.** (2003) The intraflagellar transport machinery of *Chlamydomonas reinhardtii*. *Traffic.* 4(7): 435-42.
- Czaja AD.** (2010). Early Earth: Microbes and the rise of oxygen. *Nature Geosci* 3 (8): 522–523.
- Danku JM, Lahner B, Yakubova E, Salt DE.** (2013) Large-scale plant ionomics. *Methods Mol Biol.* 2013; 953:255-76.
- Dekker JP, van Grondelle R.** (2000). Primary charge separation in Photosystem II. *Photosynthesis research* 63 (3): 195–208.
- Dent RM, Han M, Niyogi KK.** (2001) Functional genomics of plant photosynthesis in the fast lane using *Chlamydomonas reinhardtii*. *Trends Plant Sci.*6(8): 364-71.
- Desplats C, Mus F, Cuine S, Billon E, Cournac L, Peltier G.** (2009). Characterization of Nda2, a plastoquinone-reducing type II NAD(P)H dehydrogenase in *Chlamydomonas* chloroplasts. *The Journal of biological chemistry* 284 (7): 4148–4157
- Dobin A, Davis CA, Schlesinger F, Drenkow J, Zaleski C, Jha S, Batut P, Chaisson M, Gingeras TR.** (2013) STAR: ultrafast universal RNA-seq aligner. *Bioinformatics.* 29(1): 15-21.

## 5. References

---

- Docampo R, de Souza W, Miranda K, Rohloff P, Moreno SN.** (2005) Acidocalcisomes - conserved from bacteria to man. *Nat Rev Microbiol.* (3): 251-61.
- Docampo R, Ulrich P, Moreno SN.** (2010) Evolution of acidocalcisomes and their role in polyphosphate storage and osmoregulation in eukaryotic microbes. *Philos Trans R Soc Lond B Biol Sci.* 365(1541): 775-84.
- Donald R, Yocum CF, Heichel IF.** (1996). *Oxygenic photosynthesis: The light reactions.* (Dordrecht, Boston: Kluwer).
- Dudev T, Lim C.** (2008) Metal binding affinity and selectivity in metalloproteins: insights from computational studies. *Annu Rev Biophys.* 37: 97-116.
- Eberhard S, Finazzi G, Wollman FA.** (2008) The dynamics of photosynthesis. *Annu Rev Genet.* 42: 463-515.
- Ebersold WT.** (1956) Crossing over in *Chlamydomonas reinhardtii*. *Am. J. Bot.* 43: 408.
- Eide DJ, Clark S, Nair TM, Gehl M, Gribskov M, Guerinot ML, Harper JF.** (2005) Characterization of the yeast ionome: a genome-wide analysis of nutrient mineral and trace element homeostasis in *Saccharomyces cerevisiae*. *Genome Biol.* (9): R77.
- Erickson E, Wakao S, Niyogi KK.** (2015) Light stress and photoprotection in *Chlamydomonas reinhardtii*. *Plant J.* 82(3): 449-65.
- Fernández E, Schnell R, Ranum LP, Hussey SC, Silflow CD, Lefebvre PA.** (1989) Isolation and characterization of the nitrate reductase structural gene of *Chlamydomonas reinhardtii*. *Proc Natl Acad Sci USA.* 86(17): 6449-53.
- Ferris PJ, Armbrust EV, Goodenough UW** (2002). Genetic structure of the mating-type locus of *Chlamydomonas reinhardtii*. *Genetics* 160 (1): 181-200
- Field CB, Behrenfeld MJ, Randerson JT, Falkowski P.** (1998) Primary production of the biosphere: Integrating terrestrial and oceanic components. *Science* 281: 237-240.
- Fischer WW.** (2008) Biogeochemistry: Life before the rise of oxygen. *Nature.* 455(7216): 1051-2.
- Fischer WW, Hemp J, Johnson JE.** (2016) Evolution of Oxygenic Photosynthesis. *Annu. Rev. Earth Planet. Sci.* 44: 647-83.
- Flowers JM, Hazzouri KM, Pham GM, Rosas U, Bahmani T, Khraiweh B, Nelson DR, Jijakli K, Abdrabu R, Harris EH, Lefebvre PA, Hom EF, Salehi-Ashtiani K, Purugganan MD.** (2015) Whole-Genome Resequencing Reveals Extensive Natural Variation in the Model Green Alga *Chlamydomonas reinhardtii*. *Plant Cell.* (9): 2353-69.

## 5. References

---

- Galaris D, Barbouti A, Pantopoulos K.** (2019) Iron homeostasis and oxidative stress: An intimate relationship. *Biochim Biophys Acta Mol Cell Res.* 1866(12): 118535.
- Gallaher SD, Fitz-Gibbon ST, Glaesener AG, Pellegrini M, Merchant SS.** (2015) *Chlamydomonas* Genome Resource for Laboratory Strains Reveals a Mosaic of Sequence Variation, Identifies True Strain Histories, and Enables Strain-Specific Studies. *Plant Cell.* 27(9): 2335-52.
- Gallaher SD, Fitz-Gibbon ST, Strenkert D, Purvine SO, Pellegrini M, Merchant SS.** (2018) High-throughput sequencing of the chloroplast and mitochondrion of *Chlamydomonas reinhardtii* to generate improved de novo assemblies, analyze expression patterns and transcript speciation, and evaluate diversity among laboratory strains and wild isolates. *Plant J.* 93(3): 545-565.
- Gepstein S, Sabehi G, Carp MJ, Hajouj T, Neshar MF, Yariv I, Dor C, Bassani M.** (2003) Large-scale identification of leaf senescence-associated genes. *Plant J.* 36(5): 629-42.
- Ghosh S, Chan CK.** (2016) Analysis of RNA-Seq Data Using TopHat and Cufflinks. *Methods Mol Biol.* 1374:339-61.
- Glaesener AG, Merchant SS, Blaby-Haas CE.** (2013) Iron economy in *Chlamydomonas reinhardtii*. *Front Plant Sci.* Sep 2; 4:337.
- Goff LA, Trapnell C, Kelley D.** (2012). cummeRbund: Analysis, exploration, manipulation, and visualization of Cufflinks high-throughputsequencing data. R Package. Version 2.20.0
- Goodstein DM, Shu S, Howson R, Neupane R, Hayes RD, Fazo J, Mitros T, Dirks W, Hellsten U, Putnam N, Rokhsar DS.** (2012) Phytozome: a comparative platform for green plant genomics. *Nucleic Acids Res.* 40(Database issue): D1178-86.
- Grossman AR, Schaefer MR, Chiang GG, Collier JL.** (1993) The phycobilisome, a light-harvesting complex responsive to environmental conditions. *Microbiol Rev.* 57(3): 725-49.
- Grossman AR, Bhaya D, Apt KE, Kehoe DM.** (1995) Light-harvesting complexes in oxygenic photosynthesis: diversity, control, and evolution. *Annu Rev Genet.*29: 231-88.
- Grossman AR.** (2000) *Chlamydomonas reinhardtii* and photosynthesis: genetics to genomics. *Curr Opin Plant Biol.* 3(2): 132-7.

## 5. References

---

- Grossman AR, Croft M, Gladyshev VN, Merchant SS, Posewitz MC, Prochnik S, Spalding MH.** (2007) Novel metabolism in *Chlamydomonas* through the lens of genomics. *Curr Opin Plant Biol.* 10(2): 190-8.
- Grossman AR, Karpowicz SJ, Heinnickel M, Dewez D, Hamel B, Dent R, Niyogi KK, Johnson X, Alric J, Wollman FA, Li H, Merchant SS.** (2010) Phylogenomic analysis of the *Chlamydomonas* genome unmasks proteins potentially involved in photosynthetic function and regulation. *Photosynth Res.* 106(1-2): 3-17.
- Gu R, Chen F, Liu B, Wang X, Liu J, Li P, Pan Q, Pace J, Soomro AA, Lübberstedt T, Mi G, Yuan L.** (2015) Comprehensive phenotypic analysis and quantitative trait locus identification for grain mineral concentration, content, and yield in maize (*Zea mays* L.). *Theor Appl Genet.* 128(9): 1777-89.
- Guerinot ML, Yi Y.** (1994) Iron: Nutritious, Noxious, and Not Readily Available. *Plant Physiol.* 104(3): 815-820.
- Guiry MD, Guiry GM.** (2019) AlgaeBase. World-wide electronic publication, National University of Ireland, Galway. <https://www.algaebase.org>; searched on 10 October 2019.
- Han TM, Runnegar B.** (1992) Megascopic eukaryotic algae from the 2.1-billion-year-old neogaunee iron-formation, Michigan. *Science.* 257(5067): 232-5.
- Hanikenne M, Talke IN, Haydon MJ, Lanz C, Nolte A, Motte P, Kroymann J, Weigel D, Krämer U.** (2008) Evolution of metal hyperaccumulation required cis-regulatory changes and triplication of *HMA4*. *Nature.* 453(7193): 391.
- Harris EH.** (1989) *The Chlamydomonas Sourcebook: A Comprehensive Guide to Biology and Laboratory Use.* (San Diego: CA Academic press).
- Harris EH.** (2001) *Chlamydomonas* as a model organism. *Annu Rev Plant Physiol Plant Mol Biol* 52: 363-406.
- Harris EH, ed.** (2009) *The Chlamydomonas Sourcebook* (San Diego: Academic).
- Herbik A, Bölling C, Buckhout TJ.** (2002) The involvement of a multicopper oxidase in iron uptake by the green algae *Chlamydomonas reinhardtii*. *Plant Physiol.* 130(4): 2039-48.
- Hill R, Bendall F.** (1960) Crystallization of a photosynthetic reductase from a green plant. *Nature.* 187:17.
- Hoffman BJ, Broadwater JA, Johnson P, Harper J, Fox BG, Kenealy WR.** (1995) Lactose fed-batch overexpression of recombinant metalloproteins in *Escherichia coli*

## 5. References

---

- BL21 (DE3): process control yielding high levels of metal-incorporated, soluble protein. *Protein Expr Purif.* 6(5):46-54.
- Höhner R, Barth J, Magneschi L, Jaeger D, Niehues A, Bald T, Grossman A, Fufezan C, Hippler M.** (2013) The metabolic status drives acclimation of iron deficiency responses in *Chlamydomonas reinhardtii* as revealed by proteomics based hierarchical clustering and reverse genetics. *Mol Cell Proteomics.*12(10): 2774-90.
- Hong-Hermesdorf A, Miethke M, Gallaher SD, Kropat J, Dodani SC, Chan J, Barupala D, Domaille DW, Shirasaki DI, Loo JA, Weber PK, Pett-Ridge J, Stemmler TL, Chang CJ, Merchant SS.** (2014) Subcellular metal imaging identifies dynamic sites of Cu accumulation in *Chlamydomonas*. *Nat Chem Biol.* 10(12): 1034-42.
- Houille-Vernes L, Rappaport F, Wollman FA, Alric J, Johnson X.** (2011) Plastid terminal oxidase 2 (PTOX2) is the major oxidase involved in chlororespiration in *Chlamydomonas*. *Proc Natl Acad Sci USA.* 108(51):0820-5.
- Hsieh SI, Castruita M, Malasarn D, Urzica E, Erde J, Page MD, Yamasaki H, Casero D, Pellegrini M, Merchant SS, Loo JA.** (2013) The proteome of copper, iron, zinc, and manganese micronutrient deficiency in *Chlamydomonas reinhardtii*. *Mol Cell Proteomics.* 12(1): 65-86.
- Hulsen T, de Vlieg J, Alkema W.** (2008) BioVenn - a web application for the comparison and visualization of biological lists using area-proportional Venn diagrams. *BMC Genomics.* 9: 488.
- Hutner SH, Provasoli L, Schatz A, Haskins CP.** (1950). Some approaches to the study of the role of metals in the metabolism of microorganisms. *Proc. Am. Phil. Soc.* 94, 152–170
- Irving H, Williams RJP.** (1953) The stability of transition-metals complexes. *J. Chem. Soc.* 3192-3210
- Jacobs J, Pudollek S, Hemschemeier A, Happe T.** (2009) A novel, anaerobically induced ferredoxin in *Chlamydomonas reinhardtii*. *FEBS Lett.* 583(2): 325-9.
- Jacobsen FE, Kazmierczak KM, Lisher JP, Winkler ME, Giedroc DP.** (2011) Interplay between manganese and zinc homeostasis in the human pathogen *Streptococcus pneumoniae*. *Metallomics.* 3(1): 38-41.
- Jacobson L.** (1945) Iron in the leaves and chloroplasts of some plants in relation to their chlorophyll content. *Plant Physiol.* 20(2): 233–245.

## 5. References

---

- Jans F, Mignolet E, Houyoux PA, Cardol P, Ghysels B, Cuiné S, Cournac L, Peltier G, Remacle C, Franck F.** (2008) A type II NAD(P)H dehydrogenase mediates light-independent plastoquinone reduction in the chloroplast of *Chlamydomonas*. Proc Natl Acad Sci USA. 105(51): 20546-51.
- Jeong J, Guerinot ML.** (2009) Homing in on iron homeostasis in plants. Trends Plant Sci. 14(5): 280-5.
- Jiang X, Stern D.** (2009) Mating and tetrad separation of *Chlamydomonas reinhardtii* for genetic analysis. J Vis Exp. (30).
- Johnson MP.** (2016) Photosynthesis. Essays Biochem. 60(3): 255-273.
- Johnson X, Steinbeck J, Dent RM, Takahashi H, Richaud P, Ozawa S, Houille-Vernes L, Petroustos D, Rappaport F, Grossman AR, Niyogi KK, Hippler M, Alric J.** (2014) Proton gradient regulation 5-mediated cyclic electron flow under ATP- or redox-limited conditions: a study of  $\Delta ATPase\ pgr5$  and  $\Delta rbcL\ pgr5$  mutants in the green alga *Chlamydomonas reinhardtii*. Plant Physiol. 165(1): 438-52.
- Jordan P, Fromme P, Witt HT, Klukas O, Saenger W, Krauss N.** (2001) Three-dimensional structure of cyanobacterial photosystem I at 2.5 Å resolution. Nature. 411(6840): 909-17.
- Kasting JF, Catling DC, Zahnle K.** (2012) Atmospheric oxygenation and volcanism. Nature. 487(7408)
- Kautsky H, Hirsch A.** (1931) Neue Versuche zur Kohlensäureassimilation, Naturwissenschaften, 19:964-964.
- Kitayama K, Kitamaya M, Osafune T, Togasaki RK.** (2002) Subcellular localization of iron and manganese superoxide dismutase in *Chlamydomonas reinhardtii* (Chlorophyceae). Journal of Phycology, 35: 136-142.
- Kosman DJ.** (2003) Molecular mechanisms of iron uptake in fungi. Mol Microbiol. 47(5): 1185-97.
- Kosman DJ.** (2010a) Redox cycling in iron uptake, efflux, and trafficking. J Biol Chem. 285(35): 26729-35.
- Kosman DJ.** (2010b) Multicopper oxidases: a workshop on copper coordination chemistry, electron transfer, and metallophysiology. J Biol Inorg Chem. 15(1): 15-28.

## 5. References

---

- Koziol AG, Borza T, Ishida K, Keeling P, Lee RW, Durnford DG.** (2007) Tracing the evolution of the light-harvesting antennae in chlorophyll *a/b*-containing organisms. *Plant Physiol.* 143(4): 1802-16.
- Kropat J, Hong-Hermesdorf A, Casero D, Ent P, Castruita M, Pellegrini M, Merchant SS, Malasarn D.** (2011) A revised mineral nutrient supplement increases biomass and growth rate in *Chlamydomonas reinhardtii*. *Plant J.* 66(5): 770-80.
- Kropat J, Gallaher SD, Urzica EI, Nakamoto SS, Strenkert D, Tottey S, Mason AZ, Merchant SS.** (2015) Copper economy in *Chlamydomonas*: prioritized allocation and reallocation of copper to respiration vs. photosynthesis. *Proc Natl Acad Sci USA.* 112(9): 2644-51.
- Kurisu G, Zhang H, Smith JL, Cramer WA.** (2003) Structure of the cytochrome  $b_6/f$  complex of oxygenic photosynthesis: tuning the cavity. *Science.* 302(5647): 1009-14.
- La Fontaine S, Quinn JM, Nakamoto SS, Page MD, Göhre V, Moseley JL, Kropat J, Merchant S.** (2002) Copper-dependent iron assimilation pathway in the model photosynthetic eukaryote *Chlamydomonas reinhardtii*. *Eukaryot Cell.* 1(5): 736-57.
- Lahner B, Gong J, Mahmoudian M, Smith EL, Abid KB, Rogers EE, Guerinot ML, Harper JF, Ward JM, McIntyre L, Schroeder JI, Salt DE.** (2003) Genomic scale profiling of nutrient and trace elements in *Arabidopsis thaliana*. *Nat Biotechnol.* 21(10): 1215-21.
- Lander N, Cordeiro C, Huang G, Docampo R.** (2016) Polyphosphate and acidocalcisomes. *Biochem Soc Trans.* 44(1): 1-6.
- Latorre M, Low M, Gárate E, Reyes-Jara A, Murray BE, Cambiazo V, González M.** (2015) Interplay between copper and zinc homeostasis through the transcriptional regulator Zur in *Enterococcus faecalis*. *Metallomics.* 7(7): 1137-45.
- Lee JH, Lin H, Joo S, Goodenough U.** (2008) Early sexual origins of homeoprotein heterodimerization and evolution of the plant KNOX/BELL family. *Cell.* 133(5): 829-40.
- Leliaert F, Smith DR, Moreau H, Herron MD, Verbruggen CFD, De Clerck O.** (2012) Phylogeny and Molecular Evolution of the Green Algae. *Critical Reviews in Plant Sciences.* 31(1):1-46
- Levine RP.** (1960) Genetic control of photosynthesis in *Chlamydomonas reinhardtii*. *Proc Natl Acad Sci USA.* 46(7): 972-8.



## 5. References

---

- Li X, Zhang R, Patena W, Gang SS, Blum SR, Ivanova N, Yue R, Robertson JM, Lefebvre PA, Fitz-Gibbon ST, Grossman AR, Jonikas MC.** (2016) An Indexed, Mapped Mutant Library Enables Reverse Genetics Studies of Biological Processes in *Chlamydomonas reinhardtii*. *Plant Cell*. 28(2): 367-87.
- Lill R, Mühlhoff U.** (2008) Maturation of iron-sulfur proteins in eukaryotes: mechanisms, connected processes, and diseases. *Annu Rev Biochem*. 77: 669-700.
- Long JC, Sommer F, Allen MD, Lu SF, Merchant SS.** (2008) *FER1* and *FER2* encoding two ferritin complexes in *Chlamydomonas reinhardtii* chloroplasts are regulated by iron. *Genetics*. 179(1): 137-47.
- Long JC, Merchant SS.** (2008). Photo-oxidative stress impacts the expression of genes encoding iron metabolism components in *Chlamydomonas*. *Photochem. Photobiol.* 84, 1395–1403.
- Lopez D, Casero D, Cokus SJ, Merchant SS, Pellegrini M.** (2011) Algal Functional Annotation Tool: a web-based analysis suite to functionally interpret large gene lists using integrated annotation and expression data. *BMC Bioinformatics*. 12: 282.
- Lowe DR.** (1980) Stromatolites 3,400-Myr old from the Archean of Western Australia. *Nature* 284(5755): 441-443.
- Malasarn D, Kropat J, Hsieh SI, Finazzi G, Casero D, Loo JA, Pellegrini M, Wollman FA, Merchant SS.** (2013) Zinc deficiency impacts CO<sub>2</sub> assimilation and disrupts copper homeostasis in *Chlamydomonas reinhardtii*. *J Biol Chem*. 288(15): 10672-83.
- Malinouski M, Hasan NM, Zhang Y, Seravalli J, Lin J, Avanesov A, Lutsenko S, Gladyshev VN.** (2014) Genome-wide RNAi ionomics screen reveals new genes and regulation of human trace element metabolism. *Nature comm*. 5: 3301.
- Maret W, Li Y.** (2009) Coordination dynamics of zinc in proteins. *Chem. Rev.*, 109: 4682-4707
- Martin JH, Fitzwater SE, Gordon RM.** (1990) Iron deficiency limits phytoplankton growth in Antarctic waters. *Global Biogeochemical Cycles*. 4(1):5-12.
- Martinoia E, Maeshima M, Neuhaus HE.** (2007) Vacuolar transporters and their essential role in plant metabolism. *J Exp Bot*. 58(1): 83-102.
- Martinoia E, Meyer S, De Angeli A, Nagy R.** (2012) Vacuolar transporters in their physiological context. *Annu Rev Plant Biol*. 63: 183-213.

## 5. References

---

- Mascher M, Gerlach N, Gahrtz M, Bucher M, Scholz U, Dresselhaus T.** (2014) Sequence and ionomic analysis of divergent strains of maize inbred line B73 with an altered growth phenotype. *PLoS One*. 9(5): e96782.
- Maul JE, Lilly JW, Cui L, dePamphilis CW, Miller W, Harris EH, Stern DB.** (2002) The *Chlamydomonas reinhardtii* plastid chromosome: islands of genes in a sea of repeats. *Plant Cell*. 14(11): 2659-79.
- Maxwell K, Johnson GN.** (2000) Chlorophyll fluorescence—a practical guide. *J Exp Bot*. 51(345): 659-68.
- Mehler AH.** (1951) Studies on reactions of illuminated chloroplasts. I. Mechanism of the reduction of oxygen and other Hill reagents. *Arch Biochem Biophys*. 33(1): 65-77.
- Merchant SS, Allen MD, Kropat J, Moseley JL, Long JC, Tottey S, Terauchi AM.** (2006) Between a rock and a hard place: trace element nutrition in *Chlamydomonas*. *Biochim Biophys Acta*. 1763(7): 578-94.
- Merchant SS, Prochnik SE, Vallon O, Harris EH, Karpowicz SJ, Witman GB, Terry A, Salamov A, Fritz-Laylin LK, Maréchal-Drouard L, Marshall WF, Qu LH, Nelson DR, Sanderfoot AA, Spalding MH, Kapitonov VV, Ren Q, Ferris P, Lindquist E, Shapiro H, Lucas SM, Grimwood J, Schmutz J, Cardol P, Cerutti H, Chanfreau G, Chen CL, Cognat V, Croft MT, Dent R, Dutcher S, Fernández E, Fukuzawa H, González-Ballester D, González-Halphen D, Hallmann A, Hanikenne M, Hippler M, Inwood W, Jabbari K, Kalanon M, Kuras R, Lefebvre PA, Lemaire SD, Lobanov AV, Lohr M, Manuell A, Meier I, Mets L, Mittag M, Mittelmeier T, Moroney JV, Moseley J, Napoli C, Nedelcu AM, Niyogi K, Novoselov SV, Paulsen IT, Pazour G, Purton S, Ral JP, Riaño-Pachón DM, Riekhof W, Rymarquis L, Schroda M, Stern D, Umen J, Willows R, Wilson N, Zimmer SL, Allmer J, Balk J, Bisova K, Chen CJ, Elias M, Gendler K, Hauser C, Lamb MR, Ledford H, Long JC, Minagawa J, Page MD, Pan J, Pootakham W, Roje S, Rose A, Stahlberg E, Terauchi AM, Yang P, Ball S, Bowler C, Dieckmann CL, Gladyshev VN, Green P, Jorgensen R, Mayfield S, Mueller-Roeber B, Rajamani S, Sayre RT, Brokstein P, Dubchak I, Goodstein D, Hornick L, Huang YW, Jhaveri J, Luo Y, Martínez D, Ngau WC, Otiillar B, Poliakov A, Porter A, Szajkowski L, Werner G, Zhou K, Grigoriev IV, Rokhsar DS, Grossman AR.** (2007) The *Chlamydomonas* genome reveals the evolution of key animal and plant functions. *Science*. 318(5848): 245-50.

## 5. References

---

- Merchant SS, Helmann D.** (2012) Elemental economy: microbial strategies for optimizing growth in the face of nutrient limitation. *Adv Microb Physiol.* 60: 91-210
- Meyer TE.** (1994) Evolution of photosynthetic reaction centers and light harvesting chlorophyll proteins. *Biosystems.* 33(3): 167-75.
- Mitchell P. (1961) Coupling of Phosphorylation to Electron and Hydrogen Transfer by a Chemi-Osmotic type of Mechanism. *Nature* 191 (4784): 144–148.
- Moellering ER, Benning C.** (2010) RNA interference silencing of a major lipid droplet protein affects lipid droplet size in *Chlamydomonas reinhardtii*. *Eukaryot Cell.* 9(1): 97-106.
- Moore TA, Gust D, Moore AL.** (1989). The Function of Carotenoid Pigments in Photosynthesis and their Possible Involvement in the Evolution of Higher Plants. In *Carotenoids*, N.I. Krinsky, M.M. Mathews-Roth, and R.F. Taylor, eds (Boston, MA: Springer US), pp. 223–228.
- Moore JK, Doney SC, Glover DM, Fung IY.** (2002). Iron cycling and nutrient-limitation patterns in surface waters of the World Ocean. *Deep Sea Res. II* 49, 463–507
- Moseley J, Quinn J, Eriksson M, Merchant S.** (2000) The *Crd1* gene encodes a putative di-iron enzyme required for photosystem I accumulation in copper deficiency and hypoxia in *Chlamydomonas reinhardtii*. *EMBO J.* 19(10): 2139-51.
- Moseley JL, Allinger T, Herzog S, Hoerth P, Wehinger E, Merchant S, Hippler M.** (2012) Adaptation to Fe-deficiency requires remodeling of the photosynthetic apparatus. *EMBO J.* 21(24): 6709-20.
- Munekage Y, Hashimoto M, Miyake C, Tomizawa K, Endo T, Tasaka M, Shikanai T.** (2004) Cyclic electron flow around photosystem I is essential for photosynthesis. *Nature* 429 (6991): 579–582.
- Nagasaka S, Yoshimura E.** (2008) External iron regulates polyphosphate content in the acidophilic, thermophilic alga *Cyanidium caldarium*. *Biol Trace Elem Res.* 125(3): 286-9.
- Naumann B, Stauber EJ, Busch A, Sommer F, Hippler M.** (2005). N-terminal processing of Lhca3 Is a key step in remodeling of the photosystem I-light harvesting complex under iron deficiency in *Chlamydomonas reinhardtii*. *J Biol Chem.* 280(21): 20431-41.
- Naumann B, Busch A, Allmer J, Ostendorf E, Zeller M, Kirchhoff H, Hippler M.** (2007) Comparative quantitative proteomics to investigate the remodeling of

## 5. References

---

- bioenergetic pathways under iron deficiency in *Chlamydomonas reinhardtii*. *Proteomics*. 7(21): 3964-79.
- Nelson N, Ben-Shem A.** (2004) The complex architecture of oxygenic photosynthesis. *Nat Rev Mol Cell Biol* 5 (12): 971–982
- Nishimura Y.** (2010) Uniparental inheritance of cpDNA and the genetic control of sexual differentiation in *Chlamydomonas reinhardtii*. *J Plant Res*. 123(2): 149-62.
- Noack K, Jiebich H.** (1941) The iron-set of chloroplasts of spinach. *Naturwissenschaften*.29:302–302.
- Nouet C, Motte P, Hanikenne M.** (2011) Chloroplastic and mitochondrial metal homeostasis. *Trends Plant Sci*. 16(7): 395-404.
- Norton GJ, Dasgupta T, Islam MR, Islam S, Deacon CM, Zhao FJ, Stroud JL, McGrath SP, Feldmann J, Price AH, Meharg AA.** (2010) Arsenic influence on genetic variation in grain trace-element nutrient content in Bengal delta grown rice. *Environ Sci Technol*. 44(21): 8284-8.
- Ohad I, Siekevitz P, Palade GE.** (1967). Biogenesis of chloroplast membranes. I. Plastid dedifferentiation in a dark-grown algal mutant (*Chlamydomonas reinhardi*). *J. Cell Biol*. 35: 521–552.
- Olson SL, Reinhard CT, Lyons TW.** (2006) Cyanobacterial Diazotrophy and Earth's Delayed Oxygenation. *Front Microbiol*. 7: 1526.
- Page MD, Allen MD, Kropat J, Urzica EI, Karpowicz SJ, Hsieh SI, Loo JA, Merchant SS.** (2012) Fe sparing and Fe recycling contribute to increased superoxide dismutase capacity in iron-starved *Chlamydomonas reinhardtii*. *Plant Cell*. 24(6): 2649-65.
- Papageorgiou GC, Govindjee J.** (2004) Chlorophyll a fluorescence. Light-harvesting antennas in photosynthesis. Kluwer Academic Publishers, Dordrecht.43-63
- Parent SÉ, Parent LE, Rozane DE, Natale W.** (2103) Plant ionome diagnosis using sound balances: case study with mango (*Mangifera Indica*). *Front Plant Sci*. 4: 449.
- Paz Y, Shimoni E, Weiss M, Pick U.** (2007) Effects of iron deficiency on iron binding and internalization into acidic vacuoles in *Dunaliella salina*. *Plant Physiol*. 144(3): 1407-15.
- Pazour GJ, Sineshchekov OA, Witman GB.** (1995) Mutational analysis of the phototransduction pathway of *Chlamydomonas reinhardtii*. *J Cell Biol*. 131(2): 427-40.

## 5. References

---

- Peltier G, Cournac L.** (2002). Chlororespiration. Annual review of plant biology 53: 523-550.
- Philpott CC.** (2006) Iron uptake in fungi: a system for every source. Biochim Biophys Acta. 1763(7): 636-45.
- Philpott CC, Protchenko O.** (2008) Response to iron deprivation in *Saccharomyces cerevisiae*. Eukaryot Cell. 7(1): 20-7.
- Pilon M, Cohu CM, Ravet K, Abdel-Ghany SE, Gaymard F.** (2009) Essential transition metal homeostasis in plants. Curr Opin Plant Biol. 12(3): 347-57.
- Pinson SR, Tarpley L, Yan W, Yeater K, Lahner B, Yakubova E, Huang XY, Zhang M, Guerinot ML, Salt DE.** (2015) Worldwide genetic diversity for mineral element concentrations in rice grain. Crop Science. 55(1): 294-311.
- Planavsky NJ, Asael D, Hofmann A, Reinhard CT, Lalonde SV, Knudsen A, Wang X, Ossa Ossa F, Pecoits E, Smith AJB, Beukes NJ, Bekker A, Johnson TM, Konhauser KO, Lyons TW, Rouxel OJ.** (2014). Evidence for oxygenic photosynthesis half a billion years before the Great Oxidation Event. Nature Geosci 7 (4): 283–286.
- Popescu CE, Lee RW.** (2007) Mitochondrial genome sequence evolution in *Chlamydomonas*. Genetics. 175(2): 819-26.
- Porra RJ, Thompson WA, Kriedemann PE.** (1989) Determination of accurate extinction coefficients and simultaneous equations for assaying chlorophylls a and b extracted with four different solvents: verification of the concentration of chlorophyll standards by atomic absorption spectroscopy. Biochim Biophys Acta-Bioenergetics. 975(3): 384-94.
- Quarmby LM.** (1994) Signal transduction in the sexual life of *Chlamydomonas*. In Signals and Signal Transduction Pathways in Plants 1994 (pp. 35-51). Springer, Dordrecht.
- Radakovits R, Jinkerson RE, Darzins A, Posewitz MC.** (2010) Genetic engineering of algae for enhanced biofuel production. Eukaryotic cell. 9(4): 486-501.
- Radmer R, Kok B.** (1975) Energy capture in photosynthesis: photosystem II. Annual review of biochemistry. 44(1): 409-33.
- Renger G, Govindjee.** (1985) The mechanism of photosynthetic water oxidation. Photosynthesis research 6 (1): 33–55
- Reyes-Prieto A, Weber AP, Bhattacharya D.** (2007) The origin and establishment of the plastid in algae and plants. Annu. Rev. Genet. 41: 147-68.

## 5. References

---

- Rochaix JD.** (1995) *Chlamydomonas reinhardtii* as the photosynthetic yeast. *Annu Rev Genet.* 29: 209-30.
- Rockwell NC, Duanmu D, Martin SS, Bachy C, Price DC, Bhattacharya D, Worden AZ, Lagarias JC.** (2014) Eukaryotic algal phytochromes span the visible spectrum. *Proc Natl Acad Sci USA.* 111(10): 3871-6.
- Romanova ND, Sazhin AF.** (2010) Relationships between the cell volume and the carbon content of bacteria. *Oceanology.* 50(4): 522-30.
- Ruiz FA, Marchesini N, Seufferheld M, Govindjee, Docampo R.** (2001) The polyphosphate bodies of *Chlamydomonas reinhardtii* possess a proton-pumping pyrophosphatase and are similar to acidocalcisomes. *J Biol Chem.* 276(49): 46196-203.
- Rumeau D, Peltier G, Cournac L.** (2007) Chlororespiration and cyclic electron flow around PSI during photosynthesis and plant stress response. *Plant, cell & environment* 30 (9): 1041-1051.
- Sager R.** (1955) Inheritance in the Green Alga *Chlamydomonas Reinhardi*. *Genetics.* 40(4): 476-89.
- Salomé PA, Merchant SS.** (2019) A Series of Fortunate Events: Introducing *Chlamydomonas* as a Reference Organism. *Plant Cell.* 31(8): 1682-1707.
- Salt DE.** (2004) Update on plant ionomics. *Plant Physiol.* 136(1): 2451-6.
- Salt DE, Baxter I, Lahner B.** (2008) Ionomics and the study of the plant ionome. *Annu Rev Plant Biol.* 59: 709-33.
- Schopf JW.** (1993) Microfossils of the Early Archean Apex chert: new evidence of the antiquity of life. *Science.* 260: 640-6.
- Semin BK, Davletshina LN, Novakova AA, Kiseleva TY, Lanchinskaya VY, Aleksandrov AY, Seifulina N, Ivanov II, Seibert M, Rubin AB.** (2003) Accumulation of ferrous iron in *Chlamydomonas reinhardtii*. Influence of CO<sub>2</sub> and anaerobic induction of the reversible hydrogenase. *Plant Physiol.* 131(4): 1756-64.
- Shikanai T.** (2007) Cyclic electron transport around photosystem I: genetic approaches. *Annual review of plant biology* 58: 199-217.
- Siaut M, Cui n  S, Cagnon C, Fessler B, Nguyen M, Carrier P, Beyly A, Beisson F, Triantaphylid s C, Li-Beisson Y, Peltier G.** (2011) Oil accumulation in the model green alga *Chlamydomonas reinhardtii*: characterization, variability between

## 5. References

---

- common laboratory strains and relationship with starch reserves. *BMC Biotechnol.* 11: 7.
- Silflow CD, LaVoie M, Tam LW, Tousey S, Sanders M, Wu WC, Borodovsky M, Lefebvre PA.** (2001) The Vfl1 protein in *Chlamydomonas* localizes in a rotationally asymmetric pattern at the distal ends of the basal bodies. *The Journal of cell biology.* 153(1): 63-74.
- Silflow CD, Lefebvre PA.** (2001) Assembly and motility of eukaryotic cilia and flagella. Lessons from *Chlamydomonas reinhardtii*. *Plant physiology.* 127(4): 1500-7.
- Smith GM.** (1946) The nature of sexuality in *Chlamydomonas*. *Am J Bot.* 33(8): 625-30.
- Smith GM, Regnery DC.** (1950) Inheritance of sexuality in *Chlamydomonas reinhardtii*. *Proc Natl Acad Sci USA.* 36(4): 246-8.
- Snell WJ, Pan J, Wang Q.** (2004) Cilia and flagella revealed: from flagellar assembly in *Chlamydomonas* to human obesity disorders. *Cell.* 117(6): 693-7.
- Spreitzer RJ, Mets L.** (1981) Photosynthesis-deficient Mutants of *Chlamydomonas reinhardtii* with Associated Light-sensitive Phenotypes. *Plant Physiol.* 67(3): 565-9.
- Staiger D.** (2002) Chemical strategies for iron acquisition in plants. *Angew Chem Int Ed Engl.* 41(13): 2259-64.
- Stirbet A, Govindjee.** (2011) On the relation between the Kautsky effect (chlorophyll a fluorescence induction) and Photosystem II: basics and applications of the OJIP fluorescence transient. *J Photochem Photobiol B.* 104(1-2): 236-57.
- Stirbet A, Lazár D, Kromdijk J.** (2018) Chlorophyll a fluorescence induction: can just a one-second measurement be used to quantify abiotic stress responses? *Photosynthetica.* 56(1): 86-104.
- Sun L, Yu Y, Huang T, An P, Yu D, Yu Z, Li H, Sheng H, Cai L, Xue J, Jing M, Li Y, Lin X, Wang F.** (2012) Associations between Ionic Profile and Metabolic Abnormalities in Human Population. *PLoS One.* 7(6): e38845.
- Tardif M, Atteia A, Specht M, Cogne G, Rolland N, Brugière S, Hippler M, Ferro M, Bruley C, Peltier G, Vallon O, Cournac L.** (2012) PredAlgo: a new subcellular localization prediction tool dedicated to green algae. *Mol Biol Evol.* 29(12): 3625-39.
- Terauchi AM, Peers G, Kobayashi MC, Niyogi KK, Merchant SS.** (2010) Trophic status of *Chlamydomonas reinhardtii* influences the impact of iron deficiency on photosynthesis. *Photosynth Res.* 105(1): 39-49.

## 5. References

---

- Terzulli A, Kosman DJ.** (2009)
- Terzulli A, Kosman DJ.** (2010) Analysis of the high-affinity iron uptake system at the *Chlamydomonas reinhardtii* plasma membrane. *Eukaryot Cell.* 9(5): 815-26.
- Theil EC.** (2004) Iron, ferritin, and nutrition. *Annu Rev Nutr.* 24:327-43.
- Thimm O, Blaesing O, Gibon Y, Nagel A, Meyer S, Krüger P, Selbig J, Müller LA, Rhee SY, Stitt M.** (2004) MAPMAN: a user-driven tool to display genomics data sets onto diagrams of metabolic pathways and other biological processes. *Plant J.* 37(6): 914-39.
- Thomas R.** (2013) *Practical Guide to ICP-MS.* (Third edition, Boca Raton, Florida: CRC Press Taylor & Francis Group.)
- Totey S, Waldron KJ, Firbank SJ, Reale B, Bessant C, Sato K, Cheek TR, Gray J, Banfield MJ, Dennison C, Robinson NJ.** (2008) Protein-folding location can regulate manganese-binding versus copper- or zinc-binding. *Nature.* 455(7216):138-42.
- Trapnell C, Roberts A, Goff L, Pertea G, Kim D, Kelley DR, Pimentel H, Salzberg SL, Rinn JL, Pachter L.** (2012) Differential gene and transcript expression analysis of RNA-seq experiments with TopHat and Cufflinks. *Nat Protoc.* 7(3): 562-78.
- Trapnell C, Hendrickson DG, Sauvageau M, Goff L, Rinn JL, Pachter L.** (2013) Differential analysis of gene regulation at transcript resolution with RNA-seq. *Nat Biotechnol.* 31(1): 46-53.
- Tsednee M, Castruita M, Salomé PA, Sharma A, Lewis BE, Schmollinger SR, Strenkert D, Holbrook K, Otegui MS, Khatua K, Das S, Datta A, Chen S, Ramon C, Ralle M, Weber PK, Stemmler TL, Pett-Ridge J, Hoffman BM, Merchant SS.** (2019) Manganese co-localizes with calcium and phosphorus in *Chlamydomonas acidocalcisomes* and is mobilized in Mn-deficient conditions. *J Biol Chem.* pii: jbc.RA119.009130. [Epub ahead of print]
- Urzica EI, Casero D, Yamasaki H, Hsieh SI, Adler LN, Karpowicz SJ, Blaby-Haas CE, Clarke SG, Loo JA, Pellegrini M, Merchant SS.** (2012) Systems and trans-system level analysis identifies conserved iron deficiency responses in the plant lineage. *Plant Cell.* 24(10): 3921-48.
- Urzica EI, Vieler A, Hong-Hermesdorf A, Page MD, Casero D, Gallaher SD, Kropat J, Pellegrini M, Benning C, Merchant SS.** (2013) Remodeling of membrane lipids in iron-starved *Chlamydomonas*. *J Biol Chem.* 288(42): 30246-58



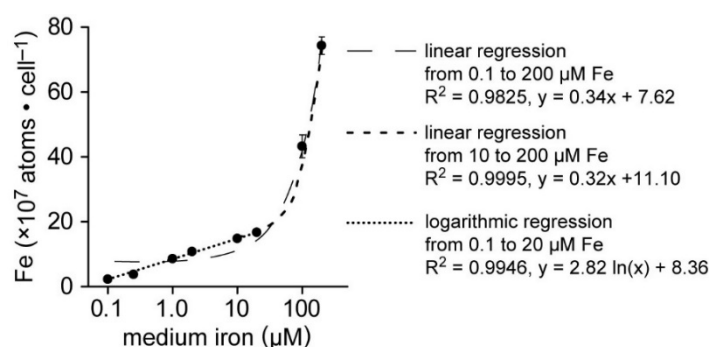
## 5. References

---

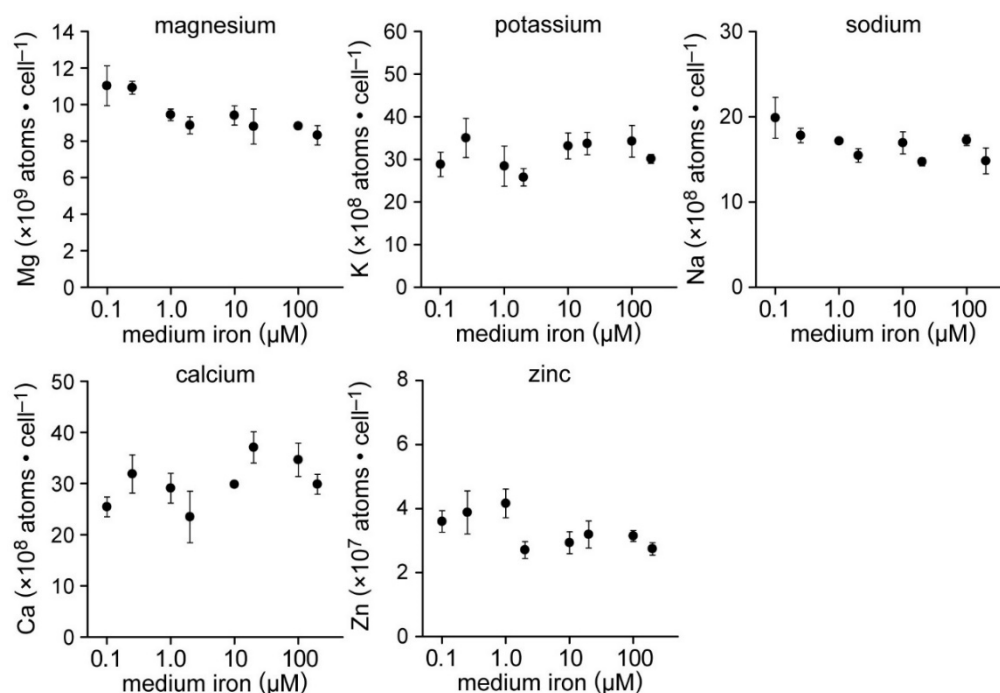
- Vasil'ev S, Bruce D.** (2004) Optimization and evolution of light harvesting in photosynthesis: the role of antenna chlorophyll conserved between photosystem II and photosystem I. *The Plant Cell*. 16(11): 3059-68.
- Waldron KJ, Rutherford JC, Ford D, Robinson NJ.** (2009) Metalloproteins and metal sensing. *Nature*. Aug 13;460(7257):823-30.
- Watanabe T, Broadley MR, Jansen S, White PJ, Takada J, Satake K, Takamatsu T, Tuah SJ, Osaki M.** (2007) Evolutionary control of leaf element composition in plants. *New Phytologist*. 174(3): 516-23.
- Wijffels RH, Barbosa MJ.** (2010) An outlook on microalgal biofuels. *Science*. 329(5993): 796-9.
- Williams RJP.** (2001) Chemical selection of elements by cells. *Coord Chem Rev* 216–217: 583–595.
- Wu D, Shen Q, Cai S, Chen ZH, Dai F, Zhang G.** (2103) Ionic responses and correlations between elements and metabolites under salt stress in wild and cultivated barley. *Plant and Cell Physiology*. 54(12): 1976-88.
- Xu W, Barrientos T, Andrews NC.** (2013) Iron and copper in mitochondrial diseases. *Cell Metab*. 17(3): 319-28.
- Ying H, Zhang Y.** (2019) Systems Biology of Selenium and Complex Disease. *Biol Trace Elem Res*. 192(1): 38-50.
- Yoshida S, Date Y, Akama M, Kikuchi J.** (2014) Comparative metabolomic and ionic approach for abundant fishes in estuarine environments of Japan. *Sci Rep*. 4: 7005.
- Yu D, Danku JM, Baxter I, Kim S, Vatamaniuk OK, Vitek O, Ouzzani M, Salt DE.** (2012) High-resolution genome-wide scan of genes, gene-networks and cellular systems impacting the yeast ionome. *BMC Genomics*. 13: 623.
- Yruela I.** (2013) Transition metals in plant photosynthesis. *Metallomics*. 5(9): 1090-109.
- Zhang M, Pinson SR, Tarpley L, Huang XY, Lahner B, Yakubova E, Baxter I, Guerinot ML, Salt DE.** (2014) Mapping and validation of quantitative trait loci associated with concentrations of 16 elements in unmilled rice grain. *Theor Appl Genet*. 127(1): 137-65.
- Zimorski V, Ku C, Martin WF, Gould SB.** (2014) Endosymbiotic theory for organelle origins. *Curr Opin Microbiol*. 22: 38-48.

## 6 Appendix

## 6.1 Supplemental Figures

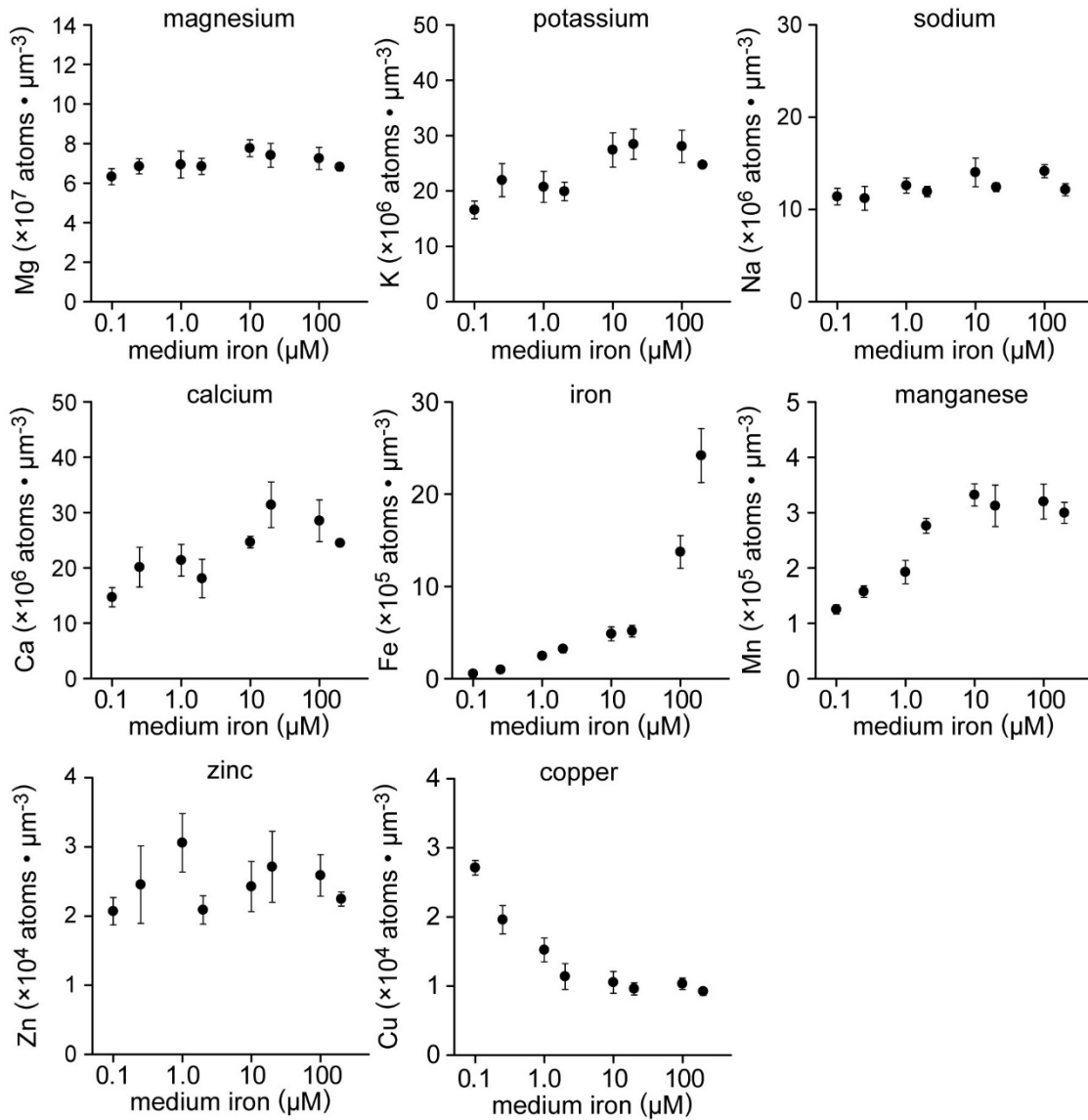


**Supplemental Figure 1. Regression analysis of intracellular and extracellular iron content.** Iron content per cell was used for regression analysis to estimate the relationship between extracellular and intracellular iron content. Linear, exponential and logarithmic regression analysis were applied to the entire range as well as two overlapping subgroups of extracellular iron concentrations and the resulting coefficients of determination ( $R^2$ ) were compared for each analysis. The regression with the highest coefficient was chosen for each group.



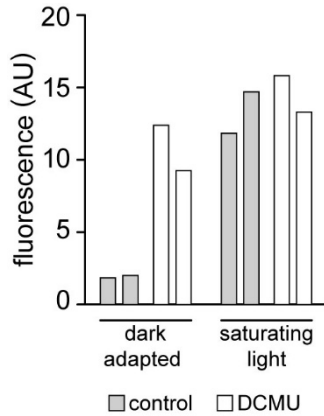
**Supplemental Figure 2. Iron-dependent elemental composition.** Photoheterotrophic cultures containing 0.10, 0.25, 1.0, 2.0, 10, 20, 100 and 200  $\mu\text{M}$  Fe, from precultures containing 1.0, 1.0, 1.0, 2.0, 10, 20, 100, and 200  $\mu\text{M}$  Fe, respectively, and grown to a density of  $2\text{--}3 \times 10^6$  cells  $\cdot\text{ml}^{-1}$  for further analysis by ICP-MS/MS from whole cell lysates. Cellular quota of the indicated elements was related to the number of cells analyzed. The mean of four replicates is shown for each extracellular iron concentration (0.1 to 200  $\mu\text{M}$  Fe), error bars represent SD.

## 6. Appendix

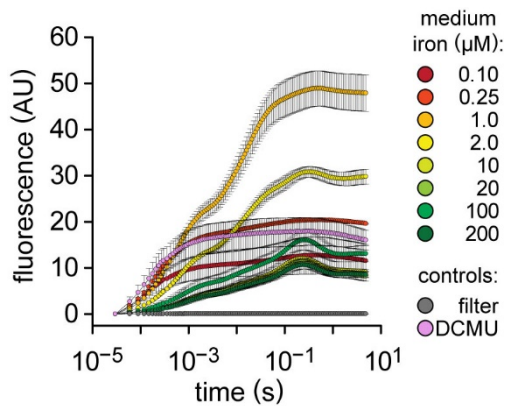


**Supplemental Figure 3. Volume-normalized elemental composition.** Photoheterotrophic cultures containing 0.10, 0.25, 1.0, 2.0, 10, 20, 100 and 200  $\mu\text{M}$  Fe, from precultures containing 1.0, 1.0, 1.0, 2.0, 10, 20, 100, and 200  $\mu\text{M}$  Fe, respectively, and grown to a density of  $2\text{-}3 \times 10^6$  cells  $\cdot \text{ml}^{-1}$  for elemental analysis ICP-MS/MS. Cellular content of the indicated elements were related to the average cell volume calculated from the median cell diameter of each culture. The mean of four replicates is shown for each extracellular iron concentration (0.1 to 200  $\mu\text{M}$  Fe), error bars represent SD.

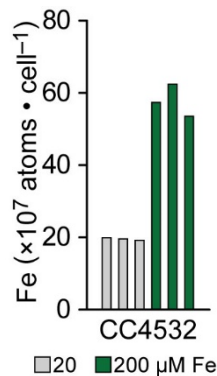
## 6. Appendix



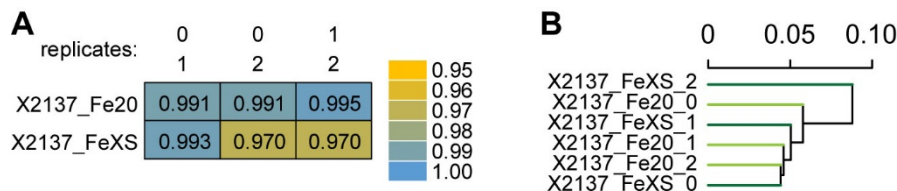
**Supplemental Figure 4. Experimental controls for maximum quantum efficiency of PSII ( $F_v/F_m$ ).** Two independent standard replete cultures were inoculated from replete precultures and grown to a density of  $2-3 \times 10^6$  cells $\cdot$ ml $^{-1}$ . Cells from two independent standard replete cultures of CC-4532 were treated with 20  $\mu$ M DCMU. Treated and untreated cells were immobilized onto 15 mm round filters and the fluorescence was measured after dark-adaptation for 12-15 min and after applying saturating light.



**Supplemental Figure 5. Raw fluorescence transients.** Photoheterotrophic cultures containing 0.1, 0.25, 0.5, 1.0, 2.0, 10, 20, 100 and 200  $\mu$ M Fe were inoculated from precultures containing 1.0, 1.0, 1.0, 1.0, 2.0, 10, 20, 100, and 200  $\mu$ M extracellular iron, respectively, and grown to a density of  $2-3 \times 10^6$  cells $\cdot$ ml $^{-1}$  for analysis. Fluorescence intensity normalized for  $F_0$  is expressed in arbitrary fluorescence units (AU), including cell-free filter and standard replete cells treated with 20  $\mu$ M DCMU. The mean of three replicates is shown, error bars represent SD.

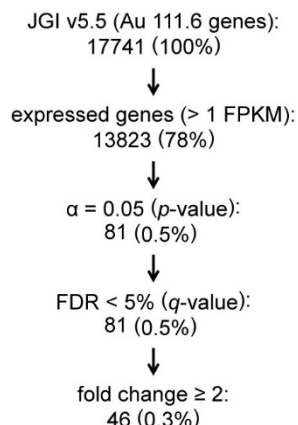


**Supplemental Figure 6. Cellular iron content.** Cells from cultures used for the RNAseq experiment were sampled for elemental analysis by ICP-MS/MS. Cellular iron content was related to the number of cells analyzed. The three independent samples “\_0”, “\_1” and “\_2” are shown from left to right for each condition.

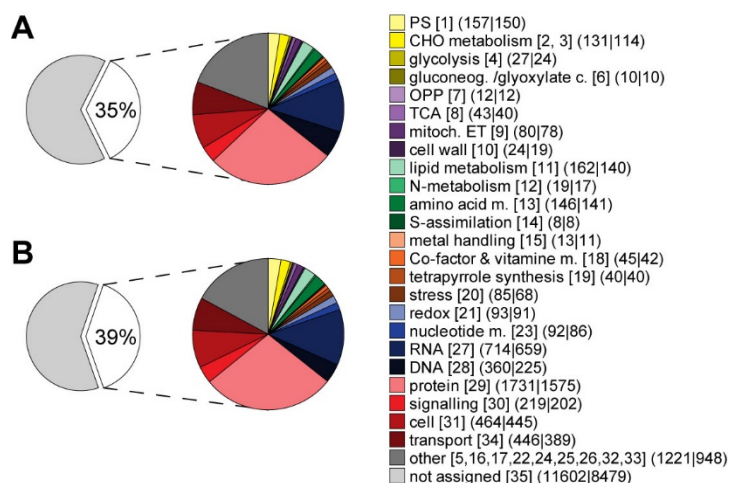


**Supplemental Figure 7. Replicate transcript expression estimates.** **A:** The Spearman's rank correlation coefficient ( $\rho$ ) was calculated between the independent biological replicates for each of the conditions. **B:** The distance relationship between all six samples based on the transcript abundance of all 17 741 gene models.

## 6. Appendix

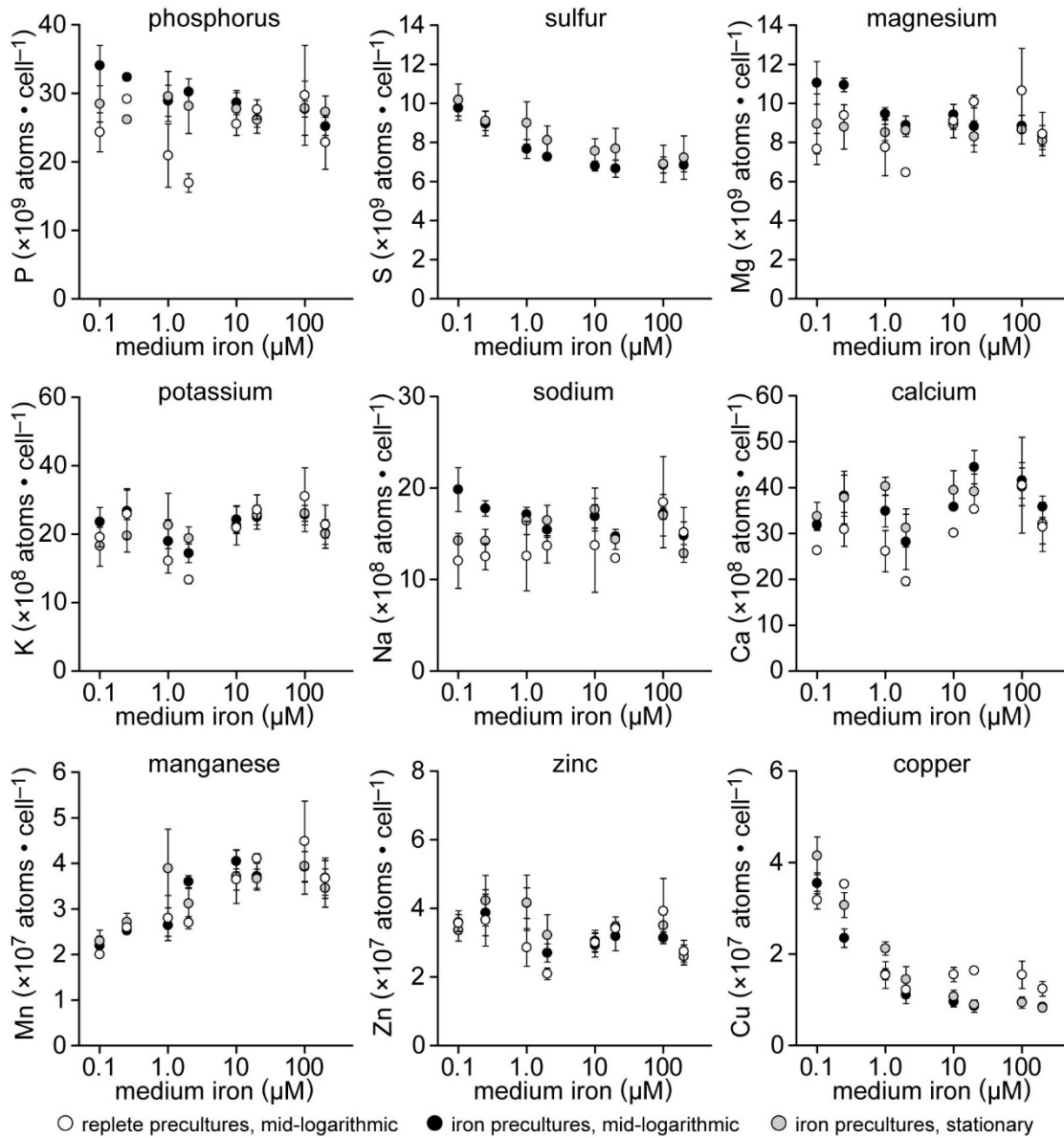


**Supplemental Figure 8. Differentially expressed genes.** The individual steps taken for the determination of differentially expressed genes (DEG).



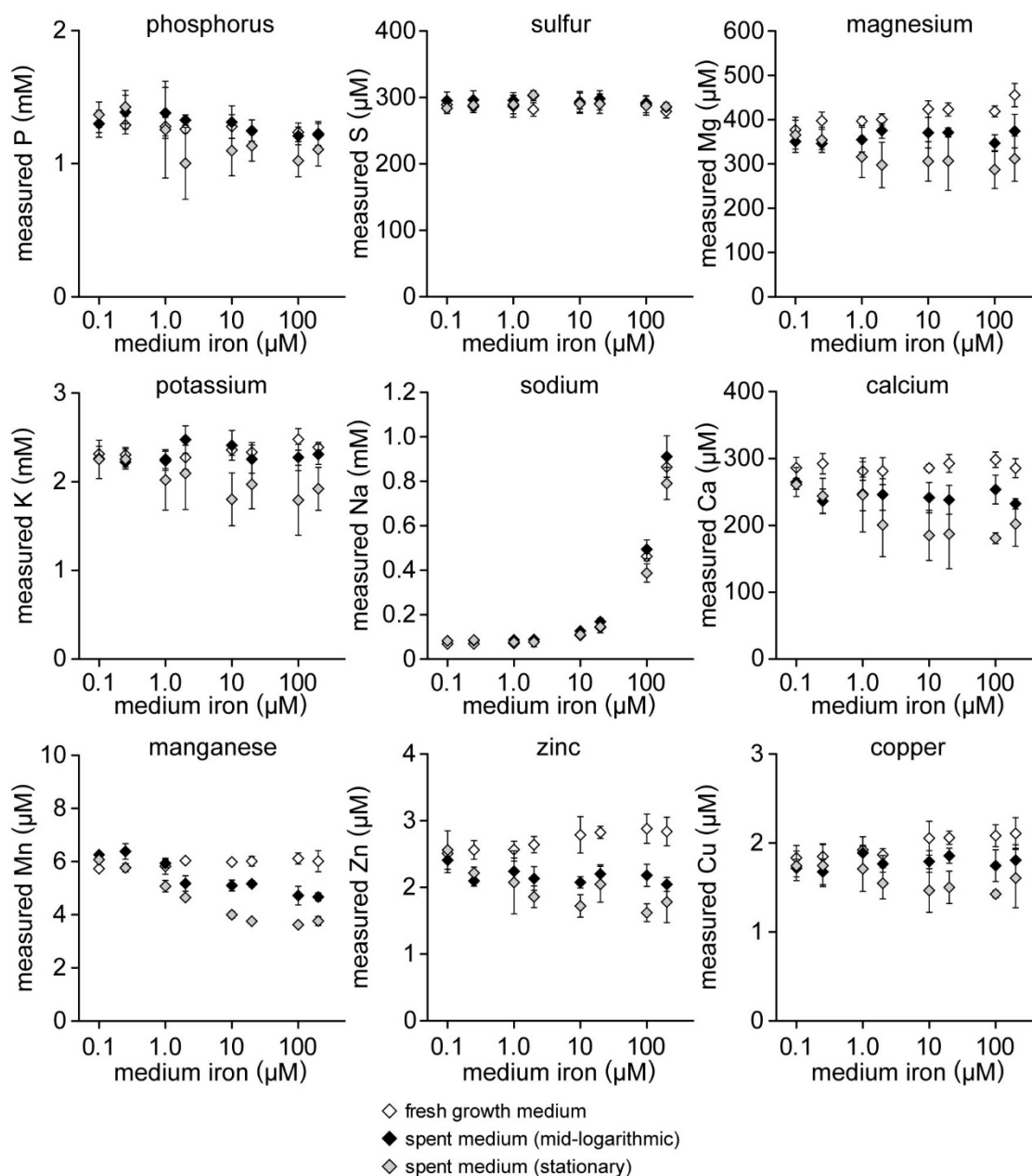
**Supplemental Figure 9. Functional annotation of the entire and the expressed genome.** **A:** Of the 17 741 genes, 6342 have annotations according to MapMan (white wedge), genes were grouped according to the functional annotation of their predicted protein sequence (colored wedges, right). Category numbers of the first bin and number of genes in each group are listed in brackets in the format of [bin number] (number of genes). **B:** Of the 17 741 genes, 13 823 genes are expressed in this experiment (>1 FPKM in at least one sample) and 5534 of the expressed genes have MapMan annotations.

## 6. Appendix



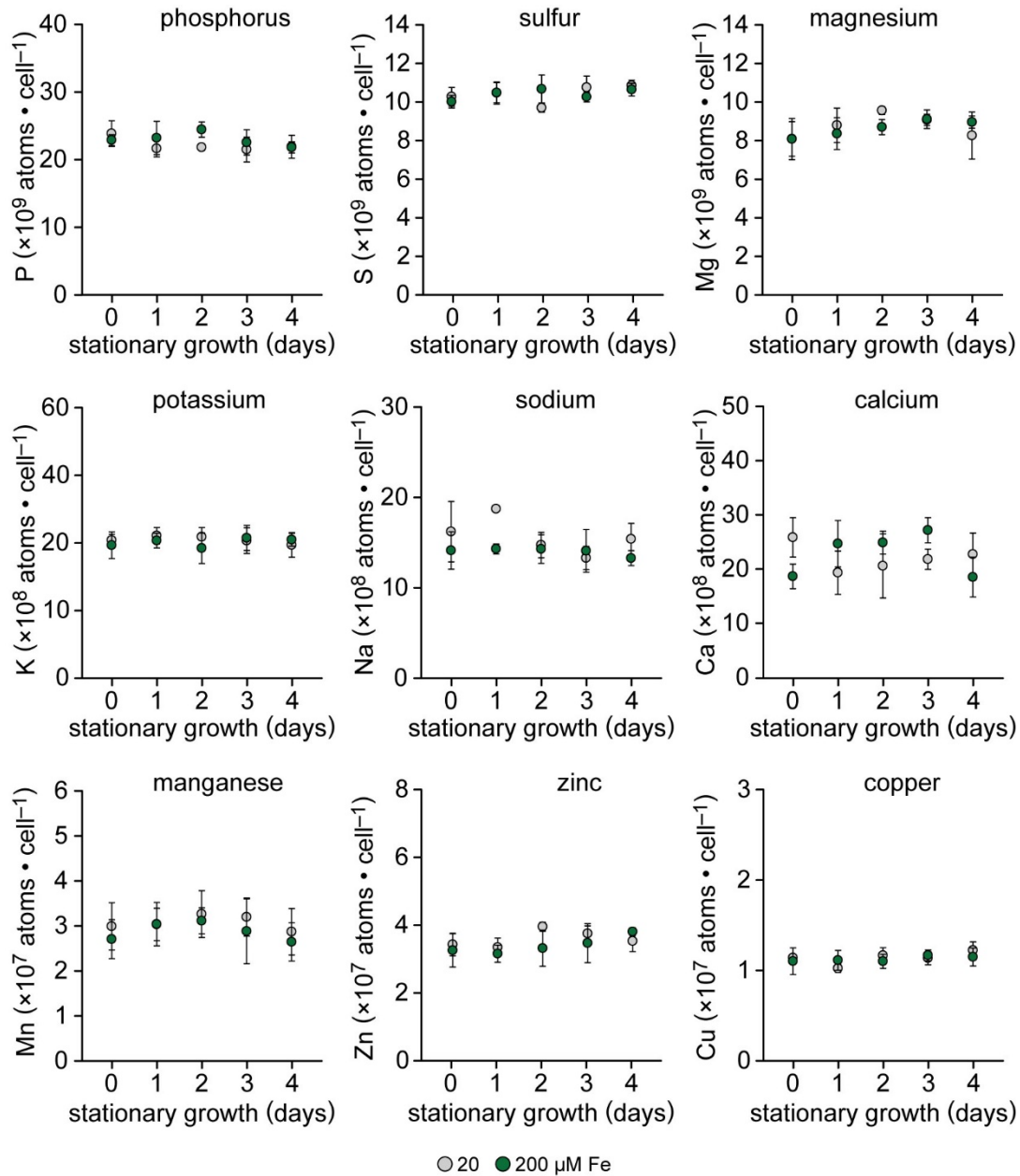
**Supplemental Figure 10. Iron-dependent elemental composition.** In one experimental setup, photoheterotrophic cultures containing 0.1, 0.25, 0.5, 1.0, 2.0, 10, 20, 100 and 200 μM Fe were inoculated from standard replete cultures and grown to a density of  $2-3 \times 10^6$  cells · ml<sup>-1</sup> (white circles). In a second experimental setup, photoheterotrophic cultures containing 0.1, 0.25, 0.5, 1.0, 2.0, 10, 20, 100 and 200 μM Fe were inoculated from precultures containing 1.0, 1.0, 1.0, 1.0, 2.0, 10, 20, 100, and 200 μM extracellular iron, respectively, and grown to a density of  $2-3 \times 10^6$  cells · ml<sup>-1</sup> for mid-logarithmic (black circles) and  $10 \times 10^6$  cells · ml<sup>-1</sup> for stationary sampling (grey circles). The elemental composition was analyzed by ICP-MS/MS from whole cell lysates and related to the number of cells analyzed. The mean of three (replete precultures, white circles) or four (iron precultures, black and grey circles) replicates is shown, error bars represent SD.

## 6. Appendix



**Supplemental Figure 11. Iron-dependent extracellular elemental concentrations.** Photoheterotrophic cultures containing 0.1, 0.25, 0.5, 1.0, 2.0, 10, 20, 100 and 200  $\mu\text{M}$  Fe were inoculated from precultures containing 1.0, 1.0, 1.0, 1.0, 2.0, 10, 20, 100, and 200  $\mu\text{M}$  extracellular iron, respectively. Elemental concentrations of freshly prepared growth medium (white diamonds), cell-free spent medium at  $2\text{-}3 \times 10^6$  cells·ml<sup>-1</sup> for mid-logarithmic (black diamonds) and at  $10 \times 10^6$  cells·ml<sup>-1</sup> for stationary growth phase (grey diamonds) were determined by ICP-MS/MS and expressed as millimolar concentration. The mean of four replicates is shown, error bars represent SD.

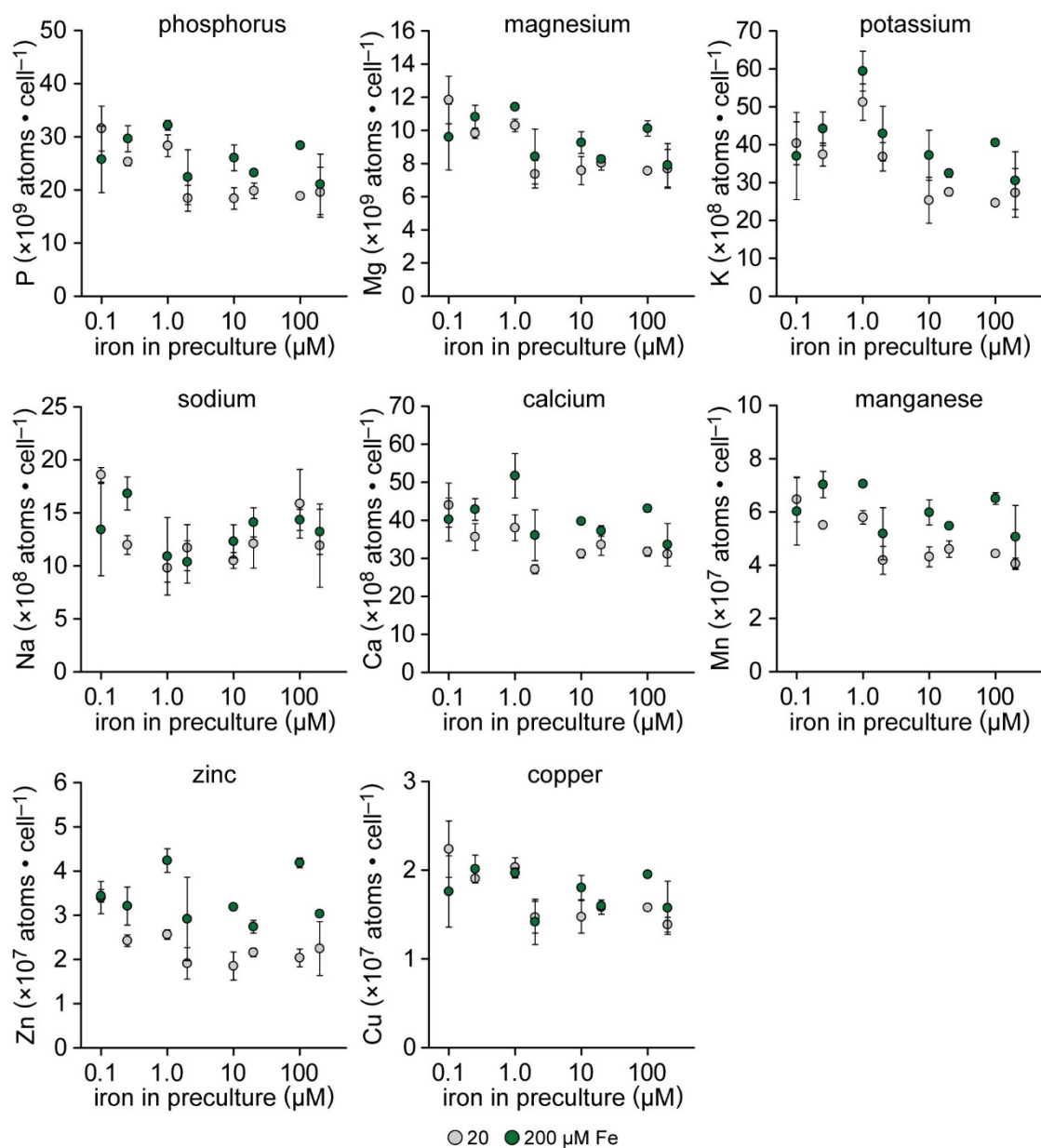
## 6. Appendix



**Supplemental Figure 12. Iron-replete and -excess elemental composition.** Photoheterotrophic cultures containing 20 and 200  $\mu\text{M}$  Fe were inoculated from standard replete cultures and the elemental composition was analyzed once the cultures reached  $10 \times 10^6 \text{ cells} \cdot \text{ml}^{-1}$  (0 days) and every 24h following (1 to 4 days) by ICP-MS/MS from whole cell lysates. The mean of three replicates is shown, error bars represent SD.

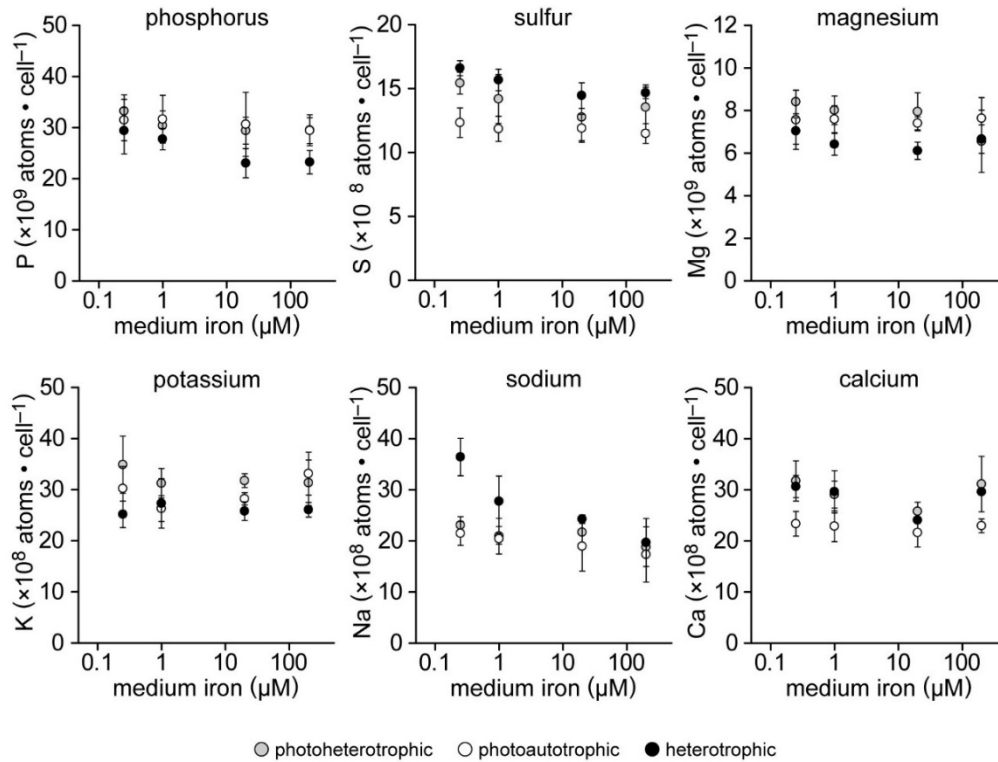


## 6. Appendix

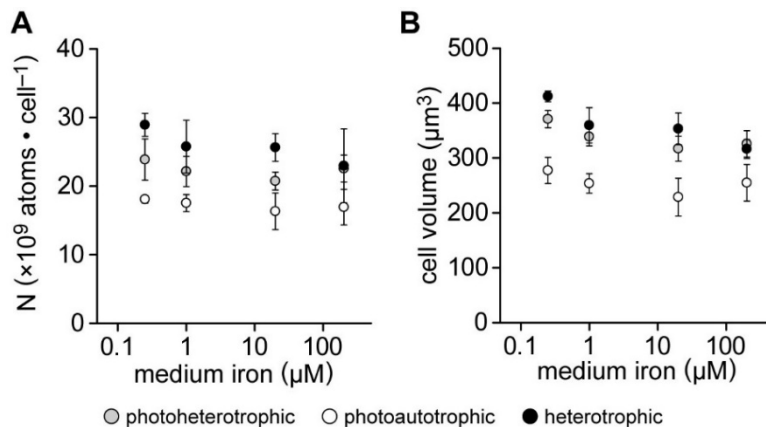


**Supplemental Figure 13. Fe-replete and -excess elemental composition.** Photoheterotrophic cultures containing 0.1, 0.25, 0.5, 1.0, 2.0, 10, 20, 100 and 200  $\mu$ M Fe were grown from inoculation to a density of  $2-3 \times 10^6$  (0.10 and 0.25  $\mu$ M) or  $\sim 8 \times 10^6$  cells  $\cdot$  ml $^{-1}$  (all other) and used to start cultures containing 20 and 200  $\mu$ M Fe. Fractions of the cultures were collected at a density of  $2-3 \times 10^6$  cells  $\cdot$  ml $^{-1}$  for analysis by ICP-MS/MS from whole cell lysates. The mean of three replicates is shown, error bars represent SD.

## 6. Appendix

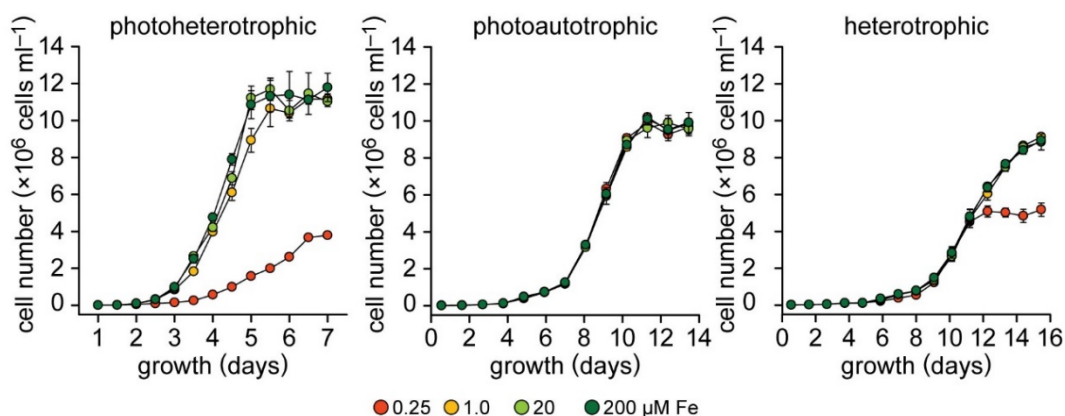


**Supplemental Figure 14. Iron- and trophic-dependent elemental composition.** Cells from a replete culture were grown in the presence of acetate and light (photoheterotrophic, grey circles), air and light (photoautotrophic, white circles), or acetate (heterotrophic, black circles) for a full growth curve before starting replicate iron precultures. For each of the three trophic conditions, cultures containing 0.25, 1.0, 20 and 200  $\mu$ M Fe were inoculated from precultures containing 1.0, 1.0, 20 and 200  $\mu$ M extracellular iron, respectively and grown to a density of  $2\text{--}3 \times 10^6$  cells  $\cdot$  ml $^{-1}$  for analysis by ICP-MS/MS from whole cell lysates. Intracellular content of the indicated elements was related to the number of cells analyzed. The mean of three replicates is shown, error bars represent SD.

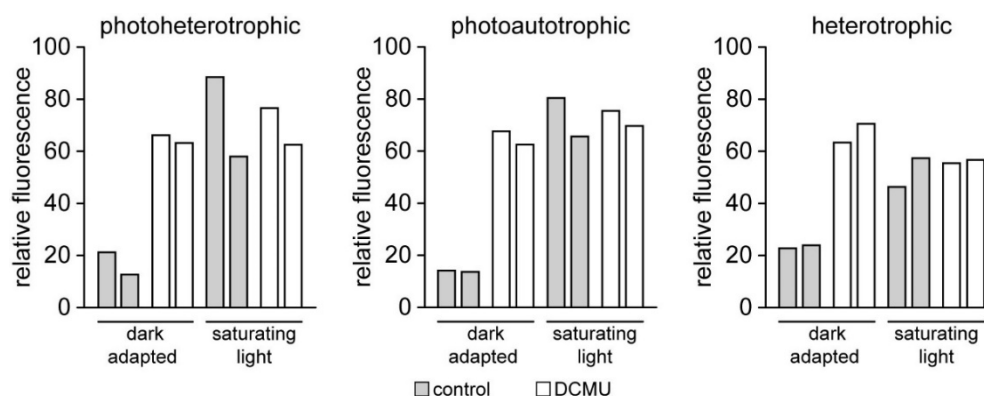


**Supplemental Figure 15. Nitrogen content and average cell volume.** Cultures containing 0.25, 1.0, 20 and 200  $\mu$ M Fe were inoculated from precultures containing 1.0, 1.0, 20 and 200  $\mu$ M extracellular iron, respectively, and were grown in the presence of acetate and light (photoheterotrophic), air and light (photoautotrophic), or acetate (heterotrophic) to a density of  $2\text{--}3 \times 10^6$  cells  $\cdot$  ml $^{-1}$  for analysis. **A:** Cellular nitrogen content was analyzed by TOC-TN and related to the number of cells analyzed. **B:** Average cell volume was calculated from the median cell diameter of each culture. The mean of three replicates is shown, error bars represent SD.

## 6. Appendix

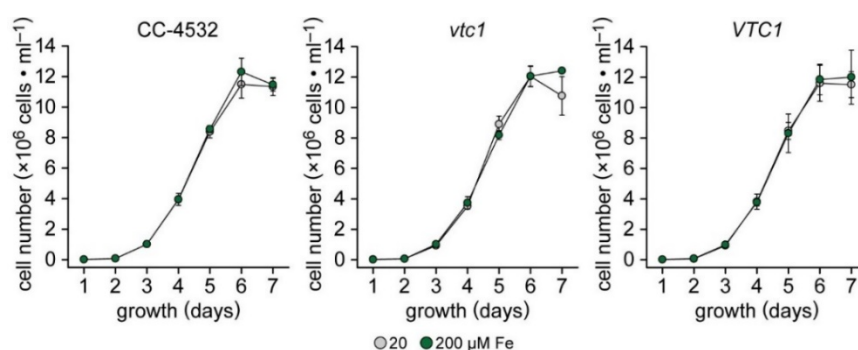


**Supplemental Figure 16. Growth curves of Fe-limited, -deficient, -replete and -excess cultures in photohetero-, photoauto- and heterotrophic conditions.** Cells from a replete culture were grown in the presence of acetate and light (photoheterotrophic), air and light (photoautotrophic), or acetate (heterotrophic) for at least one full growth curve before inoculating iron precultures. For each of the three trophic conditions, cultures containing 0.25 (orange), 1.0 (yellow), 20 (light green) and 200  $\mu\text{M}$  Fe (dark green) were inoculated from precultures containing 1.0, 1.0, 20 and 200  $\mu\text{M}$  extracellular iron, respectively. Growth was monitored from inoculation to stationary phase and the cell number was determined every 24h by manual counting (Hemocytometer). The mean of three biological replicates is shown, error bars represent SD.

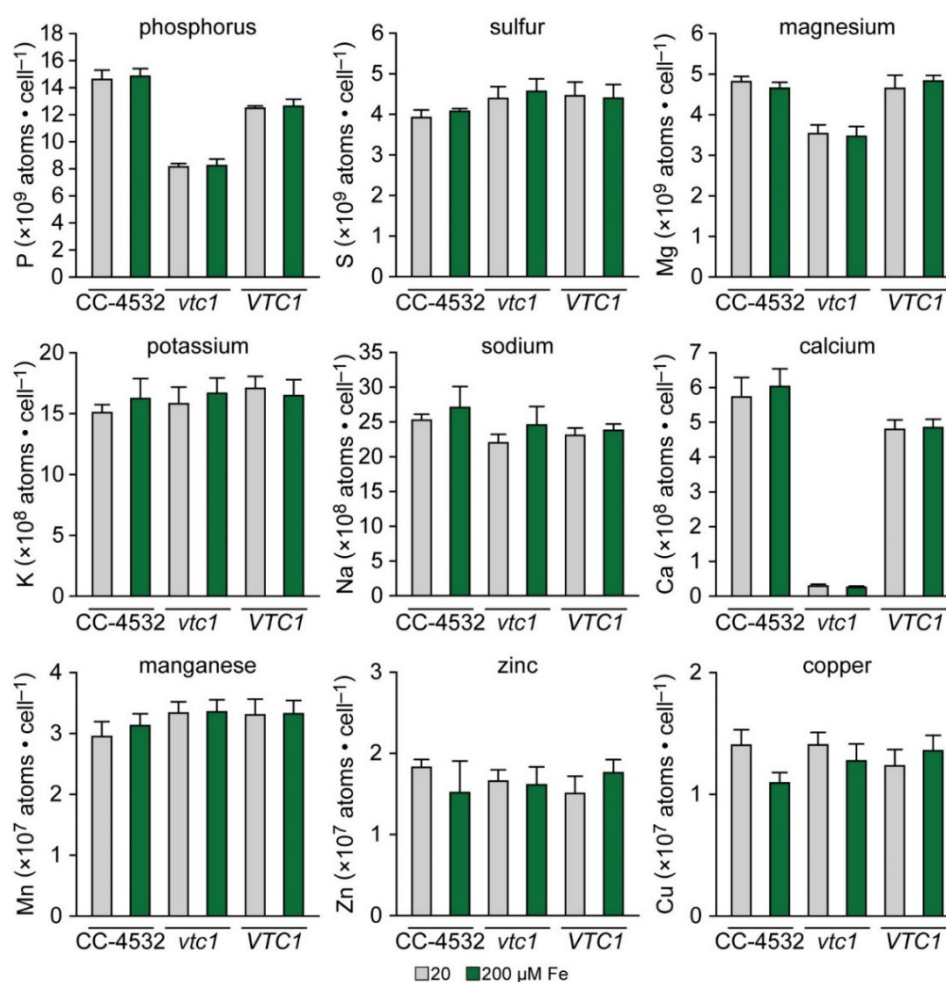


**Supplemental Figure 17. Experimental controls for the measurement of maximum quantum efficiency of PSII ( $F_v/F_m$ ).** Two independent photoheterotrophic, photoautotrophic and heterotrophic cultures were grown to a density of  $2\text{--}3 \times 10^6$  cells  $\cdot$  ml $^{-1}$  and about  $2 \times 10^6$  cells were treated with 20  $\mu\text{M}$  DCMU. Treated and untreated cells were immobilized onto 15 mm round filters and the fluorescence was measured after dark-adaptation for 10-12 Min and after applying saturating light.

## 6. Appendix

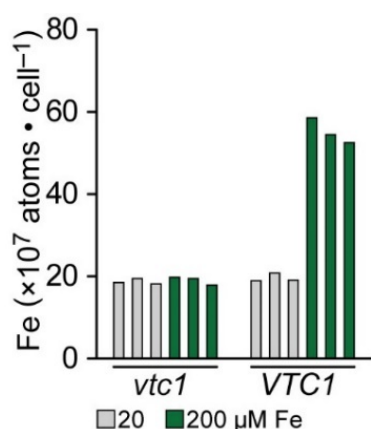


**Supplemental Figure 18. Iron-replete and -excess growth of CC-4532, *vtc1*, and *VTC1*.** Photoheterotrophic cultures containing 20 and 200  $\mu\text{M}$  Fe were inoculated with CC-4532, *vtc1* or *VTC1* from precultures containing 20 and 200  $\mu\text{M}$  Fe, respectively, to an initial cell density of  $1\text{-}2 \times 10^4 \text{ cells} \cdot \text{ml}^{-1}$ . Growth was monitored from inoculation to stationary phase and the cell number was determined every 24h by manual counting (Hemocytometer). The mean of three replicates is shown, error bars represent SD.

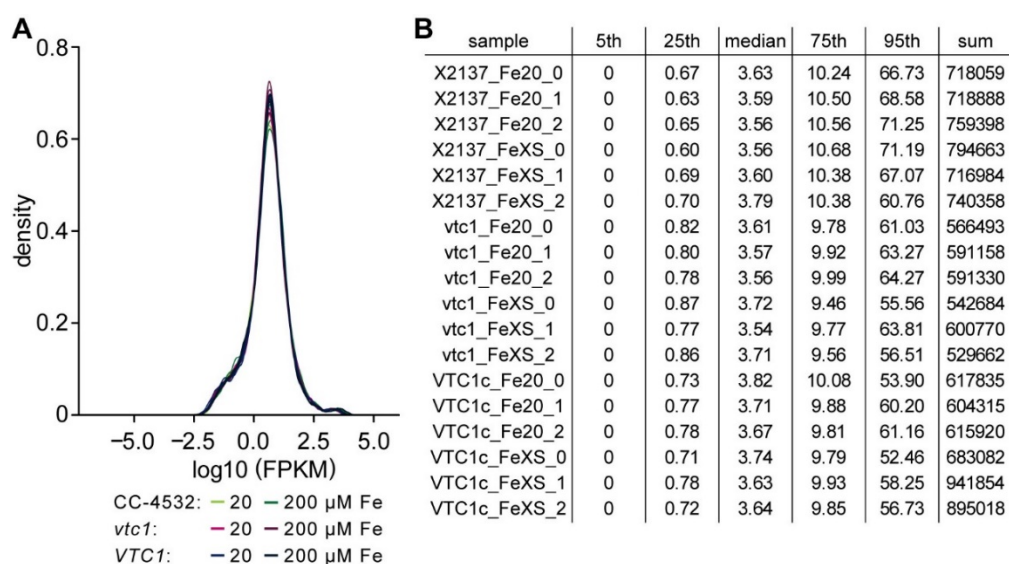


**Supplemental Figure 19. Intracellular metal content in Fe-replete and -excess growth conditions.** Photoheterotrophic cultures containing 20 and 200  $\mu\text{M}$  Fe were inoculated with CC-4532, *vtc1* or *VTC1* from precultures containing 20 and 200  $\mu\text{M}$  Fe, respectively, to an initial cell density of  $1\text{-}2 \times 10^4 \text{ cells} \cdot \text{ml}^{-1}$  and grown to a density of  $2\text{-}3 \times 10^6 \text{ cells} \cdot \text{ml}^{-1}$  for analysis by ICP-MS/MS of whole cell lysates and related to the number of cells analyzed. The mean of four replicates is shown, error bars represent SD.

## 6. Appendix

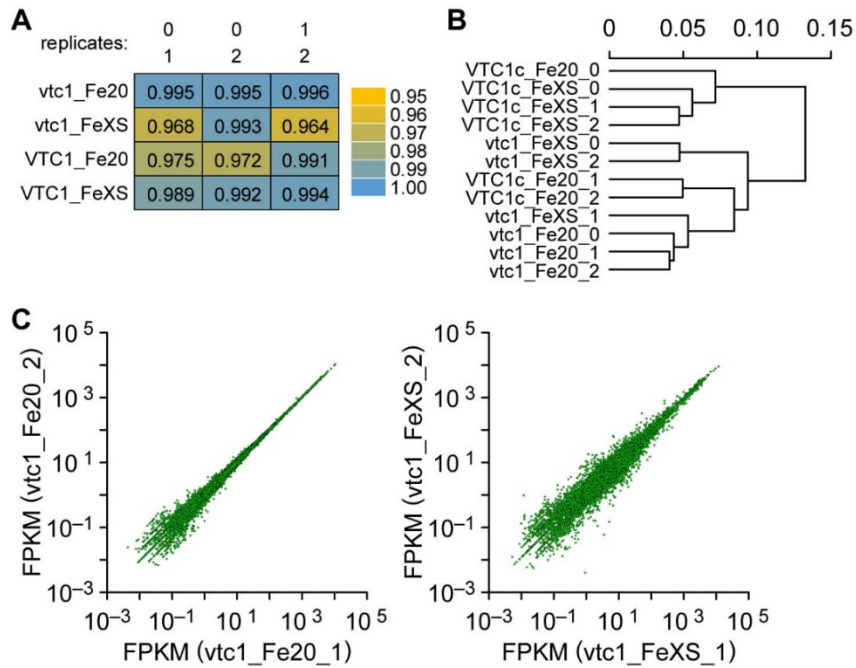


**Supplemental Figure 20. Cellular iron content.** Cells from cultures used for the RNAseq experiment were sampled for elemental analysis by ICP-MS/MS. Cellular iron content was related to the number of cells analyzed. The three independent samples “\_0”, “\_1” and “\_2” are shown from left to right for each condition and strain.

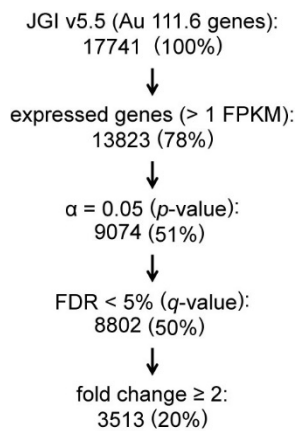


**Supplemental Figure 21. Gene expression level distribution of all 17 741 gene models of the individual replicates in all conditions.** **A:** For an across-sample comparison of expression level distribution, the expression values (FPKM) for each transcript of the replicates under each condition were transformed by decimal logarithm and plotted by density of occurrence. 18 line graphs are shown in the figure, the replicates are shown in the same color, different strains and iron-nutrition states are colored according to the key points below the graph. **B:** The table summarizes untransformed FPKM values of the 5<sup>th</sup>, 25<sup>th</sup>, 50<sup>th</sup> (median), 75<sup>th</sup>, 95<sup>th</sup> percentile, and the sum from all genes. The values are consistent among all replicates and conditions.

## 6. Appendix

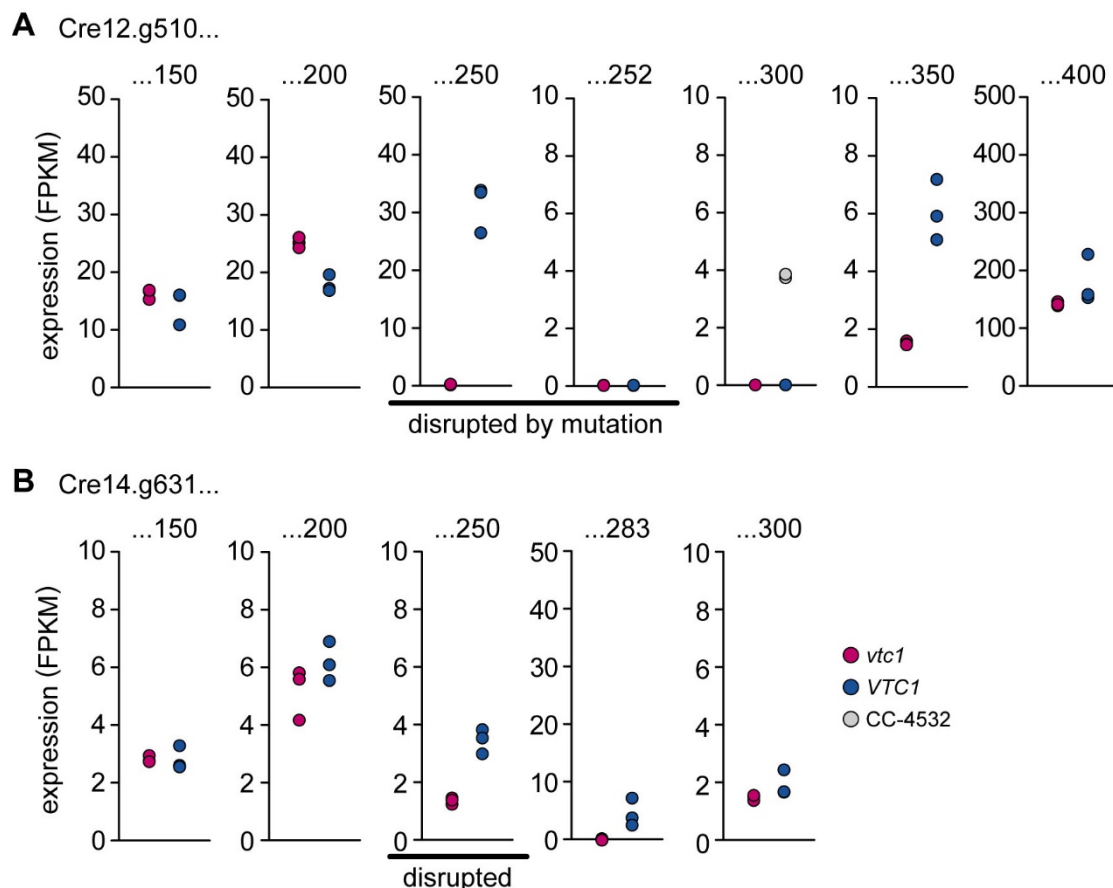


**Supplemental Figure 22. Replicate transcript expression.** **A:** The Spearman's rank correlation coefficient ( $\rho$ ) between the independent biological replicates of each conditions. **B:** The distance relationship between all twelve samples based on the transcript abundance of all 17741 gene models. **C:** Two exemplary scatter plots of vtc1 20  $\mu$ M Fe-EDTA, replicate \_1 versus \_2 and vtc1 200  $\mu$ M Fe-EDTA replicate \_1 versus \_2.

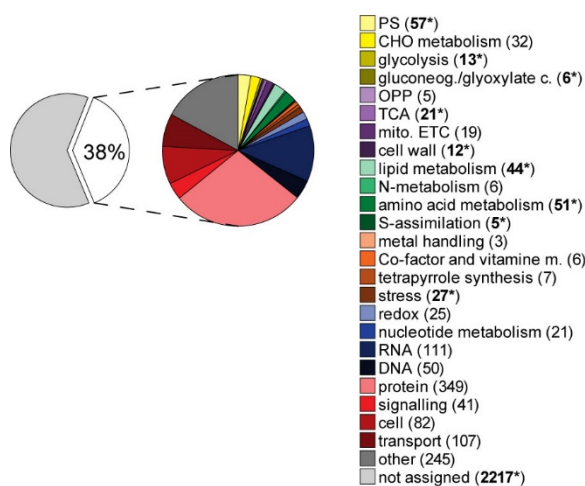


**Supplemental Figure 23. Differentially expressed genes (DEG).** The individual steps for the determination of differentially expressed genes.

## 6. Appendix

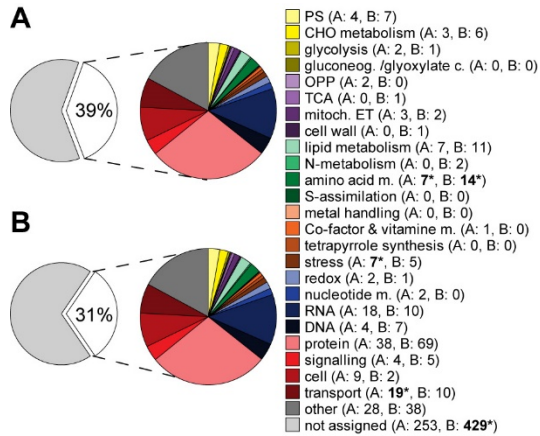


**Supplemental Figure 24. Expression of genes around the insertion sites in the strains *vtc1* and *VTC1*.** **A:** Expression estimates of neighboring genes around the insertion side of the *vtc1* mutant in genes Cre12.g510250 (*VTC1*) and Cre12.g510252 (no annotation). The disruption of the genes was verified by whole genome sequencing. The expression estimate for gene Cre12.g510300 in strain CC-4532 was added as a comparison. **B:** Expression of neighboring genes around the insertion side of the *VTC1* complementation site in gene Cre14.g531250. Disruption of the gene was verified by whole genome sequencing.



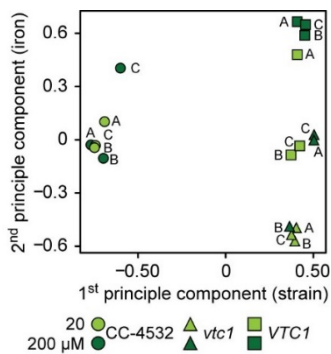
**Supplemental Figure 25. Functional annotation of DE genes.** Of the 3513 DE genes, 1345 have annotations according to MapMan, genes were grouped according to the functional annotation of their predicted protein sequence. The number of genes in each group are listed in brackets, groups that are significantly enriched ( $p$ -value  $> 0.05$ ) compared to randomly assigned genes are labeled with \* and marked in bold.

## 6. Appendix



### Supplemental Figure 26. Functional annotation of DE genes in the *vtc1* mutant.

Of the 1025 DE genes between *vtc1* and *VTC1*, 413 are induced in the mutant and 621 are repressed. **A:** Induced, and **B:** repressed genes were grouped according to the MapMan functional annotation of their predicted protein sequence. The number of genes in each group are listed in brackets for both A and B, groups that are significantly enriched (p-value > 0.05) compared to randomly assigned genes are labeled with \* and marked in bold.

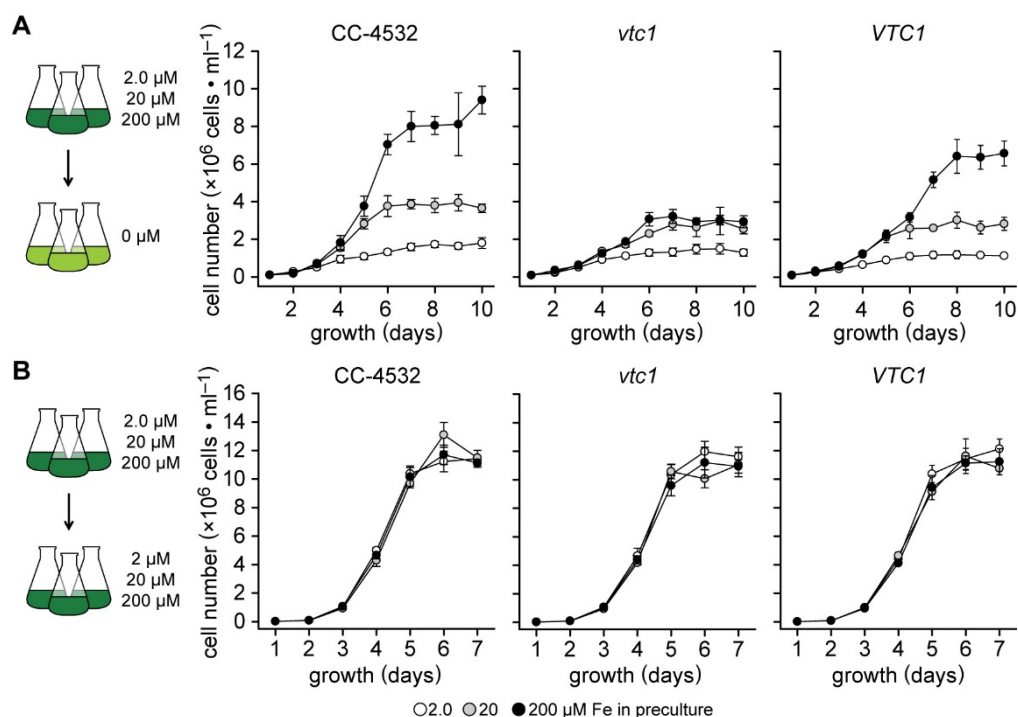


### Supplemental Figure 27. Principal component analysis of individual replicates.

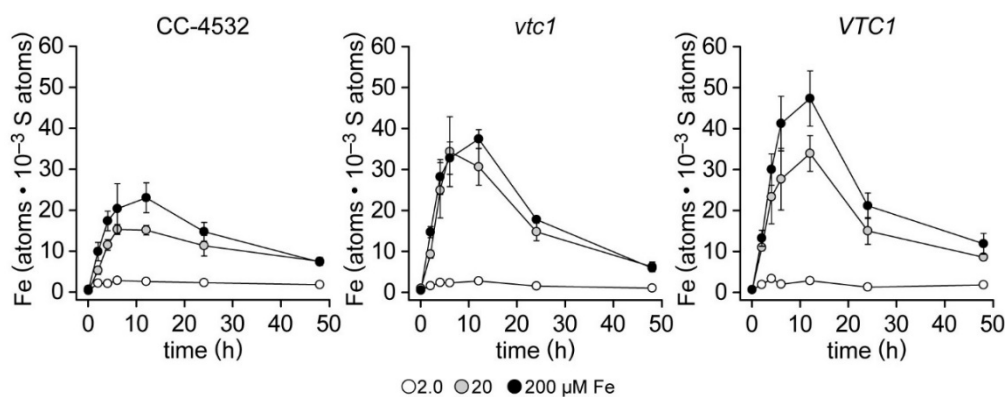
A principal component analysis was generated from the individual replicate samples (18), marked with A, B, and C. The first principal component refers to the variation due to the different strain backgrounds, The second is the extracellular iron concentration.



## 6. Appendix

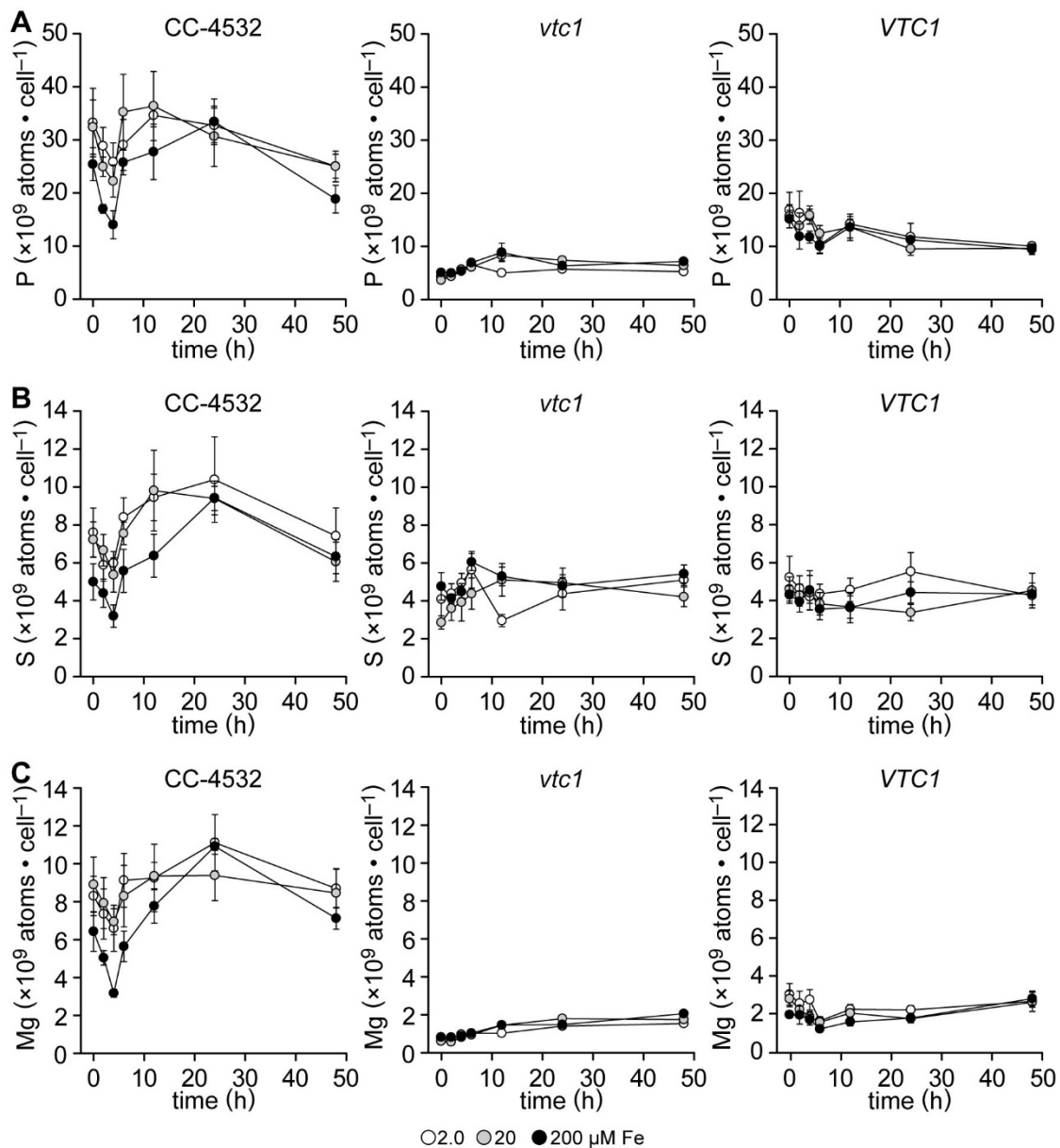


**Supplemental Figure 28. Growth curves after the transition to Fe-free growth medium.** Photoheterotrophic cultures containing 2, 20 and 200  $\mu\text{M}$  Fe were inoculated with CC-4532, *vtc1* (CC-5321) and *VTC1* (CC-5324) from precultures containing 2, 20 and 200  $\mu\text{M}$  Fe, respectively, to an initial cell density of  $1\text{--}2 \times 10^4$  cells $\cdot$ ml $^{-1}$  and grown to a density of  $2\text{--}3 \times 10^6$  cells $\cdot$ ml $^{-1}$ . Cells were washed once with 1 mM Na-EDTA and once with purified water and transferred to fresh photoheterotrophic growth medium **A**: without added iron and **B**: containing 2.0, 20 and 200  $\mu\text{M}$  Fe, respectively, to an initial cell density of  $1 \times 10^6$  cells $\cdot$ ml $^{-1}$ . Growth was monitored from inoculation to stationary phase, the cell number was determined every 24h by manual counting (Hemocytometer). The mean of four replicates is shown for each condition, error bars represent SD.



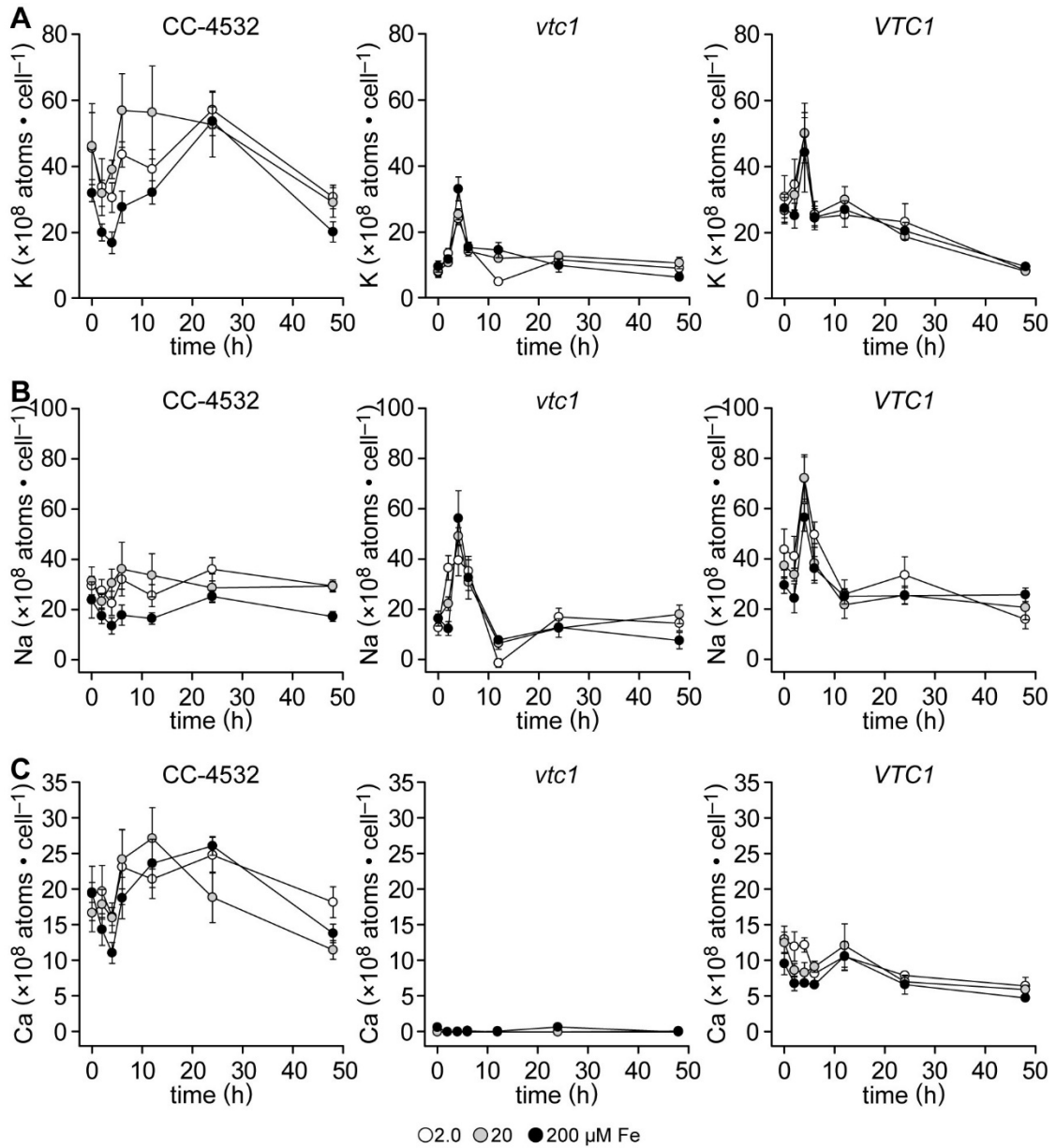
**Supplemental Figure 29. Iron content after re-supply of Fe, normalized to intracellular sulfur content.** Photoheterotrophic cultures containing no added iron were inoculated with CC-4532, *vtc1* (CC-5321) and *VTC1* (CC-5324) from precultures containing 1  $\mu\text{M}$  Fe, to an initial cell density of  $1 \times 10^4$  cells $\cdot$ ml $^{-1}$ , grown for 3 (CC-4532) or 3.5 days (*vtc1* and *VTC1*) to a density of  $1 \times 10^6$  cells $\cdot$ ml $^{-1}$  and Fe-EDTA was added to the cultures at the indicated concentrations. Cellular iron content was assessed by ICP-MS/MS analysis of whole cell lysates at 0, 2, 4, 6, 12, 24, and 48h after the addition of Fe to the cultures and was related to the sulfur content of each sample. The mean of four replicates is shown, error bars represent SD.

6. Appendix



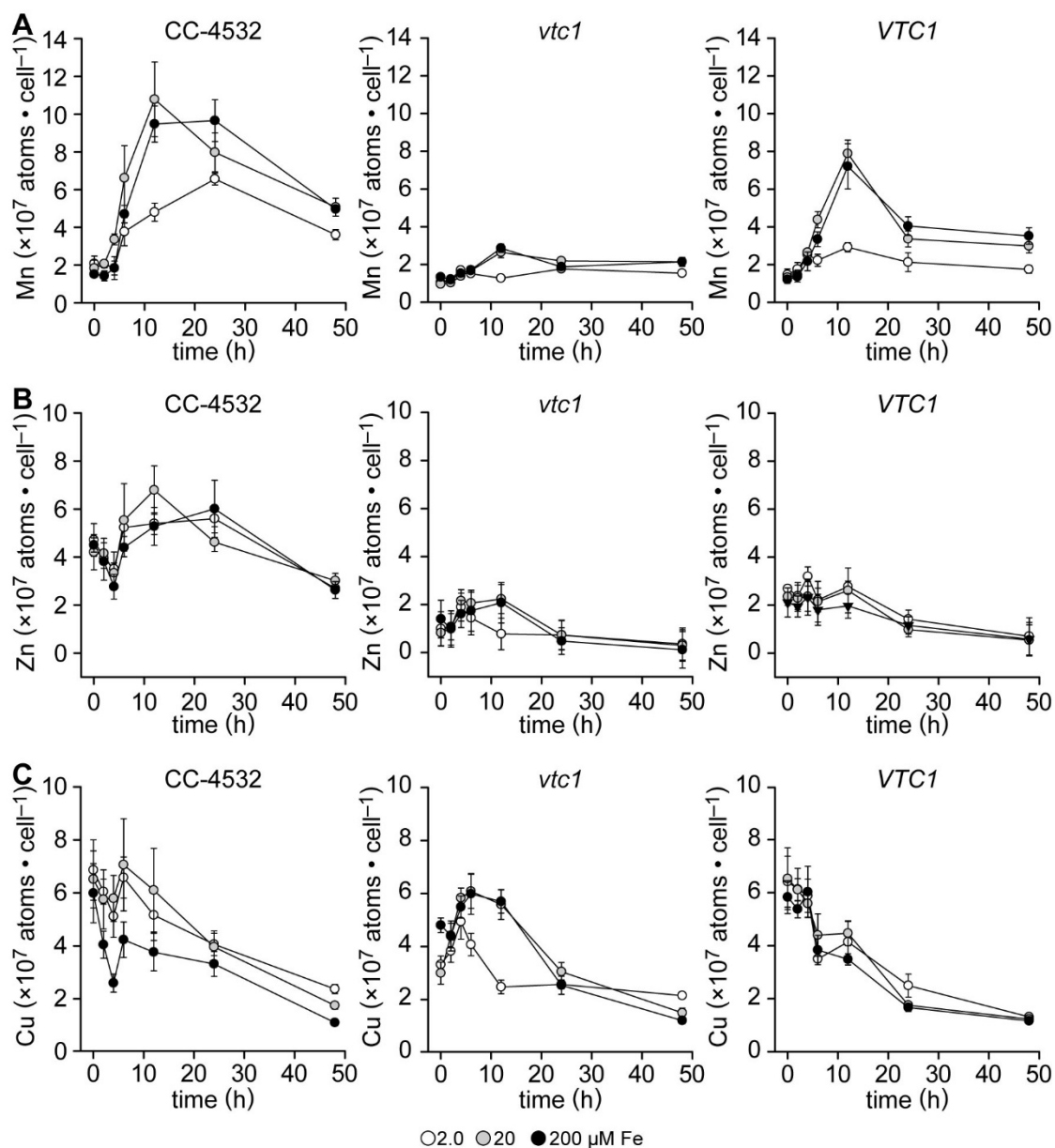
**Supplemental Figure 30. Phosphorus, sulfur and magnesium content.** Photoheterotrophic cultures containing no added iron were inoculated with CC-4532, *vtc1* (CC-5321) and VTC1 (CC-5324) from precultures containing 1  $\mu$ M Fe, to an initial cell density of  $1 \times 10^4$  cells $\cdot$ ml $^{-1}$ , grown for 3 (CC-4532) or 3.5 days (*vtc1* and VTC1) to a density of  $1 \times 10^6$  cells $\cdot$ ml $^{-1}$  and Fe-EDTA was added to the cultures at the indicated concentrations. Elemental composition was assessed by ICP-MS/MS analysis of whole cell lysates at 0, 2, 4, 6, 12, 24, and 48h after the addition of Fe to the cultures. **A:** Cellular phosphorus, **B:** sulfur, and **C:** magnesium content were related to the number of cells analyzed. The mean of four replicates is shown, error bars represent SD.

6. Appendix



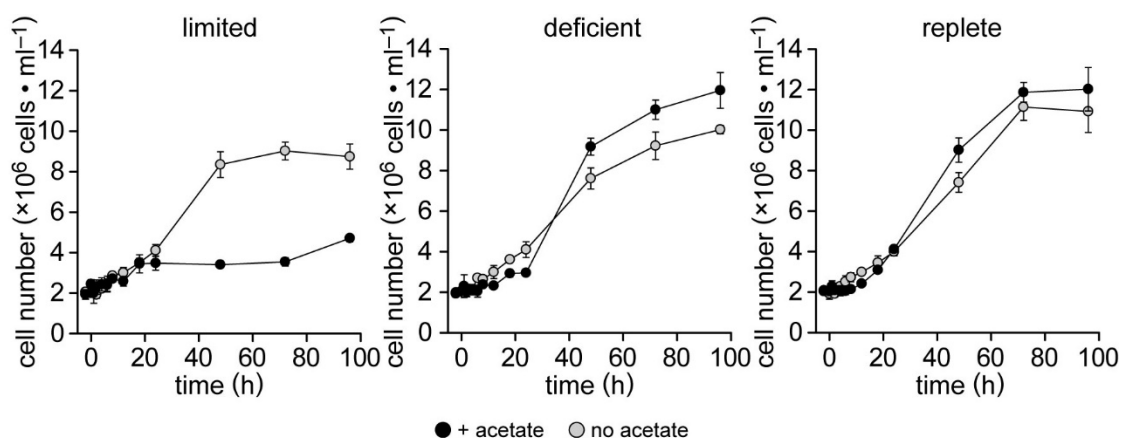
**Supplemental Figure 31. Potassium, sodium and calcium content.** Photoheterotrophic cultures containing no added iron were inoculated with CC-4532, *vtc1* (CC-5321) and VTC1 (CC-5324) from precultures containing 1  $\mu$ M Fe, to an initial cell density of  $1 \times 10^4$  cells $\cdot$ ml $^{-1}$ , grown for 3 (CC-4532) or 3.5 days (*vtc1* and VTC1) to a density of  $1 \times 10^6$  cells $\cdot$ ml $^{-1}$  and Fe was added to the cultures at the indicated concentrations. Elemental composition was assessed by ICP-MS/MS analysis of whole cell lysates at 0, 2, 4, 6, 12, 24, and 48h after the addition of Fe to the cultures. **A:** Cellular potassium, **B:** sodium, and **C:** calcium content were related to the number of cells analyzed. The mean of four replicates is shown, error bars represent SD.

## 6. Appendix

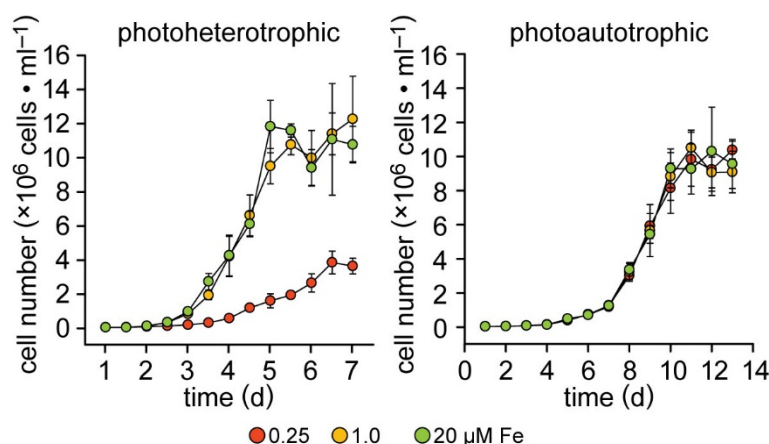


**Supplemental Figure 32. Manganese, zinc and copper content.** Photoheterotrophic cultures containing no added iron were inoculated with CC-4532, *vtc1* (CC-5321) and *VTC1* (CC-5324) from precultures containing 1  $\mu$ M Fe, to an initial cell density of  $1 \times 10^4$  cells  $\cdot$  ml $^{-1}$ , grown for 3 (CC-4532) or 3.5 days (*vtc1* and *VTC1*) to a density of  $1 \times 10^6$  cells  $\cdot$  ml $^{-1}$  and Fe-EDTA was added to the cultures at the indicated concentrations. Elemental composition was assessed by ICP-MS/MS analysis of whole cell lysates at 0, 2, 4, 6, 12, 24, and 48h after the addition of Fe to the cultures. **A:** Cellular manganese, **B:** zinc, and **C:** copper content was related to the number of cells analyzed. The mean of four replicates is shown, error bars represent SD.

## 6. Appendix

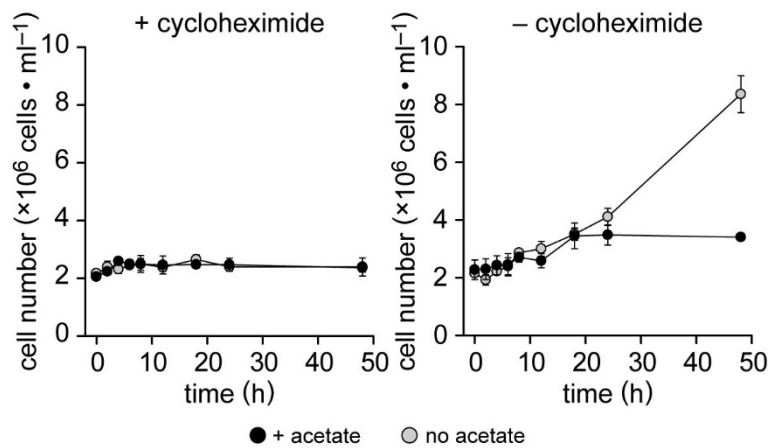


**Supplemental Figure 33. Longer growth of iron-limited, -deficient and -replete cultures after the addition of acetate.** Cells of strain CC-4532 were grown with increased aeration and light, without acetate (photoautotrophic) for a full growth curve before starting replicate precultures containing 2  $\mu\text{M}$  Fe. Photoautotrophic cultures containing 0.25 (limited), 1.0 (deficient), and 20  $\mu\text{M}$  Fe (replete) were inoculated to an initial cell density of  $2 \times 10^4$  cells  $\cdot$  ml $^{-1}$ , grown for 6-7 days to a cell density of  $2 \times 10^6$  cells  $\cdot$  ml $^{-1}$  and each culture was either supplied with 17 mM sterile sodium acetate (black circles) or with the equal volume of sterile purified water as control (grey circles). Growth was monitored up to 96h after the addition of acetate by manual counting (Hemocytometer). The mean of four independent replicates is shown, error bars represent SD.

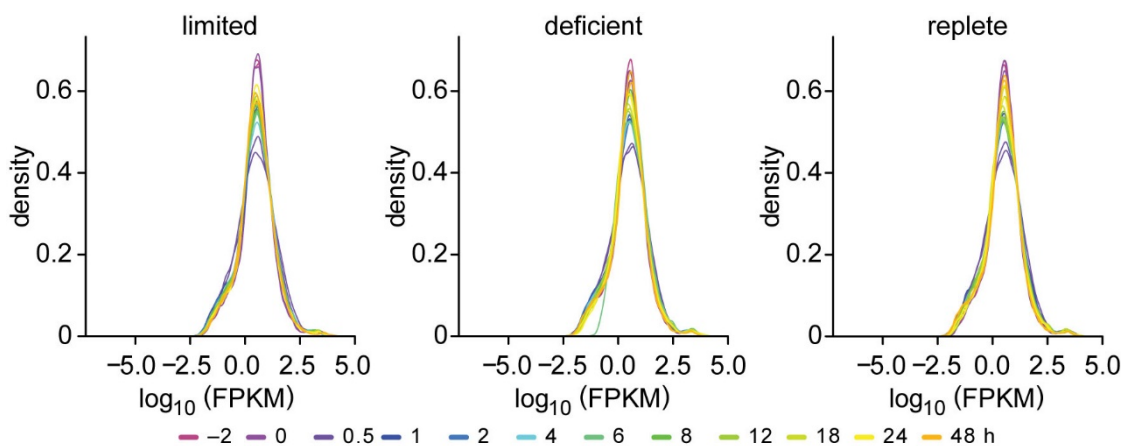


**Supplemental Figure 34. Growth of iron-limited, -deficient and -replete steady state photoheterotrophic and photoautotrophic cultures.** Cells from a replete culture were grown in the presence of acetate and light (photoheterotrophic) or increased aeration and light (photoautotrophic) in the same flasks, culture volume and incubator as the acetate addition experiments. Photoheterotrophic and photoautotrophic cultures containing 0.25 (orange), 1.0 (yellow) and 20  $\mu\text{M}$  Fe (green) were inoculated from precultures containing 1  $\mu\text{M}$  Fe to an initial cell density of  $1-2 \times 10^6$  cells  $\cdot$  ml $^{-1}$ . Growth was monitored from inoculation to stationary growth phase and the cell number was determined every 12h for the photoheterotrophic cultures and every 24h for the photoautotrophic cultures by manual counting (Hemocytometer). The mean of three independent replicates is shown, error bars represent SD.

## 6. Appendix

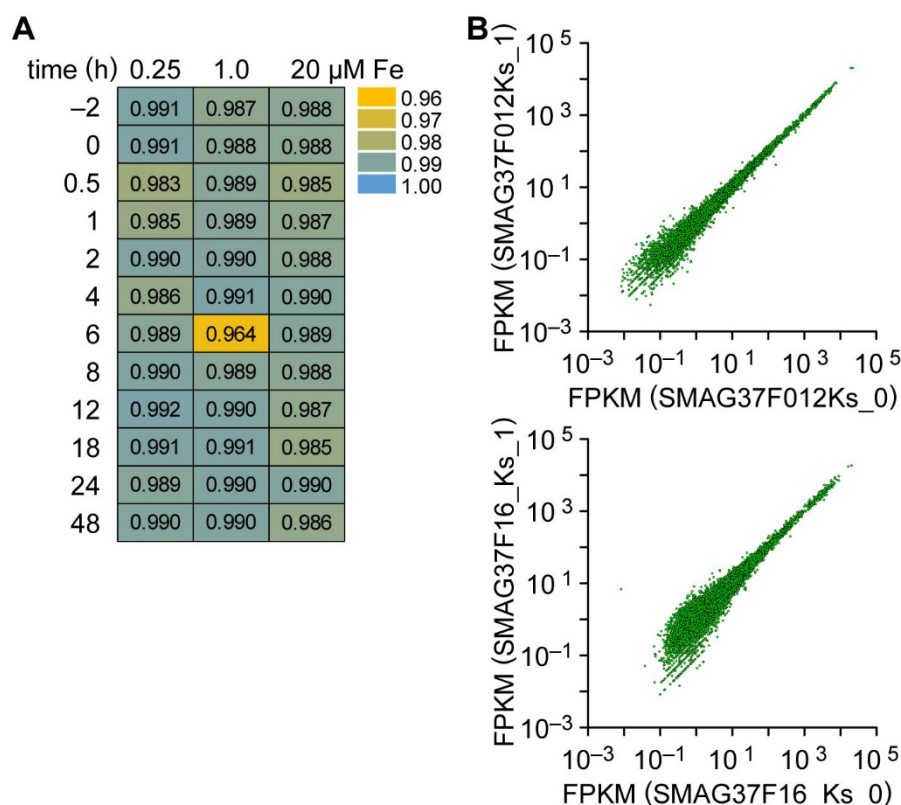


**Supplemental Figure 35. Growth of iron-limited cultures after the addition of acetate and cycloheximide.** Cells of strain CC-4532 were grown with increased aeration and light, without acetate (photoautotrophic) for a full growth curve before starting replicate precultures containing  $2 \mu\text{M}$  Fe. Photoautotrophic cultures containing  $0.25 \mu\text{M}$  Fe (limited) were inoculated to an initial cell density of  $2 \times 10^4$  cells  $\text{ml}^{-1}$ , grown for 6-7 days to a cell density of  $2 \times 10^6$  cells  $\text{ml}^{-1}$  and each culture was either supplied with 17 mM sterile sodium acetate (black circles) or with the equal volume of sterile purified water as control (grey circles) and were treated with 10  $\mu\text{g}/\text{ml}$  cycloheximide (left graph) or left untreated (right graph). Growth was monitored 0, 2, 4, 6, 8, 12, 18, 24, and 48h after the addition of acetate by manual counting (Hemocytometer). The mean of three independent biological replicates is shown, error bars represent SD.

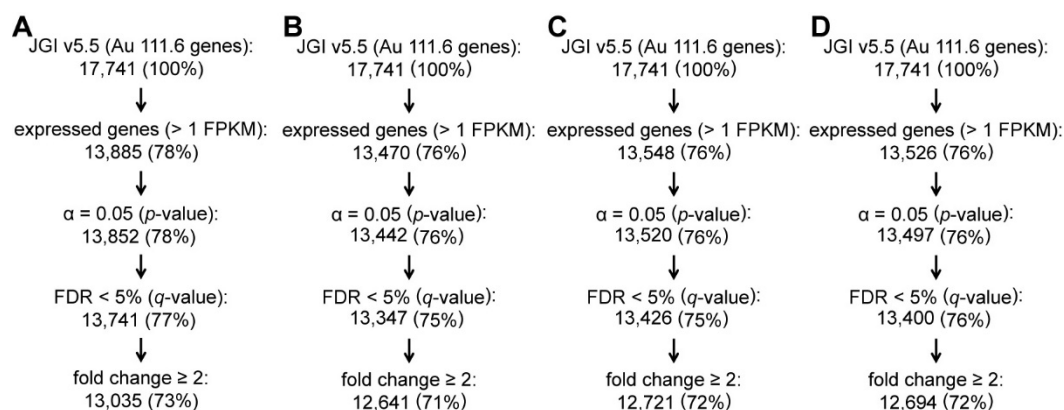


**Supplemental Figure 36. Expression level distribution of all 17 741 gene models of the individual replicates in all conditions.** For an across-sample comparison of expression level distribution, the expression values (FPKM) for each transcript under each condition were transformed by decimal logarithm and plotted by density of occurrence. 24 line graphs are shown in each graph, the two biological replicates are shown in the same color.

## 6. Appendix

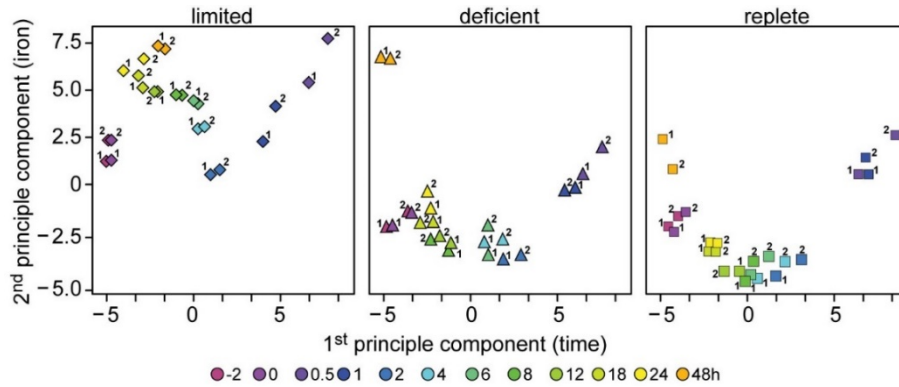


**Supplemental Figure 37. Replicate transcript expression.** **A:** The Spearman's rank correlation coefficient ( $\rho$ ) was calculated between the independent biological replicates for each of the conditions. **B:** Two exemplary scatter plots are shown, comparing the two replicates of 0.25  $\mu$ M Fe-EDTA at 12h (top) and 1  $\mu$ M Fe-EDTA at 6h (bottom).

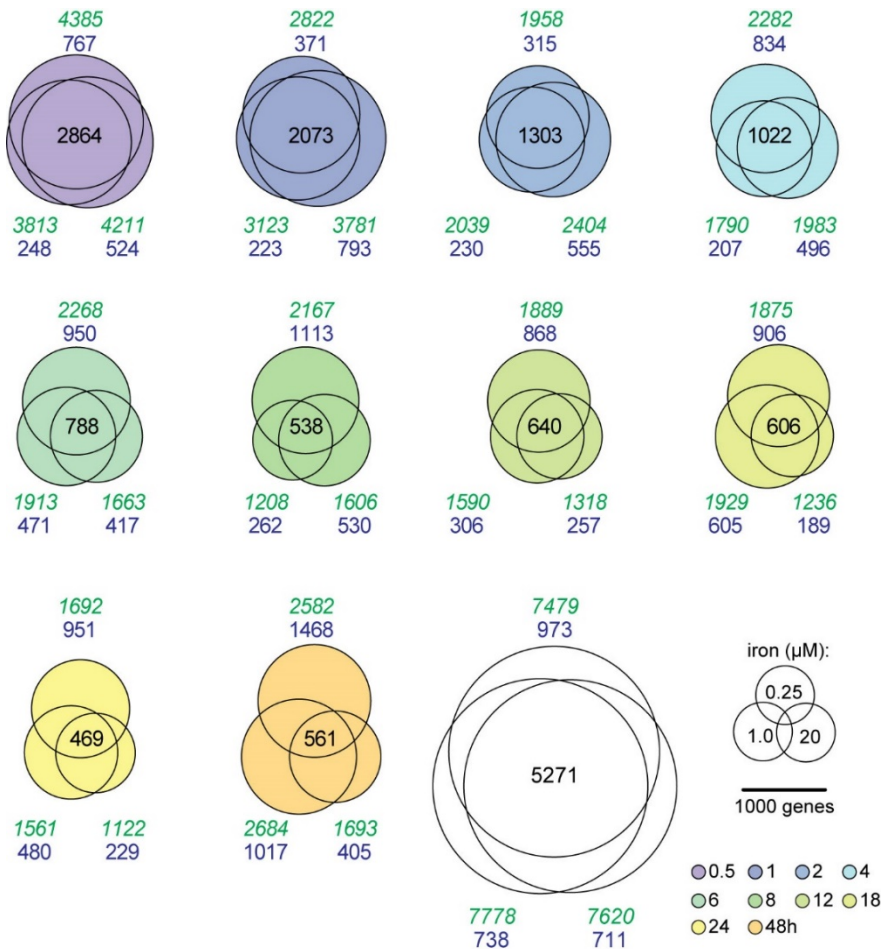


**Supplemental Figure 38. Differentially expressed genes (DEG).** The individual steps taken for the determination of differentially expressed genes. **A:** Entire dataset, **B:** Iron replete only, **C:** deficient only, and **D:** limited time course only. Percentage of differentially expressed genes from the whole genome are shown in inside parentheses.

## 6. Appendix

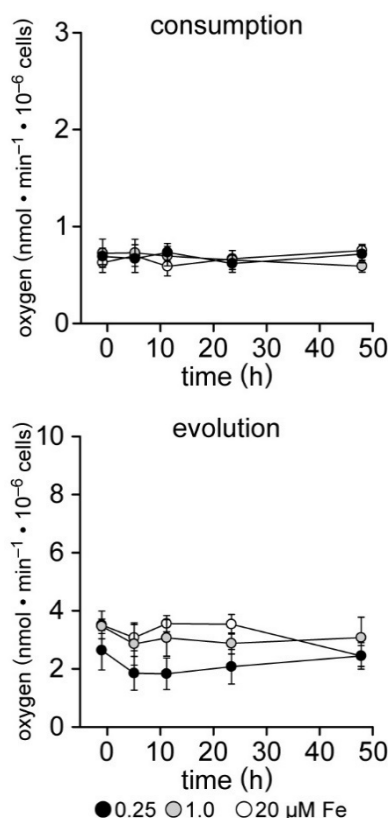


**Supplemental Figure 39. Principal component analysis of individual replicates.** A principal component analysis was generated from the individual replicate samples, labeled “1” and “2”. The first principal component refers to the time after acetate addition, the second is the extracellular iron concentration.

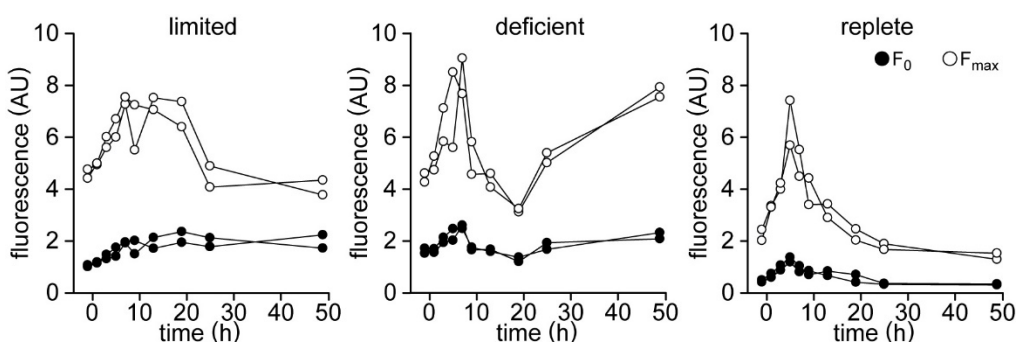


**Supplemental Figure 40. The iron-dependent transcriptome response to acetate.** Differentially expressed genes between Fe-limited (left), -deficient (middle) and -replete (right) time points compared to -2h. Size-correct Venn diagrams showing the shared response for each time point. The scale bar indicates circle diameter per 1000 genes, Fe-limited is at the top, -deficient at the bottom left and -replete at the bottom right. The green number indicate all genes within this condition, the blue number represent the number of unique genes, numbers are the shared response.



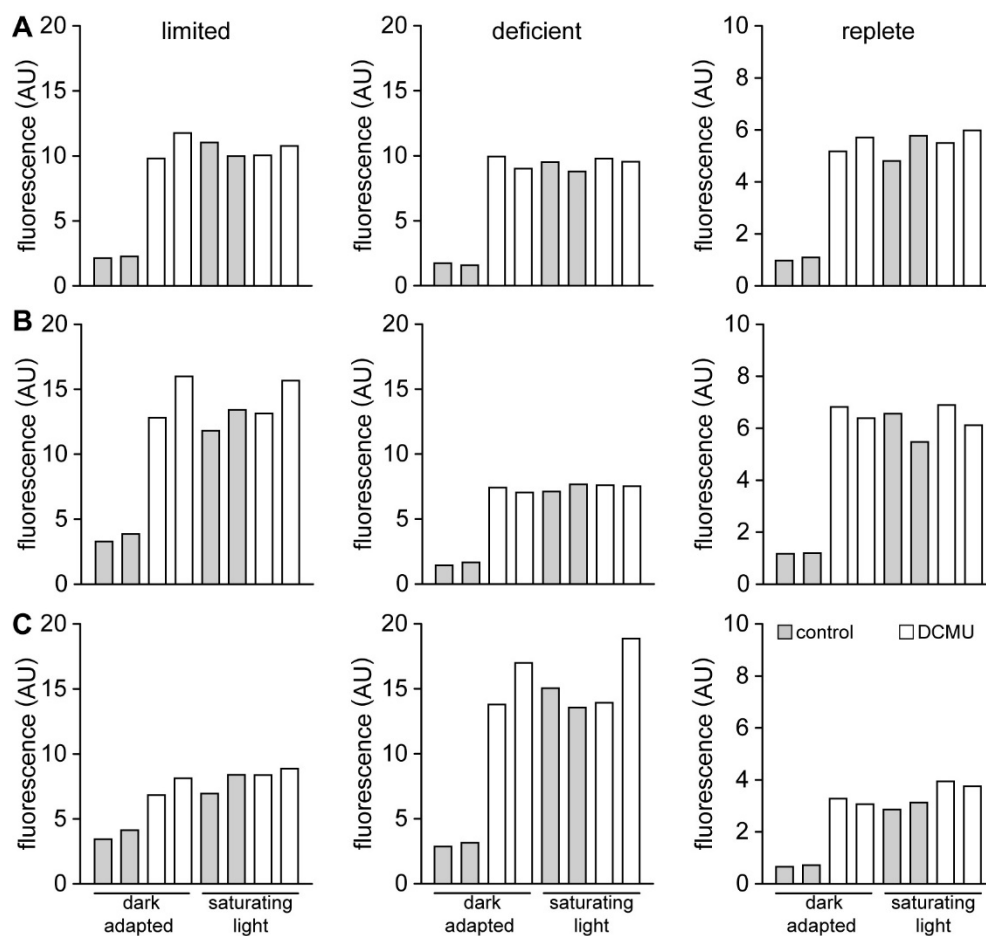


**Supplemental Figure 41. Net oxygen consumption in the dark and evolution in the light of iron limited, deficient and replete cultures without the addition of acetate.** Cells of strain CC-4532 were grown with increased aeration and light, without acetate (photoautotrophic) for a full growth curve before starting replicate precultures containing 2  $\mu\text{M}$  Fe-EDTA. Photoautotrophic cultures containing 0.25 (black circles), 1.0 (grey circles), and 20  $\mu\text{M}$  Fe-EDTA (white circles) were inoculated to an initial cell density of  $2 \times 10^4$  cells $\cdot\text{ml}^{-1}$ , grown for 6-7 days to a cell density of  $2 \times 10^6$  cells $\cdot\text{ml}^{-1}$  and each culture was supplied with sterile purified water as control. The rates of net oxygen consumption and evolution were measured from  $\sim 4 \times 10^6$  intact cells. The decrease in dissolved oxygen in the dark and the increase during constant illumination with  $100 \mu\text{mol}\cdot\text{m}^{-2}\cdot\text{s}^{-1}$  was monitored for five minutes each and the resulting rate was related to the number of cells analyzed. The mean of three independent replicates is shown, error bars represent SD.



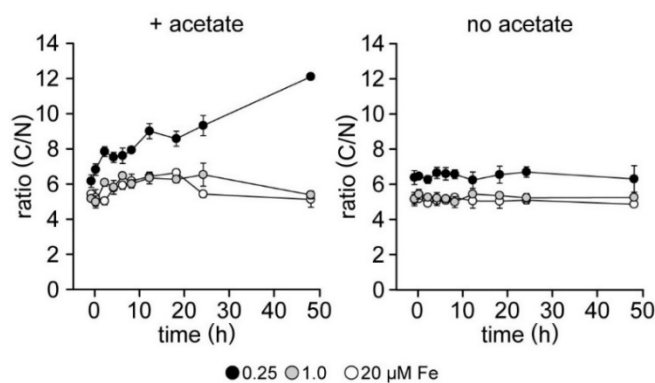
**Supplemental Figure 42. Fluorescence of dark adapted ( $F_0$ ) and light saturated ( $F_{\text{max}}$ ) cultures after the addition of acetate.** At each time point,  $1 \times 10^6$  cells were immobilized onto 15 mm round filters and fluorescence after dark-adaptation for 12-15 min ( $F_0$ ) and after saturating light ( $F_{\text{max}}$ ) was determined. Data from two independent experiments is shown and fluorescence is expressed in arbitrary units.

## 6. Appendix

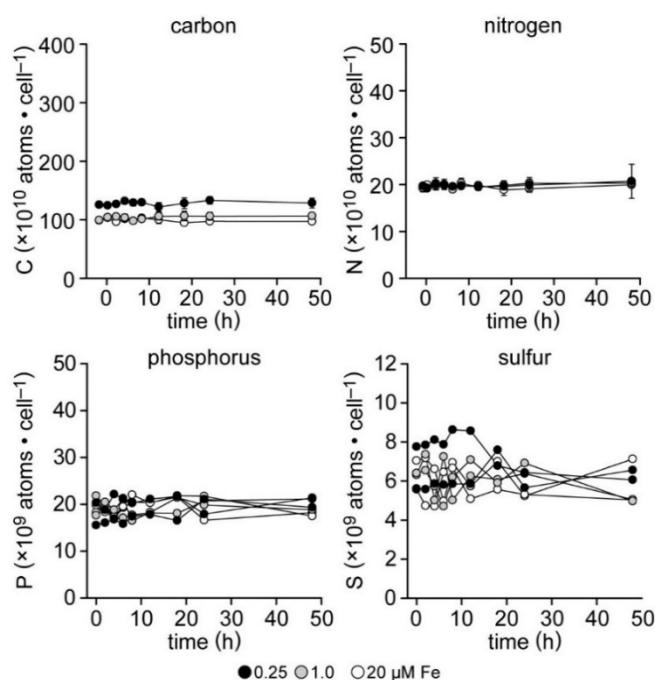


**Supplemental Figure 43. DCMU treated cultures before, 12 and 48h after the addition of acetate.** **A:** Before, **B:** 12 and **C:** 48 hours after the addition of acetate, cells were treated with 20  $\mu$ M DCMU, treated (white bars) and untreated (grey bars) cells were immobilized onto 15 mm round filters and the fluorescence was measured after dark-adaptation for 12-15 min and after applying saturating light. Data from two independent experiments is shown and fluorescence is expressed in arbitrary units.

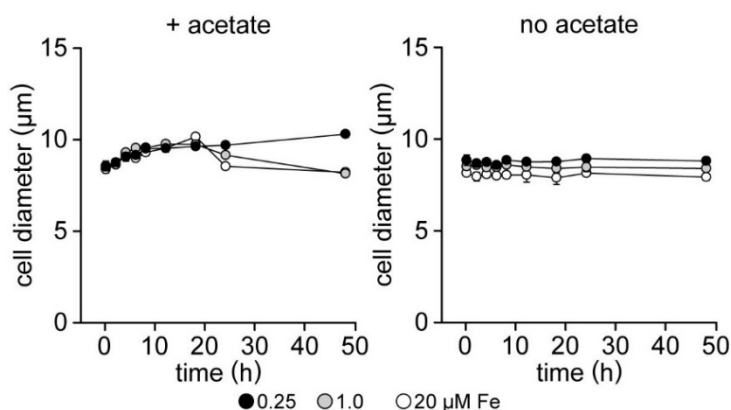
## 6. Appendix



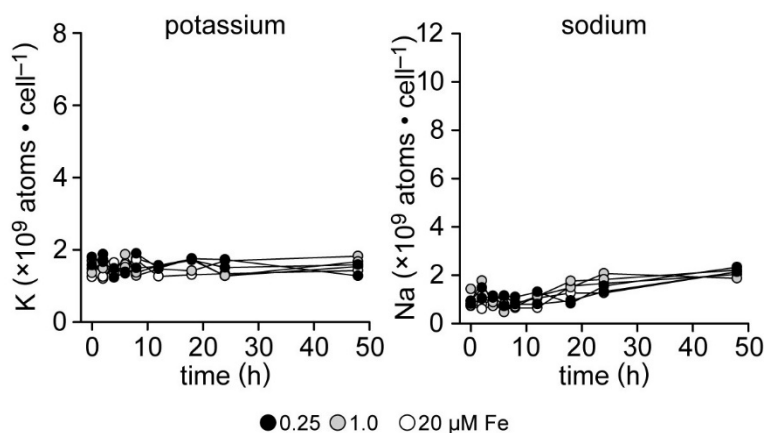
**Supplemental Figure 44. Cellular carbon to nitrogen ratio of iron limited, deficient and replete cultures without the addition of acetate.** Cells of strain CC-4532 were grown with increased aeration and light, without acetate (photoautotrophic) for a full growth curve before starting replicate precultures containing  $2 \mu\text{M}$  Fe-EDTA. Photoautotrophic cultures containing  $0.25$  (black circles),  $1.0$  (grey circles), and  $20 \mu\text{M}$  Fe-EDTA (white circles) were inoculated to an initial cell density of  $2 \times 10^4 \text{ cells} \cdot \text{ml}^{-1}$ , grown for 6-7 days to a cell density of  $2 \times 10^6 \text{ cells} \cdot \text{ml}^{-1}$ , each culture was either supplied with  $17 \text{ mM}$  sterile sodium acetate or with the equal volume of sterile purified water as control. Cellular carbon and nitrogen content were analyzed by TOC and the ratio of carbon to nitrogen atoms per cell calculated. The mean of four independent replicates is shown, error bars represent SD.



**Supplemental Figure 45. Cellular carbon, nitrogen, phosphorus and sulfur content of iron limited, deficient and replete cultures without the addition of acetate.** Cells of strain CC-4532 were grown with increased aeration and light, without acetate (photoautotrophic) for a full growth curve before starting replicate precultures containing  $2 \mu\text{M}$  Fe-EDTA. Photoautotrophic cultures containing  $0.25$  (black circles),  $1.0$  (grey circles), and  $20 \mu\text{M}$  Fe-EDTA (white circles) were inoculated to an initial cell density of  $2 \times 10^4 \text{ cells} \cdot \text{ml}^{-1}$ , grown for 6-7 days to a cell density of  $2 \times 10^6 \text{ cells} \cdot \text{ml}^{-1}$ , each culture was supplied with sterile purified water as control and cells for elemental analysis by TOC (nitrogen and carbon) and ICP-MS/MS (phosphorus and sulfur) were taken at each time point and the content related to the number of cells analyzed. The mean of four independent replicates is shown, error bars represent SD.

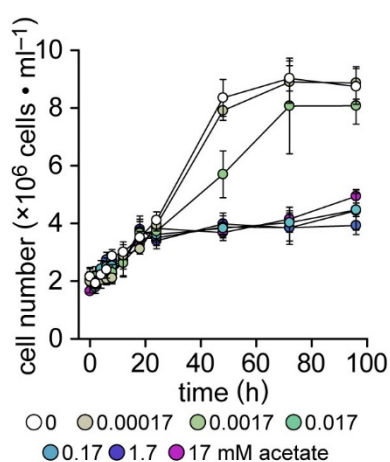


**Supplemental Figure 46. Median cell diameter used for the calculation of cell volume of iron limited, deficient and replete cultures after the addition of acetate.** Cells of strain CC-4532 were grown with increased aeration and light, without acetate (photoautotrophic) for a full growth curve before starting replicate precultures containing 2 µM Fe-EDTA. Photoautotrophic cultures containing 0.25 (black circles), 1.0 (grey circles), and 20 µM Fe-EDTA (white circles) were inoculated to an initial cell density of  $2 \times 10^4$  cells · mL<sup>-1</sup>, grown for 6-7 days to a cell density of  $2 \times 10^6$  cells · mL<sup>-1</sup> and each culture was either supplied with 17 mM sterile sodium acetate or with the equal volume of sterile purified water as control. The median diameter was determined from 500 to 600 (+ acetate) or 200 to 300 (no acetate) cells of each culture. The mean of four independent replicates is shown, error bars represent SD.

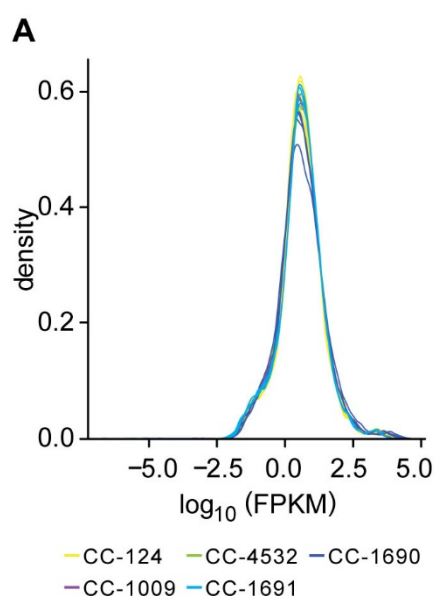


**Supplemental Figure 47. Cellular potassium and sodium content of iron limited, deficient and replete culture without the addition of acetate.** Cells of strain CC-4532 were grown with increased aeration and light, without acetate (photoautotrophic) for a full growth curve before starting replicate precultures containing 2 µM Fe-EDTA. Photoautotrophic cultures containing 0.25 (black circles), 1.0 (grey circles), and 20 µM Fe-EDTA (white circles) were inoculated to an initial cell density of  $2 \times 10^4$  cells · mL<sup>-1</sup>, grown for 6-7 days to a cell density of  $2 \times 10^6$  cells · mL<sup>-1</sup>, each culture was supplied with sterile purified water as control and cells for elemental analysis by ICP-MS/MS were taken at each time point. Two independent replicates are shown in individual line graphs.

## 6. Appendix



**Supplemental Figure 48. Growth of iron limited cultures after the addition of reduced concentrations of acetate.** Cells of strain CC-4532 were grown with increased aeration and light, without acetate (photoautotrophic) for a full growth curve before starting replicate precultures containing 2  $\mu\text{M}$  Fe-EDTA. Photoautotrophic cultures containing 0.25, 1.0, and 20  $\mu\text{M}$  Fe-EDTA were inoculated to an initial cell density of  $2 \times 10^4$  cells $\cdot\text{ml}^{-1}$ , grown for 6-7 days to a cell density of  $2 \times 10^6$  cells $\cdot\text{ml}^{-1}$  and each culture was supplied with sodium acetate at the indicated concentrations. Growth was monitored up to 96h after the addition of acetate by manual counting (Hemocytometer). The mean of three independent replicates is shown, error bars represent SD.

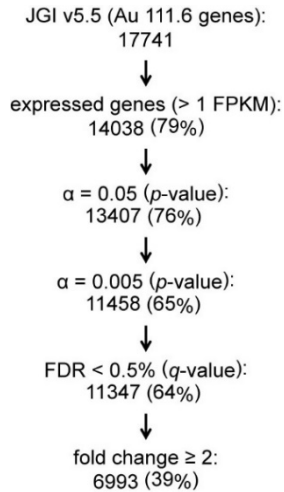


**B**

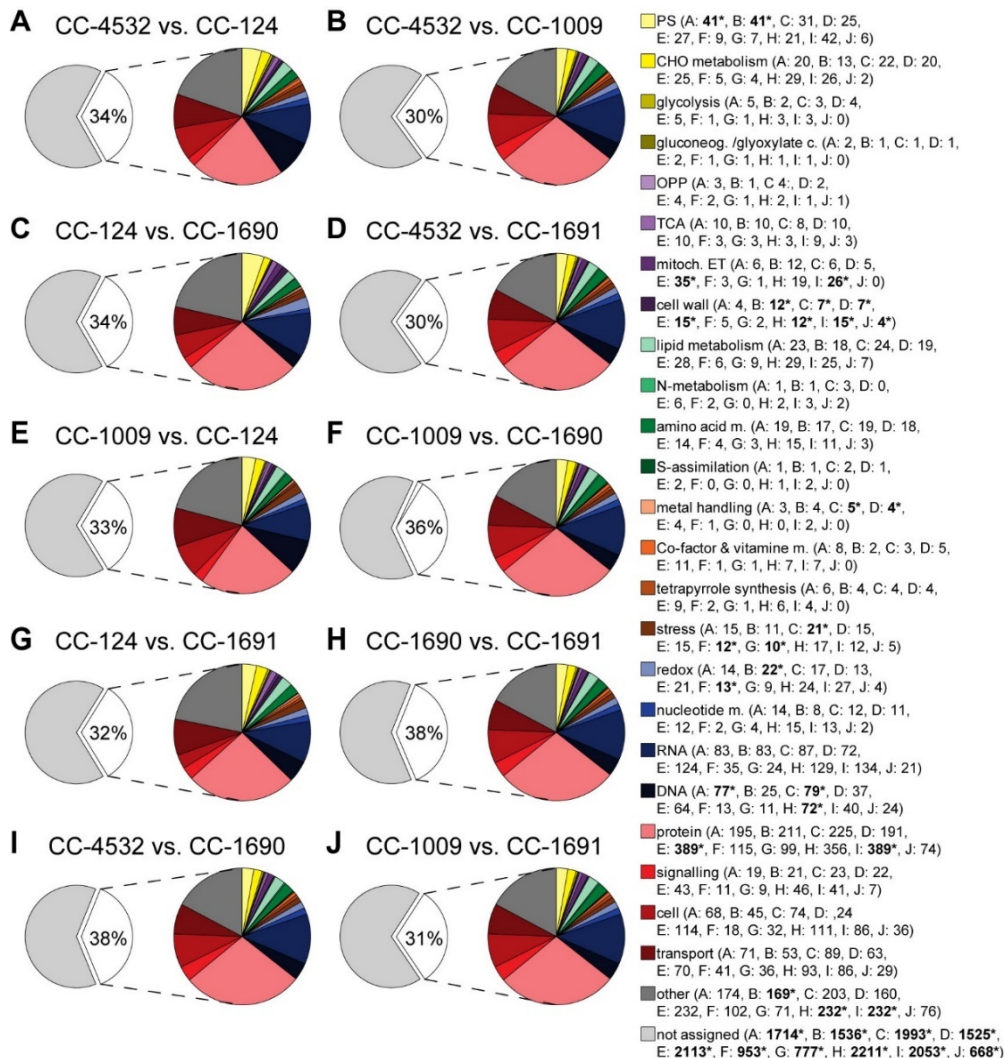
sample	25th	median	75th	95th	sum
SMAG37B2E6Ks_0	0.70	3.20	9.79	67.86	629341
SMAG37B2E6Ks_1	0.69	3.20	9.91	68.01	651950
SMAG37B2E6Ks_2	0.67	3.16	9.85	68.43	663924
SMAG37B2E6Ks_3	0.64	3.14	9.86	69.91	676758
SMAG09B2E6Ks_0	0.71	3.18	9.77	65.97	658716
SMAG09B2E6Ks_1	0.69	3.19	9.82	65.76	701814
SMAG09B2E6Ks_2	0.69	3.17	9.86	66.28	674783
SMAG09B2E6Ks_3	0.68	3.15	9.77	65.65	697329
SMAG24B2E6Ks_0	0.85	3.07	9.79	70.86	858768
SMAG24B2E6Ks_1	0.88	3.21	9.28	58.47	542590
SMAG24B2E6Ks_2	0.90	3.24	9.24	58.30	549866
SMAG24B2E6Ks_3	0.89	3.11	9.47	67.10	782644
SMAG21B2E6Ks_0	0.67	2.90	9.89	79.47	926882
SMAG21B2E6Ks_1	0.59	2.80	10.85	98.74	1537236
SMAG21B2E6Ks_2	0.67	2.94	9.81	74.94	911079
SMAG21B2E6Ks_3	0.66	2.91	9.81	78.19	1135127
SMAG91B2E6Ks_0	0.69	3.19	9.87	64.43	595961
SMAG91B2E6Ks_1	0.77	3.24	9.68	61.30	560498
SMAG91B2E6Ks_2	0.73	3.20	9.55	61.28	581195
SMAG91B2E6Ks_3	0.71	3.21	9.70	61.94	604809

**Supplemental Figure 49. Gene expression level distribution of all 17 741 gene models of the individual replicates in all conditions.** **A:** For an across-sample comparison of expression level distribution, the expression values (FPKM) for each transcript of the replicates under each condition were transformed by decimal logarithm and plotted by density of occurrence. 20 line graphs are shown in the figure, the replicates are shown in the same color, different strains are colored according to the key points below the graph. **B:** The table summarizes untransformed FPKM values of the 5<sup>th</sup>, 25<sup>th</sup>, 50<sup>th</sup> (median), 75<sup>th</sup>, 95<sup>th</sup> percentile, and the sum from all genes. The values are consistent among all replicates and conditions.expression level distribution.

## 6. Appendix

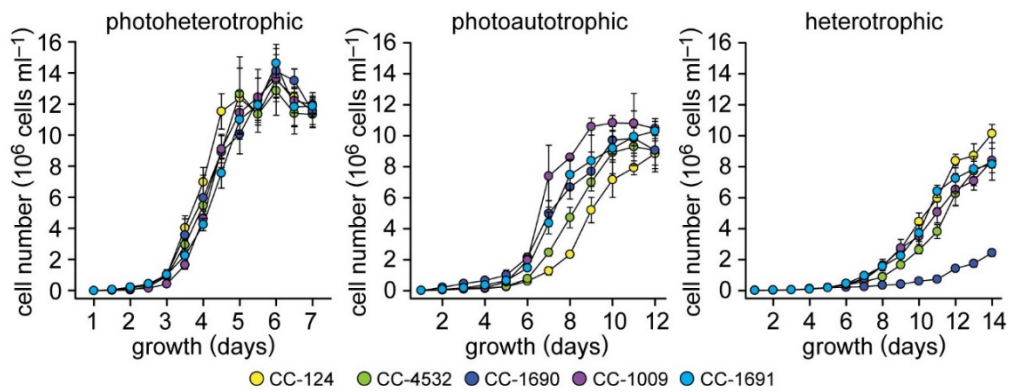


**Supplemental Figure 50. Criteria for the determination of differentially expressed genes.** The individual steps taken for the determination of differentially expressed genes (DEG).

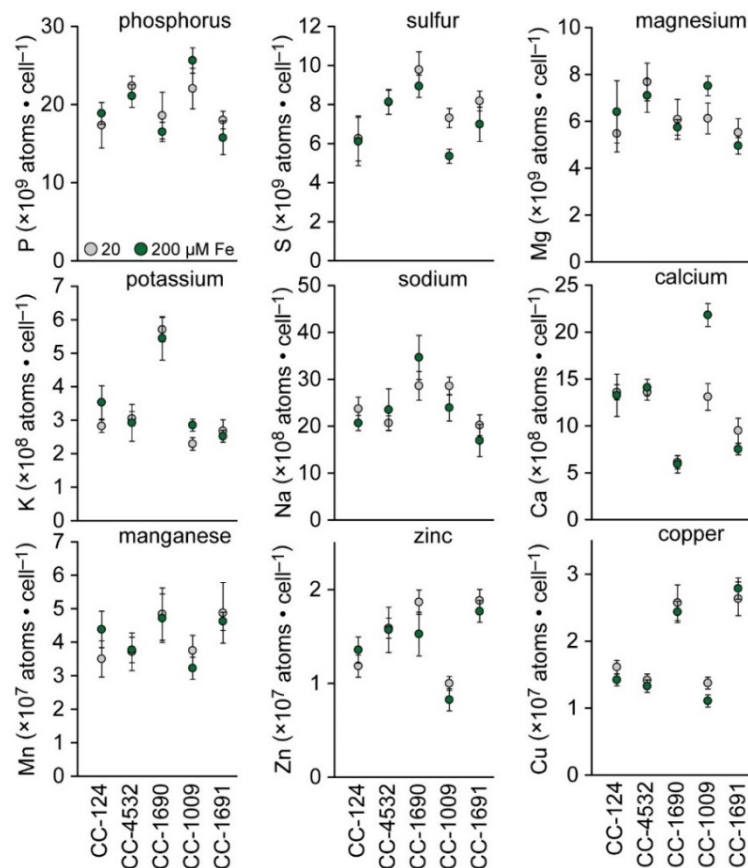


**Supplemental Figure 51. Functional annotation of DE genes between the strains.** Genes were grouped according to the MapMan functional annotation of their predicted protein sequence. The number of genes in each group are listed in brackets for comparisons A to J, groups that are significantly enriched ( $p$ -value > 0.05) compared to randomly assigned genes are labeled with \* and marked in bold.

## 6. Appendix



**Supplemental Figure 52. Growth curves of photoheterotrophic, photoautotrophic, and heterotrophic cultures of different wild-type strains.** Cells from replete cultures were grown in the presence of acetate and light (photoheterotrophic), air and light (photoautotrophic), or acetate (heterotrophic) for at least one full growth curve before starting experimental cultures. Growth was monitored from inoculation to stationary phase and the cell number was determined every 12h (photoheterotrophic) or 24h (photoautotrophic, heterotrophic) by manual counting (Hemocytometer). The mean of three biological replicates is shown, error bars represent SD.



**Supplemental Figure 53. Elemental composition of different wild-type strains grown in excess iron conditions.** Photoheterotrophic cultures containing 20 and 200  $\mu\text{M}$  Fe were inoculated from precultures containing 20 and 200  $\mu\text{M}$  Fe, grown to a cell density of  $2 \times 10^6$  cells  $\cdot$  ml $^{-1}$  and analyzed by ICP-MS/MS. The mean of three replicates is shown, error bars represent SD.

## 6.2 Supplemental Tables

**Supplemental Table 1.** Statistical significance of iron content. Cohen's  $d$ -value was computed as a measure of effect size between the individual conditions, absolute  $d$ -values are shown at the top of each cell. For statistical significance between conditions, unpaired, two-tailed Student's  $t$ -test was applied, and the resulting  $p$ -values are shown at the bottom of each cell.  $P$ -values passing a significance threshold of  $\alpha = 0.05$  are highlighted in bold,  $\alpha = 0.01$  in bold and underlined,  $\alpha = 0.001$  are labeled  $< 0.001$ .

$\mu\text{M Fe}$		0.25	1.0	2.0	10	20	100	200
0.10	$d$	3.4	14.5	15.5	18.1	26.0	16.2	37.1
	$p$	<b>0.003</b>	<b>&lt;0.001</b>	<b>&lt;0.001</b>	<b>&lt;0.001</b>	<b>&lt;0.001</b>	<b>&lt;0.001</b>	<b>&lt;0.001</b>
0.25	$d$		12.4	13.6	16.6	24.9	15.7	36.5
	$p$		<b>&lt;0.001</b>	<b>&lt;0.001</b>	<b>&lt;0.001</b>	<b>&lt;0.001</b>	<b>&lt;0.001</b>	<b>&lt;0.001</b>
1.0	$d$			4.3	9.4	15.7	13.8	34.0
	$p$			<b>0.001</b>	<b>&lt;0.001</b>	<b>&lt;0.001</b>	<b>&lt;0.001</b>	<b>&lt;0.001</b>
2.0	$d$				5.4	9.6	12.8	32.4
	$p$				<b>&lt;0.001</b>	<b>&lt;0.001</b>	<b>&lt;0.001</b>	<b>&lt;0.001</b>
10	$d$					2.5	11.0	29.7
	$p$					<b>0.012</b>	<b>&lt;0.001</b>	<b>&lt;0.001</b>
20	$d$						10.4	29.4
	$p$						<b>&lt;0.001</b>	<b>&lt;0.001</b>
100	$d$							9.9
	$p$							<b>&lt;0.001</b>

**Supplemental Table 2.** Statistical significance of manganese and copper content. **A:** Manganese and **B:** copper content. Cohen's  $d$ -value was computed as a measure of effect size between the individual conditions, absolute  $d$ -values are shown at the top of each cell. For statistical significance between conditions, unpaired, two-tailed Student's  $t$ -test was applied, and the resulting  $p$ -values are shown at the bottom of each cell.  $P$ -values passing a significance threshold of  $\alpha = 0.05$  are highlighted in bold,  $\alpha = 0.01$  in bold and underlined,  $\alpha = 0.001$  are labeled  $< 0.001$ .

<b>A</b> $\mu\text{M Fe}$		0.25	1.0	2.0	10	20	100	200
0.10	$d$	2.1	2.0	8.0	8.3	5.9	6.2	4.9
	$p$	<b>0.023</b>	<b>0.031</b>	<b>&lt;0.001</b>	<b>&lt;0.001</b>	<b>&lt;0.001</b>	<b>&lt;0.001</b>	<b>&lt;0.001</b>
0.25	$d$		0.7	10.5	8.8	5.5	5.8	4.3
	$p$		0.375	<b>&lt;0.001</b>	<b>&lt;0.001</b>	<b>&lt;0.001</b>	<b>&lt;0.001</b>	<b>0.001</b>
1.0	$d$			4.9	5.9	4.0	4.4	3.3
	$p$			<b>&lt;0.001</b>	<b>&lt;0.001</b>	<b>0.001</b>	<b>0.001</b>	<b>0.004</b>
2.0	$d$				2.3	0.5	1.3	0.3
	$p$				<b>0.016</b>	0.504	0.123	0.695
10	$d$					1.2	0.4	1.2
	$p$					0.133	0.567	0.154
20	$d$						0.7	0.1
	$p$						0.392	0.894
100	$d$							0.7
	$p$							0.378



## 6. Appendix

**Supplemental Table 3.** Statistical significance of nitrogen and carbon content. **A:** Nitrogen and **B:** carbon content. Cohen's  $d$ -value was computed as a measure of effect size between the individual conditions, absolute  $d$ -values are shown at the top of each cell. For statistical significance between conditions, unpaired, two-tailed Student's  $t$ -test was applied, and the resulting  $p$ -values are shown at the bottom of each cell.  $P$ -values passing a significance threshold of  $\alpha = 0.05$  are highlighted in bold,  $\alpha = 0.01$  in bold and underlined,  $\alpha = 0.001$  are labeled  $< 0.001$ .

<b>A</b>								<b>B</b>									
$\mu\text{M Fe}$		0.25	1.0	2.0	10	20	100	200	$\mu\text{M Fe}$		0.25	1.0	2.0	10	20	100	200
0.10	$d$	2.7	2.5	2.9	4.5	4.5	5.3	4.6	0.10	$d$	9.0	22.9	21.2	17.1	22.3	26.2	29.4
	$p$	<b><u>0.009</u></b>	<b><u>0.013</u></b>	<b><u>0.006</u></b>	<b><u>0.001</u></b>	<b><u>0.001</u></b>	<b><u>&lt;0.001</u></b>	<b><u>0.001</u></b>		$p$	<b><u>&lt;0.001</u></b>	<b><u>&lt;0.001</u></b>	<b><u>&lt;0.001</u></b>	<b><u>&lt;0.001</u></b>	<b><u>&lt;0.001</u></b>	<b><u>&lt;0.001</u></b>	<b><u>&lt;0.001</u></b>
0.25	$d$		<0.1	0.6	1.2	1.7	2.1	1.9	0.25	$d$		12.2	11.4	9.3	12.4	14.9	16.7
	$p$		0.953	0.460	0.140	0.054	<b><u>0.025</u></b>	<b><u>0.034</u></b>		$p$		<b><u>&lt;0.001</u></b>	<b><u>&lt;0.001</u></b>	<b><u>&lt;0.001</u></b>	<b><u>&lt;0.001</u></b>	<b><u>&lt;0.001</u></b>	<b><u>&lt;0.001</u></b>
1.0	$d$			0.5	1.0	1.5	1.9	1.7	1.0	$d$			0.4	0.5	1.4	2.7	3.7
	$p$			0.519	0.198	0.076	<b><u>0.040</u></b>	<b><u>0.048</u></b>		$p$			0.591	0.512	0.100	<b><u>0.009</u></b>	<b><u>0.002</u></b>
2.0	$d$				0.4	0.9	1.2	1.2	2.0	$d$				0.2	0.9	1.8	2.4
	$p$				0.614	0.237	0.144	0.147		$p$				0.802	0.273	<b><u>0.041</u></b>	<b><u>0.014</u></b>
10	$d$					0.8	1.3	1.2	10	$d$					0.5	1.1	1.4
	$p$					0.287	0.125	0.155		$p$					0.535	0.170	0.099
20	$d$						0.2	0.3	20	$d$						0.9	1.3
	$p$						0.790	0.665		$p$						0.269	0.112
100	$d$							0.2	100	$d$							0.5
	$p$							0.811		$p$							

**Supplemental Table 4.** Statistical significance of cellular phosphorus and sulfur content. **A:** Phosphorus and **B:** sulfur content. Cohen's  $d$ -value was computed as a measure of effect size between the individual conditions, absolute  $d$ -values are shown at the top of each cell. For statistical significance between conditions, unpaired, two-tailed Student's  $t$ -test was applied, and the resulting  $p$ -values are shown at the bottom of each cell.  $P$ -values passing a significance threshold of  $\alpha = 0.05$  are highlighted in bold,  $\alpha = 0.01$  in bold and underlined,  $\alpha = 0.001$  are labeled  $< 0.001$ .

<b>A</b>								<b>B</b>									
$\mu\text{M Fe}$		0.25	1.0	2.0	10	20	100	200	$\mu\text{M Fe}$		0.25	1.0	2.0	10	20	100	200
0.10	$d$	0.8	2.0	1.5	2.2	3.1	2.8	3.9	0.10	$d$	1.3	3.7	5.4	6.1	5.7	5.4	5.7
	$p$	0.292	<b><u>0.033</u></b>	0.072	<b><u>0.020</u></b>	<b><u>0.005</u></b>	<b><u>0.007</u></b>	<b><u>0.002</u></b>		$p$	0.123	<b><u>0.002</u></b>	<b><u>&lt;0.001</u></b>	<b><u>&lt;0.001</u></b>	<b><u>&lt;0.001</u></b>	<b><u>&lt;0.001</u></b>	<b><u>&lt;0.001</u></b>
0.25	$d$		2.1	1.6	2.9	4.3	5.5	7.5	0.25	$d$		2.3	3.7	4.5	4.3	4.0	4.2
	$p$		<b><u>0.024</u></b>	0.069	<b><u>0.006</u></b>	<b><u>0.001</u></b>	<b><u>&lt;0.001</u></b>	<b><u>&lt;0.001</u></b>		$p$		<b><u>0.017</u></b>	<b><u>0.002</u></b>	<b><u>0.001</u></b>	<b><u>0.001</u></b>	<b><u>0.001</u></b>	<b><u>0.001</u></b>
1.0	$d$			0.6	0.1	1.3	0.7	2.0	1.0	$d$			1.1	2.3	2.2	1.8	2.0
	$p$			0.413	0.863	0.125	0.384	<b><u>0.030</u></b>		$p$			0.168	<b><u>0.019</u></b>	<b><u>0.022</u></b>	<b><u>0.043</u></b>	<b><u>0.031</u></b>
2.0	$d$				0.8	2.0	1.6	3.0	2.0	$d$				2.2	1.8	1.3	1.6
	$p$				0.275	<b><u>0.028</u></b>	0.067	<b><u>0.005</u></b>		$p$				<b><u>0.021</u></b>	<b><u>0.043</u></b>	0.114	0.066
10	$d$					1.3	0.6	2.2	10	$d$					0.4	0.2	0.1
	$p$					0.118	0.409	<b><u>0.020</u></b>		$p$					0.609	0.831	0.839
20	$d$						0.9	0.6	20	$d$						0.4	0.5
	$p$						0.244	0.430		$p$						0.552	0.538
100	$d$							2.0	100	$d$							<0.1
	$p$							<b><u>0.030</u></b>		$p$							

## 6. Appendix

**Supplemental Table 5.** Statistical significance of cell volume. Cohen's  $d$ -value was computed as a measure of effect size between the individual conditions, absolute  $d$ -values are shown at the top of each cell. For statistical significance between conditions, unpaired, two-tailed Student's  $t$ -test was applied, and the resulting  $p$ -values are shown at the bottom of each cell.  $P$ -values passing a significance threshold of  $\alpha = 0.05$  are highlighted in bold,  $\alpha = 0.01$  in bold and underlined,  $\alpha = 0.001$  are labeled  $< 0.001$ .

$\mu\text{M Fe}$		0.25	1.0	2.0	10	20	100	200
0.10	$d$	1.3	3.4	3.9	4.7	3.9	5.8	4.9
	$p$	0.114	<b>0.003</b>	<b>0.001</b>	<b>0.001</b>	<b>0.001</b>	<b>&lt;0.001</b>	<b>&lt;0.001</b>
0.25	$d$		1.7	2.3	3.2	2.5	3.6	3.3
	$p$		<b>0.049</b>	<b>0.018</b>	<b>0.004</b>	<b>0.013</b>	<b>0.002</b>	<b>0.004</b>
1.0	$d$			0.7	1.9	1.0	1.9	1.8
	$p$			0.375	<b>0.038</b>	0.200	<b>0.035</b>	<b>0.040</b>
2.0	$d$				1.3	0.4	1.1	1.2
	$p$				0.127	0.588	0.186	0.145
10	$d$					0.8	0.5	0.1
	$p$					0.311	0.482	0.866
20	$d$						0.4	0.7
	$p$						0.549	0.364
100	$d$							0.4
	$p$							0.583

**Supplemental Table 6.** Statistical significance of generation time. Cohen's  $d$ -value was computed as a measure of effect size between the individual conditions, absolute  $d$ -values are shown at the top of each cell. For statistical significance between conditions, unpaired, two-tailed Student's  $t$ -test was applied, and the resulting  $p$ -values are shown at the bottom of each cell.  $P$ -values passing a significance threshold of  $\alpha = 0.05$  are highlighted in bold,  $\alpha = 0.01$  in bold and underlined,  $\alpha = 0.001$  are labeled  $< 0.001$ .

$\mu\text{M Fe}$		0.25	1.0	2.0	10	20	100	200
0.10	$d$	24.2	33.1	43.7	42.4	33.9	52.9	50.8
	$p$	<b>&lt;0.001</b>	<b>&lt;0.001</b>	<b>&lt;0.001</b>	<b>&lt;0.001</b>	<b>&lt;0.001</b>	<b>&lt;0.001</b>	<b>&lt;0.001</b>
0.25	$d$		21.4	44.3	39.1	22.2	88.6	66.0
	$p$		<b>&lt;0.001</b>	<b>&lt;0.001</b>	<b>&lt;0.001</b>	<b>&lt;0.001</b>	<b>&lt;0.001</b>	<b>&lt;0.001</b>
1.0	$d$			16.4	15.0	9.9	31.5	27.7
	$p$			<b>&lt;0.001</b>	<b>&lt;0.001</b>	<b>&lt;0.001</b>	<b>&lt;0.001</b>	<b>&lt;0.001</b>
2.0	$d$				0.2	0.1	12.0	10.3
	$p$				0.828	0.940	<b>&lt;0.001</b>	<b>&lt;0.001</b>
10	$d$					0.2	10.8	9.5
	$p$					0.837	<b>&lt;0.001</b>	<b>&lt;0.001</b>
20	$d$						5.7	5.5
	$p$						<b>&lt;0.001</b>	<b>&lt;0.001</b>
100	$d$							<0.1
	$p$							0.966

## 6. Appendix

**Supplemental Table 7.** Statistical significance of cellular chlorophyll content. Cohen's  $d$ -value was computed as a measure of effect size between individual conditions, absolute  $d$ -values are shown at the top of each cell. For statistical significance between conditions, unpaired, two-tailed Student's  $t$ -test was applied and the resulting  $p$ -values are shown at the bottom of each cell.  $P$ -values passing a significance threshold of  $\alpha = 0.05$  are highlighted in bold,  $\alpha = 0.01$  in bold and underlined,  $\alpha = 0.001$  are labeled  $< 0.001$ .

$\mu\text{M Fe}$		0.25	1.0	2.0	10	20	100	200
0.10	$d$	4.0	11.3	17.3	14.6	13.7	20.0	13.0
	$p$	<b><u>&lt;0.001</u></b>	<b><u>&lt;0.001</u></b>	<b><u>&lt;0.001</u></b>	<b><u>&lt;0.001</u></b>	<b><u>&lt;0.001</u></b>	<b><u>&lt;0.001</u></b>	<b><u>&lt;0.001</u></b>
0.25	$d$		9.5	14.2	12.5	11.7	16.9	11.3
	$p$		<b><u>&lt;0.001</u></b>	<b><u>&lt;0.001</u></b>	<b><u>&lt;0.001</u></b>	<b><u>&lt;0.001</u></b>	<b><u>&lt;0.001</u></b>	<b><u>&lt;0.001</u></b>
1.0	$d$			1.3	1.7	1.4	3.4	2.2
	$p$			0.119	0.057	0.087	<b><u>0.003</u></b>	<b><u>0.021</u></b>
2.0	$d$				0.6	0.3	2.5	1.3
	$p$				0.458	0.653	<b><u>0.012</u></b>	0.125
10	$d$					0.2	1.7	0.7
	$p$					0.795	0.056	0.354
20	$d$						1.8	0.9
	$p$						<b><u>0.041</u></b>	0.265
100	$d$							0.7
	$p$							0.347

**Supplemental Table 8.** Statistical significance of maximum quantum efficiency of PSII ( $F_v/F_m$ ). Cohen's  $d$ -value was computed as a measure of effect size between the individual conditions, absolute  $d$ -values are shown at the top of each cell. For statistical significance between conditions, unpaired, two-tailed Student's  $t$ -test was applied, and the resulting  $p$ -values are shown at the bottom of each cell.  $P$ -values passing a significance threshold of  $\alpha = 0.05$  are highlighted in bold,  $\alpha = 0.01$  in bold and underlined,  $\alpha = 0.001$  are labeled  $< 0.001$ .

$\mu\text{M Fe}$		0.25	1.0	2.0	10	20	100	200
0.10	$d$	3.2	12.8	13.4	14.1	15.5	14.1	10.6
	$p$	<b><u>0.004</u></b>	<b><u>&lt;0.001</u></b>	<b><u>&lt;0.001</u></b>	<b><u>&lt;0.001</u></b>	<b><u>&lt;0.001</u></b>	<b><u>&lt;0.001</u></b>	<b><u>&lt;0.001</u></b>
0.25	$d$		9.8	10.5	11.1	12.6	11.1	7.9
	$p$		<b><u>&lt;0.001</u></b>	<b><u>&lt;0.001</u></b>	<b><u>&lt;0.001</u></b>	<b><u>&lt;0.001</u></b>	<b><u>&lt;0.001</u></b>	<b><u>&lt;0.001</u></b>
1.0	$d$			1.8	1.7	3.3	1.6	0.5
	$p$			<b><u>0.045</u></b>	0.053	<b><u>0.003</u></b>	0.067	0.477
2.0	$d$				0.4	0.6	0.5	0.7
	$p$				0.589	0.420	0.468	0.374
10	$d$					1.4	0.2	0.5
	$p$					0.086	0.816	0.541
20	$d$						1.7	1.2
	$p$						0.050	0.151
100	$d$							0.4
	$p$							0.620

**Supplemental Table 9.** Statistical significance of cellular iron content. Cohen's  $d$ -value was computed as a measure of effect size between the individual conditions, absolute  $d$ -values are shown in the first and third column. For statistical significance between conditions, unpaired, two-tailed Student's  $t$ -test was applied, and the resulting  $p$ -values are shown in the second and fourth column.  $P$ -values passing a significance threshold of  $\alpha = 0.05$  are highlighted in bold,  $\alpha = 0.01$  in bold and underlined,  $\alpha = 0.001$  are labeled  $< 0.001$ .

$\mu\text{M Fe}$	replete vs. iron preculture		mid-logarithmic vs. stationary	
	$d$	$p$	$d$	$p$
0.10	5.8	<b><u>0.002</u></b>	0.6	0.459
0.25	6.9	<b><u>0.001</u></b>	4.7	<b><u>0.003</u></b>
1.0	2.2	<b><u>0.045</u></b>	10.4	<b><u>&lt;0.001</u></b>
2.0	0.8	0.339	6.9	<b><u>0.001</u></b>
10	0.4	0.660	0.1	0.932
20	0.6	0.470	5.2	<b><u>0.002</u></b>
100	2.3	<b><u>0.003</u></b>	0.8	0.317
200	9.6	<b><u>&lt;0.001</u></b>	1.0	0.239

## 6. Appendix

**Supplemental Table 10.** Statistical significance of medium iron concentrations. Cohen's  $d$ -value was computed as a measure of effect size between the individual conditions, absolute  $d$ -values are shown in the first and third column. For statistical significance between conditions, unpaired, two-tailed Student's  $t$ -test was applied, and the resulting  $p$ -values are shown in the second and fourth column.  $P$ -values passing a significance threshold of  $\alpha = 0.05$  are highlighted in bold,  $\alpha = 0.01$  in bold and underlined,  $\alpha = 0.001$  are labeled  $< 0.001$ .

$\mu\text{M Fe}$	fresh vs. mid-log.		fresh vs. stationary	
	$d$	$p$	$d$	$p$
0.10	12.9	<b><u>&lt;0.001</u></b>	12.5	<b><u>&lt;0.001</u></b>
0.25	29.2	<b><u>&lt;0.001</u></b>	28.4	<b><u>&lt;0.001</u></b>
1.0	10.7	<b><u>&lt;0.001</u></b>	21.6	<b><u>&lt;0.001</u></b>
2.0	8.3	<b><u>&lt;0.001</u></b>	14.7	<b><u>&lt;0.001</u></b>
10	2.9	<b><u>0.007</u></b>	6.8	<b><u>&lt;0.001</u></b>
20	0.3	0.737	4.4	<b><u>0.001</u></b>
100	0.8	0.308	3.5	<b><u>0.002</u></b>
200	2.4	<b><u>0.016</u></b>	7.0	<b><u>&lt;0.001</u></b>

**Supplemental Table 11.** Statistical significance of iron content. Cohen's  $d$ -value was computed as a measure of effect size between the individual conditions, absolute  $d$ -values are shown in the left column. For statistical significance between conditions, unpaired, two-tailed Student's  $t$ -test was applied, and the resulting  $p$ -values are shown in the right column.  $P$ -values passing a significance threshold of  $\alpha = 0.05$  are highlighted in bold,  $\alpha = 0.01$  in bold and underlined,  $\alpha = 0.001$  are labeled  $< 0.001$ .

stationary (days)	20 vs. 200 $\mu\text{M Fe}$	
	$d$	$p$
0	10.6	<b><u>&lt;0.001</u></b>
1	15.1	<b><u>&lt;0.001</u></b>
2	10.9	<b><u>&lt;0.001</u></b>
3	21.3	<b><u>&lt;0.001</u></b>
4	20.9	<b><u>&lt;0.001</u></b>

**Supplemental Table 12.** Statistical significance of cellular iron content. Cohen's  $d$ -value was computed as a measure of effect size between the individual conditions, absolute  $d$ -values are shown in left column. For statistical significance between conditions, unpaired, two-tailed Student's  $t$ -test was applied, and the resulting  $p$ -values are shown in the right column.  $P$ -values passing a significance threshold of  $\alpha = 0.05$  are highlighted in bold,  $\alpha = 0.01$  in bold and underlined,  $\alpha = 0.001$  are labeled  $< 0.001$ .

$\mu\text{M Fe}$ (preculture)	20 vs. 200 $\mu\text{M Fe}$	
	$d$	$p$
0.10	15.8	<b><u>&lt;0.001</u></b>
0.25	12.7	<b><u>&lt;0.001</u></b>
1.0	6.3	<b><u>0.002</u></b>
2.0	4.7	<b><u>0.004</u></b>
10	6.6	<b><u>0.001</u></b>
20	10.2	<b><u>&lt;0.001</u></b>
100	12.9	<b><u>&lt;0.001</u></b>
200	9.5	<b><u>&lt;0.001</u></b>

## 6. Appendix

**Supplemental Table 13.** Statistical significance of iron content. **A:** Photoheterotrophic, **B:** photoautotrophic, and **C:** heterotrophic growth conditions. **D:** Trophic comparison of the iron nutrition states. Cohen's *d*-value was computed as a measure of effect size between the individual conditions, absolute *d*-values are shown at the top of each cell. For statistical significance between conditions, unpaired, two-tailed Student's *t*-test was applied, and the resulting *p*-values are shown at the bottom of each cell. *P*-values passing a significance threshold of  $\alpha = 0.05$  are highlighted in bold,  $\alpha = 0.01$  in bold and underlined,  $\alpha = 0.001$  are labeled  $< 0.001$ .

A		$\mu\text{M Fe}$		
		1.0	20	200
0.25	<i>d</i>	14.2	11.2	20.0
	<i>p</i>	<b>&lt;0.001</b>	<b>&lt;0.001</b>	<b>&lt;0.001</b>
1.0	<i>d</i>		6.6	18.3
	<i>p</i>		<b>0.001</b>	<b>&lt;0.001</b>
20	<i>d</i>			15.1
	<i>p</i>			<b>&lt;0.001</b>

B		$\mu\text{M Fe}$		
		1.0	20	200
0.25	<i>d</i>	6.8	9.5	14.3
	<i>p</i>	<b>0.001</b>	<b>&lt;0.001</b>	<b>&lt;0.001</b>
1.0	<i>d</i>		3.0	11.8
	<i>p</i>		<b>0.022</b>	<b>&lt;0.001</b>
20	<i>d</i>			10.4
	<i>p</i>			<b>&lt;0.001</b>

C		$\mu\text{M Fe}$		
		1.0	20	200
0.25	<i>d</i>	8.8	15.0	11.8
	<i>p</i>	<b>0.001</b>	<b>0.001</b>	<b>0.001</b>
1.0	<i>d</i>		12.8	11.4
	<i>p</i>		<b>0.001</b>	<b>0.001</b>
20	<i>d</i>			8.6
	<i>p</i>			<b>0.001</b>

D		$\mu\text{M Fe}$		
		photoheterotrophic vs. photoautotrophic	photoautotrophic vs. heterotrophic	photoheterotrophic vs. heterotrophic
0.25	<i>d</i>	2.3	2.0	0.3
	<i>p</i>	<b>0.046</b>	0.074	0.739
1.0	<i>d</i>	3.4	5.3	4.7
	<i>p</i>	<b>0.013</b>	<b>0.003</b>	<b>0.005</b>
20	<i>d</i>	0.1	4.1	4.2
	<i>p</i>	0.895	<b>0.007</b>	<b>0.007</b>
200	<i>d</i>	2.8	3.7	2.0
	<i>p</i>	<b>0.026</b>	<b>0.010</b>	0.073

**Supplemental Table 14.** Statistical significance of manganese content. **A:** Photoheterotrophic, **B:** photoautotrophic, and **C:** heterotrophic growth conditions. **D:** Trophic comparison of the iron nutrition states. Cohen's *d*-value was computed as a measure of effect size between the individual conditions, absolute *d*-values are shown at the top of each cell. For statistical significance between conditions, unpaired, two-tailed Student's *t*-test was applied, and the resulting *p*-values are shown at the bottom of each cell. *P*-values passing a significance threshold of  $\alpha = 0.05$  are highlighted in bold,  $\alpha = 0.01$  in bold and underlined,  $\alpha = 0.001$  are labeled  $< 0.001$ .

A		$\mu\text{M Fe}$		
		1.0	20	200
0.25	<i>d</i>	2.4	2.9	3.6
	<i>p</i>	<b>0.041</b>	<b>0.024</b>	<b>0.012</b>
1.0	<i>d</i>		0.6	1.4
	<i>p</i>		0.518	0.153
20	<i>d</i>			0.9
	<i>p</i>			0.346

B		$\mu\text{M Fe}$		
		1.0	20	200
0.25	<i>d</i>	0.4	<0.1	0.9
	<i>p</i>	0.678	0.992	0.330
1.0	<i>d</i>		0.4	1.7
	<i>p</i>		0.690	0.109
20	<i>d</i>			0.9
	<i>p</i>			0.330

C		$\mu\text{M Fe}$		
		1.0	20	200
0.25	<i>d</i>	5.0	5.2	6.8
	<i>p</i>	<b>0.004</b>	<b>0.003</b>	<b>0.001</b>
1.0	<i>d</i>		2.4	3.5
	<i>p</i>		<b>0.044</b>	<b>0.013</b>
20	<i>d</i>			0.1
	<i>p</i>			0.934

D		$\mu\text{M Fe}$		
		photoheterotrophic vs. photoautotrophic	photoautotrophic vs. heterotrophic	photoheterotrophic vs. heterotrophic
0.25	<i>d</i>	2.5	3.1	1.3
	<i>p</i>	<b>0.037</b>	<b>0.020</b>	0.180
1.0	<i>d</i>	0.3	1.2	0.6
	<i>p</i>	0.754	0.204	0.493
20	<i>d</i>	<0.1	0.2	0.3
	<i>p</i>	0.995	0.793	0.761
200	<i>d</i>	<0.1	1.0	0.8
	<i>p</i>	0.992	0.286	0.396

## 6. Appendix

**Supplemental Table 15.** Statistical significance of carbon content. **A:** Photoheterotrophic, **B:** photoautotrophic, and **C:** heterotrophic growth conditions. **D:** Trophic comparison of the iron nutrition states. Cohen's *d*-value was computed as a measure of effect size between the individual conditions, absolute *d*-values are shown at the top of each cell. For statistical significance between conditions, unpaired, two-tailed Student's *t*-test was applied, and the resulting *p*-values are shown at the bottom of each cell. *P*-values passing a significance threshold of  $\alpha = 0.05$  are highlighted in bold,  $\alpha = 0.01$  in bold and underlined,  $\alpha = 0.001$  are labeled < 0.001.

A		$\mu\text{M Fe}$			D	
		1.0	20	200		
0.25	<i>d</i>	7.2	9.6	11.7	photoheterotrophic vs. photoautotrophic	12.7
	<i>p</i>	<b>&lt;0.001</b>	<b>&lt;0.001</b>	<b>&lt;0.001</b>		
1.0	<i>d</i>		0.2	0.7	photoautotrophic vs. heterotrophic	0.8
	<i>p</i>		0.808	0.467		
20	<i>d</i>			0.7	photoheterotrophic vs. heterotrophic	2.7
	<i>p</i>			0.438		
0.25	<i>d</i>	0.7	1.6	2.3	photoheterotrophic vs. photoautotrophic	4.4
	<i>p</i>	0.433	0.125	0.050		
1.0	<i>d</i>		1.7	1.7	photoautotrophic vs. heterotrophic	2.7
	<i>p</i>		0.109	0.105		
20	<i>d</i>			0.5	photoheterotrophic vs. heterotrophic	4.4
	<i>p</i>			0.590		
0.25	<i>d</i>	10.8	9.9	11.7	photoheterotrophic vs. photoautotrophic	12.7
	<i>p</i>	<b>&lt;0.001</b>	<b>&lt;0.001</b>	<b>&lt;0.001</b>		
1.0	<i>d</i>		1.3	3.4	photoautotrophic vs. heterotrophic	0.8
	<i>p</i>		0.195	<b>0.014</b>		
20	<i>d</i>			0.7	photoheterotrophic vs. heterotrophic	2.7
	<i>p</i>			0.465		

**Supplemental Table 16.** Statistical significance of growth rates. **A:** Photoheterotrophic, **B:** photoautotrophic, and **C:** heterotrophic growth conditions. **D:** Trophic comparison of the iron nutrition states. Cohen's *d*-value was computed as a measure of effect size between the individual conditions, absolute *d*-values are shown at the top of each cell. For statistical significance between conditions, unpaired, two-tailed Student's *t*-test was applied, and the resulting *p*-values are shown at the bottom of each cell. *P*-values passing a significance threshold of  $\alpha = 0.05$  are highlighted in bold,  $\alpha = 0.01$  in bold and underlined,  $\alpha = 0.001$  are labeled < 0.001.

A		$\mu\text{M Fe}$			D	
		1.0	20	200		
0.25	<i>d</i>	73.7	54.0	93.1	photoheterotrophic vs. photoautotrophic	14.4
	<i>p</i>	<b>&lt;0.001</b>	<b>&lt;0.001</b>	<b>&lt;0.001</b>		
1.0	<i>d</i>		12.1	39.8	photoautotrophic vs. heterotrophic	9.2
	<i>p</i>		<b>&lt;0.001</b>	<b>&lt;0.001</b>		
20	<i>d</i>			11.5	photoheterotrophic vs. heterotrophic	11.2
	<i>p</i>			<b>&lt;0.001</b>		
0.25	<i>d</i>	0.9	1.2	1.9	photoheterotrophic vs. photoautotrophic	14.4
	<i>p</i>	0.315	0.201	0.083		
1.0	<i>d</i>		0.2	0.6	photoautotrophic vs. heterotrophic	9.2
	<i>p</i>		0.861	0.480		
20	<i>d</i>			0.5	photoheterotrophic vs. heterotrophic	11.2
	<i>p</i>			0.557		
0.25	<i>d</i>	1.5	0.6	1.2	photoheterotrophic vs. photoautotrophic	14.4
	<i>p</i>	0.137	0.476	0.205		
1.0	<i>d</i>		1.5	0.1	photoautotrophic vs. heterotrophic	9.2
	<i>p</i>		0.133	0.920		
20	<i>d</i>			1.0	photoheterotrophic vs. heterotrophic	11.2
	<i>p</i>			0.283		

## 6. Appendix

**Supplemental Table 17.** Statistical significance of chlorophyll content. **A:** Photoheterotrophic, **B:** photoautotrophic, and **C:** heterotrophic growth conditions. **D:** Trophic comparison of the iron nutrition states. Cohen's *d*-value was computed as a measure of effect size between the individual conditions, absolute *d*-values are shown at the top of each cell. For statistical significance between conditions, unpaired, two-tailed Student's *t*-test was applied, and the resulting *p*-values are shown at the bottom of each cell. *P*-values passing a significance threshold of  $\alpha = 0.05$  are highlighted in bold,  $\alpha = 0.01$  in bold and underlined,  $\alpha = 0.001$  are labeled < 0.001.

		$\mu\text{M Fe}$		
		1.0	20	200
<b>A</b>	0.25 <i>d</i>	22.4	47.9	6.2
	<i>p</i>	<b>&lt;0.001</b>	<b>&lt;0.001</b>	<b>0.002</b>
	1.0 <i>d</i>		1.8	0.5
	<i>p</i>		0.087	0.561
	20 <i>d</i>			0.1
	<i>p</i>			0.937
<b>B</b>	0.25 <i>d</i>	2.6	3.5	1.8
	<i>p</i>	<b>0.035</b>	<b>0.013</b>	0.089
	1.0 <i>d</i>		0.7	0.3
	<i>p</i>		0.465	0.697
	20 <i>d</i>			<0.1
	<i>p</i>			0.966
<b>C</b>	0.25 <i>d</i>	2.7	4.6	5.6
	<i>p</i>	<b>0.028</b>	<b>0.005</b>	<b>0.002</b>
	1.0 <i>d</i>		3.3	4.7
	<i>p</i>		<b>0.015</b>	<b>0.005</b>
	20 <i>d</i>			0.3
	<i>p</i>			0.705

		$\mu\text{M Fe}$		
		photoheterotrophic vs. photoautotrophic	photoautotrophic vs. heterotrophic	photoheterotrophic vs. heterotrophic
<b>D</b>	0.25 <i>d</i>	7.9	4.1	4.4
	<i>p</i>	<b>0.001</b>	<b>0.007</b>	<b>0.006</b>
	1.0 <i>d</i>	2.8	7.4	8.6
	<i>p</i>	<b>0.027</b>	<b>0.001</b>	<b>&lt;0.001</b>
	20 <i>d</i>	4.2	4.2	2.1
	<i>p</i>	<b>0.007</b>	<b>0.007</b>	0.059
200 <i>d</i>	1.0	1.9	0.9	
<i>p</i>	0.309	0.083	0.332	

**Supplemental Table 18.** Statistical significance of maximum quantum efficiency of PSII ( $F_v/F_m$ ). **A:** Photoheterotrophic, **B:** photoautotrophic, and **C:** heterotrophic growth conditions. **D:** Trophic comparison of the iron nutrition states. Cohen's *d*-value was computed as a measure of effect size between the individual conditions, absolute *d*-values are shown at the top of each cell. For statistical significance between conditions, unpaired, two-tailed Student's *t*-test was applied, and the resulting *p*-values are shown at the bottom of each cell. *P*-values passing a significance threshold of  $\alpha = 0.05$  are highlighted in bold,  $\alpha = 0.01$  in bold and underlined,  $\alpha = 0.001$  are labeled < 0.001.

		$\mu\text{M Fe}$		
		1.0	20	200
<b>A</b>	0.25 <i>d</i>	11.8	14.2	12.9
	<i>p</i>	<b>&lt;0.001</b>	<b>&lt;0.001</b>	<b>&lt;0.001</b>
	1.0 <i>d</i>		4.1	2.9
	<i>p</i>		<b>0.007</b>	<b>0.023</b>
	20 <i>d</i>			0.5
	<i>p</i>			0.539
<b>B</b>	0.25 <i>d</i>	7.0	8.0	4.2
	<i>p</i>	<b>0.001</b>	<b>0.001</b>	<b>0.007</b>
	1.0 <i>d</i>		1.0	0.7
	<i>p</i>		0.288	0.435
	20 <i>d</i>			1.4
	<i>p</i>			0.158
<b>C</b>	0.25 <i>d</i>	3.8	4.6	3.7
	<i>p</i>	<b>0.010</b>	<b>0.005</b>	<b>0.011</b>
	1.0 <i>d</i>		1.4	0.5
	<i>p</i>		0.157	0.609
	20 <i>d</i>			2.2
	<i>p</i>			0.052

		$\mu\text{M Fe}$		
		photoheterotrophic vs. photoautotrophic	photoautotrophic vs. heterotrophic	photoheterotrophic vs. heterotrophic
<b>D</b>	0.25 <i>d</i>	12.3	6.7	1.3
	<i>p</i>	<b>&lt;0.001</b>	<b>0.001</b>	0.200
	1.0 <i>d</i>	5.2	7.0	5.2
	<i>p</i>	<b>0.003</b>	<b>0.001</b>	<b>0.003</b>
	20 <i>d</i>	1.0	7.9	7.2
	<i>p</i>	0.275	<b>0.001</b>	<b>0.001</b>
200 <i>d</i>	0.2	3.8	3.7	
<i>p</i>	0.842	<b>0.010</b>	<b>0.011</b>	

## 6. Appendix

**Supplemental Table 19.** Genes directly affected by the insertional mutations in *vtc1* and *VTC1*. Mutations in the strains *vtc1* (CC-5321) and *VTC1* (CC-5324) were verified by whole genome sequencing.

strain	common name	genes affected by mutation	description
CC-5321	<i>vtc1</i>	Cre12.g510250	Vacuolar Transport Chaperone-like protein
		Cre12.g510252	no annotation
CC-5324	<i>VTC1</i>	Cre14.g531250	Testis-Specific Protein PBS13 T-Complex 11

**Supplemental Table 20.** Statistical significance of iron accumulation. Cohen's *d*-value was computed as a measure of effect size between the individual conditions, absolute *d*-values are shown in the left column. For statistical significance between conditions, unpaired, two-tailed Student's *t*-test was applied, and the resulting *p*-values are shown in the right column. *P*-values passing a significance threshold of  $\alpha = 0.05$  are highlighted in bold,  $\alpha = 0.01$  in bold and underlined,  $\alpha = 0.001$  are labeled < 0.001.

	20 vs. 200 $\mu$ M Fe	
	<i>d</i>	<i>p</i>
CC-4532	11.57	<b>&lt;0.001</b>
<i>vtc1</i>	2.97	<b>0.014</b>
<i>VTC1</i>	10.78	<b>&lt;0.001</b>

**Supplemental Table 21.** Statistical significance of the cellular elemental composition. **A:** Iron replete and **B:** iron excess growth conditions. Cohen's *d*-value was computed as a measure of effect size between the individual conditions, absolute *d*-values are shown at the top of each cell. For statistical significance between conditions, unpaired, two-tailed Student's *t*-test was applied, and the resulting *p*-values are shown at the bottom of each cell. *P*-values passing a significance threshold of  $\alpha = 0.05$  are highlighted in bold,  $\alpha = 0.01$  in bold and underlined,  $\alpha = 0.001$  are labeled < 0.001.

		<b>A</b>			<b>B</b>		
		CC-4532 vs. <i>vtc1</i>	<i>vtc1</i> vs. <i>VTC1</i>	CC-4532 vs. <i>VTC1</i>	CC-4532 vs. <i>vtc1</i>	<i>vtc1</i> vs. <i>VTC1</i>	CC-4532 vs. <i>VTC1</i>
phosphorus	<i>d</i>	3.1	0.9	2.3	0.9	0.4	1.5
	<i>p</i>	<b>0.012</b>	0.256	<b>0.032</b>	0.278	0.612	0.105
sulfur	<i>d</i>	7.2	4.0	0.7	5.9	6.9	1.2
	<i>p</i>	<b>0.001</b>	<b>0.005</b>	0.386	<b>0.001</b>	<b>0.001</b>	0.153
magnesium	<i>d</i>	12.6	20.1	4.3	12.4	8.6	4.0
	<i>p</i>	<b>&lt;0.001</b>	<b>&lt;0.001</b>	<b>0.004</b>	<b>&lt;0.001</b>	<b>&lt;0.001</b>	<b>0.005</b>
potassium	<i>d</i>	1.9	0.2	2.0	2.2	0.5	1.3
	<i>p</i>	0.054	0.771	<b>0.049</b>	<b>0.035</b>	0.492	0.135
sodium	<i>d</i>	0.7	1.1	2.4	0.3	0.1	0.2
	<i>p</i>	0.384	0.210	<b>0.028</b>	0.699	0.847	0.829
calcium	<i>d</i>	13.6	23.0	2.1	16.1	26.3	3.0
	<i>p</i>	<b>&lt;0.001</b>	<b>&lt;0.001</b>	<b>0.040</b>	<b>&lt;0.001</b>	<b>&lt;0.001</b>	<b>0.014</b>
iron	<i>d</i>	1.8	0.1	1.4	1.1	0.2	0.9
	<i>p</i>	0.066	0.857	0.118	0.181	0.838	0.259
manganese	<i>d</i>	0.7	0.1	0.8	13.1	10.0	0.4
	<i>p</i>	0.399	0.852	0.332	<b>&lt;0.001</b>	<b>&lt;0.001</b>	0.611
zinc	<i>d</i>	0.0	1.4	1.3	1.6	0.6	2.4
	<i>p</i>	0.978	0.112	0.140	0.090	0.427	<b>0.026</b>
copper	<i>d</i>	1.4	0.8	1.9	0.3	0.8	0.8
	<i>p</i>	0.116	0.297	0.052	0.686	0.341	0.309



## 6. Appendix

**Supplemental Table 22.** Statistical significance of colony number. Cohen's  $d$ -value was computed as a measure of effect size between the individual conditions, absolute  $d$ -values are shown in the left column. For statistical significance between conditions, unpaired, two-tailed Student's  $t$ -test was applied, and the resulting  $p$ -values are shown in the right column.  $P$ -values passing a significance threshold of  $\alpha = 0.05$  are highlighted in bold,  $\alpha = 0.01$  in bold and underlined,  $\alpha = 0.001$  are labeled  $< 0.001$ .

20 vs. 200  $\mu\text{M}$  Fe

	$d$	$p$
CC-4532	1.7	0.109
<i>vtc1</i>	5.9	<b><u>0.002</u></b>
VTC1	1.9	0.082

**Supplemental Table 23.** Statistical significance of doublings. Cohen's  $d$ -value was computed as a measure of effect size between the individual conditions, absolute  $d$ -values are shown at the top of each cell. For statistical significance between conditions, unpaired, two-tailed Student's  $t$ -test was applied, and the resulting  $p$ -values are shown at the bottom of each cell.  $P$ -values passing a significance threshold of  $\alpha = 0.05$  are highlighted in bold,  $\alpha = 0.01$  in bold and underlined,  $\alpha = 0.001$  are labeled  $< 0.001$ .

		deficient vs. replete	deficient vs. excess	replete vs. excess
CC-4532	$d$	5.8	6.8	5.7
	$p$	<b><u>&lt;0.001</u></b>	<b><u>&lt;0.001</u></b>	<b><u>&lt;0.001</u></b>
<i>vtc1</i>	$d$	7.7	5.8	1.7
	$p$	<b><u>&lt;0.001</u></b>	<b><u>&lt;0.001</u></b>	0.075
VTC1	$d$	13.7	15.5	8.1
	$p$	<b><u>&lt;0.001</u></b>	<b><u>&lt;0.001</u></b>	<b><u>&lt;0.001</u></b>

## 6. Appendix

**Supplemental Table 24.** Statistical significance of cell number. **A:** CC-4532, **B:** *vtc1* mutant, and **C:** *VTC1* complemented. **D:** Iron deficient, **E:** iron replete, and **F:** iron excess growth conditions. Cohen's *d*-value was computed as a measure of effect size between the individual conditions, absolute *d*-values are shown at the top of each cell. For statistical significance between conditions, unpaired, two-tailed Student's *t*-test was applied, and the resulting *p*-values are shown at the bottom of each cell. *P*-values passing a significance threshold of  $\alpha = 0.05$  are highlighted in bold,  $\alpha = 0.01$  in bold and underlined,  $\alpha = 0.001$  are labeled < 0.001.

<b>A</b>			<b>B</b>			<b>C</b>					
time (h)	deficient vs. replete	deficient vs. excess	replete vs. excess	time (h)	deficient vs. replete	deficient vs. excess	replete vs. excess	time (h)	deficient vs. replete	deficient vs. excess	replete vs. excess
0	<i>d</i> 0.5	<i>d</i> 0.4	<i>d</i> 0.3	0	<i>d</i> 0.5	<i>d</i> 0.1	<i>d</i> 0.4	0	<i>d</i> 0.4	<i>d</i> 0.2	<i>d</i> 0.4
	<i>p</i> 0.491	<i>p</i> 0.612	<i>p</i> 0.685		<i>p</i> 0.544	<i>p</i> 0.887	<i>p</i> 0.589		<i>p</i> 0.567	<i>p</i> 0.834	<i>p</i> 0.568
2	<i>d</i> 1.2	<i>d</i> 0.6	<i>d</i> 1.9	2	<i>d</i> 0.2	<i>d</i> 0.4	<i>d</i> 0.2	2	<i>d</i> 0.3	<i>d</i> 0.3	<i>d</i> 0.8
	<i>p</i> 0.159	<i>p</i> 0.428	<i>p</i> 0.052		<i>p</i> 0.757	<i>p</i> 0.581	<i>p</i> 0.807		<i>p</i> 0.662	<i>p</i> 0.688	<i>p</i> 0.345
4	<i>d</i> 1.9	<i>d</i> 3.6	<i>d</i> 0.9	4	<i>d</i> 0.1	<i>d</i> 0.7	<i>d</i> 0.8	4	<i>d</i> 1.6	<i>d</i> 0.1	<i>d</i> 1.2
	<i>p</i> 0.053	<i>p</i> <b>0.007</b>	<i>p</i> 0.261		<i>p</i> 0.899	<i>p</i> 0.408	<i>p</i> 0.310		<i>p</i> 0.092	<i>p</i> 0.937	<i>p</i> 0.155
6	<i>d</i> 0.6	<i>d</i> 2.0	<i>d</i> 0.6	6	<i>d</i> 0.2	<i>d</i> 0.2	<i>d</i> 0.1	6	<i>d</i> 3.1	<i>d</i> 2.1	<i>d</i> 0.7
	<i>p</i> 0.457	<i>p</i> <b>0.048</b>	<i>p</i> 0.477		<i>p</i> 0.838	<i>p</i> 0.754	<i>p</i> 0.895		<i>p</i> <b>0.012</b>	<i>p</i> <b>0.043</b>	<i>p</i> 0.406
12	<i>d</i> 0.1	<i>d</i> 1.1	<i>d</i> 0.9	12	<i>d</i> 2.3	<i>d</i> 2.6	<i>d</i> <0.1	12	<i>d</i> 1.0	<i>d</i> 0.2	<i>d</i> 1.2
	<i>p</i> 0.911	<i>p</i> 0.197	<i>p</i> 0.283		<i>p</i> <b>0.031</b>	<i>p</i> <b>0.020</b>	<i>p</i> 0.984		<i>p</i> 0.222	<i>p</i> 0.746	<i>p</i> 0.165
24	<i>d</i> 0.9	<i>d</i> 0.1	<i>d</i> 0.9	24	<i>d</i> 2.0	<i>d</i> 1.8	<i>d</i> 0.2	24	<i>d</i> 2.5	<i>d</i> 1.6	<i>d</i> 0.9
	<i>p</i> 0.257	<i>p</i> 0.940	<i>p</i> 0.256		<i>p</i> <b>0.046</b>	<i>p</i> 0.066	<i>p</i> 0.839		<i>p</i> <b>0.023</b>	<i>p</i> 0.083	<i>p</i> 0.254
48	<i>d</i> 0.6	<i>d</i> 0.3	<i>d</i> 0.1	48	<i>d</i> <0.1	<i>d</i> 0.3	<i>d</i> 0.4	48	<i>d</i> 0.4	<i>d</i> 1.0	<i>d</i> 0.8
	<i>p</i> 0.455	<i>p</i> 0.677	<i>p</i> 0.874		<i>p</i> 1.000	<i>p</i> 0.726	<i>p</i> 0.610		<i>p</i> 0.632	<i>p</i> 0.225	<i>p</i> 0.305

<b>D</b>			<b>E</b>			<b>F</b>					
time (h)	CC-4532 vs. <i>vtc1</i>	<i>vtc1</i> vs. <i>VTC1</i>	CC-4532 vs. <i>VTC1</i>	time (h)	CC-4532 vs. <i>vtc1</i>	<i>vtc1</i> vs. <i>VTC1</i>	CC-4532 vs. <i>VTC1</i>	time (h)	CC-4532 vs. <i>vtc1</i>	<i>vtc1</i> vs. <i>VTC1</i>	CC-4532 vs. <i>VTC1</i>
0	<i>d</i> 0.3	<i>d</i> 0.3	<i>d</i> 0.6	0	<i>d</i> 0.2	<i>d</i> 0.7	<i>d</i> 0.3	0	<i>d</i> 0.2	<i>d</i> 0.1	<i>d</i> 0.4
	<i>p</i> 0.704	<i>p</i> 0.668	<i>p</i> 0.401		<i>p</i> 0.822	<i>p</i> 0.384	<i>p</i> 0.647		<i>p</i> 0.837	<i>p</i> 0.842	<i>p</i> 0.603
2	<i>d</i> 1.8	<i>d</i> 2.0	<i>d</i> 0.6	2	<i>d</i> 2.6	<i>d</i> 2.1	<i>d</i> 1.0	2	<i>d</i> 1.3	<i>d</i> 2.3	<i>d</i> 1.6
	<i>p</i> <b>0.040</b>	<i>p</i> <b>0.029</b>	<i>p</i> 0.435		<i>p</i> <b>0.011</b>	<i>p</i> <b>0.024</b>	<i>p</i> 0.223		<i>p</i> 0.114	<i>p</i> <b>0.019</b>	<i>p</i> 0.070
4	<i>d</i> 2.7	<i>d</i> 3.8	<i>d</i> 2.0	4	<i>d</i> 4.2	<i>d</i> 3.6	<i>d</i> 1.3	4	<i>d</i> 5.7	<i>d</i> 3.1	<i>d</i> 0.3
	<i>p</i> <b>0.008</b>	<i>p</i> <b>0.002</b>	<i>p</i> <b>0.028</b>		<i>p</i> <b>0.001</b>	<i>p</i> <b>0.002</b>	<i>p</i> 0.109		<i>p</i> <b>&lt;0.001</b>	<i>p</i> <b>0.004</b>	<i>p</i> 0.642
6	<i>d</i> 3.4	<i>d</i> 8.9	<i>d</i> 4.1	6	<i>d</i> 3.1	<i>d</i> 5.1	<i>d</i> <0.1	6	<i>d</i> 8.3	<i>d</i> 5.7	<i>d</i> 0.2
	<i>p</i> <b>0.003</b>	<i>p</i> <b>&lt;0.001</b>	<i>p</i> <b>0.001</b>		<i>p</i> <b>0.005</b>	<i>p</i> <b>&lt;0.001</b>	<i>p</i> 0.967		<i>p</i> <b>&lt;0.001</b>	<i>p</i> <b>&lt;0.001</b>	<i>p</i> 0.809
12	<i>d</i> 2.7	<i>d</i> 1.6	<i>d</i> 1.0	12	<i>d</i> 5.0	<i>d</i> 3.5	<i>d</i> 1.9	12	<i>d</i> 8.1	<i>d</i> 4.9	<i>d</i> 0.1
	<i>p</i> <b>0.010</b>	<i>p</i> 0.069	<i>p</i> 0.217		<i>p</i> <b>&lt;0.001</b>	<i>p</i> <b>0.002</b>	<i>p</i> <b>0.039</b>		<i>p</i> <b>&lt;0.001</b>	<i>p</i> <b>&lt;0.001</b>	<i>p</i> 0.857
24	<i>d</i> 2.6	<i>d</i> 0.8	<i>d</i> 2.7	24	<i>d</i> 5.3	<i>d</i> 7.2	<i>d</i> 0.6	24	<i>d</i> 6.2	<i>d</i> 5.2	<i>d</i> 0.6
	<i>p</i> <b>0.011</b>	<i>p</i> 0.279	<i>p</i> <b>0.010</b>		<i>p</i> <b>&lt;0.001</b>	<i>p</i> <b>&lt;0.001</b>	<i>p</i> 0.404		<i>p</i> <b>&lt;0.001</b>	<i>p</i> <b>&lt;0.001</b>	<i>p</i> 0.401
48	<i>d</i> 0.2	<i>d</i> 0.4	<i>d</i> 0.3	48	<i>d</i> 0.1	<i>d</i> 0.4	<i>d</i> 0.3	48	<i>d</i> 0.5	<i>d</i> 0.2	<i>d</i> 0.5
	<i>p</i> 0.760	<i>p</i> 0.627	<i>p</i> 0.665		<i>p</i> 0.927	<i>p</i> 0.554	<i>p</i> 0.640		<i>p</i> 0.546	<i>p</i> 0.756	<i>p</i> 0.501

## 6. Appendix

**Supplemental Table 25.** Statistical significance of cellular iron content. **A:** CC-4532, **B:** *vtc1* mutant, and **C:** *VTC1* complemented. **D:** iron deficient, **E:** iron replete, and **F:** iron excess growth conditions. Cohen’s *d*-value was computed as a measure of effect size between the individual conditions, absolute *d*-values are shown at the top of each cell. For statistical significance between conditions, unpaired, two-tailed Student’s *t*-test was applied, and the resulting *p*-values are shown at the bottom of each cell. *P*-values passing a significance threshold of  $\alpha = 0.05$  are highlighted in bold,  $\alpha = 0.01$  in bold and underlined,  $\alpha = 0.001$  are labeled  $< 0.001$ .

time (h)		<b>A</b>			<b>B</b>			<b>C</b>		
		deficient vs. replete	deficient vs. excess	replete vs. excess	deficient vs. replete	deficient vs. excess	replete vs. excess	deficient vs. replete	deficient vs. excess	replete vs. excess
0	<i>d</i>	0.3	2.4	0.8	1.3	2.1	0.3	2.1	0.3	1.0
	<i>p</i>	0.688	<b>0.028</b>	0.322	0.135	<b>0.039</b>	0.729	<b>0.043</b>	0.656	0.249
2	<i>d</i>	5.9	10.0	13.4	1.2	6.6	1.3	5.5	16.7	13.6
	<i>p</i>	<u><b>&lt;0.001</b></u>	<u><b>&lt;0.001</b></u>	<u><b>&lt;0.001</b></u>	0.161	<u><b>0.001</b></u>	0.148	<u><b>0.002</b></u>	<u><b>&lt;0.001</b></u>	<u><b>&lt;0.001</b></u>
4	<i>d</i>	12.4	21.6	16.2	1.2	3.0	2.2	8.2	11.1	7.6
	<i>p</i>	<u><b>&lt;0.001</b></u>	<u><b>&lt;0.001</b></u>	<u><b>&lt;0.001</b></u>	0.179	<b>0.014</b>	<b>0.038</b>	<u><b>&lt;0.001</b></u>	<u><b>&lt;0.001</b></u>	<u><b>&lt;0.001</b></u>
6	<i>d</i>	10.7	15.8	9.4	0.7	2.3	3.6	12.4	8.9	27.9
	<i>p</i>	<u><b>&lt;0.001</b></u>	<u><b>&lt;0.001</b></u>	<u><b>&lt;0.001</b></u>	0.398	<b>0.030</b>	<u><b>0.007</b></u>	<u><b>&lt;0.001</b></u>	<u><b>&lt;0.001</b></u>	<u><b>&lt;0.001</b></u>
12	<i>d</i>	6.9	14.2	20.2	0.0	2.9	1.8	5.8	17.0	5.8
	<i>p</i>	<u><b>0.001</b></u>	<u><b>&lt;0.001</b></u>	<u><b>&lt;0.001</b></u>	0.971	<b>0.015</b>	0.068	<u><b>0.001</b></u>	<u><b>&lt;0.001</b></u>	<u><b>0.001</b></u>
24	<i>d</i>	6.7	42.2	12.4	2.3	2.0	9.4	16.5	12.0	27.6
	<i>p</i>	<u><b>0.001</b></u>	<u><b>&lt;0.001</b></u>	<u><b>&lt;0.001</b></u>	<b>0.031</b>	0.050	<u><b>&lt;0.001</b></u>	<u><b>&lt;0.001</b></u>	<u><b>&lt;0.001</b></u>	<u><b>&lt;0.001</b></u>
48	<i>d</i>	4.8	13.2	9.5	0.0	2.3	3.0	9.2	12.4	15.4
	<i>p</i>	<u><b>0.002</b></u>	<u><b>&lt;0.001</b></u>	<u><b>&lt;0.001</b></u>	0.948	<b>0.031</b>	<b>0.013</b>	<u><b>&lt;0.001</b></u>	<u><b>&lt;0.001</b></u>	<u><b>&lt;0.001</b></u>

time (h)		<b>D</b>			<b>E</b>			<b>F</b>		
		CC-4532 vs. <i>vtc1</i>	<i>vtc1</i> vs. <i>VTC1</i>	CC-4532 vs. <i>VTC1</i>	CC-4532 vs. <i>vtc1</i>	<i>vtc1</i> vs. <i>VTC1</i>	CC-4532 vs. <i>VTC1</i>	CC-4532 vs. <i>vtc1</i>	<i>vtc1</i> vs. <i>VTC1</i>	CC-4532 vs. <i>VTC1</i>
0	<i>d</i>	5.6	0.3	5.0	3.3	0.0	1.3	0.3	0.2	1.9
	<i>p</i>	<u><b>&lt;0.001</b></u>	0.679	<u><b>&lt;0.001</b></u>	<u><b>0.003</b></u>	0.946	0.123	0.704	0.743	<b>0.039</b>
2	<i>d</i>	5.0	0.4	2.9	1.5	3.6	2.2	2.5	2.6	1.4
	<i>p</i>	<u><b>&lt;0.001</b></u>	0.620	<u><b>0.007</b></u>	0.081	<u><b>0.002</b></u>	<b>0.022</b>	<b>0.012</b>	<b>0.010</b>	0.096
4	<i>d</i>	0.4	6.7	6.3	2.6	0.8	0.5	0.5	6.3	4.8
	<i>p</i>	0.600	<u><b>&lt;0.001</b></u>	<u><b>&lt;0.001</b></u>	<b>0.011</b>	0.294	0.545	0.499	<u><b>&lt;0.001</b></u>	<u><b>&lt;0.001</b></u>
6	<i>d</i>	4.3	2.6	4.1	5.2	3.3	2.6	5.9	1.0	4.4
	<i>p</i>	<u><b>0.001</b></u>	<b>0.010</b>	<u><b>0.001</b></u>	<u><b>&lt;0.001</b></u>	<u><b>0.003</b></u>	<b>0.011</b>	<u><b>&lt;0.001</b></u>	0.218	<u><b>0.001</b></u>
12	<i>d</i>	10.9	0.4	2.2	2.3	2.8	1.0	4.9	1.3	0.7
	<i>p</i>	<u><b>&lt;0.001</b></u>	0.624	<b>0.022</b>	<b>0.016</b>	<u><b>0.007</b></u>	0.227	<u><b>&lt;0.001</b></u>	0.105	0.359
24	<i>d</i>	8.4	2.7	5.6	0.4	6.1	1.0	8.2	4.4	6.2
	<i>p</i>	<u><b>&lt;0.001</b></u>	<b>0.008</b>	<u><b>&lt;0.001</b></u>	0.625	<u><b>&lt;0.001</b></u>	0.213	<u><b>&lt;0.001</b></u>	0.001	<u><b>&lt;0.001</b></u>
48	<i>d</i>	7.6	2.9	3.6	2.7	3.6	5.4	4.1	1.0	1.0
	<i>p</i>	<u><b>&lt;0.001</b></u>	<b>0.006</b>	<b>0.002</b>	<u><b>0.009</b></u>	<u><b>0.002</b></u>	<u><b>&lt;0.001</b></u>	<u><b>0.001</b></u>	0.196	0.210

## 6. Appendix

**Supplemental Table 26.** Statistical significance of chlorophyll content (steady state). Cohen's *d*-value was computed as a measure of effect size between the individual conditions, absolute *d*-values are shown in the left column. For statistical significance between conditions, unpaired, two-tailed Student's *t*-test was applied, and the resulting *p*-values are shown in the right column. *P*-values passing a significance threshold of  $\alpha = 0.05$  are highlighted in bold,  $\alpha = 0.01$  in bold and underlined,  $\alpha = 0.001$  are labeled < 0.001.

	photoheterotrophic vs. photoautotrophic	
	<i>d</i>	<i>p</i>
limited	6.5	<b>&lt;0.001</b>
deficient	1.5	0.073
replete	0.1	0.872

**Supplemental Table 27.** Statistical significance of chlorophyll content (dynamic). **A:** Comparison of + acetate cultures and no acetate control cultures for each time and **B:** the comparison of iron concentrations with and without acetate. Cohen's *d*-value was computed as a measure of effect size between the individual conditions, absolute *d*-values are shown at the top of each cell. For statistical significance between conditions, unpaired, two-tailed Student's *t*-test was applied, and the resulting *p*-values are shown at the bottom of each cell. *P*-values passing a significance threshold of  $\alpha = 0.05$  are highlighted in bold,  $\alpha = 0.01$  in bold and underlined,  $\alpha = 0.001$  are labeled < 0.001.

<b>A</b> + acetate vs. no acetate				<b>B</b>								
				+ acetate			no acetate					
h	0.25	1.0	20 $\mu$ M Fe	0.25 vs. 1.0 $\mu$ M Fe	1.0 vs. 20 $\mu$ M Fe	0.25 vs. 20 $\mu$ M Fe	0.25 vs. 1.0 $\mu$ M Fe	1.0 vs. 20 $\mu$ M Fe	0.25 vs. 20 $\mu$ M Fe			
-2	<i>d</i> 1.2	<i>d</i> 1.0	<i>d</i> 0.2	<i>d</i> 0.5	<i>d</i> 0.1	<i>d</i> 0.8	<i>d</i> 1.6	<i>d</i> 0.6	<i>d</i> 0.4			
	<i>p</i> 0.138	<i>p</i> 0.214	<i>p</i> 0.812	<i>p</i> 0.509	<i>p</i> 0.857	<i>p</i> 0.295	<i>p</i> 0.060	<i>p</i> 0.458	<i>p</i> 0.579			
0	<i>d</i> 0.5	<i>d</i> 0.4	<i>d</i> 0.8	<i>d</i> 0.3	<i>d</i> 0.8	<i>d</i> 0.9	<i>d</i> 0.6	<i>d</i> 0.1	<i>d</i> 0.4			
	<i>p</i> 0.489	<i>p</i> 0.613	<i>p</i> 0.299	<i>p</i> 0.675	<i>p</i> 0.321	<i>p</i> 0.232	<i>p</i> 0.454	<i>p</i> 0.938	<i>p</i> 0.570			
1	<i>d</i> 1.4	<i>d</i> 0.2	<i>d</i> 2.1	<i>d</i> 0.8	<i>d</i> 0.1	<i>d</i> 1.4	<i>d</i> 0.6	<i>d</i> 1.3	<i>d</i> 1.8			
	<i>p</i> 0.101	<i>p</i> 0.774	<i>p</i> <b>0.024</b>	<i>p</i> 0.300	<i>p</i> 0.875	<i>p</i> 0.087	<i>p</i> 0.395	<i>p</i> 0.116	<i>p</i> <b>0.048</b>			
2	<i>d</i> 1.4	<i>d</i> 0.1	<i>d</i> 1.1	<i>d</i> <0.1	<i>d</i> <0.1	<i>d</i> <0.1	<i>d</i> 2.2	<i>d</i> 1.1	<i>d</i> <0.1			
	<i>p</i> 0.101	<i>p</i> 0.913	<i>p</i> 0.172	<i>p</i> 0.968	<i>p</i> 0.972	<i>p</i> 0.990	<i>p</i> <b>0.021</b>	<i>p</i> 0.156	<i>p</i> 0.971			
4	<i>d</i> 1.7	<i>d</i> 0.4	<i>d</i> 1.1	<i>d</i> 1.2	<i>d</i> 0.4	<i>d</i> 0.3	<i>d</i> 0.2	<i>d</i> 0.5	<i>d</i> 0.2			
	<i>p</i> 0.052	<i>p</i> 0.554	<i>p</i> 0.183	<i>p</i> 0.144	<i>p</i> 0.601	<i>p</i> 0.660	<i>p</i> 0.772	<i>p</i> 0.546	<i>p</i> 0.743			
6	<i>d</i> 2.6	<i>d</i> 1.4	<i>d</i> 1.1	<i>d</i> 3.7	<i>d</i> 2.7	<i>d</i> 6.4	<i>d</i> 0.8	<i>d</i> 0.5	<i>d</i> 0.2			
	<i>p</i> <b>0.010</b>	<i>p</i> 0.101	<i>p</i> 0.175	<i>p</i> <b>0.002</b>	<i>p</i> <b>0.009</b>	<i>p</i> <b>&lt;0.001</b>	<i>p</i> 0.312	<i>p</i> 0.523	<i>p</i> 0.762			
8	<i>d</i> 5.6	<i>d</i> 0.3	<i>d</i> 2.5	<i>d</i> 6.2	<i>d</i> 1.1	<i>d</i> 7.4	<i>d</i> 1.0	<i>d</i> 1.8	<i>d</i> 0.9			
	<i>p</i> <b>&lt;0.001</b>	<i>p</i> 0.734	<i>p</i> <b>0.013</b>	<i>p</i> <b>&lt;0.001</b>	<i>p</i> 0.180	<i>p</i> <b>&lt;0.001</b>	<i>p</i> 0.194	<i>p</i> <b>0.047</b>	<i>p</i> 0.272			
12	<i>d</i> 8.7	<i>d</i> 1.3	<i>d</i> 0.1	<i>d</i> 4.7	<i>d</i> 0.2	<i>d</i> 3.7	<i>d</i> 0.1	<i>d</i> 0.8	<i>d</i> 1.1			
	<i>p</i> <b>&lt;0.001</b>	<i>p</i> 0.116	<i>p</i> 0.843	<i>p</i> <b>0.001</b>	<i>p</i> 0.740	<i>p</i> <b>0.002</b>	<i>p</i> 0.911	<i>p</i> 0.297	<i>p</i> 0.158			
18	<i>d</i> 4.5	<i>d</i> 1.1	<i>d</i> 0.4	<i>d</i> 6.7	<i>d</i> 0.8	<i>d</i> 6.2	<i>d</i> 1.7	<i>d</i> 0.6	<i>d</i> 1.3			
	<i>p</i> <b>0.001</b>	<i>p</i> 0.184	<i>p</i> 0.591	<i>p</i> <b>&lt;0.001</b>	<i>p</i> 0.315	<i>p</i> <b>&lt;0.001</b>	<i>p</i> <b>0.050</b>	<i>p</i> 0.402	<i>p</i> 0.108			
24	<i>d</i> 5.2	<i>d</i> 1.2	<i>d</i> 0.8	<i>d</i> 9.0	<i>d</i> 0.1	<i>d</i> 9.9	<i>d</i> 0.8	<i>d</i> 2.2	<i>d</i> 0.3			
	<i>p</i> <b>&lt;0.001</b>	<i>p</i> 0.153	<i>p</i> 0.282	<i>p</i> <b>&lt;0.001</b>	<i>p</i> 0.906	<i>p</i> <b>&lt;0.001</b>	<i>p</i> 0.276	<i>p</i> <b>0.019</b>	<i>p</i> 0.711			
48	<i>d</i> 1.7	<i>d</i> 1.0	<i>d</i> <0.1	<i>d</i> 0.1	<i>d</i> 1.0	<i>d</i> 0.9	<i>d</i> 1.2	<i>d</i> 0.2	<i>d</i> 0.8			
	<i>p</i> 0.058	<i>p</i> 0.206	<i>p</i> 0.957	<i>p</i> 0.889	<i>p</i> 0.195	<i>p</i> 0.246	<i>p</i> 0.150	<i>p</i> 0.758	<i>p</i> 0.291			

## 6. Appendix

**Supplemental Table 28.** Statistical significance of cell density. **A:** Comparison of + acetate cultures and no acetate control cultures for each time and **B:** the comparison of iron concentrations with and without acetate. Cohen's *d*-value was computed as a measure of effect size between the individual conditions, absolute *d*-values are shown at the top of each cell. For statistical significance between conditions, unpaired, two-tailed Student's *t*-test was applied, and the resulting *p*-values are shown at the bottom of each cell. *P*-values passing a significance threshold of  $\alpha = 0.05$  are highlighted in bold,  $\alpha = 0.01$  in bold and underlined,  $\alpha = 0.001$  are labeled  $< 0.001$ .

<b>A</b>				<b>B</b>						
+ acetate vs. no acetate				+ acetate			no acetate			
	h	0.25	1.0	20 $\mu$ M Fe	0.25 vs. 1.0 $\mu$ M Fe	1.0 vs. 20 $\mu$ M Fe	0.25 vs. 20 $\mu$ M Fe	0.25 vs. 1.0 $\mu$ M Fe	1.0 vs. 20 $\mu$ M Fe	0.25 vs. 20 $\mu$ M Fe
-2	<i>d</i>	0.7	0.4	0.3	0.2	0.6	0.7	1.2	0.8	0.2
	<i>p</i>	0.384	0.619	0.655	0.754	0.455	0.338	0.146	0.295	0.793
0	<i>d</i>	0.5	<0.1	0.5	0.9	0.1	1.0	0.8	0.5	1.2
	<i>p</i>	0.502	0.976	0.486	0.272	0.846	0.211	0.287	0.471	0.143
1	<i>d</i>	<0.1	0.8	0.9	0.6	0.1	0.7	0.2	1.1	0.8
	<i>p</i>	0.974	0.289	0.263	0.449	0.945	0.362	0.818	0.186	0.278
2	<i>d</i>	1.3	0.3	1.2	0.6	<0.1	0.7	0.8	1.1	0.1
	<i>p</i>	0.111	0.694	0.152	0.417	1.000	0.334	0.300	0.187	0.942
4	<i>d</i>	0.9	0.1	1.0	1.2	0.1	1.2	0.4	0.7	0.4
	<i>p</i>	0.270	0.867	0.211	0.150	0.844	0.129	0.567	0.377	0.592
6	<i>d</i>	0.1	2.8	1.9	1.1	<0.1	1.3	1.3	0.8	0.4
	<i>p</i>	0.840	<b>0.008</b>	<b>0.034</b>	0.158	0.972	0.107	0.111	0.279	0.601
8	<i>d</i>	1.3	2.8	3.6	3.8	0.9	4.8	1.5	0.4	0.8
	<i>p</i>	0.121	<b>0.008</b>	<b>0.002</b>	<b>0.002</b>	0.228	<b>0.001</b>	0.084	0.585	0.303
12	<i>d</i>	1.7	2.7	6.3	1.3	0.8	0.9	<0.1	0.1	0.1
	<i>p</i>	0.056	<b>0.008</b>	<b>&lt;0.001</b>	0.114	0.301	0.238	0.995	0.931	0.910
18	<i>d</i>	0.2	4.4	1.4	1.5	1.1	1.1	0.6	0.7	0.2
	<i>p</i>	0.805	<b>0.001</b>	0.091	0.074	0.175	0.175	0.421	0.387	0.773
24	<i>d</i>	1.9	3.9	0.7	2.0	8.3	2.4	<0.1	0.4	0.4
	<i>p</i>	<b>0.034</b>	<b>0.001</b>	0.343	<b>0.032</b>	<b>&lt;0.001</b>	<b>0.015</b>	0.990	0.615	0.549
48	<i>d</i>	10.8	3.3	2.9	18.8	0.3	13.0	1.2	0.4	1.6
	<i>p</i>	<b>&lt;0.001</b>	<b>0.003</b>	<b>0.006</b>	<b>&lt;0.001</b>	0.651	<b>&lt;0.001</b>	0.130	0.579	0.059

**Supplemental Table 29.** Statistical significance of chlorophyll content (cycloheximide). Cohen's *d*-value was computed as a measure of effect size between the individual conditions, absolute *d*-values are shown in the first and third column. For statistical significance between conditions, unpaired, two-tailed Student's *t*-test was applied, and the resulting *p*-values are shown in the second and fourth column. *P*-values passing a significance threshold of  $\alpha = 0.05$  are highlighted in bold,  $\alpha = 0.01$  in bold and underlined,  $\alpha = 0.001$  are labeled  $< 0.001$ .

h	+ CHX		- CHX	
	<i>d</i>	<i>p</i>	<i>d</i>	<i>p</i>
0	0.4	0.617	0.5	0.480
2	0.9	0.322	1.4	0.100
4	0.1	0.864	1.7	0.053
6	0.1	0.891	2.7	<b>0.010</b>
8	0.2	0.838	5.8	<b>&lt;0.001</b>
12	0.4	0.638	8.8	<b>&lt;0.001</b>
18	1.5	0.131	4.5	<b>0.001</b>
24	0.1	0.916	5.2	<b>&lt;0.001</b>
48	0.5	0.609	6.2	<b>&lt;0.001</b>

## 6. Appendix

**Supplemental Table 30.** Statistical significance of oxygen consumption. **A:** Comparison of + acetate cultures and no acetate control cultures for each time and **B:** the comparison of iron concentrations with and without acetate. Cohen's *d*-value was computed as a measure of effect size between the individual conditions, absolute *d*-values are shown at the top of each cell. For statistical significance between conditions, unpaired, two-tailed Student's *t*-test was applied, and the resulting *p*-values are shown at the bottom of each cell. *P*-values passing a significance threshold of  $\alpha = 0.05$  are highlighted in bold,  $\alpha = 0.01$  in bold and underlined,  $\alpha = 0.001$  are labeled  $< 0.001$ .

<b>A</b>		+ acetate vs. no acetate			<b>B</b>		+ acetate			no acetate		
		0.25	1.0	20 $\mu$ M Fe			0.25 vs. 1.0 $\mu$ M Fe	1.0 vs. 20 $\mu$ M Fe	0.25 vs. 20 $\mu$ M Fe	0.25 vs. 1.0 $\mu$ M Fe	1.0 vs. 20 $\mu$ M Fe	0.25 vs. 20 $\mu$ M Fe
0	<i>d</i>	2.6	4.0	4.7								
0	<i>p</i>	<b>0.034</b>	<b>0.008</b>	<b>0.005</b>								
6	<i>d</i>	4.0	8.4	11.6								
6	<i>p</i>	<b>0.008</b>	<b>0.001</b>	<b>&lt;0.001</b>								
12	<i>d</i>	3.1	8.8	16.2								
12	<i>p</i>	<b>0.019</b>	<b>&lt;0.001</b>	<b>&lt;0.001</b>								
24	<i>d</i>	3.9	9.8	22.0								
24	<i>p</i>	<b>0.009</b>	<b>&lt;0.001</b>	<b>&lt;0.001</b>								
48	<i>d</i>	7.7	19.6	21.9								
48	<i>p</i>	<b>0.001</b>	<b>&lt;0.001</b>	<b>&lt;0.001</b>								
-2	<i>d</i>	1.0	2.3	1.5								
-2	<i>p</i>	0.292	<b>0.049</b>	0.148								
0	<i>d</i>	2.2	1.2	1.1								
0	<i>p</i>	0.057	0.228	0.244	0.740	0.414	0.474					
2	<i>d</i>	2.0	2.9	3.9								
2	<i>p</i>	0.067	<b>0.023</b>	<b>0.009</b>								
4	<i>d</i>	2.7	0.5	3.6								
4	<i>p</i>	<b>0.031</b>	0.585	<b>0.011</b>								
6	<i>d</i>	3.7	2.0	4.7								
6	<i>p</i>	<b>0.010</b>	0.069	<b>0.005</b>	0.536	0.627	0.773					
8	<i>d</i>	2.8	2.3	4.0								
8	<i>p</i>	<b>0.026</b>	<b>0.046</b>	<b>0.008</b>								
12	<i>d</i>	7.3	1.6	13.9								
12	<i>p</i>	<b>0.001</b>	0.125	<b>&lt;0.001</b>	0.732	0.252	0.154					
18	<i>d</i>	4.9	0.7	9.6								
18	<i>p</i>	<b>0.004</b>	0.420	<b>&lt;0.001</b>								
24	<i>d</i>	5.4	1.3	8.4								
24	<i>p</i>	<b>0.003</b>	0.180	<b>&lt;0.001</b>	0.657	0.846	0.448					
48	<i>d</i>	11.7	1.6	15.9								
48	<i>p</i>	<b>&lt;0.001</b>	0.121	<b>&lt;0.001</b>	0.117	<b>0.035</b>	0.624					

## 6. Appendix

**Supplemental Table 31.** Statistical significance of oxygen evolution. **A:** Comparison of + acetate cultures and no acetate control cultures for each time and **B:** the comparison of iron concentrations with and without acetate. Cohen's *d*-value was computed as a measure of effect size between the individual conditions, absolute *d*-values are shown at the top of each cell. For statistical significance between conditions, unpaired, two-tailed Student's *t*-test was applied, and the resulting *p*-values are shown at the bottom of each cell. *P*-values passing a significance threshold of  $\alpha = 0.05$  are highlighted in bold,  $\alpha = 0.01$  in bold and underlined,  $\alpha = 0.001$  are labeled  $< 0.001$ .

<b>A</b> + acetate vs. no acetate				<b>B</b>						
				+ acetate			no acetate			
h	0.25 1.0 20 $\mu$ M Fe			0.25 vs. 1.0 $\mu$ M Fe	1.0 vs. 20 $\mu$ M Fe	0.25 vs. 20 $\mu$ M Fe	0.25 vs. 1.0 $\mu$ M Fe	1.0 vs. 20 $\mu$ M Fe	0.25 vs. 20 $\mu$ M Fe	
0	<i>d</i>	2.0	4.8	1.9						
	<i>p</i>	0.068	<b>0.004</b>	0.078						
6	<i>d</i>	4.8	0.6	3.9	3.8	1.6	5.1			
	<i>p</i>	<b>0.004</b>	0.529	<b>0.009</b>	<b>0.010</b>	0.119	<b>0.003</b>			
12	<i>d</i>	5.9	5.5	4.6	3.1	2.3	4.8	1.6	0.1	
	<i>p</i>	<b>0.002</b>	<b>0.003</b>	<b>0.005</b>	<b>0.020</b>	<b>0.050</b>	<b>0.004</b>	0.120	0.923	
24	<i>d</i>	6.3	8.8	6.5	7.0	0.6	7.2			
	<i>p</i>	<b>0.001</b>	<b>&lt;0.001</b>	<b>0.001</b>	<b>0.001</b>	0.506	<b>0.001</b>			
48	<i>d</i>	9.0	4.5	6.4	10.6	3.5	15.1			
	<i>p</i>	<b>&lt;0.001</b>	<b>0.005</b>	<b>0.001</b>	<b>&lt;0.001</b>	<b>0.012</b>	<b>&lt;0.001</b>			
					11.4	5.2	18.2	1.5	0.4	
					<b>&lt;0.001</b>	<b>0.003</b>	<b>&lt;0.001</b>	0.138	0.663	
					27.3	1.7	24.3			
					<b>&lt;0.001</b>	0.102	<b>&lt;0.001</b>			
					20.5	0.9	14.8	2.1	1.0	
					<b>&lt;0.001</b>	0.342	<b>&lt;0.001</b>	0.059	0.296	
					25.3	0.9	29.4			
					<b>&lt;0.001</b>	0.341	<b>&lt;0.001</b>			
					21.1	0.2	19.5	1.6	1.9	
					<b>&lt;0.001</b>	0.853	<b>&lt;0.001</b>	0.119	0.075	
					14.2	0.6	14.1	1.1	1.1	
					<b>&lt;0.001</b>	0.498	<b>&lt;0.001</b>	0.236	0.263	
									3.0	
									<b>0.021</b>	
									$<0.1$	
									0.985	

**Supplemental Table 32.** Statistical significance of maximum quantum efficiency of PSII ( $F_v/F_m$ ). Cohen's *d*-value was computed as a measure of effect size between the individual conditions, absolute *d*-values are shown in the first, third, and fifth column. For statistical significance between conditions, unpaired, two-tailed Student's *t*-test was applied, and the resulting *p*-values are shown in the second, fourth, and sixth column. *P*-values passing a significance threshold of  $\alpha = 0.05$  are highlighted in bold,  $\alpha = 0.01$  in bold and underlined,  $\alpha = 0.001$  are labeled  $< 0.001$ .

+ acetate vs. no acetate						
0.25 1.0 20 $\mu$ M Fe						
h	<i>d</i>	<i>p</i>	<i>d</i>	<i>p</i>	<i>d</i>	<i>p</i>
-2	0.4	0.554	0.8	0.304	0.5	0.496
0	0.1	0.931	0.4	0.577	0.2	0.764
2	0.3	0.718	0.0	1.000	1.8	<b>0.045</b>
4	0.9	0.264	0.4	0.620	0.9	0.253
6	0.4	0.566	1.2	0.147	1.2	0.140
8	1.4	0.092	1.4	0.094	0.9	0.253
12	0.8	0.299	0.9	0.254	0.1	0.908
18	2.7	<b>0.008</b>	0.3	0.660	0.4	0.599
24	6.0	<b>&lt;0.001</b>	0.7	0.331	0.1	0.908
48	5.1	<b>&lt;0.001</b>	0.7	0.387	0.8	0.286

## 6. Appendix

**Supplemental Table 33.** Statistical significance of carbon to nitrogen ratio. **A:** Comparison of + acetate cultures and no acetate control cultures for each time and **B:** comparing +acetate with no acetate control. Cohen's *d*-value was computed as a measure of effect size between the individual conditions, absolute *d*-values are shown at the top of each cell. For statistical significance between conditions, unpaired, two-tailed Student's *t*-test was applied, and the resulting *p*-values are shown at the bottom of each cell. *P*-values passing a significance threshold of  $\alpha = 0.05$  are highlighted in bold,  $\alpha = 0.01$  in bold and underlined,  $\alpha = 0.001$  are labeled < 0.001.

<b>A</b> + acetate vs. no acetate				<b>B</b>						
				+ acetate			no acetate			
h	0.25	1.0	20 $\mu$ M Fe	0.25 vs. 1.0 $\mu$ M Fe	1.0 vs. 20 $\mu$ M Fe	0.25 vs. 20 $\mu$ M Fe	0.25 vs. 1.0 $\mu$ M Fe	1.0 vs. 20 $\mu$ M Fe	0.25 vs. 20 $\mu$ M Fe	
0	<i>d</i> 0.6	<i>d</i> 1.5	<i>d</i> 0.1	<i>d</i> 5.4	<i>d</i> 0.6	<i>d</i> 3.9	<i>d</i> 5.1	<i>d</i> 1.3	<i>d</i> 28.1	
	<i>p</i> 0.155	<i>p</i> 0.138	<i>p</i> 0.944	<i>p</i> <b>0.003</b>	<i>p</i> 0.521	<i>p</i> <b>0.009</b>	<i>p</i> <b>0.003</b>	<i>p</i> 0.188	<i>p</i> <b>&lt;0.001</b>	
2	<i>d</i> 1.4	<i>d</i> 5.1	<i>d</i> 0.6	<i>d</i> 7.3	<i>d</i> 5.0	<i>d</i> 11.4	<i>d</i> 6.1	<i>d</i> 3.7	<i>d</i> 8.0	
	<i>p</i> <b>0.002</b>	<i>p</i> <b>0.003</b>	<i>p</i> 0.521	<i>p</i> <b>0.001</b>	<i>p</i> <b>0.004</b>	<i>p</i> <b>&lt;0.001</b>	<i>p</i> <b>0.002</b>	<i>p</i> <b>0.011</b>	<i>p</i> <b>0.001</b>	
4	<i>d</i> 2.8	<i>d</i> 1.6	<i>d</i> 3.3	<i>d</i> 4.9	<i>d</i> 0.2	<i>d</i> 8.0	<i>d</i> 4.5	<i>d</i> 0.5	<i>d</i> 5.3	
	<i>p</i> <b>0.028</b>	<i>p</i> 0.118	<i>p</i> <b>0.016</b>	<i>p</i> <b>0.004</b>	<i>p</i> 0.856	<i>p</i> <b>0.001</b>	<i>p</i> <b>0.005</b>	<i>p</i> 0.583	<i>p</i> <b>0.003</b>	
6	<i>d</i> 2.5	<i>d</i> 12.3	<i>d</i> 4.0	<i>d</i> 3.6	<i>d</i> 3.0	<i>d</i> 4.8	<i>d</i> 5.5	<i>d</i> 0.6	<i>d</i> 5.4	
	<i>p</i> <b>0.039</b>	<i>p</i> <b>&lt;0.001</b>	<i>p</i> <b>0.008</b>	<i>p</i> <b>0.012</b>	<i>p</i> <b>0.020</b>	<i>p</i> <b>0.004</b>	<i>p</i> <b>0.002</b>	<i>p</i> 0.472	<i>p</i> <b>0.003</b>	
8	<i>d</i> 7.3	<i>d</i> 3.6	<i>d</i> 3.1	<i>d</i> 11.6	<i>d</i> 0.5	<i>d</i> 6.2	<i>d</i> 5.6	<i>d</i> 1.1	<i>d</i> 6.7	
	<i>p</i> <b>0.001</b>	<i>p</i> <b>0.011</b>	<i>p</i> <b>0.020</b>	<i>p</i> <b>&lt;0.001</b>	<i>p</i> 0.572	<i>p</i> <b>0.002</b>	<i>p</i> <b>0.002</b>	<i>p</i> 0.262	<i>p</i> <b>0.001</b>	
12	<i>d</i> 6.1	<i>d</i> 3.4	<i>d</i> 4.0	<i>d</i> 6.9	<i>d</i> 0.3	<i>d</i> 7.3	<i>d</i> 2.3	<i>d</i> 1.3	<i>d</i> 2.7	
	<i>p</i> <b>0.002</b>	<i>p</i> <b>0.014</b>	<i>p</i> <b>0.008</b>	<i>p</i> <b>0.001</b>	<i>p</i> 0.731	<i>p</i> <b>0.001</b>	<i>p</i> <b>0.048</b>	<i>p</i> 0.196	<i>p</i> <b>0.030</b>	
18	<i>d</i> 4.4	<i>d</i> 5.0	<i>d</i> 4.9	<i>d</i> 7.0	<i>d</i> 1.9	<i>d</i> 5.8	<i>d</i> 3.3	<i>d</i> 1.0	<i>d</i> 3.4	
	<i>p</i> <b>0.006</b>	<i>p</i> <b>0.004</b>	<i>p</i> <b>0.004</b>	<i>p</i> <b>0.001</b>	<i>p</i> 0.082	<i>p</i> <b>0.002</b>	<i>p</i> <b>0.015</b>	<i>p</i> 0.278	<i>p</i> <b>0.015</b>	
24	<i>d</i> 5.7	<i>d</i> 2.6	<i>d</i> 1.6	<i>d</i> 4.6	<i>d</i> 2.3	<i>d</i> 9.1	<i>d</i> 5.4	<i>d</i> 0.6	<i>d</i> 6.2	
	<i>p</i> <b>0.002</b>	<i>p</i> <b>0.034</b>	<i>p</i> 0.129	<i>p</i> <b>0.005</b>	<i>p</i> <b>0.048</b>	<i>p</i> <b>&lt;0.001</b>	<i>p</i> <b>0.003</b>	<i>p</i> 0.494	<i>p</i> <b>0.002</b>	
48	<i>d</i> 10.7	<i>d</i> 0.6	<i>d</i> 0.8	<i>d</i> 37.8	<i>d</i> 0.7	<i>d</i> 21.5	<i>d</i> 2.0	<i>d</i> 4.4	<i>d</i> 2.7	
	<i>p</i> <b>&lt;0.001</b>	<i>p</i> 0.507	<i>p</i> 0.409	<i>p</i> <b>&lt;0.001</b>	<i>p</i> 0.429	<i>p</i> <b>&lt;0.001</b>	<i>p</i> 0.075	<i>p</i> <b>0.006</b>	<i>p</i> <b>0.030</b>	

**Supplemental Table 34.** Statistical significance of carbon content. **A:** Comparison of + acetate cultures and no acetate control cultures for each time and **B:** comparing +acetate with no acetate control. Cohen's *d*-value was computed as a measure of effect size between the individual conditions, absolute *d*-values are shown at the top of each cell. For statistical significance between conditions, unpaired, two-tailed Student's *t*-test was applied, and the resulting *p*-values are shown at the bottom of each cell. *P*-values passing a significance threshold of  $\alpha = 0.05$  are highlighted in bold,  $\alpha = 0.01$  in bold and underlined,  $\alpha = 0.001$  are labeled < 0.001.

<b>A</b> + acetate vs. no acetate				<b>B</b>						
				+ acetate			no acetate			
h	0.25	1.0	20 $\mu$ M Fe	0.25 vs. 1.0 $\mu$ M Fe	1.0 vs. 20 $\mu$ M Fe	0.25 vs. 20 $\mu$ M Fe	0.25 vs. 1.0 $\mu$ M Fe	1.0 vs. 20 $\mu$ M Fe	0.25 vs. 20 $\mu$ M Fe	
-2	<i>d</i> 0.4	<i>d</i> 0.2	<i>d</i> 2.3	<i>d</i> 4.1	<i>d</i> 1.3	<i>d</i> 3.7	<i>d</i> 8.0	<i>d</i> 0.2	<i>d</i> 8.5	
	<i>p</i> 0.659	<i>p</i> 0.786	<i>p</i> <b>0.048</b>	<i>p</i> <b>0.007</b>	<i>p</i> 0.177	<i>p</i> <b>0.010</b>	<i>p</i> <b>0.001</b>	<i>p</i> 0.793	<i>p</i> <b>&lt;0.001</b>	
0	<i>d</i> 3.9	<i>d</i> 1.6	<i>d</i> 1.0	<i>d</i> 15.0	<i>d</i> 0.3	<i>d</i> 8.8	<i>d</i> 5.3	<i>d</i> 0.2	<i>d</i> 6.7	
	<i>p</i> <b>0.009</b>	<i>p</i> 0.117	<i>p</i> 0.278	<i>p</i> <b>&lt;0.001</b>	<i>p</i> 0.762	<i>p</i> <b>&lt;0.001</b>	<i>p</i> <b>0.003</b>	<i>p</i> 0.815	<i>p</i> <b>0.001</b>	
2	<i>d</i> 8.2	<i>d</i> 1.6	<i>d</i> 4.0	<i>d</i> 10.9	<i>d</i> 0.8	<i>d</i> 8.9	<i>d</i> 6.6	<i>d</i> 2.5	<i>d</i> 8.4	
	<i>p</i> <b>0.001</b>	<i>p</i> 0.119	<i>p</i> <b>0.008</b>	<i>p</i> <b>&lt;0.001</b>	<i>p</i> 0.407	<i>p</i> <b>&lt;0.001</b>	<i>p</i> <b>0.001</b>	<i>p</i> <b>0.036</b>	<i>p</i> <b>0.001</b>	
4	<i>d</i> 5.7	<i>d</i> 6.1	<i>d</i> 10.5	<i>d</i> 3.8	<i>d</i> 1.2	<i>d</i> 2.8	<i>d</i> 5.3	<i>d</i> 0.5	<i>d</i> 9.3	
	<i>p</i> <b>0.002</b>	<i>p</i> <b>0.002</b>	<i>p</i> <b>&lt;0.001</b>	<i>p</i> <b>0.010</b>	<i>p</i> 0.224	<i>p</i> <b>0.026</b>	<i>p</i> <b>0.003</b>	<i>p</i> 0.600	<i>p</i> <b>&lt;0.001</b>	
6	<i>d</i> 6.1	<i>d</i> 16.9	<i>d</i> 15.6	<i>d</i> 2.0	<i>d</i> 1.7	<i>d</i> 0.9	<i>d</i> 7.8	<i>d</i> <0.1	<i>d</i> 6.0	
	<i>p</i> <b>0.002</b>	<i>p</i> <b>&lt;0.001</b>	<i>p</i> <b>&lt;0.001</b>	<i>p</i> 0.072	<i>p</i> 0.105	<i>p</i> 0.317	<i>p</i> <b>0.001</b>	<i>p</i> 0.987	<i>p</i> <b>0.002</b>	
8	<i>d</i> 7.1	<i>d</i> 8.1	<i>d</i> 14.3	<i>d</i> 1.0	<i>d</i> 0.9	<i>d</i> 0.2	<i>d</i> 8.1	<i>d</i> 1.1	<i>d</i> 7.3	
	<i>p</i> <b>0.001</b>	<i>p</i> <b>0.001</b>	<i>p</i> <b>&lt;0.001</b>	<i>p</i> 0.306	<i>p</i> 0.353	<i>p</i> 0.811	<i>p</i> <b>0.001</b>	<i>p</i> 0.255	<i>p</i> <b>0.001</b>	
12	<i>d</i> 8.1	<i>d</i> 12.9	<i>d</i> 14.6	<i>d</i> 0.6	<i>d</i> 0.6	<i>d</i> 0.1	<i>d</i> 2.3	<i>d</i> 0.9	<i>d</i> 3.1	
	<i>p</i> <b>0.001</b>	<i>p</i> <b>&lt;0.001</b>	<i>p</i> <b>&lt;0.001</b>	<i>p</i> 0.537	<i>p</i> 0.489	<i>p</i> 0.925	<i>p</i> 0.050	<i>p</i> 0.336	<i>p</i> <b>0.020</b>	
18	<i>d</i> 13.8	<i>d</i> 9.0	<i>d</i> 43.4	<i>d</i> 1.1	<i>d</i> 2.3	<i>d</i> 2.5	<i>d</i> 2.5	<i>d</i> 1.8	<i>d</i> 4.8	
	<i>p</i> <b>&lt;0.001</b>	<i>p</i> <b>&lt;0.001</b>	<i>p</i> <b>&lt;0.001</b>	<i>p</i> 0.254	<i>p</i> <b>0.048</b>	<i>p</i> <b>0.037</b>	<i>p</i> <b>0.037</b>	<i>p</i> 0.089	<i>p</i> <b>0.004</b>	
24	<i>d</i> 9.5	<i>d</i> 14.1	<i>d</i> 17.9	<i>d</i> 0.8	<i>d</i> 7.7	<i>d</i> 6.6	<i>d</i> 4.0	<i>d</i> 1.7	<i>d</i> 7.5	
	<i>p</i> <b>&lt;0.001</b>	<i>p</i> <b>&lt;0.001</b>	<i>p</i> <b>&lt;0.001</b>	<i>p</i> 0.405	<i>p</i> <b>0.001</b>	<i>p</i> <b>0.001</b>	<i>p</i> <b>0.008</b>	<i>p</i> 0.103	<i>p</i> <b>0.001</b>	
48	<i>d</i> 17.4	<i>d</i> 0.3	<i>d</i> 0.3	<i>d</i> 14.6	<i>d</i> 1.0	<i>d</i> 22.1	<i>d</i> 3.5	<i>d</i> 2.6	<i>d</i> 4.7	
	<i>p</i> <b>&lt;0.001</b>	<i>p</i> 0.718	<i>p</i> 0.700	<i>p</i> <b>&lt;0.001</b>	<i>p</i> 0.289	<i>p</i> <b>&lt;0.001</b>	<i>p</i> <b>0.013</b>	<i>p</i> <b>0.034</b>	<i>p</i> <b>0.004</b>	



## 6. Appendix

**Supplemental Table 35.** Statistical significance of nitrogen content. **A:** Comparison of + acetate cultures and no acetate control cultures for each time and **B:** comparing +acetate with no acetate control. Cohen's *d*-value was computed as a measure of effect size between the individual conditions, absolute *d*-values are shown at the top of each cell. For statistical significance between conditions, unpaired, two-tailed Student's *t*-test was applied, and the resulting *p*-values are shown at the bottom of each cell. *P*-values passing a significance threshold of  $\alpha = 0.05$  are highlighted in bold,  $\alpha = 0.01$  in bold and underlined,  $\alpha = 0.001$  are labeled < 0.001.

<b>A</b> + acetate vs. no acetate				<b>B</b> + acetate							no acetate					
		20 $\mu$ M Fe			0.25 vs. 1.0 $\mu$ M Fe		1.0 vs. 20 $\mu$ M Fe		0.25 vs. 20 $\mu$ M Fe		0.25 vs. 1.0 $\mu$ M Fe		1.0 vs. 20 $\mu$ M Fe		0.25 vs. 20 $\mu$ M Fe	
h		0.25	1.0	20 $\mu$ M Fe	h	d	p	d	p	d	p	d	p	d	p	
-2	d	0.8	0.2	0.1	-2	d	1.2	0.4	2.0	0.5	0.1	0.8				
	p	0.363	0.810	0.921		p	0.221	0.684	0.068	0.567	0.864	0.360				
0	d	0.1	0.9	1.2	0	d	0.4	0.8	0.4	0.3	1.6	1.3				
	p	0.900	0.341	0.212		p	0.612	0.373	0.650	0.715	0.129	0.199				
2	d	0.1	3.2	4.8	2	d	2.0	7.4	2.5	0.3	0.7	0.6				
	p	0.876	<b>0.017</b>	<b>0.004</b>		p	0.066	<b>0.001</b>	<b>0.037</b>	0.773	0.438	0.471				
4	d	5.0	8.0	4.6	4	d	2.9	1.2	3.1	0.0	0.2	0.2				
	p	<b>0.004</b>	<b>0.001</b>	<b>0.005</b>		p	<b>0.023</b>	0.206	<b>0.019</b>	0.979	0.798	0.837				
6	d	6.4	11.1	10.4	6	d	2.9	4.5	6.3	1.6	0.5	0.6				
	p	<b>0.001</b>	<b>&lt;0.001</b>	<b>&lt;0.001</b>		p	<b>0.024</b>	<b>0.005</b>	<b>0.002</b>	0.122	0.544	0.536				
8	d	3.3	7.7	20.6	8	d	4.4	0.8	5.9	0.7	0.9	0.4				
	p	<b>0.015</b>	<b>0.001</b>	<b>&lt;0.001</b>		p	<b>0.006</b>	0.406	<b>0.002</b>	0.431	0.326	0.644				
12	d	11.8	22.0	11.3	12	d	15.2	0.4	7.3	0.3	0.7	0.9				
	p	<b>&lt;0.001</b>	<b>&lt;0.001</b>	<b>&lt;0.001</b>		p	<b>&lt;0.001</b>	0.671	<b>0.001</b>	0.765	0.412	0.323				
18	d	8.4	11.2	14.0	18	d	5.0	1.3	6.9	0.3	0.9	0.8				
	p	<b>0.001</b>	<b>&lt;0.001</b>	<b>&lt;0.001</b>		p	<b>0.004</b>	0.187	<b>0.001</b>	0.693	0.323	0.366				
24	d	6.6	8.4	10.1	24	d	4.9	2.7	2.9	0.3	1.1	0.8				
	p	<b>0.001</b>	<b>&lt;0.001</b>	<b>&lt;0.001</b>		p	<b>0.004</b>	<b>0.028</b>	<b>0.023</b>	0.745	0.242	0.399				
48	d	2.7	0.1	0.3	48	d	3.3	0.4	4.6	0.2	0.5	0.3				
	p	<b>0.029</b>	0.873	0.730		p	<b>0.015</b>	0.618	<b>0.005</b>	0.860	0.577	0.739				

**Supplemental Table 36.** Statistical significance of phosphorus content. **A:** Comparison of + acetate cultures and no acetate control cultures for each time and **B:** comparing +acetate with no acetate control. Cohen's *d*-value was computed as a measure of effect size between the individual conditions, absolute *d*-values are shown at the top of each cell. For statistical significance between conditions, unpaired, two-tailed Student's *t*-test was applied, and the resulting *p*-values are shown at the bottom of each cell. *P*-values passing a significance threshold of  $\alpha = 0.05$  are highlighted in bold,  $\alpha = 0.01$  in bold and underlined,  $\alpha = 0.001$  are labeled < 0.001.

<b>A</b> + acetate vs. no acetate				<b>B</b> + acetate							no acetate					
		20 $\mu$ M Fe			0.25 vs. 1.0 $\mu$ M Fe		1.0 vs. 20 $\mu$ M Fe		0.25 vs. 20 $\mu$ M Fe		0.25 vs. 1.0 $\mu$ M Fe		1.0 vs. 20 $\mu$ M Fe		0.25 vs. 20 $\mu$ M Fe	
h		0.25	1.0	20 $\mu$ M Fe	h	d	p	d	p	d	p	d	p	d	p	
0	d	3.6	0.9	2.5	0	d	1.7	0.5	1.5	0.6	0.3	0.4				
	p	<b>0.015</b>	0.353	<b>0.044</b>		p	0.050	0.468	0.081	0.626	0.783	0.703				
2	d	4.3	0.4	2.1	2	d	4.4	2.2	2.3	1.8	0.8	1.1				
	p	<b>0.007</b>	0.654	0.072		p	<b>0.001</b>	<b>0.021</b>	<b>0.018</b>	0.210	0.505	0.383				
4	d	2.7	1.5	1.9	4	d	2.1	0.4	1.2	0.6	0.7	0.8				
	p	<b>0.037</b>	0.157	0.097		p	<b>0.025</b>	0.555	0.132	0.637	0.535	0.485				
6	d	2.5	1.0	1.4	6	d	1.6	0.4	1.0	0.2	0.2	0.3				
	p	<b>0.045</b>	0.299	0.190		p	0.068	0.565	0.192	0.891	0.888	0.788				
8	d	3.5	3.1	1.1	8	d	1.1	0.4	0.5	1.1	4.2	1.5				
	p	<b>0.015</b>	<b>0.022</b>	0.272		p	0.156	0.565	0.498	0.383	0.053	0.270				
12	d	3.4	5.7	2.2	12	d	0.1	0.4	0.3	0.8	26.0	0.5				
	p	<b>0.017</b>	<b>0.003</b>	0.065		p	0.848	0.579	0.684	0.524	<b>0.001</b>	0.652				
18	d	3.2	3.6	3.5	18	d	0.3	0.2	0.5	0.2	1.2	1.0				
	p	<b>0.020</b>	<b>0.014</b>	<b>0.015</b>		p	0.696	0.837	0.546	0.861	0.363	0.424				
24	d	1.1	4.8	3.8	24	d	5.9	0.4	7.6	0.5	0.4	0.1				
	p	0.270	<b>0.005</b>	<b>0.012</b>		p	<b>&lt;0.001</b>	0.621	<b>&lt;0.001</b>	0.678	0.708	0.924				
48	d	2.4	2.4	1.0	48	d	4.9	1.7	0.8	0.2	1.8	2.3				
	p	<b>0.048</b>	0.053	0.306		p	<b>&lt;0.001</b>	0.056	0.324	0.836	0.217	0.144				

## 6. Appendix

**Supplemental Table 37.** Statistical significance of sulfur content. **A:** Comparison of + acetate cultures and no acetate control cultures for each time and **B:** comparing +acetate with no acetate control. Cohen's *d*-value was computed as a measure of effect size between the individual conditions, absolute *d*-values are shown at the top of each cell. For statistical significance between conditions, unpaired, two-tailed Student's *t*-test was applied, and the resulting *p*-values are shown at the bottom of each cell. *P*-values passing a significance threshold of  $\alpha = 0.05$  are highlighted in bold,  $\alpha = 0.01$  in bold and underlined,  $\alpha = 0.001$  are labeled < 0.001.

<b>A</b> + acetate vs. no acetate				<b>B</b> + acetate vs. no acetate						
				+ acetate			no acetate			
h	20 $\mu$ M Fe			0.25 vs. 1.0 $\mu$ M Fe	1.0 vs. 20 $\mu$ M Fe	0.25 vs. 20 $\mu$ M Fe	0.25 vs. 1.0 $\mu$ M Fe	1.0 vs. 20 $\mu$ M Fe	0.25 vs. 20 $\mu$ M Fe	
0	<i>d</i>	1.0	2.4	1.4						
	<i>p</i>	0.298	<b>0.049</b>	0.182						
2	<i>d</i>	0.6	6.2	0.4						
	<i>p</i>	0.498	<b>0.002</b>	0.672						
4	<i>d</i>	1.8	0.4	<0.1						
	<i>p</i>	0.103	0.699	0.984						
6	<i>d</i>	0.9	0.4	0.4						
	<i>p</i>	0.344	0.674	0.675						
8	<i>d</i>	1.6	0.4	0.7						
	<i>p</i>	0.139	0.666	0.466						
12	<i>d</i>	0.1	1.8	2.2						
	<i>p</i>	0.897	0.109	0.067						
18	<i>d</i>	0.9	3.5	2.8						
	<i>p</i>	0.345	<b>0.016</b>	<b>0.031</b>						
24	<i>d</i>	3.3	5.0	3.4						
	<i>p</i>	<b>0.018</b>	<b>0.004</b>	<b>0.017</b>						
48	<i>d</i>	<0.1	2.45	1.2						
	<i>p</i>	0.932	<b>0.046</b>	0.233						

**Supplemental Table 38.** Statistical significance of median cell volume. **A:** Comparison of + acetate cultures and no acetate control cultures for each time and **B:** comparing +acetate with no acetate control. Cohen's *d*-value was computed as a measure of effect size between the individual conditions, absolute *d*-values are shown at the top of each cell. For statistical significance between conditions, unpaired, two-tailed Student's *t*-test was applied, and the resulting *p*-values are shown at the bottom of each cell. *P*-values passing a significance threshold of  $\alpha = 0.05$  are highlighted in bold,  $\alpha = 0.01$  in bold and underlined,  $\alpha = 0.001$  are labeled < 0.001.

<b>A</b> + acetate vs. no acetate				<b>B</b> + acetate vs. no acetate						
				+ acetate			no acetate			
h	20 $\mu$ M Fe			0.25 vs. 1.0 $\mu$ M Fe	1.0 vs. 20 $\mu$ M Fe	0.25 vs. 20 $\mu$ M Fe	0.25 vs. 1.0 $\mu$ M Fe	1.0 vs. 20 $\mu$ M Fe	0.25 vs. 20 $\mu$ M Fe	
0	<i>d</i>	0.3	0.1	3.2						
	<i>p</i>	0.728	0.863	<b>0.004</b>						
2	<i>d</i>	3.2	6.9	7.6						
	<i>p</i>	<b>0.004</b>	<b>&lt;0.001</b>	<b>&lt;0.001</b>						
4	<i>d</i>	3.4	6.0	7.1						
	<i>p</i>	<b>0.003</b>	<b>&lt;0.001</b>	<b>&lt;0.001</b>						
6	<i>d</i>	4.6	10.1	5.1						
	<i>p</i>	<b>0.001</b>	<b>&lt;0.001</b>	<b>&lt;0.001</b>						
8	<i>d</i>	6.1	9.0	8.8						
	<i>p</i>	<b>&lt;0.001</b>	<b>&lt;0.001</b>	<b>&lt;0.001</b>						
12	<i>d</i>	5.0	3.3	5.0						
	<i>p</i>	<b>&lt;0.001</b>	<b>0.003</b>	<b>&lt;0.001</b>						
18	<i>d</i>	7.3	2.3	1.8						
	<i>p</i>	<b>&lt;0.001</b>	<b>0.016</b>	<b>0.042</b>						
24	<i>d</i>	7.5	1.0	5.2						
	<i>p</i>	<b>&lt;0.001</b>	0.225	<b>&lt;0.001</b>						
48	<i>d</i>	14.6	1.4	7.4						
	<i>p</i>	<b>&lt;0.001</b>	0.099	<b>&lt;0.001</b>						

## 6. Appendix

**Supplemental Table 39.** Statistical significance of iron content. **A:** Comparison of cellular iron content of + acetate cultures and no acetate control cultures for each time and **B:** comparing +acetate with no acetate control. **C:** Comparison of iron content normalized to sulfur content of + acetate cultures and no acetate control cultures for each time and **D:** comparing +acetate with no acetate control. Cohen's *d*-value was computed as a measure of effect size between the individual conditions, absolute *d*-values are shown at the top of each cell. For statistical significance between conditions, unpaired, two-tailed Student's *t*-test was applied, and the resulting *p*-values are shown at the bottom of each cell. *P*-values passing a significance threshold of  $\alpha = 0.05$  are highlighted in bold,  $\alpha = 0.01$  in bold and underlined,  $\alpha = 0.001$  are labeled < 0.001.

<b>A</b> + acetate vs. no acetate				<b>B</b> + acetate vs. no acetate								
h	0.25	1.0	20 $\mu$ M Fe	+ acetate			no acetate					
				0.25 vs. 1.0 $\mu$ M Fe	1.0 vs. 20 $\mu$ M Fe	0.25 vs. 20 $\mu$ M Fe	0.25 vs. 1.0 $\mu$ M Fe	1.0 vs. 20 $\mu$ M Fe	0.25 vs. 20 $\mu$ M Fe			
0	d 1.6	d 2.8	d 1.2	d 3.9	d 2.9	d 6.8	d 7.6	d 6.0	d 12.9			
	p 0.141	p <b>0.030</b>	p 0.239	p <b>0.001</b>	p <b>0.006</b>	p <b>&lt;0.001</b>	p <b>0.017</b>	p <b>0.026</b>	p <b>0.006</b>			
2	d 2.3	d 1.0	d 0.8	d 2.3	d 3.0	d 11.5	d 10.2	d 2.6	d 4.8			
	p 0.054	p 0.329	p 0.389	p <b>0.019</b>	p <b>0.005</b>	p <b>&lt;0.001</b>	p <b>0.009</b>	p 0.124	p <b>0.041</b>			
4	d 2.0	d 2.9	d 1.4	d 5.1	d 2.2	d 4.6	d 7.0	d 9.2	d 11.5			
	p 0.079	p <b>0.030</b>	p 0.185	p <b>&lt;0.001</b>	p <b>0.022</b>	p <b>0.001</b>	p <b>0.020</b>	p <b>0.012</b>	p <b>0.008</b>			
6	d 2.0	d 2.0	d 0.3	d 3.5	d 2.4	d 4.9	d 3.3	d 0.9	d 8.2			
	p 0.085	p 0.085	p 0.786	p <b>0.002</b>	p <b>0.016</b>	p <b>&lt;0.001</b>	p 0.082	p 0.472	p <b>0.014</b>			
8	d 2.4	d 3.3	d 0.8	d 9.9	d 2.3	d 5.6	d 9.6	d 2.3	d 6.5			
	p 0.053	p <b>0.020</b>	p 0.406	p <b>&lt;0.001</b>	p <b>0.017</b>	p <b>&lt;0.001</b>	p <b>0.011</b>	p 0.149	p <b>0.023</b>			
12	d 1.1	d 1.7	d 0.9	d 6.8	d 2.0	d 3.8	d 56.3	d 14.7	d 71.8			
	p 0.259	p 0.119	p 0.337	p <b>&lt;0.001</b>	p <b>0.030</b>	p <b>0.002</b>	p <b>&lt;0.001</b>	p <b>0.005</b>	p <b>&lt;0.001</b>			
18	d 5.2	d 0.1	d 2.4	d 12.2	d 5.1	d 13.2	d 12.1	d 3.9	d 15.1			
	p <b>0.004</b>	p 0.920	p <b>0.048</b>	p <b>&lt;0.001</b>	p <b>&lt;0.001</b>	p <b>&lt;0.001</b>	p <b>0.007</b>	p 0.060	p <b>0.004</b>			
24	d 5.5	d 6.6	d 7.0	d 2.7	d 1.8	d 3.7	d 13.6	d 6.0	d 10.1			
	p <b>0.003</b>	p <b>0.002</b>	p 0.001	p <b>0.010</b>	p <b>0.043</b>	p <b>0.002</b>	p <b>0.005</b>	p <b>0.027</b>	p <b>0.010</b>			
48	d 1.4	d 1.4	d 0.3	d 6.9	d 5.6	d 7.1	d 8.7	d 64.1	d 35.8			
	p 0.171	p 0.183	p 0.786	p <b>&lt;0.001</b>	p <b>&lt;0.001</b>	p <b>&lt;0.001</b>	p <b>0.013</b>	p <b>&lt;0.001</b>	p <b>0.001</b>			

<b>C</b> + acetate vs. no acetate				<b>D</b> + acetate vs. no acetate								
h	0.25	1.0	20 $\mu$ M Fe	+ acetate			no acetate					
				0.25 vs. 1.0 $\mu$ M Fe	1.0 vs. 20 $\mu$ M Fe	0.25 vs. 20 $\mu$ M Fe	0.25 vs. 1.0 $\mu$ M Fe	1.0 vs. 20 $\mu$ M Fe	0.25 vs. 20 $\mu$ M Fe			
0	d 0.4	d 0.7	d 0.5	d 27.4	d 8.9	d 22.6	d 3.5	d 1.5	d 3.6			
	p 0.687	p 0.474	p 0.605	p <b>&lt;0.001</b>	p <b>&lt;0.001</b>	p <b>&lt;0.001</b>	p 0.073	p 0.268	p 0.069			
2	d 0.7	d 0.8	d 0.4	d 2.5	d 1.2	d 18.8	d 2.1	d 1.4	d 1.9			
	p 0.448	p 0.398	p 0.705	p <b>0.012</b>	p 0.130	p <b>&lt;0.001</b>	p 0.169	p 0.302	p 0.192			
4	d 0.7	d 3.4	d 1.6	d 42.6	d 8.5	d 20.3	d 7.0	d 1.3	d 3.6			
	p 0.484	p <b>0.017</b>	p 0.148	p <b>&lt;0.001</b>	p <b>&lt;0.001</b>	p <b>&lt;0.001</b>	p <b>0.020</b>	p 0.318	p 0.069			
6	d 0.9	d 1.1	d 0.9	d 9.5	d 8.5	d 24.0	d 1.6	d 0.3	d 3.3			
	p 0.376	p 0.278	p 0.348	p <b>&lt;0.001</b>	p <b>&lt;0.001</b>	p <b>&lt;0.001</b>	p 0.242	p 0.786	p 0.080			
8	d 0.4	d 3.8	d 0.7	d 14.0	d 5.2	d 18.8	d 7.7	d 0.6	d 7.4			
	p 0.646	p <b>0.012</b>	p 0.479	p <b>&lt;0.001</b>	p <b>&lt;0.001</b>	p <b>&lt;0.001</b>	p <b>0.016</b>	p 0.635	p <b>0.018</b>			
12	d 1.0	d 4.6	d 3.2	d 13.6	d 4.7	d 10.7	d 5.1	d 3.6	d 8.1			
	p 0.323	p <b>0.006</b>	p <b>0.021</b>	p <b>&lt;0.001</b>	p <b>0.001</b>	p <b>&lt;0.001</b>	p <b>0.037</b>	p 0.068	p <b>0.015</b>			
18	d 8.0	d 11.0	d 2.1	d 21.8	d 7.3	d 17.8	d 20.7	d 1.9	d 7.9			
	p <b>0.001</b>	p <b>&lt;0.001</b>	p 0.074	p <b>&lt;0.001</b>	p <b>&lt;0.001</b>	p <b>&lt;0.001</b>	p <b>0.002</b>	p 0.198	p <b>0.016</b>			
24	d 0.7	d 0.6	d 5.7	d 11.5	d 7.9	d 29.5	d 5.2	d 6.6	d 9.2			
	p 0.454	p 0.522	p <b>0.003</b>	p <b>&lt;0.001</b>	p <b>&lt;0.001</b>	p <b>&lt;0.001</b>	p <b>0.036</b>	p <b>0.022</b>	p <b>0.012</b>			
48	d 2.7	d 15.9	d 2.1	d 30.1	d 11.9	d 16.1	d 16.5	d 3.3	d 5.0			
	p <b>0.037</b>	p <b>&lt;0.001</b>	p 0.072	p <b>&lt;0.001</b>	p <b>&lt;0.001</b>	p <b>&lt;0.001</b>	p <b>0.004</b>	p 0.079	p <b>0.038</b>			

6. Appendix

**Supplemental Table 40.** Statistical significance of magnesium content. **A:** Comparison of cellular magnesium content of + acetate cultures and no acetate control cultures for each time and **B:** comparing +acetate with no acetate control. **C:** Comparison of magnesium content normalized to sulfur content of + acetate cultures and no acetate control cultures for each time and **D:** comparing +acetate with no acetate control. Cohen's *d*-value was computed as a measure of effect size between the individual conditions, absolute *d*-values are shown at the top of each cell. For statistical significance between conditions, unpaired, two-tailed Student's *t*-test was applied, and the resulting *p*-values are shown at the bottom of each cell. *P*-values passing a significance threshold of  $\alpha = 0.05$  are highlighted in bold,  $\alpha = 0.01$  in bold and underlined,  $\alpha = 0.001$  are labeled < 0.001.

		+ acetate vs. no acetate					+ acetate			no acetate		
		0.25	1.0	20 $\mu$ M Fe			0.25 vs. 1.0 $\mu$ M Fe	1.0 vs. 20 $\mu$ M Fe	0.25 vs. 20 $\mu$ M Fe	0.25 vs. 1.0 $\mu$ M Fe	1.0 vs. 20 $\mu$ M Fe	0.25 vs. 20 $\mu$ M Fe
h	d	3.8	2.3	4.4	1.1	0.5	0.8	0.6	1.5	1.3		
	p	<b>0.012</b>	0.059	<b>0.007</b>	0.160	0.534	0.300	0.626	0.268	0.320		
2	d	4.6	2.1	5.6	3.9	2.4	1.9	0.8	0.3	2.0		
	p	<b>0.006</b>	0.071	<b>0.003</b>	<b>0.002</b>	<b>0.014</b>	<b>0.035</b>	0.521	0.765	0.187		
4	d	2.1	2.6	3.6	1.2	0.3	0.6	1.2	0.6	2.1		
	p	0.076	<b>0.042</b>	<b>0.014</b>	0.153	0.662	0.420	0.366	0.630	0.167		
6	d	2.3	3.1	2.9	0.9	0.3	0.6	1.3	1.7	0.7		
	p	0.058	<b>0.022</b>	<b>0.030</b>	0.239	0.684	0.409	0.318	0.227	0.554		
8	d	2.1	3.5	5.1	0.3	0.1	0.1	2.4	2.1	13.5		
	p	0.074	<b>0.016</b>	<b>0.004</b>	0.699	0.871	0.847	0.141	0.171	<b>0.005</b>		
12	d	2.9	7.6	3.3	0.8	0.2	0.7	2.4	<0.1	1.8		
	p	<b>0.028</b>	<b>0.001</b>	<b>0.020</b>	0.316	0.796	0.396	0.135	0.984	0.219		
18	d	5.1	4.8	5.3	1.8	0.3	1.4	0.1	0.1	0.1		
	p	<b>0.004</b>	<b>0.005</b>	<b>0.004</b>	<b>0.048</b>	0.653	0.102	0.940	0.902	0.927		
24	d	3.5	3.1	3.5	4.5	0.4	5.0	1.8	0.5	1.8		
	p	<b>0.015</b>	<b>0.022</b>	<b>0.016</b>	<b>0.001</b>	0.584	<b>&lt;0.001</b>	0.220	0.655	0.212		
48	d	5.5	0.6	1.5	5.3	1.1	1.7	1.3	2.3	0.1		
	p	<b>0.003</b>	0.522	0.149	<b>&lt;0.001</b>	0.180	0.051	0.313	0.144	0.920		

		+ acetate vs. no acetate					+ acetate			no acetate		
		0.25	1.0	20 $\mu$ M Fe			0.25 vs. 1.0 $\mu$ M Fe	1.0 vs. 20 $\mu$ M Fe	0.25 vs. 20 $\mu$ M Fe	0.25 vs. 1.0 $\mu$ M Fe	1.0 vs. 20 $\mu$ M Fe	0.25 vs. 20 $\mu$ M Fe
h	d	15.3	14.5	6.8	0.7	0.9	0.2	0.5	0.5	0.7		
	p	<b>&lt;0.001</b>	<b>&lt;0.001</b>	<b>0.001</b>	0.346	0.276	0.758	0.641	0.663	0.572		
2	d	8.3	5.1	3.4	1.4	1.2	2.4	0.7	0.3	0.3		
	p	<b>0.001</b>	<b>0.004</b>	<b>0.017</b>	0.105	0.142	<b>0.016</b>	0.535	0.821	0.795		
4	d	14.1	5.4	4.0	1.3	1.2	3.0	0.1	0.5	0.6		
	p	<b>&lt;0.001</b>	<b>0.003</b>	<b>0.010</b>	0.120	0.142	<b>0.006</b>	0.927	0.678	0.600		
6	d	13.5	4.2	2.4	1.4	1.4	2.8	0.3	0.5	0.4		
	p	<b>&lt;0.001</b>	<b>0.008</b>	<b>0.049</b>	0.103	0.097	<b>0.007</b>	0.805	0.665	0.712		
8	d	3.0	2.2	14.7	1.8	1.7	3.0	0.1	1.8	1.6		
	p	<b>0.026</b>	0.061	<b>&lt;0.001</b>	<b>0.045</b>	0.058	<b>0.005</b>	0.904	0.211	0.256		
12	d	5.1	17.9	1.7	1.9	2.7	4.0	1.8	1.1	0.1		
	p	<b>0.004</b>	<b>&lt;0.001</b>	0.127	<b>0.036</b>	<b>0.009</b>	<b>0.001</b>	0.223	0.400	0.942		
18	d	7.9	2.7	8.7	3.5	2.7	6.7	1.1	0.5	1.1		
	p	<b>0.001</b>	<b>0.034</b>	<b>0.001</b>	<b>0.003</b>	<b>0.009</b>	<b>&lt;0.001</b>	0.395	0.684	0.375		
24	d	5.4	6.3	0.9	5.1	2.8	9.7	0.7	3.9	2.1		
	p	<b>0.003</b>	<b>0.002</b>	0.365	<b>&lt;0.001</b>	<b>0.008</b>	<b>&lt;0.001</b>	0.575	0.059	0.174		
48	d	7.6	11.3	0.4	12.2	1.3	10.4	4.8	4.2	0.3		
	p	<b>0.001</b>	<b>&lt;0.001</b>	0.670	<b>&lt;0.001</b>	0.113	<b>&lt;0.001</b>	<b>0.041</b>	0.052	0.794		

## 6. Appendix

**Supplemental Table 41.** Statistical significance of calcium content. **A:** Comparison of cellular calcium content of + acetate cultures and no acetate control cultures for each time and **B:** comparing +acetate with no acetate control. **C:** Comparison of calcium content normalized to sulfur content of + acetate cultures and no acetate control cultures for each time and **D:** comparing +acetate with no acetate control. Cohen's *d*-value was computed as a measure of effect size between the individual conditions, absolute *d*-values are shown at the top of each cell. For statistical significance between conditions, unpaired, two-tailed Student's *t*-test was applied, and the resulting *p*-values are shown at the bottom of each cell. *P*-values passing a significance threshold of  $\alpha = 0.05$  are highlighted in bold,  $\alpha = 0.01$  in bold and underlined,  $\alpha = 0.001$  are labeled < 0.001.

		+ acetate vs. no acetate					+ acetate			no acetate		
		0.25	1.0	20 $\mu$ M Fe			0.25 vs. 1.0 $\mu$ M Fe	1.0 vs. 20 $\mu$ M Fe	0.25 vs. 20 $\mu$ M Fe	0.25 vs. 1.0 $\mu$ M Fe	1.0 vs. 20 $\mu$ M Fe	0.25 vs. 20 $\mu$ M Fe
0	<i>d</i>	3.8	1.3	2.8	2.3	1.2	1.4	0.1	0.1	0.2		
	<i>p</i>	<b>0.012</b>	0.214	<b>0.032</b>	<b>0.017</b>	0.150	0.093	0.940	0.955	0.884		
2	<i>d</i>	4.8	0.3	1.4	6.0	2.4	2.3	0.2	2.0	2.0		
	<i>p</i>	<b>0.005</b>	0.734	0.195	<b>&lt;0.001</b>	<b>0.014</b>	<b>0.018</b>	0.859	0.180	0.186		
4	<i>d</i>	3.0	0.7	1.4	3.0	1.4	1.0	0.3	<0.1	0.2		
	<i>p</i>	<b>0.025</b>	0.474	0.184	<b>0.005</b>	0.099	0.224	0.789	0.973	0.892		
6	<i>d</i>	2.6	1.0	1.6	2.0	1.1	0.5	0.3	0.5	1.7		
	<i>p</i>	<b>0.041</b>	0.308	0.134	<b>0.028</b>	0.180	0.533	0.822	0.644	0.227		
8	<i>d</i>	1.7	1.8	3.3	1.1	2.4	0.9	0.5	0.6	1.0		
	<i>p</i>	0.124	0.108	<b>0.020</b>	0.164	<b>0.016</b>	0.250	0.693	0.607	0.421		
12	<i>d</i>	1.3	4.3	2.5	0.8	1.0	1.4	0.3	0.4	<0.1		
	<i>p</i>	0.214	<b>0.008</b>	<b>0.047</b>	0.284	0.210	0.098	0.774	0.753	0.990		
18	<i>d</i>	0.3	5.6	6.0	4.7	2.3	5.6	0.2	1.0	0.7		
	<i>p</i>	0.749	<b>0.003</b>	<b>0.002</b>	<b>0.001</b>	<b>0.019</b>	<b>&lt;0.001</b>	0.863	0.432	0.567		
24	<i>d</i>	8.0	11.2	9.7	4.9	0.1	4.3	1.5	1.5	0.7		
	<i>p</i>	<b>0.001</b>	<b>&lt;0.001</b>	<b>&lt;0.001</b>	<b>&lt;0.001</b>	0.885	<b>0.001</b>	0.272	0.271	0.546		
48	<i>d</i>	27.2	16.7	2.4	2.4	6.9	6.5	0.6	3.4	4.0		
	<i>p</i>	<b>&lt;0.001</b>	<b>&lt;0.001</b>	0.051	<b>0.015</b>	<b>&lt;0.001</b>	<b>&lt;0.001</b>	0.602	0.079	0.058		

		+ acetate vs. no acetate					+ acetate			no acetate		
		0.25	1.0	20 $\mu$ M Fe			0.25 vs. 1.0 $\mu$ M Fe	1.0 vs. 20 $\mu$ M Fe	0.25 vs. 20 $\mu$ M Fe	0.25 vs. 1.0 $\mu$ M Fe	1.0 vs. 20 $\mu$ M Fe	0.25 vs. 20 $\mu$ M Fe
0	<i>d</i>	11.0	5.0	6.3	2.8	0.7	1.7	0.3	0.2	0.5		
	<i>p</i>	<b>&lt;0.001</b>	<b>0.004</b>	<b>0.002</b>	<b>0.007</b>	0.380	0.058	0.812	0.880	0.648		
2	<i>d</i>	5.0	5.0	1.1	4.0	0.7	3.0	0.4	1.1	0.7		
	<i>p</i>	<b>0.005</b>	<b>0.004</b>	0.260	<b>0.001</b>	0.349	<b>0.005</b>	0.747	0.392	0.573		
4	<i>d</i>	4.2	1.0	0.8	3.3	0.6	3.0	1.2	0.1	0.7		
	<i>p</i>	<b>0.009</b>	0.311	0.394	<b>0.003</b>	0.408	<b>0.006</b>	0.347	0.952	0.563		
6	<i>d</i>	4.5	0.5	1.3	2.1	0.4	1.4	0.6	0.1	0.7		
	<i>p</i>	<b>0.007</b>	0.601	0.195	<b>0.023</b>	0.601	0.088	0.627	0.920	0.535		
8	<i>d</i>	2.3	0.1	3.0	1.9	0.5	1.0	0.8	1.4	0.2		
	<i>p</i>	0.054	0.904	<b>0.027</b>	<b>0.037</b>	0.540	0.203	0.509	0.301	0.850		
12	<i>d</i>	1.2	2.6	0.4	0.1	0.5	0.4	0.1	2.9	1.2		
	<i>p</i>	0.228	<b>0.040</b>	0.672	0.911	0.533	0.581	0.962	0.103	0.352		
18	<i>d</i>	1.4	1.8	0.6	0.3	1.3	1.2	2.2	0.8	0.9		
	<i>p</i>	0.189	0.112	0.515	0.728	0.121	0.132	0.158	0.513	0.477		
24	<i>d</i>	1.7	2.5	7.4	0.5	0.3	0.2	0.1	2.7	1.6		
	<i>p</i>	0.119	<b>0.047</b>	<b>0.001</b>	0.519	0.644	0.812	0.951	0.112	0.257		
48	<i>d</i>	10.5	22.7	0.1	2.5	10.2	9.1	4.6	0.5	0.7		
	<i>p</i>	<b>&lt;0.001</b>	<b>&lt;0.001</b>	0.891	<b>0.011</b>	<b>&lt;0.001</b>	<b>&lt;0.001</b>	<b>0.044</b>	0.689	0.537		

## 6. Appendix

**Supplemental Table 42.** Statistical significance of potassium content. **A:** Comparison of cellular potassium content of + acetate cultures and no acetate control cultures for each time and **B:** comparing +acetate with no acetate control. Cohen's *d*-value was computed as a measure of effect size between the individual conditions, absolute *d*-values are shown at the top of each cell. For statistical significance between conditions, unpaired, two-tailed Student's *t*-test was applied, and the resulting *p*-values are shown at the bottom of each cell. *P*-values passing a significance threshold of  $\alpha = 0.05$  are highlighted in bold,  $\alpha = 0.01$  in bold and underlined,  $\alpha = 0.001$  are labeled < 0.001.

		+ acetate vs. no acetate					+ acetate			no acetate		
		0.25	1.0	20 $\mu$ M Fe			0.25 vs. 1.0 $\mu$ M Fe	1.0 vs. 20 $\mu$ M Fe	0.25 vs. 20 $\mu$ M Fe	0.25 vs. 1.0 $\mu$ M Fe	1.0 vs. 20 $\mu$ M Fe	0.25 vs. 20 $\mu$ M Fe
0	<i>d</i>	5.6	3.1	4.4	1.7	1.1	0.7	2.2	0.3	0.8		
0	<i>p</i>	<b>0.003</b>	<b>0.024</b>	<b>0.007</b>	0.050	0.179	0.352	0.162	0.822	0.490		
2	<i>d</i>	8.2	10.0	10.1	5.1	4.0	0.6	1.0	3.1	5.0		
2	<i>p</i>	<b>0.001</b>	<b>&lt;0.001</b>	<b>&lt;0.001</b>	<b>&lt;0.001</b>	<b>0.001</b>	0.442	0.416	0.091	<b>0.038</b>		
4	<i>d</i>	10.0	9.0	4.9	0.6	1.2	0.9	0.3	1.8	1.4		
4	<i>p</i>	<b>&lt;0.001</b>	<b>&lt;0.001</b>	<b>0.005</b>	0.423	0.133	0.249	0.807	0.211	0.292		
6	<i>d</i>	9.1	7.3	6.3	0.7	1.3	0.8	1.8	1.0	1.2		
6	<i>p</i>	<b>&lt;0.001</b>	<b>0.001</b>	<b>0.002</b>	0.364	0.111	0.321	0.207	0.414	0.357		
8	<i>d</i>	8.2	19.0	7.0	1.9	1.1	2.1	1.8	8.7	0.2		
8	<i>p</i>	<b>0.001</b>	<b>&lt;0.001</b>	<b>0.001</b>	<b>0.038</b>	0.189	<b>0.027</b>	0.212	<b>0.013</b>	0.853		
12	<i>d</i>	6.4	11.9	5.4	0.3	0.5	0.7	<0.1	0.7	0.7		
12	<i>p</i>	<b>0.002</b>	<b>&lt;0.001</b>	<b>0.003</b>	0.644	0.527	0.395	0.989	0.577	0.564		
18	<i>d</i>	7.5	1.2	1.8	3.7	0.6	4.1	1.1	0.2	0.9		
18	<i>p</i>	<b>0.001</b>	0.247	0.114	<b>0.002</b>	0.416	<b>0.001</b>	0.390	0.888	0.445		
24	<i>d</i>	5.9	6.4	6.9	2.6	0.6	2.4	0.6	0.9	2.7		
24	<i>p</i>	<b>0.002</b>	<b>0.002</b>	<b>0.001</b>	<b>0.010</b>	0.449	<b>0.015</b>	0.635	0.477	0.114		
48	<i>d</i>	1.4	1.2	4.2	0.3	4.5	5.6	1.8	2.8	0.3		
48	<i>p</i>	0.181	0.244	<b>0.009</b>	0.730	<b>0.001</b>	<b>&lt;0.001</b>	0.209	0.106	0.790		

**Supplemental Table 43.** Statistical significance of sodium content. **A:** Comparison of cellular sodium content of + acetate cultures and no acetate control cultures for each time and **B:** the comparison of sodium concentrations with and without acetate. Cohen's *d*-value was computed as a measure of effect size between the individual conditions, absolute *d*-values are shown at the top of each cell. For statistical significance between conditions, unpaired, two-tailed Student's *t*-test was applied, and the resulting *p*-values are shown at the bottom of each cell. *P*-values passing a significance threshold of  $\alpha = 0.05$  are highlighted in bold,  $\alpha = 0.01$  in bold and underlined,  $\alpha = 0.001$  are labeled < 0.001.

		+ acetate vs. no acetate					+ acetate			no acetate		
		0.25	1.0	20 $\mu$ M Fe			0.25 vs. 1.0 $\mu$ M Fe	1.0 vs. 20 $\mu$ M Fe	0.25 vs. 20 $\mu$ M Fe	0.25 vs. 1.0 $\mu$ M Fe	1.0 vs. 20 $\mu$ M Fe	0.25 vs. 20 $\mu$ M Fe
0	<i>d</i>	0.8	0.1	1.0	0.2	0.3	0.2	1.2	1.8	2.3		
0	<i>p</i>	0.388	0.920	0.329	0.802	0.650	0.775	0.368	0.221	0.150		
2	<i>d</i>	0.1	1.7	0.6	1.4	0.5	1.8	0.4	1.9	2.3		
2	<i>p</i>	0.916	0.129	0.529	0.105	0.542	<b>0.042</b>	0.746	0.195	0.151		
4	<i>d</i>	0.2	0.2	0.9	1.1	0.6	2.0	3.4	0.5	1.9		
4	<i>p</i>	0.805	0.823	0.370	0.171	0.405	<b>0.032</b>	0.075	0.667	0.201		
6	<i>d</i>	0.8	1.7	0.3	0.6	0.4	1.3	1.5	2.0	0.1		
6	<i>p</i>	0.389	0.120	0.723	0.401	0.559	0.122	0.270	0.180	0.956		
8	<i>d</i>	0.5	1.3	1.6	0.1	0.6	0.6	1.2	<0.1	1.1		
8	<i>p</i>	0.598	0.208	0.142	0.911	0.413	0.422	0.355	0.974	0.400		
12	<i>d</i>	7.2	8.6	3.9	1.1	0.5	1.0	0.3	1.4	0.6		
12	<i>p</i>	<b>0.001</b>	<b>0.001</b>	<b>0.011</b>	0.190	0.550	0.190	0.779	0.300	0.597		
18	<i>d</i>	16.2	10.4	8.3	0.9	<0.1	0.8	5.0	1.1	3.4		
18	<i>p</i>	<b>&lt;0.001</b>	<b>&lt;0.001</b>	<b>0.001</b>	0.245	0.985	0.310	<b>0.037</b>	0.386	0.078		
24	<i>d</i>	23.2	4.6	5.4	6.1	0.3	6.9	3.0	2.1	0.1		
24	<i>p</i>	<b>&lt;0.001</b>	<b>0.006</b>	<b>0.003</b>	<b>&lt;0.001</b>	0.654	<b>&lt;0.001</b>	0.096	0.173	0.933		
48	<i>d</i>	22.1	8.4	6.8	2.0	3.1	6.8	1.0	0.3	1.3		
48	<i>p</i>	<b>&lt;0.001</b>	<b>0.001</b>	<b>0.001</b>	<b>0.029</b>	<b>0.005</b>	<b>&lt;0.001</b>	0.435	0.818	0.327		

## 6. Appendix

**Supplemental Table 44.** Statistical significance of manganese content. **A:** Comparison of cellular manganese content of + acetate cultures and no acetate control cultures for each time and **B:** comparing +acetate with no acetate control. **C:** Comparison of manganese content normalized to sulfur content of + acetate cultures and no acetate control cultures for each time and **D:** comparing +acetate with no acetate control. Cohen's *d*-value was computed as a measure of effect size between the individual conditions, absolute *d*-values are shown at the top of each cell. For statistical significance between conditions, unpaired, two-tailed Student's *t*-test was applied, and the resulting *p*-values are shown at the bottom of each cell. *P*-values passing a significance threshold of  $\alpha = 0.05$  are highlighted in bold,  $\alpha = 0.01$  in bold and underlined,  $\alpha = 0.001$  are labeled < 0.001.

		+ acetate vs. no acetate			+ acetate						no acetate					
		0.25	1.0	20 $\mu$ M Fe	0.25 vs. 1.0 $\mu$ M Fe	1.0 vs. 20 $\mu$ M Fe	0.25 vs. 20 $\mu$ M Fe	0.25 vs. 1.0 $\mu$ M Fe	1.0 vs. 20 $\mu$ M Fe	0.25 vs. 20 $\mu$ M Fe	0.25 vs. 1.0 $\mu$ M Fe	1.0 vs. 20 $\mu$ M Fe	0.25 vs. 20 $\mu$ M Fe			
h	d	6.8	4.4	5.3	1.6	1.6	3.6	3.1	8.8	7.4	1.6	1.6	3.6			
	<i>p</i>	<b><u>&lt;0.001</u></b>	<b><u>0.007</u></b>	<b><u>0.004</u></b>	0.062	0.070	<b><u>0.002</u></b>	0.093	<b><u>0.013</u></b>	<b><u>0.018</u></b>	0.158	<b><u>&lt;0.001</u></b>	<b><u>&lt;0.001</u></b>			
2	d	6.3	15.9	8.9	1.1	5.7	4.8	4.8	1.3	3.2	2.9	1.3	3.2			
	<i>p</i>	<b><u>0.002</u></b>	<b><u>&lt;0.001</u></b>	<b><u>0.001</u></b>	0.158	<b><u>&lt;0.001</u></b>	<b><u>&lt;0.001</u></b>	<b><u>0.041</u></b>	0.327	0.084	<b><u>0.006</u></b>	0.128	<b><u>0.004</u></b>			
4	d	6.7	5.7	4.3	2.9	1.3	3.2	4.9	0.9	14.6	1.9	1.3	3.2			
	<i>p</i>	<b><u>0.002</u></b>	<b><u>0.003</u></b>	<b><u>0.008</u></b>	<b><u>0.006</u></b>	0.128	<b><u>0.004</u></b>	<b><u>0.039</u></b>	0.483	<b><u>0.005</u></b>	0.036	0.113	<b><u>0.004</u></b>			
6	d	6.7	5.7	5.2	3.6	1.2	3.6	5.3	2.0	3.7	3.6	1.2	3.6			
	<i>p</i>	<b><u>0.002</u></b>	<b><u>0.003</u></b>	<b><u>0.004</u></b>	<b><u>0.002</u></b>	0.132	<b><u>0.002</u></b>	<b><u>0.034</u></b>	0.180	0.065	4.1	1.0	3.1			
8	d	7.0	9.5	5.2	4.1	1.0	3.1	29.9	8.0	21.9	7.8	1.2	6.7			
	<i>p</i>	<b><u>0.001</u></b>	<b><u>&lt;0.001</u></b>	<b><u>0.004</u></b>	<b><u>0.001</u></b>	0.228	<b><u>0.004</u></b>	<b><u>0.001</u></b>	<b><u>0.015</u></b>	<b><u>0.002</u></b>	<b><u>&lt;0.001</u></b>	0.131	<b><u>&lt;0.001</u></b>			
12	d	7.9	8.1	4.4	0.5	0.2	0.1	5.0	1.6	7.7	0.5	0.2	0.1			
	<i>p</i>	<b><u>0.001</u></b>	<b><u>0.001</u></b>	<b><u>0.007</u></b>	0.497	0.782	0.869	<b><u>0.038</u></b>	0.247	<b><u>0.016</u></b>	2.9	1.8	2.9			
18	d	8.2	13.3	8.3	7.8	1.2	6.7	1.9	17.4	6.8	0.5	0.2	0.1			
	<i>p</i>	<b><u>0.001</u></b>	<b><u>&lt;0.001</u></b>	<b><u>0.001</u></b>	<b><u>&lt;0.001</u></b>	0.131	<b><u>&lt;0.001</u></b>	0.201	<b><u>0.003</u></b>	<b><u>0.021</u></b>	0.006	<b><u>0.042</u></b>	<b><u>0.006</u></b>			
24	d	8.7	0.4	0.2	0.5	0.2	0.1	5.0	1.6	7.7	0.5	0.2	0.1			
	<i>p</i>	<b><u>0.001</u></b>	0.655	0.809	0.497	0.782	0.869	<b><u>0.038</u></b>	0.247	<b><u>0.016</u></b>	2.9	1.8	2.9			
48	d	10.8	4.9	3.2	2.9	1.8	2.9	5.2	0.5	5.6	0.5	0.2	0.1			
	<i>p</i>	<b><u>&lt;0.001</u></b>	<b><u>0.005</u></b>	<b><u>0.020</u></b>	<b><u>0.006</u></b>	<b><u>0.042</u></b>	<b><u>0.006</u></b>	<b><u>0.035</u></b>	0.643	<b><u>0.030</u></b>						

		+ acetate vs. no acetate			+ acetate						no acetate					
		0.25	1.0	20 $\mu$ M Fe	0.25 vs. 1.0 $\mu$ M Fe	1.0 vs. 20 $\mu$ M Fe	0.25 vs. 20 $\mu$ M Fe	0.25 vs. 1.0 $\mu$ M Fe	1.0 vs. 20 $\mu$ M Fe	0.25 vs. 20 $\mu$ M Fe	0.25 vs. 1.0 $\mu$ M Fe	1.0 vs. 20 $\mu$ M Fe	0.25 vs. 20 $\mu$ M Fe			
h	d	15.5	13.1	11.8	7.2	2.0	12.0	3.0	1.7	3.0	7.2	2.0	12.0			
	<i>p</i>	<b><u>&lt;0.001</u></b>	<b><u>&lt;0.001</u></b>	<b><u>&lt;0.001</u></b>	<b><u>&lt;0.001</u></b>	<b><u>0.033</u></b>	<b><u>&lt;0.001</u></b>	0.098	0.228	0.097	7.2	1.4	8.7			
2	d	8.0	14.4	8.9	7.2	1.4	8.7	0.9	2.2	2.2	6.4	1.2	8.4			
	<i>p</i>	<b><u>0.001</u></b>	<b><u>&lt;0.001</u></b>	<b><u>0.001</u></b>	<b><u>&lt;0.001</u></b>	0.102	<b><u>&lt;0.001</u></b>	0.470	0.165	0.157	6.4	1.2	8.4			
4	d	8.4	11.2	6.9	6.4	1.2	8.4	3.8	0.1	2.2	6.4	1.2	8.4			
	<i>p</i>	<b><u>0.001</u></b>	<b><u>&lt;0.001</u></b>	<b><u>0.001</u></b>	<b><u>&lt;0.001</u></b>	0.155	<b><u>&lt;0.001</u></b>	0.064	0.932	0.157	6.0	1.0	6.0			
6	d	10.2	5.8	8.2	6.0	1.0	6.0	1.2	0.8	4.0	6.0	1.0	6.0			
	<i>p</i>	<b><u>&lt;0.001</u></b>	<b><u>0.003</u></b>	<b><u>0.001</u></b>	<b><u>&lt;0.001</u></b>	0.211	<b><u>&lt;0.001</u></b>	0.347	0.490	0.057	4.4	1.3	5.9			
8	d	9.0	11.4	17.5	4.4	1.3	5.9	2.4	0.3	2.5	4.4	1.3	5.9			
	<i>p</i>	<b><u>&lt;0.001</u></b>	<b><u>&lt;0.001</u></b>	<b><u>&lt;0.001</u></b>	<b><u>0.001</u></b>	0.118	<b><u>&lt;0.001</u></b>	0.137	0.765	0.128	5.8	0.8	5.9			
12	d	7.9	15.0	9.2	5.8	0.8	5.9	1.5	4.0	3.8	5.8	0.8	5.9			
	<i>p</i>	<b><u>0.001</u></b>	<b><u>&lt;0.001</u></b>	<b><u>&lt;0.001</u></b>	<b><u>&lt;0.001</u></b>	0.288	<b><u>&lt;0.001</u></b>	0.263	0.058	0.062	6.6	1.9	11.8			
18	d	10.8	16.3	9.8	6.6	1.9	11.8	2.8	1.5	2.7	6.6	1.9	11.8			
	<i>p</i>	<b><u>&lt;0.001</u></b>	<b><u>&lt;0.001</u></b>	<b><u>&lt;0.001</u></b>	<b><u>&lt;0.001</u></b>	<b><u>0.040</u></b>	<b><u>&lt;0.001</u></b>	0.111	0.269	0.113	6.6	1.2	14.2			
24	d	14.0	10.2	18.7	6.6	1.2	14.2	1.6	4.2	9.5	6.6	1.2	14.2			
	<i>p</i>	<b><u>&lt;0.001</u></b>	<b><u>&lt;0.001</u></b>	<b><u>&lt;0.001</u></b>	<b><u>&lt;0.001</u></b>	0.156	<b><u>&lt;0.001</u></b>	0.261	0.053	<b><u>0.011</u></b>	6.2	5.7	9.8			
48	d	11.4	15.5	6.0	6.2	5.7	9.8	24.2	0.9	1.7	6.2	5.7	9.8			
	<i>p</i>	<b><u>&lt;0.001</u></b>	<b><u>&lt;0.001</u></b>	<b><u>0.002</u></b>	<b><u>&lt;0.001</u></b>	<b><u>&lt;0.001</u></b>	<b><u>&lt;0.001</u></b>	<b><u>0.002</u></b>	0.472	0.227						

## 6. Appendix

**Supplemental Table 45.** Statistical significance of zinc content. **A:** Comparison of cellular zinc content of + acetate cultures and no acetate control cultures for each time and **B:** comparing +acetate with no acetate control. **C:** Comparison of zinc content normalized to sulfur content of + acetate cultures and no acetate control cultures for each time and **D:** comparing +acetate with no acetate control. Cohen's *d*-value was computed as a measure of effect size between the individual conditions, absolute *d*-values are shown at the top of each cell. For statistical significance between conditions, unpaired, two-tailed Student's *t*-test was applied, and the resulting *p*-values are shown at the bottom of each cell. *P*-values passing a significance threshold of  $\alpha = 0.05$  are highlighted in bold,  $\alpha = 0.01$  in bold and underlined,  $\alpha = 0.001$  are labeled < 0.001.

		+ acetate vs. no acetate					+ acetate			no acetate		
		0.25	1.0	20 $\mu$ M Fe			0.25 vs. 1.0 $\mu$ M Fe	1.0 vs. 20 $\mu$ M Fe	0.25 vs. 20 $\mu$ M Fe	0.25 vs. 1.0 $\mu$ M Fe	1.0 vs. 20 $\mu$ M Fe	0.25 vs. 20 $\mu$ M Fe
h	d	6.1	1.5	2.5								
	p	<b>0.002</b>	0.150	<b>0.047</b>								
2	d	6.1	0.3	1.9								
	p	<b>0.002</b>	0.738	0.091								
4	d	3.8	0.7	1.3								
	p	<b>0.012</b>	0.455	0.211								
6	d	4.6	3.3	2.5								
	p	<b>0.006</b>	<b>0.019</b>	<b>0.048</b>								
8	d	4.9	0.8	2.9								
	p	<b>0.005</b>	0.389	<b>0.029</b>								
12	d	4.2	3.3	2.7								
	p	<b>0.008</b>	<b>0.018</b>	<b>0.036</b>								
18	d	6.9	3.0	5.2								
	p	<b>0.001</b>	0.026	<b>0.004</b>								
24	d	4.9	4.4	2.7								
	p	<b>0.005</b>	<b>0.007</b>	<b>0.037</b>								
48	d	7.5	0.1	1.3								
	p	<b>0.001</b>	0.903	0.206								
h	d	4.3	1.2	2.6	0.3	0.4	<0.1					
	p	<b>0.001</b>	0.156	<b>0.011</b>	0.793	0.718	0.971					
2	d	6.1	1.5	3.8	0.6	0.5	1.1					
	p	<b>&lt;0.001</b>	0.080	<b>0.002</b>	0.608	0.642	0.379					
4	d	3.6	0.8	2.3	<0.1	0.3	0.3					
	p	<b>0.002</b>	0.307	<b>0.019</b>	1.000	0.750	0.774					
6	d	1.6	1.2	2.7	1.9	3.9	2.1					
	p	0.064	0.140	<b>0.010</b>	0.201	0.059	0.177					
8	d	3.8	1.0	2.7	3.7	5.0	0.1					
	p	<b>0.002</b>	0.203	<b>0.008</b>	0.067	<b>0.038</b>	0.903					
12	d	2.8	0.7	1.2	2.1	<0.1	1.9					
	p	<b>0.015</b>	0.344	0.130	0.173	0.970	0.206					
18	d	3.7	0.6	3.7	3.5	3.0	5.5					
	p	<b>0.002</b>	0.464	<b>0.002</b>	0.072	0.097	<b>0.032</b>					
24	d	6.8	0.3	5.8	4.7	2.4	3.5					
	p	<b>&lt;0.001</b>	0.727	<b>&lt;0.001</b>	0.042	0.137	0.075					
48	d	7.0	1.1	3.9	0.9	0.8	0.2					
	p	<b>&lt;0.001</b>	0.176	<b>0.001</b>	0.453	0.513	0.865					
h	d	7.87	4.22	5.99								
	p	<b>0.001</b>	<b>0.008</b>	<b>0.002</b>								
2	d	9.66	3.36	1.76								
	p	<b>&lt;0.001</b>	<b>0.018</b>	0.111								
4	d	4.95	2.07	1.66								
	p	<b>0.005</b>	0.075	0.128								
6	d	7.14	0.65	2.21								
	p	<b>0.001</b>	0.492	0.063								
8	d	7.52	0.32	5.14								
	p	<b>0.001</b>	0.731	<b>0.004</b>								
12	d	5.75	3.32	2.19								
	p	<b>0.003</b>	<b>0.018</b>	0.065								
18	d	7.78	1.84	2.11								
	p	<b>0.001</b>	0.101	0.071								
24	d	6.59	0.44	0.11								
	p	<b>0.002</b>	0.637	0.902								
48	d	8.34	2.57	0.02								
	p	<b>0.001</b>	<b>0.041</b>	0.981								
h	d	5.2	1.0	4.4	0.2	0.4	<0.1					
	p	<b>&lt;0.001</b>	0.224	<b>0.001</b>	0.886	0.743	0.959					
2	d	6.7	0.5	6.2	0.5	0.4	0.2					
	p	<b>&lt;0.001</b>	0.543	<b>&lt;0.001</b>	0.672	0.712	0.897					
4	d	4.7	0.6	3.4	1.1	0.7	0.6					
	p	<b>0.001</b>	0.438	<b>0.003</b>	0.405	0.544	0.598					
6	d	7.5	2.5	3.8	0.8	0.5	0.6					
	p	<b>&lt;0.001</b>	<b>0.013</b>	<b>0.002</b>	0.516	0.670	0.637					
8	d	7.3	0.8	6.2	1.7	2.4	0.1					
	p	<b>&lt;0.001</b>	0.308	<b>&lt;0.001</b>	0.238	0.144	0.929					
12	d	5.8	0.4	5.0	0.5	1.5	0.5					
	p	<b>&lt;0.001</b>	0.578	<b>&lt;0.001</b>	0.665	0.278	0.646					
18	d	7.6	0.4	6.8	1.8	0.9	0.5					
	p	<b>&lt;0.001</b>	0.596	<b>&lt;0.001</b>	0.216	0.467	0.689					
24	d	5.4	0.4	3.6	3.4	4.7	10.2					
	p	<b>&lt;0.001</b>	0.638	<b>0.002</b>	0.075	<b>0.042</b>	<b>0.010</b>					
48	d	9.3	<0.1	9.2	2.5	2.7	0.4					
	p	<b>&lt;0.001</b>	0.925	<b>&lt;0.001</b>	0.128	0.114	0.704					



## 6. Appendix

**Supplemental Table 46.** Statistical significance of copper content. **A:** Comparison of cellular copper content of + acetate cultures and no acetate control cultures for each time and **B:** comparing +acetate with no acetate control. **C:** Comparison of copper content normalized to sulfur content of + acetate cultures and no acetate control cultures for each time and **D:** comparing +acetate with no acetate control. Cohen's *d*-value was computed as a measure of effect size between the individual conditions, absolute *d*-values are shown at the top of each cell. For statistical significance between conditions, unpaired, two-tailed Student's *t*-test was applied, and the resulting *p*-values are shown at the bottom of each cell. *P*-values passing a significance threshold of  $\alpha = 0.05$  are highlighted in bold,  $\alpha = 0.01$  in bold and underlined,  $\alpha = 0.001$  are labeled < 0.001.

<b>A</b> + acetate vs. no acetate				<b>B</b>							
h	+ acetate vs. no acetate			+ acetate			no acetate				
	0.25	1.0	20 $\mu$ M Fe	0.25 vs. 1.0 $\mu$ M Fe	1.0 vs. 20 $\mu$ M Fe	0.25 vs. 20 $\mu$ M Fe	0.25 vs. 1.0 $\mu$ M Fe	1.0 vs. 20 $\mu$ M Fe	1.0 vs. 20 $\mu$ M Fe	0.25 vs. 20 $\mu$ M Fe	
0	d	2.0	7.4	6.9	d	7.5	0.7	8.1	6.1	5.3	7.34
0	p	0.079	<b><u>0.001</u></b>	<b><u>0.001</u></b>	p	<0.001	0.363	<0.001	<b><u>0.026</u></b>	<b><u>0.034</u></b>	<b><u>0.018</u></b>
2	d	3.9	10.1	7.5	d	8.9	<0.1	8.7	20.0	1.1	13.2
2	p	<b><u>0.011</u></b>	<b><u>&lt;0.001</u></b>	<b><u>0.001</u></b>	p	<0.001	0.952	<0.001	<b><u>0.002</u></b>	0.393	<b><u>0.006</u></b>
4	d	3.0	5.8	7.5	d	8.2	1.0	8.4	5.8	0.9	6.1
4	p	<b><u>0.027</u></b>	<b><u>0.003</u></b>	<b><u>0.001</u></b>	p	<0.001	0.217	<0.001	<b><u>0.028</u></b>	0.462	<b><u>0.026</u></b>
6	d	0.9	2.9	6.2	d	5.8	1.3	6.8	9.0	1.0	9.5
6	p	0.352	<b><u>0.029</u></b>	<b><u>0.002</u></b>	p	<0.001	0.128	<0.001	<b><u>0.012</u></b>	0.429	<b><u>0.011</u></b>
8	d	5.1	4.7	3.4	d	6.7	1.4	7.4	33.7	11.6	35.5
8	p	<b><u>0.004</u></b>	<b><u>0.006</u></b>	<b><u>0.018</u></b>	p	<0.001	0.090	<0.001	<b><u>0.001</u></b>	<b><u>0.007</u></b>	<b><u>0.001</u></b>
12	d	0.3	2.3	0.1	d	3.9	1.0	4.2	12.2	1.7	24.9
12	p	0.773	0.055	0.931	p	<b><u>0.001</u></b>	0.209	<b><u>0.001</u></b>	<b><u>0.007</u></b>	0.231	<b><u>0.002</u></b>
18	d	2.1	4.5	2.5	d	4.1	3.0	6.1	9.4	0.6	14.9
18	p	0.069	<b><u>0.007</u></b>	<b><u>0.045</u></b>	p	<b><u>0.001</u></b>	<b><u>0.005</u></b>	<0.001	<b><u>0.011</u></b>	0.602	<b><u>0.004</u></b>
24	d	1.0	1.7	5.3	d	9.3	2.0	12.2	10.1	0.4	22.2
24	p	0.311	0.126	<b><u>0.004</u></b>	p	<0.001	<b><u>0.032</u></b>	<0.001	<b><u>0.010</u></b>	0.715	<b><u>0.002</u></b>
48	d	4.3	4.2	1.4	d	4.6	1.9	6.0	7.4	0.3	7.8
48	p	<b><u>0.008</u></b>	<b><u>0.008</u></b>	0.192	p	<b><u>0.001</u></b>	<b><u>0.034</u></b>	<0.001	<b><u>0.018</u></b>	0.826	<b><u>0.016</u></b>

<b>C</b> + acetate vs. no acetate				<b>D</b>							
h	+ acetate vs. no acetate			+ acetate			no acetate				
	0.25	1.0	20 $\mu$ M Fe	0.25 vs. 1.0 $\mu$ M Fe	1.0 vs. 20 $\mu$ M Fe	0.25 vs. 20 $\mu$ M Fe	0.25 vs. 1.0 $\mu$ M Fe	1.0 vs. 20 $\mu$ M Fe	1.0 vs. 20 $\mu$ M Fe	0.25 vs. 20 $\mu$ M Fe	
0	d	0.4	10.9	4.2	d	29.2	6.1	42.7	1.7	1.0	1.9
0	p	0.683	<0.001	<b><u>0.009</u></b>	p	<0.001	<0.001	<0.001	0.229	0.412	0.194
2	d	1.5	5.8	2.4	d	26.9	6.0	29.3	3.1	1.0	1.8
2	p	0.150	<b><u>0.003</u></b>	<b><u>0.049</u></b>	p	<0.001	<0.001	<0.001	0.088	0.437	0.207
4	d	0.2	35.5	4.7	d	32.3	11.0	38.2	2.8	0.2	1.7
4	p	0.874	<0.001	<b><u>0.006</u></b>	p	<0.001	<0.001	<0.001	0.106	0.872	0.241
6	d	0.3	2.4	3.7	d	27.5	9.5	32.4	1.7	0.5	1.1
6	p	0.754	<b><u>0.049</u></b>	<b><u>0.013</u></b>	p	<0.001	<0.001	<0.001	0.232	0.644	0.394
8	d	0.8	4.3	41.7	d	16.9	13.0	21.1	1.8	2.9	3.1
8	p	0.431	<b><u>0.008</u></b>	<0.001	p	<0.001	<0.001	<0.001	0.211	0.099	0.092
12	d	0.2	1.0	10.2	d	26.5	7.2	38.8	2.8	2.5	1.9
12	p	0.857	0.321	<0.001	p	<0.001	<0.001	<0.001	0.105	0.131	0.199
18	d	16.9	3.0	1.3	d	43.2	17.1	66.8	8.5	0.8	8.3
18	p	<0.001	<b><u>0.026</u></b>	0.195	p	<0.001	<0.001	<0.001	<b><u>0.014</u></b>	0.508	<b><u>0.014</u></b>
24	d	4.7	4.3	6.0	d	30.7	12.0	68.6	7.0	1.9	7.6
24	p	<b><u>0.005</u></b>	<b><u>0.008</u></b>	<b><u>0.002</u></b>	p	<0.001	<0.001	<0.001	<b><u>0.020</u></b>	0.204	<b><u>0.017</u></b>
48	d	6.6	6.5	<0.1	d	13.8	15.5	22.6	3.9	1.1	4.9
48	p	<b><u>0.002</u></b>	<b><u>0.002</u></b>	0.977	p	<0.001	<0.001	<0.001	0.060	0.398	<b><u>0.039</u></b>

## 6. Appendix

**Supplemental Table 47.** Statistical significance of chlorophyll content (Fe-excess). Cohen's  $d$ -value was computed as a measure of effect size between the individual conditions, absolute  $d$ -values are shown at the top of each cell. For statistical significance between conditions, unpaired, two-tailed Student's  $t$ -test was applied, and the resulting  $p$ -values are shown at the bottom of each cell.  $P$ -values passing a significance threshold of  $\alpha = 0.05$  are highlighted in bold,  $\alpha = 0.01$  in bold and underlined,  $\alpha = 0.001$  are labeled  $< 0.001$ .

h	0.25 vs. 20 $\mu\text{M}$ Fe	1.0 vs. 20 $\mu\text{M}$ Fe	20 vs. 200 $\mu\text{M}$ Fe
0	$d$ 1.2	$d$ 1.5	$d$ $< 0.1$
	$p$ 0.232	$p$ 0.139	$p$ 0.793
2	$d$ 0.9	$d$ 0.6	$d$ $< 0.1$
	$p$ 0.345	$p$ 0.488	$p$ 0.362
4	$d$ 0.3	$d$ 0.1	$d$ $< 0.1$
	$p$ 0.723	$p$ 0.914	$p$ 0.779
6	$d$ 2.9	$d$ 0.8	$d$ $< 0.1$
	$p$ <b>0.024</b>	$p$ 0.369	$p$ 0.744
8	$d$ 5.2	$d$ $< 0.1$	$d$ $< 0.1$
	$p$ <b><u>0.003</u></b>	$p$ 0.976	$p$ 0.821
12	$d$ 2.6	$d$ 0.4	$d$ $< 0.1$
	$p$ <b>0.034</b>	$p$ 0.616	$p$ 0.207
24	$d$ 10.0	$d$ 0.1	$d$ $< 0.1$
	$p$ <b><u>&lt; 0.001</u></b>	$p$ 0.880	$p$ 0.610

**Supplemental Table 48.** Statistical significance of chlorophyll content (cell density). Cohen's  $d$ -value was computed as a measure of effect size between the individual conditions, absolute  $d$ -values are shown in the first, third and fifth column. For statistical significance between conditions, unpaired, two-tailed Student's  $t$ -test was applied, and the resulting  $p$ -values are shown in the second, fourth and sixth column.  $P$ -values passing a significance threshold of  $\alpha = 0.05$  are highlighted in bold,  $\alpha = 0.01$  in bold and underlined,  $\alpha = 0.001$  are labeled  $< 0.001$ .

h	2 vs. 0.5 $\times 10^6$ cells $\text{ml}^{-1}$	2 vs. 1 $\times 10^6$ cells $\text{ml}^{-1}$	2 vs. 4 $\times 10^6$ cells $\text{ml}^{-1}$
0	$d$ 1.9	$d$ 1.3	$d$ 2.2
	$p$ 0.142	$p$ 0.151	$p$ <b>0.037</b>
2	$d$ 0.4	$d$ 0.2	$d$ 2.3
	$p$ 0.902	$p$ 0.779	$p$ <b>0.030</b>
4	$d$ 1.0	$d$ 1.1	$d$ 3.0
	$p$ 0.828	$p$ 0.215	$p$ <b>0.012</b>
6	$d$ 0.1	$d$ 0.1	$d$ 1.1
	$p$ 0.365	$p$ 0.899	$p$ 0.226
8	$d$ $< 0.1$	$d$ 2.0	$d$ 0.9
	$p$ 0.090	$p$ <b>0.045</b>	$p$ 0.280
12	$d$ 1.5	$d$ 2.5	$d$ 4.4
	$p$ 0.134	$p$ <b>0.024</b>	$p$ <b>0.002</b>
18	$d$ 2.5	$d$ 0.5	$d$ 0.1
	$p$ 0.144	$p$ 0.509	$p$ 0.909
24	$d$ 0.9	$d$ 1.6	$d$ 2.8
	$p$ 0.565	$p$ 0.096	$p$ <b>0.015</b>

## 6. Appendix

**Supplemental Table 49.** Statistical significance of chlorophyll content (acetate concentration). Cohen's *d*-value was computed as a measure of effect size between the individual conditions, absolute *d*-values are shown at the top of each cell. For statistical significance between conditions, unpaired, two-tailed Student's *t*-test was applied, and the resulting *p*-values are shown at the bottom of each cell. *P*-values passing a significance threshold of  $\alpha = 0.05$  are highlighted in bold,  $\alpha = 0.01$  in bold and underlined,  $\alpha = 0.001$  are labeled < 0.001.

h		17 vs. 1.7 mM	17 vs. 0.17 mM	17 vs. 0.017 mM	17 vs. 0.0017 mM	17 vs. 0.00017 mM	17 vs. 0 mM
0	<i>d</i>	1.3	0.6	0.6	<0.1	0.4	0.2
	<i>p</i>	0.176	0.535	0.488	0.995	0.671	0.801
2	<i>d</i>	1.7	0.3	1.2	0.1	0.8	1.3
	<i>p</i>	0.103	0.722	0.211	0.944	0.409	0.154
4	<i>d</i>	1.0	0.1	1.1	0.9	1.0	1.7
	<i>p</i>	0.286	0.953	0.236	0.340	0.291	0.073
6	<i>d</i>	1.3	1.0	0.5	2.5	4.1	3.2
	<i>p</i>	0.185	0.276	0.575	<b>0.039</b>	<b>0.007</b>	<b>0.009</b>
8	<i>d</i>	0.1	1.3	0.9	2.7	3.4	5.8
	<i>p</i>	0.900	0.187	0.351	<b>0.031</b>	<b>0.014</b>	<b>0.001</b>
12	<i>d</i>	2.0	0.5	0.8	6.7	2.8	20.0
	<i>p</i>	0.071	0.569	0.364	<b>0.001</b>	<b>0.026</b>	<b>&lt;0.001</b>
18	<i>d</i>	0.1	0.6	1.1	7.1	5.0	5.9
	<i>p</i>	0.896	0.518	0.268	<b>0.001</b>	<b>0.004</b>	<b>0.001</b>
24	<i>d</i>	0.1	0.2	0.5	5.3	2.7	6.5
	<i>p</i>	0.900	0.821	0.608	<b>0.003</b>	<b>0.030</b>	<b>&lt;0.001</b>

**Supplemental Table 50.** Statistical significance of chlorophyll content (*vtc1*, *VTC1*). **A:** Comparison of + acetate cultures and no acetate control cultures for each time and **B:** comparing +acetate with no acetate control. Cohen's *d*-value was computed as a measure of effect size between the individual conditions, absolute *d*-values are shown at the top of each cell. For statistical significance between conditions, unpaired, two-tailed Student's *t*-test was applied, and the resulting *p*-values are shown at the bottom of each cell. *P*-values passing a significance threshold of  $\alpha = 0.05$  are highlighted in bold,  $\alpha = 0.01$  in bold and underlined,  $\alpha = 0.001$  are labeled < 0.001.

<b>A</b>				<b>B</b>						
<i>vtc1</i> vs. <i>VTC1</i>				<i>vtc1</i>			<i>VTC1</i>			
h		0.25	1.0	20 $\mu$ M Fe	0.25 vs. 1.0 $\mu$ M Fe	1.0 vs. 20 $\mu$ M Fe	0.25 vs. 20 $\mu$ M Fe	0.25 vs. 1.0 $\mu$ M Fe	1.0 vs. 20 $\mu$ M Fe	0.25 vs. 20 $\mu$ M Fe
-2	<i>d</i>	0.2	0.1	0.3	0.1	0.3	0.3	0.2	0.1	0.2
	<i>p</i>	0.855	0.907	0.699	0.925	0.729	0.746	0.783	0.894	0.807
0	<i>d</i>	0.8	1.4	0.9	0.3	2.0	1.7	0.6	0.6	0.1
	<i>p</i>	0.362	0.170	0.347	0.732	0.069	0.103	0.527	0.523	0.905
2	<i>d</i>	1.4	2.5	0.4	0.1	1.1	0.5	0.4	2.0	1.3
	<i>p</i>	0.170	<b>0.036</b>	0.650	0.875	0.251	0.576	0.670	0.069	0.178
4	<i>d</i>	0.6	1.7	0.2	<0.1	1.3	0.8	2.2	1.7	0.3
	<i>p</i>	0.478	0.112	0.859	0.983	0.193	0.374	0.055	0.101	0.766
6	<i>d</i>	0.4	0.2	0.6	2.5	1.1	4.7	2.1	1.7	4.8
	<i>p</i>	0.689	0.850	0.477	<b>0.038</b>	0.246	<b>0.004</b>	0.063	0.100	<b>0.004</b>
8	<i>d</i>	0.4	0.6	0.4	11.6	1.3	4.8	3.4	0.6	3.9
	<i>p</i>	0.627	0.500	0.677	<b>&lt;0.001</b>	0.197	<b>0.004</b>	<b>0.015</b>	0.511	<b>0.009</b>
12	<i>d</i>	0.5	0.9	0.5	4.4	0.3	2.8	2.0	0.1	2.3
	<i>p</i>	0.596	0.353	0.559	<b>0.006</b>	0.740	<b>0.028</b>	0.070	0.934	0.047
18	<i>d</i>	2.5	0.3	0.4	5.4	0.8	3.2	7.6	0.0	4.9
	<i>p</i>	<b>0.037</b>	0.698	0.631	<b>0.003</b>	0.386	<b>0.016</b>	<b>0.001</b>	0.982	<b>0.004</b>
24	<i>d</i>	0.4	0.4	0.7	4.4	0.3	7.1	2.8	1.0	2.8
	<i>p</i>	0.637	0.663	0.456	<b>0.006</b>	0.771	<b>0.001</b>	<b>0.027</b>	0.293	<b>0.027</b>
48	<i>d</i>	0.4	0.8	1.6	0.7	0.8	0.1	0.6	1.4	2.0
	<i>p</i>	0.624	0.363	0.117	0.436	0.368	0.878	0.497	0.163	0.071

## 6. Appendix

---

**Supplemental Table 51.** Statistical significance of chlorophyll content (Cu-deficiency). Cohen's *d*-value was computed as a measure of effect size between the individual conditions, absolute *d*-values are shown in the first, third and fifth column. For statistical significance between conditions, unpaired, two-tailed Student's *t*-test was applied, and the resulting *p*-values are shown in the second, fourth and sixth column. *P*-values passing a significance threshold of  $\alpha = 0.05$  are highlighted in bold,  $\alpha = 0.01$  in bold and underlined,  $\alpha = 0.001$  are labeled  $< 0.001$ .

	Cu replete vs. Cu deficient		Cu deficient vs. Cu deficient & Fe excess		Cu replete vs. Cu deficient & Fe excess	
	<i>d</i>	<i>p</i>	<i>d</i>	<i>p</i>	<i>d</i>	<i>p</i>
	CC-4402	10.1	<b><u>&lt;0.001</u></b>	9.1	<b><u>&lt;0.001</u></b>	0.5
CC-4532	<0.1	0.972	2.0	0.073	1.8	0.087

**Supplemental Table 52.** Statistical significance of chlorophyll content (heterotrophic). Cohen's *d*-value was computed as a measure of effect size between the individual conditions, absolute *d*-values are shown in the left column. For statistical significance between conditions, unpaired, two-tailed Student's *t*-test was applied, and the resulting *p*-values are shown in right column. *P*-values passing a significance threshold of  $\alpha = 0.05$  are highlighted in bold,  $\alpha = 0.01$  in bold and underlined,  $\alpha = 0.001$  are labeled  $< 0.001$ .

	photoheterotrophic vs. heterotrophic	
	<i>d</i>	<i>p</i>
CC-1009	14.0	<b><u>&lt;0.001</u></b>
CC-4532	0.9	0.267

## 6. Appendix

**Supplemental Table 53.** Statistical significance of growth rates. **A:** Photoheterotrophic, **B:** photoautotrophic, **C:** heterotrophic cultures, and **D:** trophic growth conditions for each strain. Cohen's  $d$ -value was computed as a measure of effect size between the individual conditions, absolute  $d$ -values are shown at the top of each cell. For statistical significance between conditions, unpaired, two-tailed Student's  $t$ -test was applied, and the resulting  $p$ -values are shown at the bottom of each cell.  $P$ -values passing a significance threshold of  $\alpha = 0.05$  are highlighted in bold,  $\alpha = 0.01$  in bold and underlined,  $\alpha = 0.001$  are labeled  $< 0.001$ .

		CC-4532	CC-1690	CC-1009	CC-1691					
CC-124	$d$	0.2	1.1	0.4	0.6	CC-124	$d$	16.3	2.4	14.6
	$p$	0.788	0.157	0.606	0.401		$p$	<u><b>&lt;0.001</b></u>	<b>0.029</b>	<u><b>&lt;0.001</b></u>
CC-4532	$d$		1.8	0.8	1.3	CC-4532	$d$	16.1	3.6	18.8
	$p$		<b>0.040</b>	0.289	0.117		$p$	<u><b>&lt;0.001</b></u>	<b>0.007</b>	<u><b>&lt;0.001</b></u>
CC-1690	$d$			1.1	0.9	CC-1690	$d$	9.9	3.7	6.2
	$p$			0.176	0.245		$p$	<u><b>&lt;0.001</b></u>	<b>0.006</b>	<b>0.001</b>
CC-1009	$d$				0.4	CC-1009	$d$	12.3	8.9	22.6
	$p$				0.632		$p$	<u><b>&lt;0.001</b></u>	<u><b>&lt;0.001</b></u>	<u><b>&lt;0.001</b></u>
		CC-4532	CC-1690	CC-1009	CC-1691					
CC-124	$d$	0.4	3.0	4.4	1.3	CC-124	$d$	24.5	4.6	19.2
	$p$	0.607	<b>0.005</b>	<b>0.001</b>	0.124		$p$	<u><b>&lt;0.001</b></u>	<b>0.003</b>	<u><b>&lt;0.001</b></u>
CC-4532	$d$		3.3	4.6	1.7	CC-4532	$d$			
	$p$		<b>0.003</b>	<b>0.001</b>	0.056		$p$			
CC-1690	$d$			0.8	2.4	CC-1690	$d$			
	$p$			0.325	<b>0.014</b>		$p$			
CC-1009	$d$				4.1	CC-1009	$d$			
	$p$				<b>0.001</b>		$p$			
		CC-4532	CC-1690	CC-1009	CC-1691					
CC-124	$d$	1.3	2.0	1.0	0.1	CC-124	$d$			
	$p$	0.125	<b>0.032</b>	0.190	0.919		$p$			
CC-4532	$d$		1.5	0.4	1.4	CC-4532	$d$			
	$p$		0.075	0.636	0.103		$p$			
CC-1690	$d$			1.6	2.0	CC-1690	$d$			
	$p$			0.059	<b>0.032</b>		$p$			
CC-1009	$d$				1.1	CC-1009	$d$			
	$p$				0.159		$p$			

**Supplemental Table 54.** Statistical significance of chlorophyll content. Cohen's  $d$ -value was computed as a measure of effect size between the individual conditions, absolute  $d$ -values are shown at the top of each cell. For statistical significance between conditions, unpaired, two-tailed Student's  $t$ -test was applied, and the resulting  $p$ -values are shown at the bottom of each cell.  $P$ -values passing a significance threshold of  $\alpha = 0.05$  are highlighted in bold,  $\alpha = 0.01$  in bold and underlined,  $\alpha = 0.001$  are labeled  $< 0.001$ .

		CC-4532	CC-1690	CC-1009	CC-1691
CC-124	$d$	0.1	5.0	3.7	1.1
	$p$	0.903	<u><b>&lt;0.001</b></u>	<b>0.002</b>	0.156
CC-4532	$d$		4.0	2.5	0.5
	$p$		<b>0.001</b>	<b>0.012</b>	0.485
CC-1690	$d$			2.1	5.2
	$p$			<b>0.025</b>	<u><b>&lt;0.001</b></u>
CC-1009	$d$				3.9
	$p$				<b>0.001</b>

## 6. Appendix

**Supplemental Table 55.** Statistical significance of maximum quantum efficiency of PSII ( $F_v/F_m$ ). Cohen's  $d$ -value was computed as a measure of effect size between the individual conditions, absolute  $d$ -values are shown at the top of each cell. For statistical significance between conditions, unpaired, two-tailed Student's  $t$ -test was applied, and the resulting  $p$ -values are shown at the bottom of each cell.  $P$ -values passing a significance threshold of  $\alpha = 0.05$  are highlighted in bold,  $\alpha = 0.01$  in bold and underlined,  $\alpha = 0.001$  are labeled  $< 0.001$ .

		CC-4532	CC-1690	CC-1009	CC-1691
CC-124	$d$	1.4	1.2	3.6	2.3
	$p$	0.086	0.134	<b><u>0.002</u></b>	<b>0.018</b>
CC-4532	$d$		0.6	2.5	0.7
	$p$		0.414	<b>0.013</b>	0.382
CC-1690	$d$			3.1	1.4
	$p$			<b><u>0.005</u></b>	0.086
CC-1009	$d$				2.0
	$p$				<b>0.028</b>

**Supplemental Table 56.** Statistical significance of oxygen consumption and evolution. **A:** Net oxygen consumption in the dark and **B:** net oxygen evolution in constant illumination. Effect Cohen's  $d$ -value was computed as a measure of effect size between the individual conditions, absolute  $d$ -values are shown at the top of each cell. For statistical significance between conditions, unpaired, two-tailed Student's  $t$ -test was applied, and the resulting  $p$ -values are shown at the bottom of each cell.  $P$ -values passing a significance threshold of  $\alpha = 0.05$  are highlighted in bold,  $\alpha = 0.01$  in bold and underlined,  $\alpha = 0.001$  are labeled  $< 0.001$ .

<b>A</b>					<b>B</b>						
		CC-4532	CC-1690	CC-1009	CC-1691			CC-4532	CC-1690	CC-1009	CC-1691
CC-124	$d$	0.2	2.4	8.1	3.5	CC-124	$d$	4.9	3.0	9.8	5.0
	$p$	0.820	<b>0.045</b>	<b><u>0.001</u></b>	<b>0.013</b>		$p$	<b><u>0.004</u></b>	<b>0.021</b>	<b><u>&lt;0.001</u></b>	<b>0.004</b>
CC-4532	$d$		2.2	8.6	3.9	CC-4532	$d$		7.2	4.0	0.2
	$p$		0.052	<b><u>&lt;0.001</u></b>	<b>0.009</b>		$p$		<b>0.001</b>	<b>0.008</b>	0.787
CC-1690	$d$			8.3	5.1	CC-1690	$d$			11.4	7.3
	$p$			<b><u>0.001</u></b>	<b>0.003</b>		$p$			<b><u>&lt;0.001</u></b>	<b>0.001</b>
CC-1009	$d$				6.1	CC-1009	$d$				4.7
	$p$				<b>0.002</b>		$p$				<b>0.004</b>

**Supplemental Table 57.** Statistical significance of carbon, nitrogen, phosphorus and sulfur content. **A:** Carbon, **B:** nitrogen, **C:** phosphorus, and **D:** sulfur content. Cohen's  $d$ -value was computed as a measure of effect size between the individual conditions, absolute  $d$ -values are shown at the top of each cell. For statistical significance between conditions, unpaired, two-tailed Student's  $t$ -test was applied, and the resulting  $p$ -values are shown at the bottom of each cell.  $P$ -values passing a significance threshold of  $\alpha = 0.05$  are highlighted in bold,  $\alpha = 0.01$  in bold and underlined,  $\alpha = 0.001$  are labeled  $< 0.001$ .

<b>A</b>					<b>B</b>						
		CC-4532	CC-1690	CC-1009	CC-1691			CC-4532	CC-1690	CC-1009	CC-1691
CC-124	$d$	0.4	5.3	3.7	2.5	CC-124	$d$	2.4	1.3	0.5	1.0
	$p$	0.675	<b>0.003</b>	0.011	<b>0.035</b>		$p$	<b>0.042</b>	0.186	0.584	0.287
CC-4532	$d$		4.5	3.8	2.0	CC-4532	$d$		2.8	2.4	1.4
	$p$		<b>0.005</b>	<b>0.010</b>	0.075		$p$		<b>0.026</b>	<b>0.042</b>	0.166
CC-1690	$d$			8.3	2.8	CC-1690	$d$			0.8	2.0
	$p$			<b>0.001</b>	<b>0.026</b>		$p$			0.363	0.070
CC-1009	$d$				6.0	CC-1009	$d$				1.3
	$p$				<b>0.002</b>		$p$				0.174

<b>C</b>					<b>D</b>						
		CC-4532	CC-1690	CC-1009	CC-1691			CC-4532	CC-1690	CC-1009	CC-1691
CC-124	$d$	0.7	0.1	3.7	2.7	CC-124	$d$	1.1	5.7	0.3	1.6
	$p$	0.362	0.883	<b>0.002</b>	<b>0.008</b>		$p$	0.187	<b><u>&lt;0.001</u></b>	0.649	0.066
CC-4532	$d$		1.3	3.4	4.5	CC-4532	$d$		7.0	1.0	0.6
	$p$		0.125	<b>0.003</b>	<b>0.001</b>		$p$		<b><u>&lt;0.001</u></b>	0.189	0.445
CC-1690	$d$			4.5	9.4	CC-1690	$d$			3.7	13.7
	$p$			<b>0.001</b>	<b><u>&lt;0.001</u></b>		$p$			<b>0.002</b>	<b><u>&lt;0.001</u></b>
CC-1009	$d$				6.2	CC-1009	$d$				1.3
	$p$				<b><u>&lt;0.001</u></b>		$p$				0.109

## 6. Appendix

**Supplemental Table 58.** Statistical significance of cell volume. Cohen's  $d$ -value was computed as a measure of effect size between the individual conditions, absolute  $d$ -values are shown at the top of each cell. For statistical significance between conditions, unpaired, two-tailed Student's  $t$ -test was applied, and the resulting  $p$ -values are shown at the bottom of each cell.  $P$ -values passing a significance threshold of  $\alpha = 0.05$  are highlighted in bold,  $\alpha = 0.01$  in bold and underlined,  $\alpha = 0.001$  are labeled  $< 0.001$ .

	CC-4532	CC-1690	CC-1009	CC-1691
CC-124 $d$	0.6	1.5	3.9	1.0
CC-124 $p$	0.453	0.072	<b><u>0.001</u></b>	0.219
CC-4532 $d$		1.8	2.6	0.3
CC-4532 $p$		<b>0.040</b>	<b>0.010</b>	0.680
CC-1690 $d$			4.1	2.2
CC-1690 $p$			<b><u>0.001</u></b>	<b>0.021</b>
CC-1009 $d$				2.6
CC-1009 $p$				<b>0.011</b>

**Supplemental Table 59.** Statistical significance of potassium, sodium, magnesium, and calcium content. **A:** Cellular K, **B:** Mg, **C:** Ca, **D:** Fe, **E:** Mn, and **F:** Cu content. Cohen's  $d$ -value was computed as a measure of effect size between the individual conditions, absolute  $d$ -values are shown at the top of each cell. For statistical significance between conditions, unpaired, two-tailed Student's  $t$ -test was applied, and the resulting  $p$ -values are shown at the bottom of each cell.  $P$ -values passing a significance threshold of  $\alpha = 0.05$  are highlighted in bold,  $\alpha = 0.01$  in bold and underlined,  $\alpha = 0.001$  are labeled  $< 0.001$ .

<b>A</b>					<b>B</b>				
	CC-4532	CC-1690	CC-1009	CC-1691		CC-4532	CC-1690	CC-1009	CC-1691
CC-124 $d$	0.4	8.8	0.4	1.0	CC-124 $d$	0.8	0.1	1.3	3.4
CC-124 $p$	0.626	<b><u>&lt;0.001</u></b>	0.570	0.194	CC-124 $p$	0.313	0.880	0.112	<b><u>0.003</u></b>
CC-4532 $d$		13.7	0.8	0.9	CC-4532 $d$		1.6	1.1	6.8
CC-4532 $p$		<b><u>&lt;0.001</u></b>	0.312	0.245	CC-4532 $p$		0.061	0.188	<b><u>&lt;0.001</u></b>
CC-1690 $d$			6.3	36.7	CC-1690 $d$			1.4	16.4
CC-1690 $p$			<b><u>&lt;0.001</u></b>	<b><u>&lt;0.001</u></b>	CC-1690 $p$			0.089	<b><u>&lt;0.001</u></b>
CC-1009 $d$				1.3	CC-1009 $d$				2.6
CC-1009 $p$				0.107	CC-1009 $p$				<b>0.011</b>

<b>C</b>					<b>D</b>				
	CC-4532	CC-1690	CC-1009	CC-1691		CC-4532	CC-1690	CC-1009	CC-1691
CC-124 $d$	0.3	6.9	2.7	4.2	CC-124 $d$	0.3	16.3	0.6	11.7
CC-124 $p$	0.716	<b><u>&lt;0.001</u></b>	<b>0.009</b>	<b>0.001</b>	CC-124 $p$	0.710	<b><u>&lt;0.001</u></b>	0.401	<b><u>&lt;0.001</u></b>
CC-4532 $d$		15.8	2.7	9.9	CC-4532 $d$		5.6	0.7	3.3
CC-4532 $p$		<b><u>&lt;0.001</u></b>	<b>0.009</b>	<b><u>&lt;0.001</u></b>	CC-4532 $p$		<b><u>&lt;0.001</u></b>	0.358	<b>0.003</b>
CC-1690 $d$			5.2	17.6	CC-1690 $d$			3.2	8.2
CC-1690 $p$			<b><u>&lt;0.001</u></b>	<b><u>&lt;0.001</u></b>	CC-1690 $p$			<b>0.004</b>	<b><u>&lt;0.001</u></b>
CC-1009 $d$				4.3	CC-1009 $d$				2.2
CC-1009 $p$				<b>0.001</b>	CC-1009 $p$				<b>0.022</b>

<b>E</b>					<b>F</b>				
	CC-4532	CC-1690	CC-1009	CC-1691		CC-4532	CC-1690	CC-1009	CC-1691
CC-124 $d$	0.5	3.4	0.1	4.1	CC-124 $d$	0.3	1.3	0.8	1.5
CC-124 $p$	0.491	<b>0.003</b>	0.870	<b>0.001</b>	CC-124 $p$	0.663	0.126	0.300	0.083
CC-4532 $d$		7.0	0.1	8.4	CC-4532 $d$		1.0	1.2	1.1
CC-4532 $p$		<b><u>&lt;0.001</u></b>	0.861	<b><u>&lt;0.001</u></b>	CC-4532 $p$		0.226	0.154	0.188
CC-1690 $d$			1.7	2.4	CC-1690 $d$			2.1	0.2
CC-1690 $p$			0.052	<b>0.014</b>	CC-1690 $p$			<b>0.026</b>	0.778
CC-1009 $d$				2.0	CC-1009 $d$				2.8
CC-1009 $p$				<b>0.031</b>	CC-1009 $p$				<b><u>0.007</u></b>

## 6. Appendix

**Supplemental Table 60.** Statistical significance of iron content (Fe-excess). Cohen's *d*-value was computed as a measure of effect size between the individual conditions, absolute *d*-values are shown in the left column. For statistical significance between conditions, unpaired, two-tailed Student's *t*-test was applied, and the resulting *p*-values are shown in the right column. *P*-values passing a significance threshold of  $\alpha = 0.05$  are highlighted in bold,  $\alpha = 0.01$  in bold and underlined,  $\alpha = 0.001$  are labeled  $< 0.001$ .

20 vs. 200 $\mu\text{M}$ Fe		
strain	<i>d</i>	<i>p</i>
CC-124	8.1	<b>0.001</b>
CC-4532	7.3	<b>0.001</b>
CC-1690	8.9	<b><u>&lt;0.001</u></b>
CC-1009	6.8	<b>0.001</b>
CC-1691	6.1	<b>0.001</b>

**Supplemental Table 61.** Calibration levels for ICP-MS/MS analysis. 13 different calibration solutions were prepared using a multi-element environmental calibration standard and single element standards for P and S.

level	P, S	Mg, K, Na, Ca, Fe	Mn, Cu, Zn
1	0	0	0
2	0	2 $\mu\text{g/l}$	20 ng/l
3	0	5 $\mu\text{g/l}$	50 ng/l
4	50 $\mu\text{g/l}$	10 $\mu\text{g/l}$	100 ng/l
5	100 $\mu\text{g/l}$	50 $\mu\text{g/l}$	500 ng/l
6	200 $\mu\text{g/l}$	100 $\mu\text{g/l}$	1 $\mu\text{g/l}$
7	500 $\mu\text{g/l}$	200 $\mu\text{g/l}$	2 $\mu\text{g/l}$
8	1 mg/l	500 $\mu\text{g/l}$	5 $\mu\text{g/l}$
9	2 mg/l	1 mg/l	10 $\mu\text{g/l}$
10	5 mg/l	2 mg/l	20 $\mu\text{g/l}$
11	10 mg/l	5 mg/l	50 $\mu\text{g/l}$
12	20 mg/l	10 mg/l	100 $\mu\text{g/l}$
13	50 mg/l	20 mg/l	200 $\mu\text{g/l}$



## **Eidesstattliche Erklärung**

Ich erkläre hiermit, dass ich die vorliegende Arbeit selbstständig und ohne unerlaubte Hilfe verfasst und keine anderen Quellen und Hilfsmittel als die angegebenen verwendet habe. Weiterhin versichere ich, dass diese Dissertation weder ganz noch in Teilen einer anderen Prüfungskommission vorgelegt wurde.

Berkeley, 20. Oktober 2019

---

Anne G. Glaesener



## **Acknowledgments**

A Ph.D. thesis cannot be conducted alone, there are lots of people behind the scene who contributed directly or indirectly with their constant support to this work.

I would like to express my sincere gratitude to Sabeeha for accepting me in her lab, for being my supervisor throughout the years and for her constant support and generosity. I am especially thankful that she gave me the opportunity and freedom to perform and develop my research independently. She has been, and still is, a big example of dedication and devotion to science.

I would like to thank Michael Schroda for being my German host and supervisor from afar and for all his support and understanding in navigating a Ph.D. across continents.

I would also like to thank my thesis committee chair Prof. Dr. Neuhaus for his support.

My sincere thank you goes to the entire Merchant group – everyone through the years – too many friends and acquaintances to name. Specifically, I would like to thank Ian and Crysten for their help and support while getting settled in LA and starting my research, Sean for his endless wisdom regarding everything RNA-Seq, and Dani and Stefan for their endless support during the last years.

I am thankful for my friends for their company, encouragement, and open ears - we made it all work, even over continents and time zone.

Throughout the years I could always count on the backup and support of my family. I especially want to thank my parents who have guided me through the different stages of my personal and professional growth, enabled me to study and move abroad and who were always the safety net and haven.



## Anne G. Glaesener

### EDUCATION

---

**Ph.D. Candidate** **2013 – 2019**

Technical University Kaiserslautern, Germany  
Thesis supervised by Prof. Dr. S. Merchant, Department of Chemistry and Biochemistry, University of California Los Angeles (now QB3, University of California Berkeley), USA and Prof. Dr. M. Schroda, Department of Molecular Biotechnology and Systems Biology, Technical University Kaiserslautern, Germany.

**Master of Science Biotechnology** **2009 –2011**

with specialization in Applied Cell Biology, awarded from Technical University Braunschweig, Germany. Graded thesis with seminar presentation and defense in the group of Prof. Dr. R. Mendel.

**Bachelor of Science Biotechnology** **2006 –2009**

with specialization in Applied Cell Biology, awarded from Technical University Braunschweig, Germany. Graded thesis with seminar presentation in the group of Prof. Dr. H.-H. Arnold.

**Biochemistry Studies** **2004 –2006**

University Greifswald, Germany

**Abitur (higher education entrance qualification)** **2004**

Jade-Gymnasium, Germany

### RESEARCH EXPERIENCE

---

**Assistant Specialist** **2019**

Prof. Dr. S. Merchant, University of California Berkeley, USA

**Graduate Student** **2013 – 2019**

Prof. Dr. S. Merchant, University of California Los Angeles, USA and Prof. Dr. M. Schroda, Technical University Kaiserslautern, Germany

**Research Assistant** **2011 –2013**

Staff Research Associate (SRA I), Prof. Dr. S. Merchant, University of California Los Angeles, USA

**Student Researcher** **2011**

Independent research under the supervision of a postdoctoral fellow in the group of Prof. Dr. R. Mendel, Department of Plant Biology, Technical University Braunschweig, Germany

**Student Researcher** **2011**

Mostly independent research under the supervision of a graduate student in the group of Prof. Dr. H.-H. Arnold, Department of Biochemistry, Biotechnology and Bioinformatics, Technical University Braunschweig, Germany

PUBLICATIONS

---

- **Glaesener AG**, Merchant SS and Blaby-Haas CE (2013) Iron economy in *Chlamydomonas reinhardtii*. *Front. Plant Sci.* 4:337.
- Blaby IK, **Glaesener AG**, Mettler T, Fitz-Gibbon ST, Gallaher SD, Liu B, Boyle NR, Kropat J, Stitt M, Johnson S, Benning C, Pellegrini M, Casero D and Merchant SS (2013) Systems-Level Analysis of Nitrogen Starvation-Induced Modifications of Carbon Metabolism in a *Chlamydomonas reinhardtii* Starchless Mutant. *The Plant Cell* 25 (11) 4305-4323.
- Gallaher SD, Fitz-Gibbon ST, **Glaesener AG**, Pellegrini M and Merchant SS (2015) *Chlamydomonas* Genome Resource for Laboratory Strains Reveals a Mosaic of Sequence Variation, Identifies True Strain Histories, and Enables Strain-Specific Studies. *The Plant Cell* 27 (9) 2335-2352.
- **Glaesener AG**, Gallaher SD, Merchant SS (in preparation) *Chlamydomonas* iron homeostasis during transition from photoautotrophic to photoheterotrophic growth.
- **Glaesener AG**, Gallaher SD, Merchant SS (in preparation) Transcriptomic variance in *Chlamydomonas reinhardtii* laboratory strains.